



2020

A BIOPHYSICAL INVESTIGATION OF STABILITY, LIGAND BINDING, AND IRON STATE OF CYP102A1

Catherine A. Denning-Jannace

University of Kentucky, cadenning0791@gmail.com

Author ORCID Identifier:

 <https://orcid.org/0000-0003-1750-1197>

Digital Object Identifier: <https://doi.org/10.13023/etd.2020.201>

[Right click to open a feedback form in a new tab to let us know how this document benefits you.](#)

Recommended Citation

Denning-Jannace, Catherine A., "A BIOPHYSICAL INVESTIGATION OF STABILITY, LIGAND BINDING, AND IRON STATE OF CYP102A1" (2020). *Theses and Dissertations--Chemistry*. 121.
https://uknowledge.uky.edu/chemistry_etds/121

This Doctoral Dissertation is brought to you for free and open access by the Chemistry at UKnowledge. It has been accepted for inclusion in Theses and Dissertations--Chemistry by an authorized administrator of UKnowledge. For more information, please contact UKnowledge@lsv.uky.edu.

STUDENT AGREEMENT:

I represent that my thesis or dissertation and abstract are my original work. Proper attribution has been given to all outside sources. I understand that I am solely responsible for obtaining any needed copyright permissions. I have obtained needed written permission statement(s) from the owner(s) of each third-party copyrighted matter to be included in my work, allowing electronic distribution (if such use is not permitted by the fair use doctrine) which will be submitted to UKnowledge as Additional File.

I hereby grant to The University of Kentucky and its agents the irrevocable, non-exclusive, and royalty-free license to archive and make accessible my work in whole or in part in all forms of media, now or hereafter known. I agree that the document mentioned above may be made available immediately for worldwide access unless an embargo applies.

I retain all other ownership rights to the copyright of my work. I also retain the right to use in future works (such as articles or books) all or part of my work. I understand that I am free to register the copyright to my work.

REVIEW, APPROVAL AND ACCEPTANCE

The document mentioned above has been reviewed and accepted by the student's advisor, on behalf of the advisory committee, and by the Director of Graduate Studies (DGS), on behalf of the program; we verify that this is the final, approved version of the student's thesis including all changes required by the advisory committee. The undersigned agree to abide by the statements above.

Catherine A. Denning-Jannace, Student

Dr. Edith C. Glazer, Major Professor

Dr. Yinan Wei, Director of Graduate Studies

A BIOPHYSICAL INVESTIGATION OF STABILITY, LIGAND BINDING,
AND IRON STATE OF CYP102A1

DISSERTATION

A dissertation submitted in partial fulfillment of the
requirements for the degree of Doctor of Philosophy in the
College of Arts and Sciences
at the University of Kentucky

By

Catherine Alexandria Denning-Jannace
Lexington, Kentucky

Director: Dr. Edith C. Glazer, Professor of Chemistry
Lexington, Kentucky

2020

Copyright © Catherine Alexandria Denning-Jannace 2020

<https://orcid.org/0000-0003-1750-1197>

ABSTRACT OF DISSERTATION

A BIOPHYSICAL INVESTIGATION OF STABILITY, LIGAND BINDING, AND IRON STATE OF CYP102A1

Cytochrome P450s (CYPs) are cysteine ligated Fe-heme monooxygenases that are found in all domains of life. In mammals, they have a role in xenobiotic metabolism and steroid synthesis, making them a fundamental requirement for survival. In addition, their ability to perform a variety of chemical reactions on an array of substrates makes CYPs highly sought for biotechnical applications such as wastewater remediation, production of potential drug candidates, and creation of drug metabolites. By mutating specific amino acids, these enzymes can be engineered to change their substrate binding profiles and achieve stereo- and regio-specific chemistry. While these mutations are essential to change CYP activity, the major drawback to using them on an industrial scale is a decrease in stability of the enzyme. This work elaborated how CYP stability is effected by mutations, binding of native and non-native substrates, and changes in iron oxidation state.

Cytochrome P450_{BM3} (BM3, or CYP102A1), a bacterial enzyme, was used as a model system. In contrast to membrane associated human CYPs, BM3 is soluble and has efficient turnover due to the fusion of the reductase partner the heme domain. BM3 is naturally selective, but mutations can be incorporated to make it promiscuous, similar to CYPs responsible for xenobiotic breakdown. This allowed for the comparison of a selective vs. a promiscuous CYP while conserving the greatest possible sequence identity. An approach was used combining experimental solution phase data, x-ray crystallography, and molecular dynamic simulations. The results showed that mutations resulted in an cumulative decrease in stability as promiscuity increased. This reduction in stability was due to a decrease in the number of salt bridges and disruption of hydrophobic contacts. Regions of P450_{BM3} were found that could be targeted through mutation to increase the stability of a highly promiscuous and active variant known as the pentuple mutant (PM). Further investigations demonstrated the impact of native and non-native substrate binding. The Gibbs free energy of binding (ΔG_b°) was determined for a small library of molecules and was rationalized computationally, concluding that attractive dispersion forces negated the impact of electrostatic and repulsive forces. In addition, the impact of the iron-heme

charge state on CYP stability was examined as a function of promiscuity. In general, there was an association between promiscuity and similarities in the stability of the Fe(III) and Fe(II) states. This is consistent with a model where the promiscuous variants of the enzyme are in a more “reduction-ready” state, and can undergo catalysis with greater ease than the wild type enzyme. These findings have implications for the role of CYPs in human health and for biotechnical applications.

KEYWORDS: Cytochrome P450s, Cytochrome P450_{BM3} (CYP102A1), enzyme stability, heme oxidation state

Catherine Alexandria Denning-Jannace

(Name of Student)

01/15/2020

Date

A BIOPHYSICAL INVESTIGATION OF STABILITY, LIGAND BINDING,
AND IRON STATE OF CYP102A1

By

Catherine Alexandria Denning-Jannace

Dr. Edith C. Glazer

Director of Dissertation

Dr. Yinan Wei

Director of Graduate Studies

01/15/2020

Date

DEDICATION

To Cole Rain & Kai Alexander, my two favorite boys.

ACKNOWLEDGMENTS

The past six and a half years have been the most challenging of my life. None of my accomplishments would have been possible without the support of my advisors, family, and friends. I have to begin by thanking my advisor Dr. Phoebe Glazer. None of this could have been possible without her advice, encouragement, and constant belief in me. She has always pushed me to be the best scientist possible, even when I wasn't sure I could be. I would also like to thank Drs. Anne Frances Miller, Stephen Testa, and Michael Fried for serving on my committee and advocating for me. Your immense pool of knowledge is inspirational.

Next I would like to thank Dr. David Heidary who has spent hours upon hours giving me advice, helping me plan experiments, analyze results, and generally be a thoughtful scientist. I have been very lucky to be surrounded by the best labmates in the Glazer lab, there isn't enough room here to thank them all but I would be remiss to not mention a few. I have to start with my first friend in Kentucky, Dr. Erin Wachter. My life would be so different without you in it. You're always there when I need you from research to life and I can't imagine a better friend and chosen sister. I also have to thank Dr. Elise Wright: you entered my life at such a tumultuous time and were genuinely there for me when you didn't have to be and I will always appreciate you. To Dr. Dymtro Havrylyuk, thank you for all of the help and advice through the years, I'll miss all of our talks.

My family and friends have constantly been there to encourage me, especially when I wasn't able to believe in myself. Specifically, my Mom, Dad, and sister for their love and continual support. Christine, thank you for being there for me, you've truly become a part of my family. Nicole, Cassandra, Kim, Heather, and Raphael thank you for your friendship over the years; keep pushing and I know you'll all do great things.

I have to thank the three most important people in my life. Timothy, you're truly the best husband ever. You're the one person who I know will always have my back above all others and I love you for it. You're the foundation of my support system and I'm thankful for you and the whole Jannace clan. Finally, to Cole and Kai, you are the two things I didn't realize I needed, and I can't wait to watch you grow up; mommy loves you.

TABLE OF CONTENTS

ACKNOWLEDGMENTS	iii
LIST OF TABLES	vii
LIST OF FIGURES	viii
ABBREVIATIONS.....	xi
CHAPTER 1. Introduction.....	1
1.1 Cytochrome P450s (CYPs).....	1
1.1.1 Catalytic cycle.....	1
1.1.2 CYP chemistry	6
1.2 Human Cytochrome P450s	9
1.2.1 Role in steroid and fatty acid turnover.....	11
1.2.2 Role in xenobiotic metabolism	13
1.3 Bacterial Cytochrome P450s.....	17
1.3.1 P450 _{BM3} – Use as a model system	18
1.4 Summary	20
CHAPTER 2. Effect of mutation and substrate binding on the stability of Cytochrome P450 _{BM3} variants.....	22
2.1 Introduction.....	22
2.2 Experimental procedures	26
2.2.1 Biochemical procedures.....	26
2.2.2 Crystallography procedures.	29
2.2.3 MD simulations.....	32
2.3 Results.....	36
2.3.1 Mutation-induced substrate promiscuity is correlated with reduced P450 _{BM3} stability	36
2.3.2 Inhibitor and substrate binding modulates stability	39
2.3.3 X-ray crystal structure of the P450 _{BM3} heme domain is in a closed confirmation.....	41
2.3.4 The X-ray crystal structure of PM P450 _{BM3} is similar to that of WT45	
2.3.5 X-ray co-crystal structures of WT and PM P450 _{BM3} with substrate or inhibitor.....	46
2.3.6 Molecular dynamic simulations.....	48
2.4 Discussion.....	51
2.5 Conclusions.....	58
CHAPTER 3.Molecular determinants of small molecule affinity and enzyme activity of a Cytochrome P450 _{BM3} variant.	60

3.1	Introduction.....	60
3.2	Experimental procedures	67
3.2.1	Biochemical procedures.....	67
3.2.2	Computational procedures	71
3.3	Results and discussion	75
3.3.1	Experimental and calculated binding free energies	75
3.3.2	Protein-ligand interactions in the PM BM3 active site.....	80
3.3.3	Factors contributing to uncoupling.	87
3.3.4	Heme interactions affecting oxidizing ability.....	90
3.4	Conclusions.....	92
CHAPTER 4. Correlations between the promiscuity of Cytochrome P450 _{BM3} variants and oxidation state dependent stability.....		93
4.1	Introduction.....	93
4.2	Experimental procedures	95
4.2.1	Cloning and site-directed mutagenesis of P450 _{BM3}	95
4.2.2	Expression and purification	96
4.2.3	Pulse proteolysis	97
4.2.4	Circular dichroism (CD)	98
4.2.5	UV/Vis spectroscopy	98
4.2.6	Determination of reduction potential	99
4.3	Results.....	99
4.3.1	Selectivity of P450 _{BM3} can be modulated by strategic mutations.	99
4.3.2	Changes in active site stability are observed by UV/Vis spectroscopy.	102
4.3.3	Circular dichroism monitored changes in α -helical content.....	109
4.3.4	Pulse proteolysis uses a protease to investigate global structure stability.....	111
4.3.5	Promiscuous P450 _{BM3} variants have a more positive reduction potential than more selective variants.....	113
4.4	Discussion.....	115
CHAPTER 5. Ruthenium-containing P450 inhibitors for dual enzyme inhibition and DNA damage.....		120
5.1	Introduction.....	120
5.2	Experimental Procedures	123
5.2.1	Materials and instrumentation.....	123
5.2.2	Compound synthesis, characterization, and ion exchange.....	124
5.2.3	Photoejection studies	127
5.2.4	Expression and purification of P450 _{BM3}	128
5.2.5	P450 _{BM3} binding affinity.....	129
5.2.6	Enzyme inhibition assay	130
5.2.7	<i>In vitro</i> transcription and translation.....	131
5.2.8	DNA gel electrophoresis.....	131

5.2.9	Singlet oxygen assay.....	132
5.3	Results and Discussion	132
5.3.1	Light triggered P450 inhibitors were synthesized from Ru(bpy) ₂ Cl ₂	132
5.3.2	Complex 2-4 bind and inhibit P450 _{BM3} and human liver microsomes (HLMs) after light irradiation.	134
5.3.3	DNA damage is induced by complex 2-4 after light irradiation.....	137
5.3.4	Transcription and translation in the presence of P450 _{BM3} and complex 2-4 after light irradiation is inhibited.	139
5.4	Conclusions.....	140
CHAPTER 6. Conclusions.....		142
Appendices.....		144
Appendix A: Chapter 2 Additional Figures and Tables.....		144
Appendix B: Chapter 3 Additional Figures and Tables.....		157
Appendix C: Chapter 4 Additional Figures and Tables.....		167
Appendix D: Chapter 5 Additional Figures and Tables.....		176
REFERENCES.....		192
VITA.....		216

LIST OF TABLES

Table 2.1 Data Collection, Structure Solution, and Model Refinement Statistics of Forms of the P450 _{BM3} Heme Domain.	31
Table 2.2 Urea concentration at the denaturation midpoint (C_m , M) determined by pulse proteolysis for substrate-free and bound P450 _{BM3} variants.	37
Table 2.3. Urea concentration at the denaturation midpoint (C_m , M) determined by CD of substrate-free and bound BM3 variants.	41
Table 3.1. List of mutations in functional BM3 variants.	64
Table 3.2 Drug molecules used in this study with function and CYP chemistry.	66
Table 3.3 High spin fractions, dissociation constants (K_d), and binding free energies (ΔG_b) of palmitic acid and various drug molecules in PM BM3.	80
Table 4.1 Concentration midpoint (C_m) values of P450 _{BM3} variants determined by UV/Vis spectroscopy.	102
Table 4.2 Concentration midpoint (C_m) values of P450 _{BM3} variants by circular dichroism spectroscopy.	110
Table 4.3 Concentration midpoint (C_m) values of P450 _{BM3} variants by pulse proteolysis.	112

LIST OF FIGURES

Figure 1.1 Catalytic cycle of Cytochrome P450s.	2
Figure 1.2. Insertion of oxygen into an inactivated C-H bond as shown by chemotherapeutic cyclophosphamide.	7
Figure 1.3 Possible reactions performed by Cytochrome P450s.	8
Figure 1.4 Human Cytochrome P450 characteristics.	10
Figure 1.5 Structure of an example steroid and fatty acid that both undergo modification by CYPs.	11
Figure 1.6 Activation and deactivation of a 2-aryl-benzothiazole by CYPs.	15
Figure 1.7 Reductive activation of the prodrug AQ4N by CYPs.	16
Figure 1.8 Ru(II) complexes capable of P450 inhibition and DNA damage.	17
Figure 1.9 Crystal structure of the heme domain of wild type P450 _{BM3}	18
Figure 1.10 FMN quinone electron cycling that details how electrons are transferred in the CYP reductase partner.	19
Figure 2.1. Mutations in P450 _{BM3} that result in substrate promiscuity destabilize the protein.	36
Figure 2.2. Mutations induce destabilization of secondary and active site structure.	38
Figure 2.3. The inhibitor, metyrapone, shifts the stability of WT and PM in opposite directions.	40
Figure 2.4. Crystal structures of substrate-free (open conformation) and substrate-bound (closed conformation) WT P450 _{BM3}	42
Figure 2.5 Omit maps for bound ligands in WT and PM P450 _{BM3} X-ray crystal structures.	44
Figure 2.6 Crystal structures of WT and PM BM3.	45
Figure 2.7 Snapshots at 25 ns from the 550 K simulations of substrate-free WT and PM viewed through the channel entrance.	49
Figure 3.1 Peroxide and oxidase uncoupling pathways.	60
Figure 3.2 P450 _{BM3} structure.	62

Figure 3.3 Comparison of a full type I spectral shift to the water bound resting state.	70
Figure 3.4 Spectral titration of PM BM3 with the native substrate palmitic acid and inhibitor metyrapone.	76
Figure 3.5 Difference spectra of all compounds bound to PM P450 _{BM3} studied experimentally.	77
Figure 3.6 An EROD activity assay determined if compounds that induced a type II spectral shift efficiently inhibited metabolism of the fluorescent substrate.	79
Figure 3.7 MD-averaged structures superimposed on the PM-palmitic acid crystal structure for naproxen, diclofenac, S-/R-warfarin, and lovastatin.	82
Figure 3.8 MD-averaged structures superimposed on the PM-palmitic acid crystal structure.	84
Figure 3.9 MD-averaged structures of superimposed on the PM-palmitic acid crystal structure for cotinine, nicotine, and metyrapone.	86
Figure 3.10 Water density at the PM P450 _{BM3} substrate channel.	89
Figure 4.1 Crystal structures of the active site of WT and PM P450 _{BM3}	99
Figure 4.2 Reduction of P450 _{BM3} variants impacts stability as detected by UV/Vis spectroscopy.	104
Figure 4.3 Unfolding of WT and PM P450 _{BM3} as detected by UV/Vis spectroscopy.	106
Figure 4.4 Reduction from Fe(III) to Fe(II) states of selective and promiscuous variants has an opposing effect on secondary structure stability.	109
Figure 4.5 A greater disparity in stability of the global structure occurred as a function of iron oxidation state for selective P450 _{BM3} variants.	111
Figure 4.6 Redox potential is correlated to iron state stability of selective vs. promiscuous P450 _{BM3} variants.	114
Figure 4.7 Change in concentration midpoint (C_m) of all tested variants by pulse proteolysis.	116
Figure 4.8 Possible pathways for biphasic unfolding.	117
Figure 5.1 Design of dual action inhibitors.	120
Figure 5.2 Structures of P450 inhibitors and Ru(II) complexes.	122
Figure 5.3 Absorption spectrum of P450 _{BM3} inhibitor saturated and Ru(II) dark and light systems: 2, 3, 4	134

Figure 5.4 Relative activity of P450 _{BM3} in the presence of 1 and 4 in the dark and following irradiation.....	136
Figure 5.5 Agarose gels showing the dose response of 2 , 3 , and 4 with pUC19 plasmid with and without irradiation.....	138
Figure 5.6 An <i>in vitro</i> transcription and translation experiment allowed for detection of DNA damage that results in inhibition of GFP production.	139

ABBREVIATIONS

$^1\text{O}_2$	Singlet oxygen
AST	Astemizole
bpy	2,2'-bipyridine
CD	Circular dichroism spectroscopy
C_m	Concentration midpoint of denaturation
CNPY	4-Cyanopyridine
CPO	Chloroperoxidase
CPR	Cytochrome P450 reductase
CTN	Cotinine
CYP	Cytochrome P450
DEX	Dextromethorphan
DIF	Diclofenac
DNA	Deoxyribonucleic acid
e^-	Electron
EDTA	Ethylenediaminetetraacetic acid
EET	Epoxyeicosatrienoic acid
EROD	7-Ethoxyresorufin-O-deethylase

ESI-MS	Electrospray ionization mass spectrometry
Eto	Etomidate
EtOH	Ethanol
FAD	Flavin adenine dinucleotide
FdR	Ferredoxin reductase
Fdx	Fe-S containing ferredoxin
FEP/ λ -REMD	Free energy perturbation with Hamiltonian replica-exchange molecular dynamics
FMN	Flavin mononucleotide
FMNH	Flavin mononucleotide semiquinone
FMNH ₂	Flavin mononucleotide hydroquinone
G _b [°]	Gibbs free energy of binding
GFP	Green fluorescent protein
HETE	Hydroxyeicosatetraenoic acids
HPLC	High pressure liquid phase chromatography
HS	High spin
I	Intermediate state
IPTG	Isopropyl β -d-1-thiogalactopyranoside
IVTT	<i>In vitro</i> transcription and translation

K _d	Binding dissociation constant
L	Ligand
LB	Luria broth
LED	Light emitting diode
LS	Low Spin
LVA	Lovastatin
<i>m/z</i>	Mass to charge
MD	Molecular dynamics
MLCT	Metal-to-ligand charge transfer state
mRNA	Messenger ribonucleic acid
MYT or met	Metyrapone
N	Native state
NADPH	Nicotinamide adenine dinucleotide phosphate
NCT	Nicotine
NMR	Nuclear magnetic resonance
NOS	Nitric oxide synthase
NPS	Naproxen
PAH	Polyaromatic hydrocarbon

PBS	Phosphate buffered saline
PDB	Protein Data Bank
PDT	Photodynamic therapy
PEG	Polyethylene glycol
phen	1,10-phenanthroline
PIE-FRET	Pulsed interleaved excitation Förster resonance energy transfer
PM	Pentuple mutant P450 _{BM3} (R47L/F81I/F87V/L188Q/E267V)
PMSF	Phenylmethylsulfonyl fluoride
PUFA	Polyunsaturated fatty acids
QM	Quadruple mutant P450 _{BM3} (R47L/F87V/L188Q/E267V)
RMSD	Root-mean-square deviation
ROS	Radical oxygen species
RT	Room temperature
RWF	R-warfarin
SDS- PAGE	Sodium dodecyl sulfate-polyacrylamide gel
SOSG	Singlet oxygen sensor green
SRS	Substrate recognition sites
SWF	S-warfarin

$t_{1/2}$	Half life
TB	Terrific broth
T_m	Temperature midpoint of denaturation
TM	Triple mutant P450 _{BM3} (R47L/F87V/L188Q)
U	Unfolded/denatured state
WT	Wild-type P450 _{BM3}

CHAPTER 1. INTRODUCTION

1.1 Cytochrome P450s (CYPs)

Cytochrome P450s (CYPs) were first named by Omura and Sato in 1964 due to their observation that these enzymes had an absorbance band at 450 nm when reduced and CO-bound, leading to the name “pigment-450”.³ Since then, CYPs have been intensively studied in relation to their health implications in humans, biological roles in other species, and biotechnical applications.

Cytochrome P450s are a superfamily of Fe-heme cysteine-ligated monooxygenases that exist in almost all life forms, including viruses, with approximately 20,000 genes currently known.^{4, 5} Astonishingly, they are all characterized by a similar fold and carry out somewhat similar reactions even though they have evolved to have distinct substrates and perform various functions that benefit a particular species. This includes steroid synthesis and xenobiotic metabolism in mammals,⁶ and playing a major role in the chemical defense of plants.⁴ The importance of CYPs’ roles in nature has made them highly studied, but much more work is needed to fully characterize and understand the biophysical properties that are important for them to function properly. This work is focused on parsing some of these biophysical properties to elucidate further how these amazing enzymes work.

1.1.1 Catalytic cycle

As CYPs are monooxygenases, the most common reaction is to use O₂ to incorporate one oxygen atom into a substrate. Taking advantage of the Fe-heme active site, in which the Fe is able to cycle through multiple charge and spin states, allows CYPs to perform chemistry that is difficult for most organic chemists to accomplish. All CYPs are believed to utilize the catalytic cycle shown in Figure 1.1. The enzyme

is considered in the resting state (1) when the Fe in the heme porphyrin is hexa-coordinated. The four nitrogens of the porphyrin are ligated in the plane, and a thiol from a cysteine residue is coordinated in the distal position. This ligand plays an essential role in the generation of compound I (7). Lastly, a water molecule is bound in the proximal position, and is the labile ligand. At rest, the d electrons (e^-) of Fe(III) occupy the lowest energy molecular orbitals, producing a low spin (LS) complex.

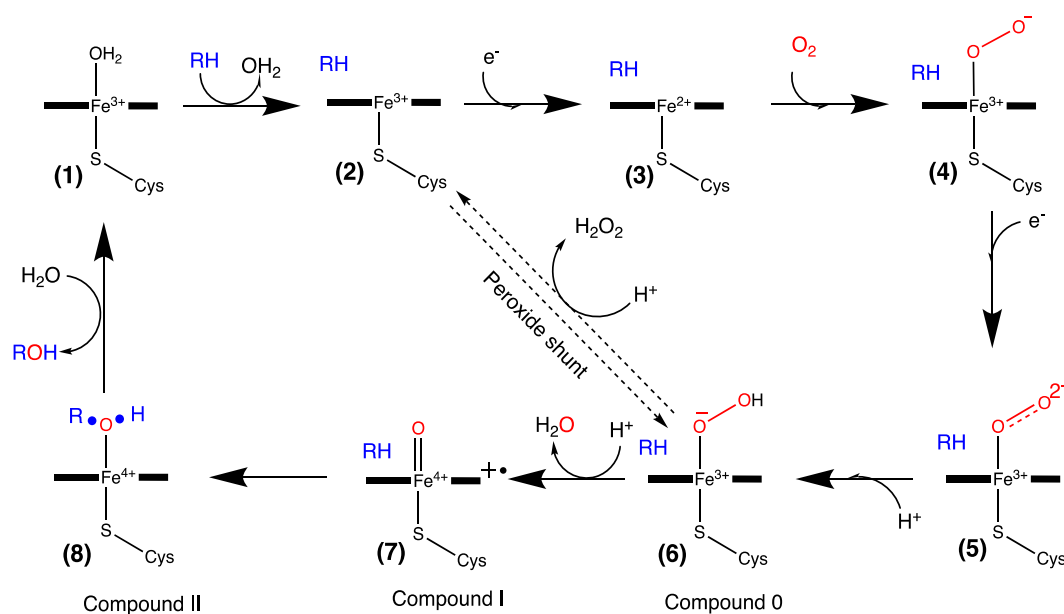


Figure 1.1 Catalytic cycle of Cytochrome P450s.

When substrate (RH) enters the active site, it occupies space near the Fe heme, which causes the bound H_2O molecule to dissociate (2). Upon this dissociation, the Fe-heme becomes penta-coordinate, causing the Fe to move slightly below the plane of the heme. This movement leads to a weakening of the interactions of the Fe-heme, causing the d-block electrons to occupy higher molecular orbitals, producing a high spin (HS) state⁷, and making the complex a better e^- acceptor. This triggers the transfer of one e^- from the reductase partner, converting the HS ferric species to a HS ferrous species (3). At this point, molecular oxygen (O_2) is able to bind, returning the Fe-heme to a low

spin state (4).⁸ This species is a good e⁻ acceptor, facilitating the second e⁻ transfer from the reductase partner. The ferric-dioxo state of the heme⁹ (5) is an excellent Lewis base and readily accepts a proton to produce the ferric-hydroperoxy complex, also known as compound 0 (6). This complex is also a good Lewis base that allows a second protonation step to occur. Upon the release of a H₂O molecule, the heme is now in its most active state, having formed a short lived iron-oxo intermediate called compound I (7)¹⁰. In this state, the oxygen bound can now be transferred to the substrate (8)¹¹⁻¹³ and the enzyme returned to resting state.

It has taken decades and the collaborative efforts of several research groups to fully characterize the complete catalytic cycle of CYPs. In fact, the existence of compound I was finally confirmed only recently in 2010 by Prof. Michael Green.¹⁰ Though the general cycle is agreed upon, there are still several questions that remain. Recently, it was reported by Johnston *et al.* that a mixture of the Fe(III) and Fe(II) state were present at rest, not just Fe(III) state, for two bacterial and five mammalian CYPs expressed in *Escherichia coli* as well as rat hepatocytes.¹⁴ The ratio of Fe(III) to Fe(II) at rest can also be altered by the presence of substrate or electron donors,¹⁴ meaning the current catalytic cycle isn't as static as previously believed. Our group is interested in probing overall protein stability in regards to the ease of transition from the Fe(III) to Fe(II) state and how substrates or inhibitors modulates this transition.

1.1.1.1 Importance of the Fe-cysteine bond on catalysis

Though the metal center is necessary for catalytic modification of substrates to occur, it is the protein environment that regulates the chemistry the metal is able to accomplish. In CYPs, the tuning ability comes from the thiolate ligand. The Fe-Cys bond plays an essential role in the function and stability of cytochrome P450s. Most

CYPs have a similar secondary structure, though they can differ in amino acid sequence by as much as 85%.¹⁵ There are some conserved sequences in most CYPs, such as an alcohol residue in the active site necessary for O₂ activation^{16, 17} and a second acidic residue critical for proton transfer to O₂,^{18, 19} but the one mainstay is the cysteine residue that ligates the heme.

The only heme proteins other than P450s that can cleave C-H bonds are chloroperoxidases (CPO).²⁰ Both enzymes, like nitric oxide synthase (NOS), have Fe-hemes that are Cys-ligated, in contrast to other heme proteins that store or transport O₂. What makes heme-thiolate chemistry unique is that these enzymes are capable of 2 e⁻ transfers, in contrast to His-ligated heme proteins.²¹ The Cys-ligation decreases the reduction potential of the Fe-heme which makes it one of the most powerful oxidants in nature²¹ and has been compared to a biological blowtorch.⁸

This reduction in the Fe-heme potential is based on the fact that the Cys-ligand is a good electron donor. The electron donating ability of the thiolate drives the complex towards protonation, which leads to the incorporation of an oxygen into the substrate.²¹ This is often referred to as the “push effect” which encourages the O₂ molecule bound to the Fe to cleave, leading to the formation of compound I.²² In this way, the thiolate ligand impacts the stability of the enzyme when compound I is formed. This stabilization also occurs as a result of hydrogen bonding in the Cys-ligand loop between the cysteine ligand and other residues.²³

1.1.1.2 Implications of uncoupled catalysis

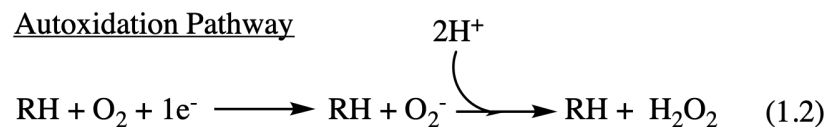
The catalytic cycle of CYPs is tightly regulated to use one molecule of atmospheric dioxygen and two reducing equivalents to produce an oxygenated product and molecule of water (Figure 1.1, Equation 1.1). Misregulation of the catalytic cycle

leads to uncoupled catalysis in which the dioxygen molecule is diverted from forming product from the substrate. The unintended consequence of unproductive catalysis is not only stalled metabolism of substrates but also the creation of radical oxygen species (ROS).

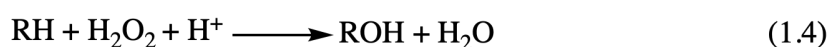
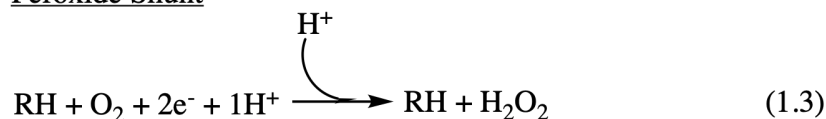
Normal Catalysis



Autoxidation Pathway



Peroxide Shunt



Oxidase Pathway



There are three main pathways in which uncoupled catalysis can occur in CYPs. The first is the autoxidation pathway in which the free radical superoxide (O_2^-) is released from the Fe(III) complex, shown in step 4 in Figure 1.1 and Equation 1.2. Superoxide is quickly converted to hydrogen peroxide (H_2O_2), another potentially damaging compound. The second pathway is the peroxide shunt (Equation 1.3), in which H_2O_2 is released from the Fe(III) complex, shown as step 6 in Figure 1.1 reverting to the HS Fe(III) state (Figure 1.1, step 2). This pathway can also be exploited to jumpstart catalysis without the presence of reducing agents (NADPH), as shown in

Equation 1.4. Addition of H₂O₂ allows for steps 3–5 to be skipped and still get productive metabolism of substrate. The peroxide shunt has been used to bypass the need for expensive reducing agents for CYP catalysis for large-scale biotechnical applications.²⁴ The oxidase pathway is the third uncoupling pathway possible in the CYP catalytic cycle, shown in Equation 1.5. Compound I, which in itself is a radical, has very high reduction potential, which can lead to it being reduced twice more, leading to the formation of a second water molecule if misregulated.

Several factors lead to uncoupled catalysis, including but not limited to identity of the substrate/inhibitor bound²⁵⁻²⁸, mutation of residues^{7, 17, 29}, source of electrons³⁰⁻³² (ex. Cytochrome b5 vs. FAD-FMN reductase), and enzyme promiscuity.³³⁻³⁵ Regardless of cause, the immediate result of ROS production is damage to the enzyme itself, leading to decrease in function, degradation, and aggregation.³⁶ In humans, the highest concentration of P450s are found in the liver, but CYPs are also present in the majority of organ systems. On a molecular level, the creation of ROS by CYPs leads to lipid peroxidation, protein degradation, and cell death. Over time, these molecular damages build up and are implicated in aging³⁷⁻³⁹, carcinogenesis⁴⁰⁻⁴², and several other disease states.

1.1.2 CYP chemistry

The canonical CYP reaction is insertion of oxygen into an unactivated C-H bond, as seen in the first step of modification of the chemotherapeutic cyclophosphamide by liver CYPs (Figure 1.2). Though hydroxylation is an important reaction catalyzed by CYPs, they are capable of carrying out a diverse range of reactions, including but not limited to sulfoxidation, oxidation, and oxidative dehalogenation (Figure 1.3). Of particular interest to xenobiotic metabolism is O- and

N-dealkylation (Figure 1.3) as many compounds go through this process to become more hydrophilic before elimination.

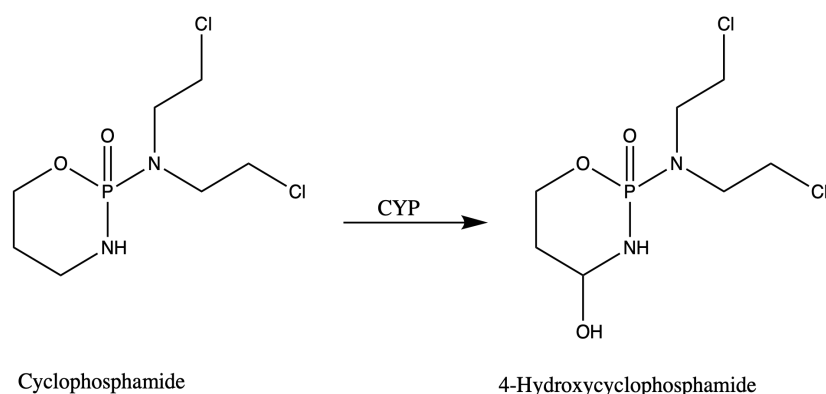


Figure 1.2. Insertion of oxygen into an inactivated C-H bond as shown by chemotherapeutic cyclophosphamide.

As CYPs are capable of such complex chemistries, efforts have been made to harness their power for biotechnical applications, with an emphasis on controlling selectivity and specificity. Highlighting the importance of this field of research is the fact that Professor Frances Arnold won the 2018 Nobel Prize in Chemistry for her work on directed evolution of enzymes. Much of her research has been dedicated to engineering enzymes (particularly CYPs) to perform specific chemistries with high efficiencies and sufficient stability for use for commercial purposes.

This use of engineered enzymes is particularly prominent in the development of pharmaceuticals. Whenever a new drug is tested, all metabolites that are made formed with percentages over a certain threshold must also be tested for toxicity. Many of these metabolites are difficult to synthesize, and those that can be made often use protocols that entail the use of harsh chemicals that are bad for the environment. As a result, a more efficient source is needed, and biocatalysts are a good solution. In addition,

chemistry performed on a large scale can lead to significant impurities, which means extra steps are needed to purify the molecule of interest.

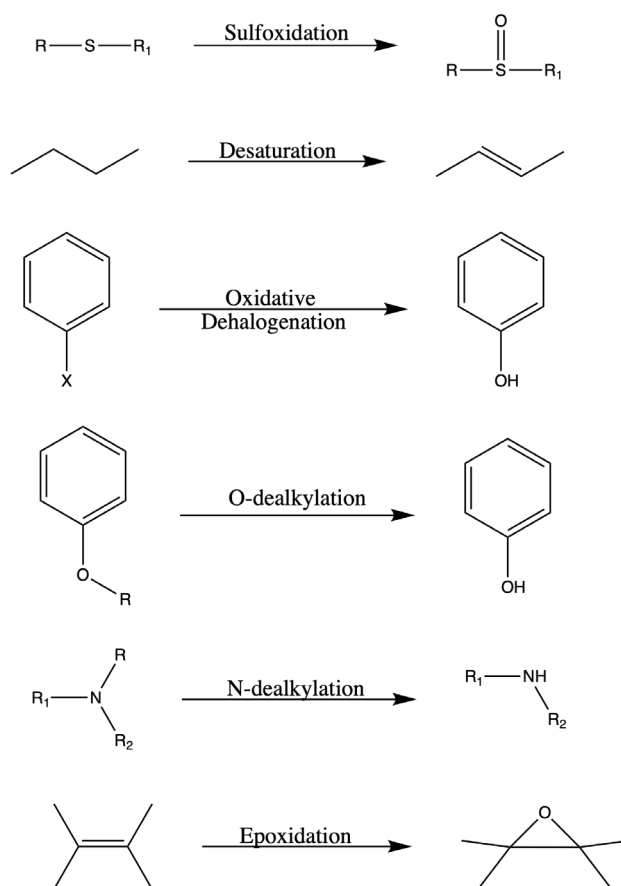


Figure 1.3 Possible reactions performed by Cytochrome P450s.

In 2013, Dennig et al. showed that introduction of three mutations (R47S/Y51W/I401M) to cytochrome P450_{BM3} (CYP102A1), a bacterial CYP, made it able to hydroxylate monosubstituted benzene rings in the ortho-position, with a selectivity of 99:1 as compared to the meta- and para-positions. This finding is interesting as it means P450_{BM3} has potential to be used to make precursors for further synthesis of vitamins, flavorings, and several drug molecules.⁴³ The L75/V78/F87 P450_{BM3} variant was able to selectively hydroxylate and epoxidize β -cembrenediol, a terpenoid natural product, that is being investigated for its antitumor, anti-

inflammatory, and neuroprotective properties. Of 13 possible hydroxylation positions and three epoxidation positions, these three mutations only hydroxylated the substrate at 2 specific positions (C-9 and C-10), and introduced the epoxide at one position. However, this increase in specificity came at the detriment of coupling efficiency, with the highest reported as 56%.⁴⁴ Reactivity can also be tuned by changing the residue ligated to the heme. Wang et al. showed that mutating the cysteine to a histidine diminished the oxidation abilities of P450_{BM3} but allowed it to be competent as a catalyst for cyclopropanation. Cyclopropanation of N,N-diethyl-2-phenylacrylamide and ethyl diazoacetate by His-ligated BM3 (with 4 added mutations) produced levomilnacipran, a serotonin-norepinephrine reuptake inhibitor used to treat depression. Surprisingly, levomilnacipran was produced with a yield greater than 92% in anaerobic conditions and 90% when aerobic. Diastereoselectivity of 98% was obtained, favoring the cis form with enantioselectivity of 92%.⁴⁵

1.2 Human Cytochrome P450s

Human cytochrome P450s have evolved to be a very diverse family of enzymes. They are found in all organs, are involved in a variety of processes, and, if misregulated, can be involved in a plethora of disease states. Of the approximately 60 human CYPs, most have been characterized, though six still have unknown functions. Of the known CYPs, 12% are located in the mitochondrial membrane (Figure 1.4A) and are of the class I electron transfer type (electron transferred to CYP via ferredoxin reductase (FdR) and Fe-S containing ferredoxin (Fdx) proteins).⁴⁶ All 12% are selective and modify steroids or are involved in vitamin D metabolism. The remaining majority of CYPs are localized in the endoplasmic reticulum (ER) and utilize the class II electron transfer system (electron transferred to CYP via FAD-FMN containing cytochrome

P450 reductase (CPR)) to carry out catalysis.⁴⁶ Those in the ER range from being selective and only able to modify steroids, fatty acids, or vitamins (Figure 1.4C), to being extremely promiscuous. CYP3A4 is an example of a promiscuous CYP and metabolizes over 50% of xenobiotics in the liver (Figure 1.4D). This highlights the fascinating fact that one family of enzymes, all with similar structures, is able to perform a wide variety of functions.

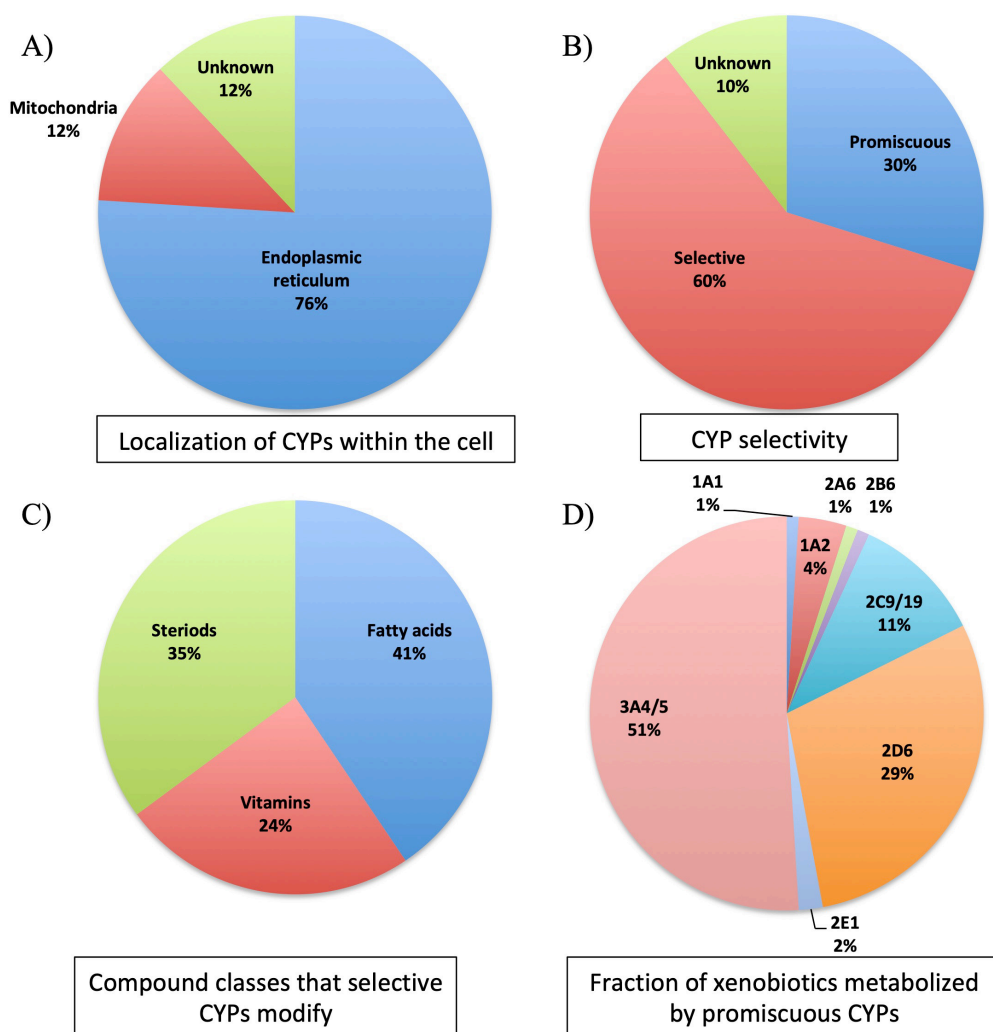


Figure 1.4 Human Cytochrome P450 characteristics.

1.2.1 Role in steroid and fatty acid turnover

One of the main functions of human P450s is their role in steroid and fatty acid modification. All steroids have the same base structure of four fused rings, and differ in the functional groups on those rings, as shown in cholesterol (Figure 1.5A). In humans, steroids are necessary for sodium and potassium transport, stimulation of gluconeogenesis, and transport and synthesis of amino acids. This is in addition to the more commonly known roles, such as cortisol in the fight or flight response, and sex hormones in defining secondary sexual characteristics. Cytochrome P450s are involved in nearly every avenue of steroid synthesis or metabolism. For example, lanosterol 14 α -desmethylase (CYP51A1) removes 2 methyl groups from lanosterol, a necessary step in cholesterol formation that allows it to further differentiate into bile acids and hormones.

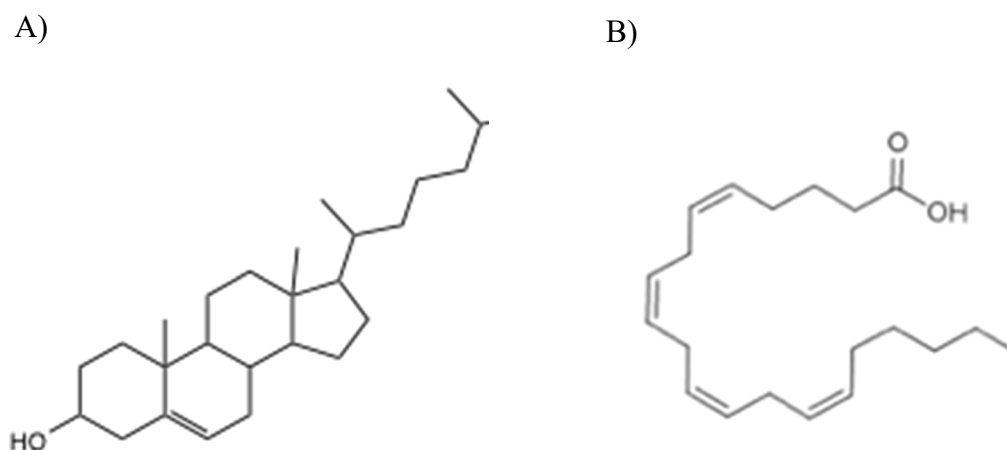


Figure 1.5 Structure of an example (A) steroid and (B) fatty acid that both undergo modification by CYPs.

Six CYPs are involved in the formation of hormones from cholesterol in a tightly regulated system. They are also extremely selective; for instance, CYP19A1 (aromatase) selectively binds androstenedione and testosterone and converts them to

estrone and estradiol, respectively. Though this system is tightly regulated, loss of function and gain of function mutations occur. Inversions in the CYP19A1 gene cause it to be regulated by a different promotor, which leads to overexpression of the enzyme, leading to aromatase excess syndrome, resulting in shorten stature, osteoporosis, early onset of puberty, irregular menstrual cycles in females, and gynecomastia in males.⁴⁷ ⁴⁸ Conversely, lack of CYP19A1 expression leads to aromatase deficiency syndrome, in which pseudo-hermaphroditism is reported in females and hypervirilization in males.⁴⁹

Fatty acids, like steroids, also play several important roles in the human body. An example structure, arachidonic acid, is shown in Figure 1.5B. There are two main classes: saturated and unsaturated fatty acids. Saturated fatty acids mostly come from animal sources, are linear, and tend to pack together, making them solid at room temperature. Unsaturated fatty acids usually come from plant and fish sources, contain double bounds that causes them to kink, and are liquid at room temperature. Unsaturated fatty acids are mostly obtained from our diet, and as they are integral to cell membranes, are necessary to maintain shape and porosity of our cells.⁵⁰ In addition to allowing normal metabolic processes to occur,⁵¹ unsaturated fats are cardioprotective in that they decrease blood pressure and decrease aggregation of blood cells.^{52, 53} They are also involved in movement of smooth muscle and inflammation response an several other processes that occur in the human body.⁵⁴

It has long been speculated that xenobiotic-metabolizing human CYPs have at least one endogenous substrate, and for many of them, it has been found to be polyunsaturated fatty acids (PUFA), specifically arachidonic acid.⁵⁵ CYPs are responsible for modifying arachidonic acid by hydroxylation, epoxidation, and allylic oxidation⁵⁶⁻⁵⁸ into over 100 distinct bioactive molecules.^{55, 59} These metabolites can be

separated into various classes, including hydroxyeicosatetraenoic acids (HETEs), epoxyeicosatrienoic acids (EETs), leukotrienes, and prostaglandins, all of which are considered eicosanoids or secondary messengers in signaling pathways derived from PUFAs. HETEs and EETs are involved in pathways that lead to vasodilation or constriction, promotion or reduction of inflammation, as well as salt uptake and cell injury.⁵⁹ Prostaglandins are important for contractions and relaxations of smooth muscle and cardioprotective functions,⁵⁴ whereas leukotrienes are necessary in the signaling pathway that regulates immune responses.⁶⁰

As expected for compounds so important to homeostasis of the human body, this system is highly regulated. CYP8A1, also known as prostacyclin synthase, a member of the class X electron transfer family (CYPs that don't have a reductase partner),⁴⁶ hydroxylates prostaglandin H2 to prostacyclin. As prostacyclin is a potent vasodilator, when too much is produced, prostaglandin H2 can also act as an irreversible inhibitor of CYP8A1 stopping catalysis.⁶¹ Tyrosine nitration is also known to occur in the active site of CYP8A1 to regulate prostacyclin production.⁶² Changes in expression of CYP8A1 that lead to a decrease in prostacyclin production can lead to pulmonary hypertension and cerebral infraction.^{63, 64}

1.2.2 Role in xenobiotic metabolism

Most xenobiotic metabolism by CYPs in humans occurs in the liver, where enzymes convert their substrates into more hydrophilic products that can then be excreted from the body. In addition to breakdown of substrates, xenobiotic metabolizing CYPs can also activate prodrugs as well as create toxic by-products.

CYP3A4 is the most prevalent and promiscuous P450 in the liver, making up approximately 30% of expressed CYPs in the liver and metabolizing over 50% of

current pharmaceuticals.⁶⁵ To accomplish this, 3A4 has an extremely large and flexible active site that is able to accept molecules as large as the antibiotic erythromycin and the immunosuppressant cyclosporin, to smaller molecules such as the three ring containing omeprazole and two ring containing nifedipine.⁶⁶ One way these large molecules are accommodated is that, unlike other xenobiotic-metabolizing CYPs, helices F and G, which are usually positioned directly over the active site and are considered its “lid” aren’t positioned this way for 3A4, and have less of a defined helical structure.⁶⁷ The result of the flexibility and therefore promiscuity of CYP3A4 is a decrease in stability⁶⁸ and an increase in drug interactions, whether from induction, inhibition, or activation.⁶⁵

As a direct consequence of their ability to eliminate foreign substances from the body, xenobiotic metabolizing P450s are implicated in the creation of mutagenic, carcinogenic, and toxic metabolites. It is thought that at least three-fourths of all possible carcinogens must first be activated by P450s.^{69, 70} Of particular interest is the role of the CYP1 family (CYP1A1, CYP1A2, and CYP1B1) in the activation of polycyclic aromatic hydrocarbons (PAHs). These planar aromatic compounds are very hydrophobic, making them a good substrate for the hydrophobic active site of cytochrome P450s. CYP1 enzymes hydroxylate PAHs, and, with the help of epoxide hydrolase, make compounds that can covalently bind and damage DNA.⁷¹ Compounding the problem is the fact that PAHs induce expression of CYP1 enzymes by binding to the arylhydrocarbon receptor,⁷² so that the presence of PAHs leads to an increase in the concentration of their carcinogenic metabolites. Xenobiotic metabolizing CYPs convert exogenous compounds to carcinogens, but they can also do the same with endogenous compounds. One of the most prevalent examples of this is estrogen metabolism. CYP1B1 hydroxylates 17 β -estradiol in the 4-position instead of

the 2-position, unlike other P450s,⁷³ which leads to a compound able to covalently modify DNA; this has been identified as leading to progression of breast cancer.⁷⁴ As CYP1B1 is mostly expressed in tumors as opposed to healthy tissue, one chemotherapeutic strategy is to selectively inhibit 1B1 so it will no longer be able to interact with procarcinogens, estradiol, and won't be able to inactivate other chemotherapeutics used to fight the disease.⁷⁵⁻⁷⁷

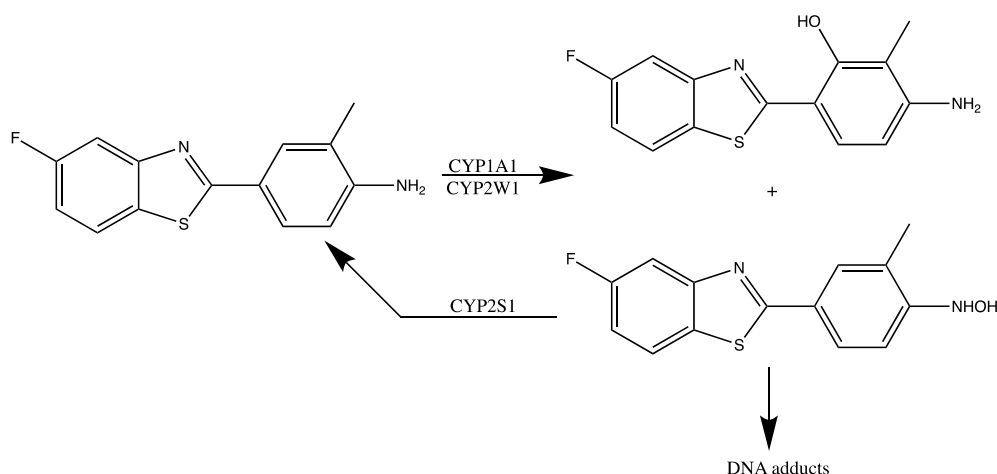


Figure 1.6 Activation and deactivation of a 2-aryl-benzothiazole by CYPs.⁷⁷

Xenobiotic metabolizing CYPs are also investigated for their role in activating pro-drugs. The use of pro-drugs in the fight against disease is an attractive strategy as the drug isn't activated until an action is done upon it. This makes targeted delivery possible, therefore limiting unexpected reactions and decreasing side effects. As a chemotherapeutic strategy, currently, most prodrugs are made active by an oxidative mechanism, as shown in Figure 1.2, with the hydroxylation of cyclophosphamide. The drawback of oxidative activation is that it usually occurs in the liver, and therefore the activated drug must travel to the affected area, causing potentially negative interactions with healthy tissues along the way.⁷⁸ As this is a large drawback, more recent strategies involve targeting CYPs overly expressed in tumors as well as those that use reductive

mechanisms to be activated. An example of the first strategy is 2-aryl-benzothiazoles.⁷⁹⁻
⁸² Though these compounds have not yet entered clinical trials, they are activated by CYP1A1 and CYP2W1, where metabolites can either form DNA adducts or revert to the prodrug form by CYP2S1 (Figure 1.6).⁷⁸ Neither of these enzymes is expressed in the liver, and CYP2W1 and CYP2S1 have been found to be more highly expressed in tumors as opposed to healthy tissue.⁸³⁻⁸⁵ AQ4N (Figure 1.7) is an example of a prodrug that uses a reductive mechanism for activation, which is especially important as tumors have a hypoxic core, making it difficult for reactions that involve insertion of oxygen to proceed. AQ4N is a topoisomerase II poison that is anaerobically activated by deoxygenation by CYP3A4, CYP2W1, and CYP2S1.⁸⁶

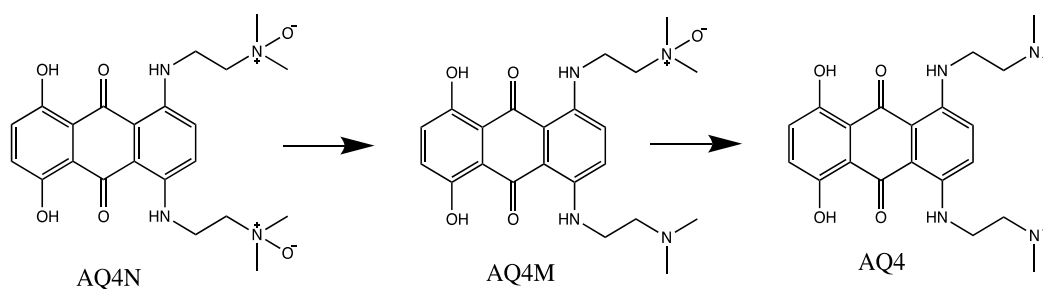


Figure 1.7 Reductive activation of the prodrug AQ4N by CYPs.⁸⁴

A third promising strategy to develop prodrugs combines manipulation of CYP activity, coordination compounds, and photodynamic therapy (PDT). As proof of concept we synthesized three ruthenium (II) complexes with coordinated P450 inhibitors (Figure 1.8). When irradiated with light, the inhibitors were released from the complex and bound to the P450, while the remaining Ru complex was able to interact with DNA as a dual targeting strategy. Compound **3**, after exposure to light inhibited P450 activity with an IC_{50} of $0.05 \pm 0.00 \mu\text{M}$, while simultaneously inducing DNA damage that significantly diminished protein production.⁸⁷

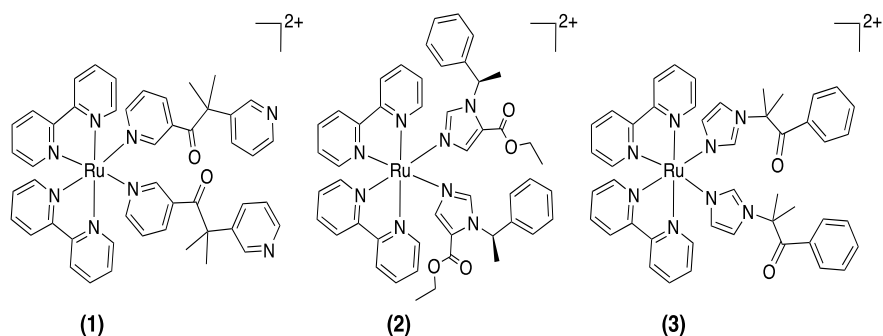


Figure 1.8 Ru(II) complexes capable of P450 inhibition and DNA damage.⁸⁷

1.3 Bacterial Cytochrome P450s

Since the discovery of the first bacterial P450 isolated from a *Rhizobium* spp. in 1967,⁸⁸ over 1,000 bacterial P450s have been classified and named.⁸⁹ Unlike their eukaryotic counterparts, bacterial P450s were found to be soluble, use more diverse electron transfer systems, and have a wider variety of functions. Additionally, unlike eukaryotes that need CYPs to survive, many bacteria, including *Escherichia coli*, don't express any P450s. As P450s are mostly nonessential in bacteria, their main roles are in formation of secondary metabolites, detoxification, and enabling growth on alternative carbon sources.⁹⁰

Of the bacterial P450s, P450cam (CYP101) isolated from *Pseudomonas putida* is considered the archetypal P450 and is perhaps the most studied. P450cam, a class I P450, catalyzes the 5-exo hydroxylation of camphor that can be used as a carbon source for *P. putida*. P450cam was the first P450 for which the crystal structure was solved⁷ and has been instrumental in piecing together the elusive steps of the P450 catalytic cycle.^{8, 16, 18, 91-93}

1.3.1 P450_{BM3} – Use as a model system

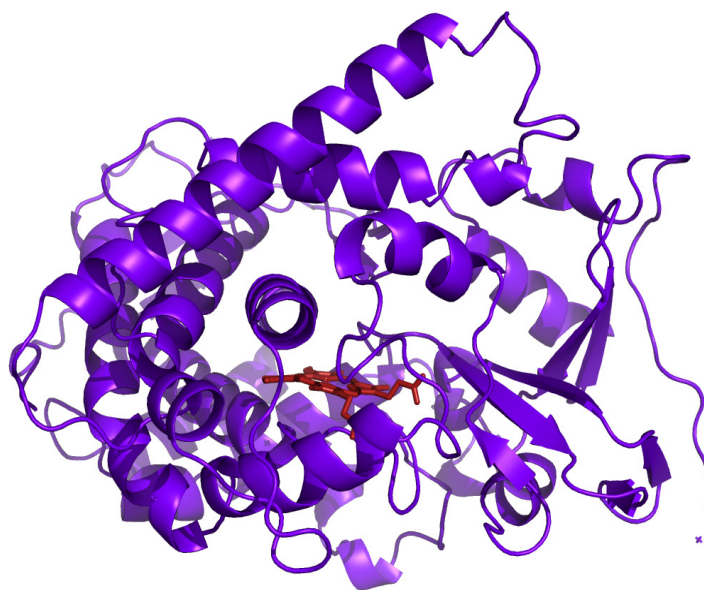


Figure 1.9 Crystal structure of the heme domain of wild type P450_{BM3} (PDB ID 4ZFA).

Competing with P450_{cam} for most studied bacterial P450 is CYP102A1, commonly referred to as P450_{BM3} (Figure 1.9). P450_{BM3} was first isolated from *Bacillus megaterium* by Miura and Fulco in 1974 as a “system” able to hydroxylate fatty acids.⁹⁴ Over a decade later, in 1986, Narhi and Fulco demonstrated the novel (at that time) finding that this system is a self-sufficient P450 with a high binding affinity for medium to long chain fatty acids.⁹⁵ In a subsequent publication, Narhi and Fulco showed that P450_{BM3} is self-sufficient as a result of having a mammalian CPR-like FMN-FAD reductase fused to the heme domain.⁹⁶ This fusion allows for extremely efficient turnover, and P450_{BM3} is considered to be the CYP with the highest activity discovered to date, with a k_{cat} of 17,000 min⁻¹ for hydroxylation of arachidonic acid.⁹⁷

Due to the solubility of P450_{BM3} and its similarity to class II mammalian microsomal CYPs, P450_{BM3} has been heavily investigated as a model system.¹⁵ P450_{BM3} can be purified in its full-length form, or alternatively, just the heme or

reductase domains separately. As a result, studies on electron transfer can be performed that are extrapolated to class II P450s. Particular attention has been focused on the impact of how the linker connecting the reductase and heme domains of P450_{BM3} modulates how the two partners interact, as compared to the CPR and its P450 partners. Both the reductase domain of P450_{BM3} and CPR bind close to the Cys-ligand loop of the P450 via the FMN-containing portion of the reductase so that electrons can be transferred easily to the heme.

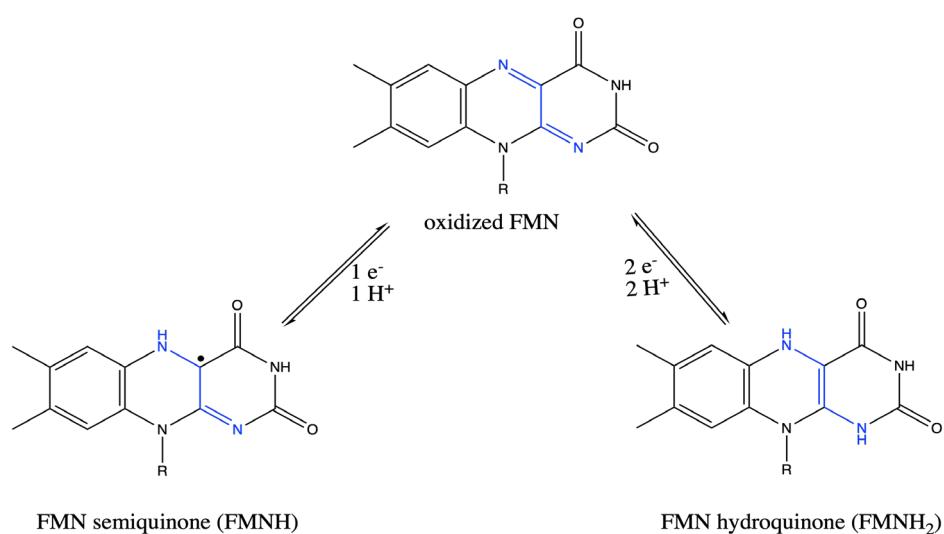


Figure 1.10 FMN quinone electron cycling that details how electrons are transferred in the CYP reductase partner.

Differences are apparent in how this binding occurs, as P450_{BM3} interactions between the domains can be attributed mostly to weak electrostatic affects seen by complementary surface potentials on both domains. In contrast, CPR-P450 binding seems to be driven by ionic forces, as there is a cluster of negatively charged residues on the CPR surface where it interacts with its P450 partner.² The impact of this difference in residues manifests in the reduction potentials of the FMN cofactor. The negatively charged residues at the CPR surface leads to destabilization of the FMN

semiquinone (FMNH), the one e^- reduced species, and stabilization of the FMN hydroquinone (FMNH₂), the two e^- reduced species, so that electron transfer to the heme occurs from FMNH₂ (Figure 1.10). In P450_{BM3}, the hydrophobic and neutral residues at the reductase surface lead to a stabilization of FMNH over FMNH₂ so that electron transfer occurs from FMNH to the substrate bound heme.² Electron transfer from FMNH allows for quick transfer to the heme but also gives P450_{BM3} tighter control of catalysis to decrease the rate of uncoupled catalysis, which is especially important as the two domains are connected.

P450_{BM3} is naturally a selective enzyme, but mutations can be made that make it more promiscuous, and thus similar in function to xenobiotic metabolizing human CYPs. Mutagenesis allows for study of the role of residues important for P450_{BM3} catalysis, but also the study of conserved residues in order to elucidate their function. In addition, the biophysical properties of promiscuous P450_{BM3} variants can be compared to the selective WT enzyme to determine the impact of promiscuity on enzyme structure and function. For example, we showed that mutations that increased promiscuity of P450_{BM3} also decreased its stability as a result of a decrease in the number of highly stabilizing salt bridges and disruptions to the hydrophobic core.⁹⁸ Though there is a decrease in stability, non-native substrates are still able to bind favorably by overcoming negative repulsive and electrostatic effects with positive dispersion forces with active site residues.⁹⁸

1.4 Summary

Cytochrome P450s are a large family of enzymes that are of continual interest to the scientific community due to their role in human health, prevalence in nature, vast chemical repertoire, and many more factors. Though much is already known, there are

still gaps in our understanding, and methods by which these enzymes can be manipulated to our advantage. This dissertation focuses on the biophysical properties of P450s to attempt to fill some of these knowledge gaps. Specifically, it focuses on the impact of substrate selectivity and iron oxidation state on enzyme stability and function as well as how P450s can be exploited to make new potential drug candidates.

CHAPTER 2. EFFECT OF MUTATION AND SUBSTRATE BINDING ON THE STABILITY OF CYTOCHROME P450 BM3 VARIANTS.

Chapter adapted from: Geronimo, I., Denning, C. A., Rogers, W. E., Othman, T., Huxford, T., Heidary, D. K., Glazer, E. C., Payne, C. M. (2016). "Effect of mutation and substrate binding on the stability of cytochrome P450_{BM3} variants." Biochemistry **55**: 3594-3606.

Author Contributions: IG, ECG, DKH, TH, and CMP designed the study, analyzed the data, and wrote the paper. IG conducted the molecular dynamics simulations. CAD and DKH expressed and purified the proteins, conducted the stability assays, and analyzed the data. WER, TO, and TH crystallized the proteins and solved the structures.

2.1 Introduction

Protein stability pertains to (a) thermodynamic stability, the resistance to unfolding defined by the free energy difference between the folded and unfolded states (ΔG_{stab}), and melting temperature (T_m , the temperature at which 50% of the protein is unfolded), and (b) kinetic stability, the resistance to irreversible inactivation defined by the half-life of the enzyme ($t_{1/2}$) at a specific temperature.^{99, 100} These two definitions of stability involve different processes but are usually related when the protein follows the classical two-step process $N \leftrightarrow I \rightarrow U$, where the native structure (N) first undergoes reversible unfolding to an intermediate state (I), leading to an irreversibly denatured/unfolded state (U), and eventually, to permanent inactivation due to aggregation, misfolding, covalent changes, cofactor loss, or oxidation of sulfur-containing residues.¹⁰⁰⁻¹⁰³

Traditionally, thermodynamic stability has been thought of in regards to unfolding of an enzyme as a result of temperature, in which a T_m is determined.

Alternatively, thermodynamic stability can be probed by chemical denaturation in which a C_m – concentration midpoint (denaturation concentration at which the protein is 50% unfolded) is determined. Though chemical denaturation is highly amino acid dependent, it has been found that thermal and chemical denaturation impact protein unfolding in comparable fashion.^{104, 105} In addition, similar $\Delta G_{\text{folding}}$ values are reported from chemical denaturation and temperature studies when extrapolated to no chemical denaturant or low temperature.^{106, 107} A linear relationship has also been established between denaturation with urea and temperature the caveat being a deviation at high urea concentrations,¹⁰⁸ Chemical denaturation of proteins can be studied in a variety of solvents, at various temperatures, and by a plethora of techniques including UV-Vis, circular dichroism (CD), fluorescence, and many more. Though kinetic stability may be a more important parameter in cost-effective industrial enzyme utilization, thermodynamic stability is inextricably linked to kinetic stability through the unfolding process. As increasing resistance to unfolding, via any mechanism, will likely also enhance kinetic stability, we focus our work on thermodynamic stability given the relative accessibility of thermodynamic stability as an engineering target.

Human health and biotechnical applications are two fields in which understanding thermodynamic stability of proteins is crucial. Cytochrome P450s (CYPs) are a super family of heme dependent monooxygenases that have essential functions in organisms from all domains of life. Humans have approximately 60 CYP enzymes that are necessary for steroidogenesis and xenobiotic metabolism. CYPs involved in steroidogenesis tend to be selective whereas those involved in xenobiotic metabolism tend to be more promiscuous and turnover a wider variety of substrates. Many disease states, including certain cancers,^{109, 110} liver diseases,¹¹¹⁻¹¹³ glaucoma,¹¹⁴⁻¹¹⁶ and vitamin deficiencies^{117, 118} can be traced to mutation and misregulation of

particular CYPs. Mutations, in particular, impact protein folding, which can therefore lead to differences in stability. Understanding the thermodynamic stability of enzymes in various disease states could help develop possible remedies to improve those afflicted.

Additionally, compounds and drugs made for commercial use are produced in large-scale preparations that often involve the use of harsh and toxic chemicals that have to be disposed of. Using biocatalysts, such as CYPs, is an attractive solution as reactions can be done without the use of organic solvents and the chemistry done can be highly tuned. One of the main drawbacks to this strategy reaching fruition is the lowered stability of enzymes typically able to perform the reactions of interest. Understanding how to increase enzyme stability while not impacting their activity is of extreme importance.

Cytochrome P450_{BM3} (CYP102A1) is a bacterial CYP from *Bacillus megaterium* that has been extensively studied in recent years because of its potential as a biocatalyst in the production of fine chemicals, environmental remediation, as well as a model for human CYPs. P450_{BM3} is an excellent candidate because it has the highest known monooxygenase activity among the P450 enzymes,⁹⁷ which is attributed to efficient electron transfer due to fusion of the mammalian-like FAD-FMN reductase and heme domain in the single polypeptide chain.¹¹⁹ P450_{BM3} catalyzes the hydroxylation and/or epoxidation of fatty acids, fatty amides, and alcohols but can be engineered to bind non-native substrates. Random mutagenesis and directed evolution have produced more promiscuous variants capable of catalyzing the oxidation of non-native substrates, particularly drugs normally metabolized by human P450s. For example, P450_{BM3} containing the D251G and Q307H mutations is active toward nonsteroidal anti-inflammatory drugs,¹²⁰ that containing F87V and A82F toward proton pump

inhibitors,¹²¹ and that containing R47L, F87V, and L188Q [triple mutant (TM)] toward drug-like molecules such as dextromethorphan and 3,4-methylenedioxymethylamphetamine.^{122 123}

There has been interest in using TM P450_{BM3} as a platform from which to develop additional variants that exhibit activity toward other nonnative substrates.¹²⁴⁻¹²⁷ A prior computational study of TM, as well as the R47L/F87V/L188Q/E267V quadruple mutant (QM) and R47L/F87V/L188Q/E267V/F81I pentuple mutant (PM), linked the enhanced catalytic activity of the mutants to the more closed conformation of the substrate channel and possibly to electrostatic effects resulting from the bending of heme propionate A toward the active site.¹²⁸ Mutations that are beneficial for nonnative substrate catalysis, however, often cause loss of protein stability, limiting the application of P450_{BM3} mutants as industrial biocatalysts. It also precludes their use as a starting point in engineering more promiscuous and active variants, as they are less tolerant of destabilizing mutations that may be required for nonnative substrate binding.¹²⁹⁻¹³¹

Effective means of overcoming the destabilization of TM (and other variants derived from it) remain largely unknown because the mechanisms behind the phenomenon are not well understood. In the case of full-length wild-type (WT) P450_{BM3}, the relatively low stability results from the low T_m of the reductase domain (47.5°C) compared to the heme domain (64.9°C and a shoulder at 58.7°C) as determined by differential scanning calorimetry.¹³² The appearance of a shoulder at the lower temperature for heme domain unfolding suggests WT may unfold by a biphasic transition. Thus, one approach to improving stability has been to replace the reductase domain with a more thermostable analogue, for example, that of CYP102A3.¹³³ However, chimeras such as this generally have lower coupling efficiencies and turnover

rates.¹³⁴ Alternatively, Arnold, *et al.* developed an efficient peroxide-driven variant of the P450_{BM3} heme domain, 21B3, which requires neither the reductase domain nor NADPH or O₂.²⁴ The 21B3 variant has since been used as a starting point to create more thermostable variants through directed evolution,^{129, 135, 136} though this approach suffers from the required time-intensive variant screening process.

As a rational approach to selection of mutation sites for the stabilization of P450_{BM3} variants, the molecular-level contributions to the stability of the heme domain were determined using biochemical, structural, and computational methods. As the heme domain can be used as a catalytic center using the peroxide shunt, the studies were focused on this one domain. The stabilities of WT, TM, QM, PM, and the single mutants E267V and F81I, in the presence and absence of small active site ligands, were experimentally measured by chemical denaturation using pulse proteolysis and circular dichroism (CD).¹³⁷ Structural data for WT and PM, as well as PM in complex with the native substrate, palmitic acid, and the inhibitor, metyrapone, were obtained to directly examine the effects of mutation and binding. High-temperature molecular dynamics (MD) simulations were performed to model the unfolding process and describe the interactions underlying the biochemical results. Labile regions in PM, which can be targeted for mutation to improve stability, were identified based on the experimental and computational findings.

2.2 Experimental procedures

2.2.1 Biochemical procedures

2.2.1.1 Cloning and site-directed mutagenesis of P450_{BM3}

The heme domain (Thr 1 to Thr 463) of P450_{BM3} containing a C-terminal 6xHis tag was cloned into the pCWori vector. All point mutations were incorporated into the

heme domain using the QuikChange (Stratagene) site-directed mutagenesis procedure. The DpnI-digested PCR reaction was transformed into ultracompetent cells (Stratagene) and screened for ampicillin resistance. Colonies were grown in Luria Broth with 100 µg/ml ampicillin, followed by plasmid isolation. All mutations were confirmed by sequence analysis (Eurofins Scientific).

2.2.1.2 Expression and purification

The P450_{BM3} heme domain proteins were expressed in *E. coli* BL21(DE3) cells. Cells were grown in 1 L of Terrific Broth at 37°C with shaking at 180 rpm until an OD₆₀₀ of 0.7–0.8 was reached. Protein expression was then induced with addition of isopropyl β-D-1-thiogalactopyranoside (IPTG) at a final concentration of 0.5 mM. Expression was continued for 20 h before the cells were harvested by centrifugation at 4000 xg for 15 min at 4°C. The supernatant was decanted, and the cell pellet was stored at -80°C. For purification, the cell pellets were resuspended in Buffer A (50 mM NaH₂PO₄, 300 mM NaCl, 10 mM imidazole, and 0.1 mM EDTA, pH 8.0 with the addition of 0.1 mM phenylmethylsulfonyl fluoride. Lysis was then carried out by sonication on ice for 15 min using a microtip with output control of 3 and duty cycle of 50% (Branson Sonifier 250). Cell debris was cleared by centrifugation at 20000 xg for 1 h at 4°C. The supernatant was decanted and passed through a 0.45-µm polytetrafluoroethylene filter before loading onto a His-Trap column (GE Healthcare) equilibrated with five column volumes of Buffer A. The protein was eluted over a gradient where the imidazole concentration was linearly increased from 20 to 200 mM using buffer B (50 mM NaH₂PO₄, 300 mM NaCl, and 20 mM imidazole, pH 8.0). The fractions containing heme-bound protein were identified by measuring absorption at 420 nm by UV-Vis spectroscopy (Figure A1), and concentrated to approximately 2 ml using Amicon Ultracel-30K Millipore centrifugal units at 4500 xg and 4°C. The protein

was then loaded onto a Hi-Prep 26/60 Sephacryl S200 HR column equilibrated in 20 mM Tris and 150 mM NaCl, pH 8.0. Protein fractions containing an $A_{420/280}$ absorption ratio >1.4 for WT, >1.3 for TM, and >1.2 for F81I, QM, and PM were collected and concentrated to between 10 and 20 mg/ml using an Ultracel-30K centrifugal filter unit. For E267V, the protein was isolated in the high-spin state, so fractions with an $A_{394/280}$ of >1.3 were collected and concentrated. Protein concentration and quality was determined by CO binding (Figure A2).¹³⁸ For storage, glycerol was added to the protein for a final concentration of 20%, and aliquots were frozen in a dry ice ethanol bath and placed at -80°C .

2.2.1.3 Pulse proteolysis

The pulse proteolysis procedure was adapted from the work of Park and Marqusee.¹³⁹ The protein was prepared by thawing on ice followed by buffer exchange into 10 mM Tris (pH 7.4) using a Micro Bio-Spin 6 chromatography column (Bio-Rad). The protein was then diluted to 1.7 mg/ml in pulse buffer (20 mM Tris, 10 mM CaCl_2 , and 20 mM NaCl, pH 7.4) with urea added to achieve concentrations ranging from 0 to 6.8 M. The samples were then incubated for 2 h at room temperature. For experiments involving ligands, the midpoint concentration required to saturate binding (K_d) was first determined by measuring the change in heme absorption as a function of ligand concentration. The protein was then equilibrated in pulse buffer containing the ligand at 10x the K_d for 10 min prior to the addition of urea.

After incubation with urea, thermolysin was added to the solution at a final concentration of 0.6 mg/ml, gently vortexed to mix, and allowed to react for 1 min at room temperature. The reaction was immediately quenched by addition of EDTA to give a final concentration of 37 mM and placed on ice. Laemlli sample buffer was added, and the samples were placed at 95°C for 1 min, followed by centrifugation for

30 s at 17000 \times g. Samples (7 μ g P450_{BM3}) were resolved on a 4–12% Tris-glycine gel, followed by Coomassie Blue staining. Gels were then imaged and quantified using a ChemiDoc™ MP equipped with Image Quant software (Biorad), where the intensity of the P450_{BM3} bands were quantified and plotted against urea concentration. The concentration midpoint (C_m) was determined by normalizing the data to the fraction folded at 0 M denaturant. The data were fit on Graphpad Prism software with a sigmoidal dose response equation with variable slope. C_m values were averaged and error is reported as the standard deviation from three replicate experiments.

2.2.1.4 Circular Dichroism

The heme domain was equilibrated with urea (varying from 0 – 6.8 M) at a concentration of 1.7 mg/ml for near UV-visible spectra and 0.1 mg/ml for far UV spectra at room temperature as described above, and spectra were taken using a Jasco J-815 CD Spectrometer. Due to spectral interference, far UV spectra were taken from 190–250 nm in 50 mM KH₂PO₄ buffer at pH 7.6, while near UV-visible spectra were taken between 300 and 450 nm with the sample in 20 mM Tris, 10 mM CaCl₂, and 20 mM NaCl at pH 7.6. The addition of ligands was carried out as described for pulse proteolysis. The change in ellipticity at 222 and 415 nm was determined and the data plotted as a function of urea concentration.

2.2.2 Crystallography procedures.

2.2.2.1 Complex formation for crystallization

Separate samples of both purified WT and PM P450_{BM3} heme domain proteins were diluted in 20 mM Tris-HCl and 150 mM NaCl (pH 8.0) to a final concentration of 20 mg/ml with either 3 mM metyrapone (Sigma) or 5 mM sodium palmitate (Sigma).

Free protein and small molecule complexes were flash frozen in liquid nitrogen and stored in 50 μ l aliquots at -80 °C.

2.2.2.2 Crystallization

P450_{BM3} heme domain protein crystals and complex co-crystals were grown at room temperature by the hanging-drop vapor-diffusion method. One microliter of protein or protein:small molecule complex (~20 mg/ml) was mixed with 1 μ l of reservoir solution containing 0.10–0.25 M NiCl₂ and 5–10% polyethylene glycol monomethyl ether (PEG 2000 MME) and then suspended in a sealed compartment over 1 ml of reservoir solution. Ruby red hexagonal disc crystals grew to a final size of up to 0.3 \times 0.3 \times 0.2 mm in 3–4 days.

2.2.2.3 Diffraction data collection and processing

P450_{BM3} heme crystals and ligand-bound co-crystals were harvested with nylon loops and immersed in reservoir solution supplemented with 20 or 30% ethylene glycol before being flash-cooled directly in liquid nitrogen. Diffraction data were collected at 100 K with 0.1° oscillations in continuous (shutterless) mode on a Pilatus-6MF pixel array detector at Advanced Photon Source (Argonne National Laboratory) NE-CAT Beamline 24ID-C. Because of one large unit cell dimension ($c = 705\text{--}720$ Å) in the crystals, diffraction data were collected using a mounted mini-kappa goniometer at a crystal-to-detector distance of 900 mm. Raw diffraction intensities were indexed, integrated, and scaled in X-ray Detector Software as part of the RAPD package.¹⁴⁰ Data collection statistics are presented in Table 2.1.

Table 2.1 Data Collection, Structure Solution, and Model Refinement Statistics of Forms of the P450_{BM3} Heme Domain.

	Wild-type	Pentuple mutant		
	No substrate	No substrate	Metyrapone	Palmitic acid
<i>Data Collection</i>				
X-ray source	APS 24ID-C	APS 24ID-C	APS 24ID-C	APS 24ID-C
Wavelength (Å)	0.9792	0.9792	0.9792	0.9792
Space group	P6 ₅ 22	P6 ₅ 22	P6 ₅ 22	P6 ₅ 22
Unit cell (Å)				
a	55.5	56.0	55.9	55.9
b	55.5	56.0	55.9	55.9
c	717.7	711.2	711.0	707.6
Molecules/asymmetric unit	1	1	1	1
Resolution range ^a	179.44-2.76 (2.91-2.76)	177.81-2.77 (2.92-2.77)	177.76-2.77 (2.92-2.77)	176.89-2.84 (2.99-2.84)
R_{symm}	0.077 (0.435)	0.070 (0.323)	0.065 (0.373)	0.091 (0.431)
Observations	135,949	136,501	134,033	127,981
Unique reflections	18,145	18,183	18,059	16,866
Completeness (%)	97.0 (80.2)	97.2 (80.6)	96.2 (74.7)	98.5 (92.3)
Redundancy	7.5 (3.5)	7.5 (3.4)	7.4 (3.7)	7.6 (5.0)
Average intensity (I/σ)	16.2 (2.3)	17.7 (3.1)	18.0 (2.4)	14.2 (2.8)
<i>Structure Solution by Molecular Replacement</i>				
Probe	3NPL	3NPL		
Resolution range (Å)	10.0-4.0	10.0-4.0		
Z-score ^b	11.1	12.8		
LLG ^b	3113.11	3083.44		
<i>Refinement</i>				
Resolution range (Å)	59.83-2.77 (2.92-2.77)	59.27-2.77 (2.92-2.77)	48.42-2.77 (2.91-2.77)	117.93-2.84 (3.02-2.84)
Unique reflections	17,928 (1,853)	17,997 (1,228)	17,883 (1,732)	16,706 (2,322)
Protein atoms	3,699	3,688	3,688	3,688
Ligand atoms	67	67	64	69
Water atoms	57	61	83	56
R_{work}	0.2466 (0.3347)	0.2008 (0.2923)	0.2176 (0.3219)	0.2207 (0.3075)
R_{free}^c	0.3017 (0.4245)	0.2572 (0.4153)	0.2627 (0.4448)	0.2741 (0.3784)
Geometry				
Rmsd bond lengths (Å)	0.002	0.004	0.003	0.003
Rmsd. bond angles (°)	0.689	0.947	0.739	0.785
Mean B (Å ²)				
Protein	51.96	49.11	59.21	49.98
Ligands	46.73	46.97	49.54	45.47
Waters	47.97	39.33	51.77	43.22
Clashscore	5.61	4.55	5.09	4.94
Ramachandran plot ^d				
Favored	93.9	94.3	95.5	92.6
Disallowed	0.2	0.2	0.2	0
MolProbity score ^e	1.71	1.62	1.64	1.72
PDB accession code	4ZFA	4ZF6	4ZF8	4ZFB

^a Data in parentheses are for the highest resolution shell. ^b PHENIX.¹⁴¹ ^c Calculated against a cross-validation set of 5% of the data selected at random prior to refinement. ^d MolProbity.¹⁴² ^e Combines clashscore, rotamer, and Ramachandran evaluations into a single score, normalized to the same scale as x-ray resolution.

2.2.2.4 X-ray structure solution and refinement.

The X-ray crystal structures of the P450_{BM3} heme domains were determined by molecular replacement using PHASER within the PHENIX crystallography suite.^{141, 143} The coordinates that were used for molecular replacement were from the P450_{BM3} heme domain in space group P4₁2₁2 [Protein Data Bank (PDB) entry 3NPL, no associated publication]. The structure was modified to remove all nonbonded atoms other than those in the heme prosthetic group, which were set to an occupancy of zero, and the sites of the five mutated amino acids were replaced with alanine. The raw data scaled as P622, and systematic absences along the *001* face suggested a six-fold screw axis along *c*. When rotation and translation functions were performed on the probe against data from 10 to 4 Å, a clear solution arose for space group P6₅22. The solution contained one complex in the asymmetric unit. Model building was conducted in COOT using $2F_o - F_c$ electron density maps and maximum likelihood refinement with REFMAC5.^{144, 145} Stereochemical analysis and final adjustments to the model were directed by MolProbity.¹⁴² WT and PM models were then used to determine complex co-crystal structures by removing nonbonded atoms, reassigning *B*-factors to 15.00 Å², and performing rigid body refinement against all data to a limit of 3.4 Å. The resulting models were then refined against all data and the electron density of the bound small molecules was identified unambiguously from $F_o - F_c$ difference maps. Statistics for the refined crystallographic models are presented in Table 2.1.

2.2.3 MD simulations

A total of 11 systems were simulated: (1) substrate-free WT, R47L, F81I, F87V, L188Q, E267V, and PM; (2) WT and PM in complex with palmitic acid (modeled as palmitate); and (3) WT and PM in complex with metyrapone. The enzyme was modeled using the AMBER ff14SB force field¹⁴⁶ and the solvent using TIP3P.¹⁴⁷ Force field

parameters for the heme-Cys moiety and partial charges for the high-spin, pentacoordinate form (characteristic of the substrate-bound enzyme) were taken from a previous study.⁷² Partial charges for the low-spin, hexacoordinate (water being the sixth ligand) form (characteristic of the substrate-free enzyme) were calculated using the method described therein. The suitability of the heme-Cys parameters was verified by monitoring the rmsd and planarity of the heme (Figure A3). Parameters for unbound metyrapone and palmitate were derived using the *antechamber* module¹⁴⁸ at the HF/6-31G* level to be consistent with the GAFF force field.¹⁴⁹ The bond between the pyridine N and heme Fe in the metyrapone complexes was restrained using a harmonic force constant of 10 kcal/mol/Å and an equilibrium bond length of 2.6 Å.

Using AMBER 14,¹⁵⁰ production MD simulations in the *NVT* ensemble at 300 K were run for 100 ns using the same simulation parameters that were used during equilibration. For the high-temperature simulations, 550 K was chosen for the observation of significant structural changes in the protein on a feasible simulation time scale (50 ns). A similar temperature (500 K) was used to study substrate-bound mesophilic (CYP101 and CYP176A) and thermophilic (CYP119, CYP231A2, and CYP175A1) P450s.¹⁵¹ Previous MD studies, employing a temperature as high as 600 K, have demonstrated that the unfolding mechanism of an enzyme remains essentially the same regardless of the simulation temperature.¹⁵²⁻¹⁵⁴ Three independent trials, each with a new set of velocities, were performed for the 550 K simulations. Trajectories were analyzed using the *cpptraj* module of AmberTools 14.^{150, 155} Native contacts and salt bridge networks were determined from the 300 K simulations. A native contact is defined as contact between C α atoms that is (a) at least three residues away in sequence, (b) is within a distance cutoff of 6.5 Å, and (c) has an occupancy greater than 67%. A

salt bridge is defined as interaction between the O atom of Asp/Glu and protonated N atom of Arg/Lys/His within a distance cutoff of 4.0 Å.

2.2.3.1 Preparation of systems for MD simulations

The systems were prepared using the *tleap* module of AmberTools 14.¹⁵⁰⁷⁸ Initial coordinates of the substrate-free wild-type (WT) P450_{BM3} and R47L/F87V/L188Q/E267V/F81I pentuple mutant (PM) were taken from the crystal structures 1BU7 (molecule B)² and 4ZF6, respectively. Substrate-free, single-point mutants were prepared from 1BU7 (molecule B). For the substrate-bound enzymes, 4ZFA, 4ZFB, 4ZFD, and 4ZF8, were used as starting structures for the WT:palmitic acid, PM:palmitic acid, WT:metyrapone, and PM:metyrapone complexes, respectively. Protonation states of titratable residues were assigned based on pK values calculated using H++¹⁵⁶⁻¹⁵⁸ and visual inspection at pH 7.4. Asp and Glu residues were deprotonated, except for the buried residue E409, while Arg and Lys residues were protonated. H361 was assigned as HID (N δ protonated); H116, H171, H388, and H408 as HIE (N ϵ protonated); and H92, H100, H138, H285, H410, and H426 as HIP (both N protonated). H236 and H266 were assigned as HIP and HID in the substrate-free enzyme, and HIE and HIP in the substrate-bound enzyme. The total charge of WT P450_{BM3} is -7. The appropriate number of sodium ions, depending on the mutation and substrate present, was added to neutralize each system. Crystallographic water molecules were retained, and the whole system was solvated in a truncated octahedral box of TIP3P water,¹⁴⁷ with a buffer distance of 12 Å between each wall and the closest atom in each direction. After solvation, each system consisted of approximately 53,000 atoms.

All simulations were performed using AMBER 14.¹⁵⁰⁷⁸ The force constants used are discussed in the main text. Periodic boundary conditions were applied using

the Particle Mesh Ewald method¹⁵⁹ with a non-bonded cutoff of 10 Å. Energy minimization was done in two stages: (1) with the solute initially restrained with a harmonic force constant of 5.0 kcal/mol/Å² to allow water and ions to relax, followed by (2) minimization of the entire system. At each stage, minimization was done using the steepest descent algorithm for the first 1000 steps and conjugate gradient algorithm for the last 1000 steps. In the case of the mutants, residues within 5 Å of the mutated residue were allowed to relax for 2000 steps prior to unrestrained minimization of the entire system.

The system was then heated from 0 to 300 K for 50 ps with C α atoms restrained with a harmonic force constant of 5.0 kcal/mol/Å². Bonds involving hydrogen were constrained using the SHAKE algorithm,¹⁶⁰ and a 2-fs time step was used for time integration. The temperature was controlled using Langevin dynamics¹⁶¹ with a collision frequency of 1.0 ps⁻¹. NMR weight restraints were also used to linearly increase the temperature to avoid instabilities in the simulation. The system was equilibrated at constant pressure over a 200-ps period, during which the force constant was incrementally reduced (5.0, 2.0, 1.0, and 0.5 kcal/mol/Å²). Equilibration of the unrestrained system was then continued for 2 ns. Isotropic position scaling was used to maintain the pressure at 1 atm, with a relaxation time of 2 ps. As the system proved to be initially unstable in the case of substrate-free enzymes, heating was done in two stages (0–100 K for 20 ps at constant volume followed by 100–300 K for 80 ps at constant pressure), the duration of restrained equilibration was doubled, and a smaller time step of 1 fs was used.

The final structure was used as the starting point for production simulations in the *NVT* ensemble at 300 and 550 K using a 2-fs time step. Heating from 300 to 550 K and equilibration of the system prior to production followed the same procedure

described above, except for unrestrained equilibration, which was conducted for only 200 ps.

2.3 Results

2.3.1 Mutation-induced substrate promiscuity is correlated with reduced P450_{BM3} stability

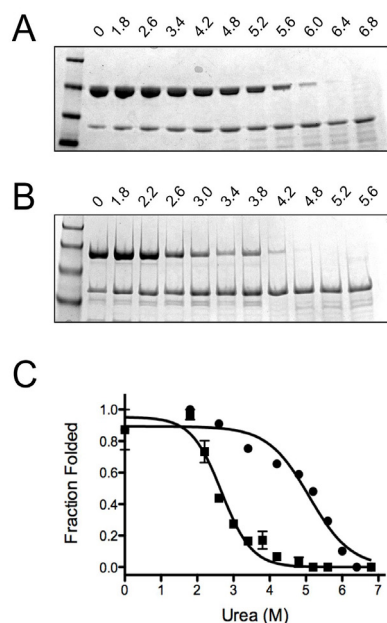


Figure 2.1. Mutations in P450_{BM3} that result in substrate promiscuity destabilize the protein. (A) Wild-type (WT) P450_{BM3} (1.7 mg/ml) was equilibrated in urea for 2 hr, followed by a 1 min incubation with thermolysin (10 mg/ml) and then resolved by SDS-PAGE. The upper band corresponds to P450_{BM3} and the lower band to thermolysin. The amount of intact P450_{BM3} was quantified for each urea concentration to determine the midpoint for stability. Pulse proteolysis experiments were done at room temperature in pulse buffer (20 mM Tris, 10mM CaCl₂, 20 mM NaCl pH 7.6). (B) SDS-PAGE of the pentuple mutant, PM, after pulse proteolysis at varying urea concentrations. The procedure followed was the same as that for WT. (C) Normalized data from panels A and B, where the fraction of intact P450_{BM3} is plotted vs. urea concentration. The filled squares correspond to data for PM and filled circles for WT.

It has previously been shown that the introduction of five mutations (R47L, F81I, F87V, L188Q, and E267V) into the heme domain of P450_{BM3} allows the enzyme to shift from selectively oxidizing fatty acids to modifying larger, more complicated

drug-like molecules.^{124, 127, 162, 163} To gain insight into the effect of these mutations on the global stability of the protein, the heme domain of WT and the promiscuous mutant, PM, were subjected to chemical denaturation studies (Figure 2.1). The urea concentration midpoint for stability (C_m) was measured for WT and PM (Table 2.2), with a C_m of 5.4 ± 0.5 M for substrate-free WT. The PM P450_{BM3} protein was much less stable, with a midpoint of 2.7 ± 0.2 M. Subsequent studies of WT unfolding by pulse proteolysis, similar to results published by Munro,¹³² indicated a biphasic unfolding with a higher C_m of 5.3 ± 0.4 M and a lower C_m of 3.2 ± 0.2 M.

Table 2.2 Urea concentration at the denaturation midpoint (C_m , M) determined by pulse proteolysis for substrate-free and bound P450_{BM3} variants.^a

Variant	Substrate		
	None	Metyrapone	Palmitic acid
WT	5.4 ± 0.5^b	3.9 ± 0.2	4.9 ± 0.4
F81I	4.7 ± 0.1	4.8 ± 0.1	4.8 ± 0.1
E267V	4.4 ± 0.1	3.6 ± 0.2	4.5 ± 0.1
TM	3.2 ± 0.1	3.4 ± 0.2	3.3 ± 0.1
QM	3.2 ± 0.2	4.0 ± 0.2	3.3 ± 0.1
PM	2.7 ± 0.2	3.8 ± 0.2	2.7 ± 0.2

^a Error is report as standard deviation from three independent experiments. ^b WT exhibits biphasic unfolding. The higher C_m is reported, but other experiments demonstrate more clear biphasic character resulting in two C_m values.

Because pulse proteolysis primarily uncovers changes in tertiary structure, the effect of the mutations on the stability of protein secondary structure, particularly α -helical content, was measured in the presence of urea by CD (Figure 2.2A). As anticipated, the WT and PM denaturation C_m values were higher than those observed by pulse proteolysis, with values of 5.9 M for WT and 4.1 M for PM. This is consistent

with the expectation that loss of secondary structure will require higher concentrations of denaturant than for disruption of the tertiary structure. The stability of the heme cofactor environment was also measured by following the change in the Soret region at 415 nm (Figure 2.2B). The implication of different C_m values by various techniques suggests a number of intermediate states of unfolding are present that can only be found by probing the enzyme by numerous methods. The stability of the heme in PM was reduced compared to that of WT, with a C_m of 3.1 M versus a C_m of 5.4 M for WT. In both cases, the stability of the heme environment was lower than that of the overall protein secondary structure. As the protein concentration was held constant for CD experiments, the difference in the baselines is the result of differentness of compaction (Figure 2.2A) and heme environment (Figure 2.2B) between the WT and PM. Pulse proteolysis of the single-point variants, E267V and F81I, and multiple mutants, TM and QM, indicated that all mutations had a destabilizing effect on the substrate-free enzyme (Table 2.2).

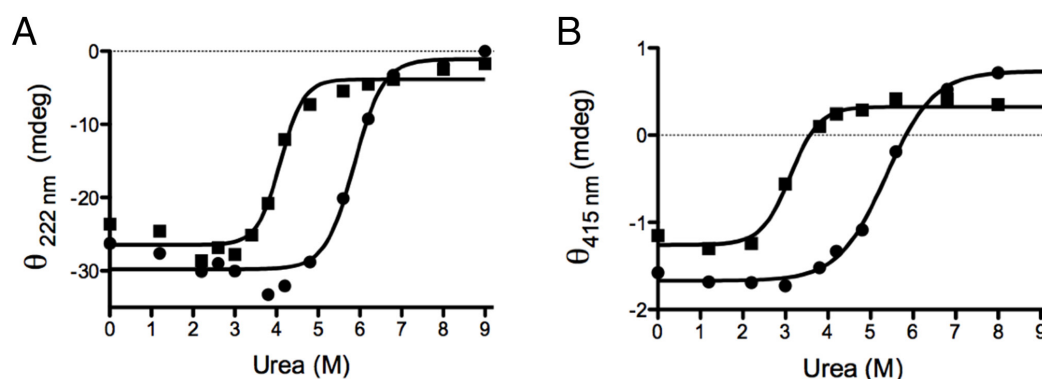


Figure 2.2. Mutations induce destabilization of secondary and active site structure. (A) Changes in secondary structure measured by circular dichroism as a function of urea. P450_{BM3} (0.1 mg/ml) was incubated in varying concentrations of urea (in 50 mM KH₂PO₄ buffer pH 7.6) for 2 hr before CD spectra were obtained. (B) Stability of the heme monitored in the Soret region. To monitor active site stability, P450_{BM3} (1.7 mg/ml) was incubated in varying concentrations of urea for 2 hr before spectra were taken. Due to spectral interference, pulse buffer (20 mM Tris, 10 mM CaCl₂, 20 mM NaCl, pH 7.6) was used. In all plots, WT is shown as filled circles and PM as filled squares.

2.3.2 Inhibitor and substrate binding modulates stability

The effects of inhibitor binding on the stability of WT and PM BM3 were measured using metyrapone, which inhibits P450 enzymes through direct coordination of the pyridine nitrogen with the heme Fe; this prevents the enzyme from oxidizing its substrate. Surprisingly, by pulse proteolysis, the stability of the WT enzyme decreased when it was bound to metyrapone, from 5.4 ± 0.5 to 3.9 ± 0.2 M (Figure 2.3A). The destabilizing effect of metyrapone on WT secondary structure was also observed by CD by which the C_m reduced from 5.9 to 5.1 M. The heme environment too reflected a disruption, with a reduction in the C_m from 5.4 to 4.7 M (Figure 2.3C, D). In marked contrast, the tertiary structure stability of metyrapone-bound PM increased from a C_m of 2.7 ± 0.2 to 3.8 ± 0.2 M (Figure 2.3B). No significant modulations in the stability of the secondary structure were observed by CD, with C_m values of 4.1 M vs 4.2 M (Figure 2.3C). However, the stability of the heme environment increased, with a shift from 3.1 to 4.1 M (Figure 2.3D). The tertiary structure of metyrapone-bound E267V was less stable, while the F81I, TM, and QM complexes were more stable than their respective substrate-free forms, with the greatest effect seen for the least stable variants (Table 2.2).

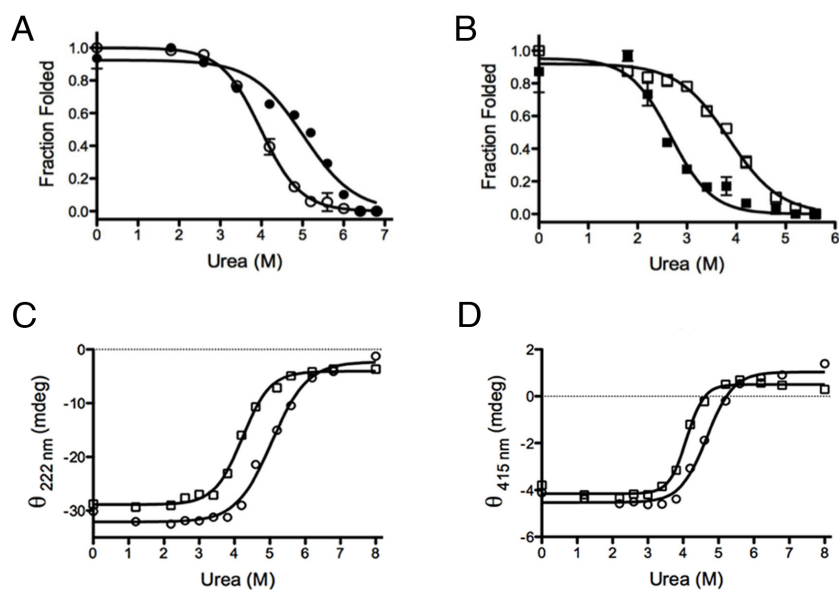


Figure 2.3. The inhibitor, metyrapone, shifts the stability of WT and PM in opposite directions. (A) WT stability as measured by pulse proteolysis, where filled circles correspond to the enzyme without the inhibitor and open circles to the enzyme with the inhibitor. (B) PM stability measured by pulse proteolysis, where filled squares correspond to the enzyme without the inhibitor and open squares to the enzyme with the inhibitor. (C) Stability of the secondary structure and (D) heme environment in the presence of metyrapone measured by circular dichroism. For all data in panels (C) and (D), WT is shown as open circles and PM as open squares.

The WT P450_{BM3} enzyme is selective for the hydroxylation of fatty acid substrates, such as palmitic acid. Binding requires the hydrophobic tail of the fatty acid hydrocarbon chain to be in the proximity of the heme for hydroxylation to occur. Substrate binding was expected to increase the stability of WT based on previous studies.¹⁶⁴ Instead, only a minor change was observed, with a decrease to 4.9 ± 0.4 M determined by pulse proteolysis, and a slight decrease detected by CD, to 5.7 M. For PM, palmitic acid had no significant impact on the stability of the secondary structure, with the C_m decreasing from 4.1 to 4.0 M (Table 2.3). This was also seen with pulse proteolysis, where the C_m was 2.7 ± 0.2 M in the presence or absence of palmitic acid. The stabilities of E267V, F81I, TM, and QM were also unaffected by palmitic acid binding.

Table 2.3. Urea concentration at the denaturation midpoint (C_m , M) determined by CD of substrate-free and bound BM3 variants.

Variant	Ligand	Active Site	Secondary Structure
WT	None	5.4	5.9
	Metyrapone	4.7	5.1
	Palmitic acid	-	5.7
PM	None	3.1	4.1
	Metyrapone	4.1	4.2
	Palmitic acid	-	4.0

2.3.3 X-ray crystal structure of the P450_{BM3} heme domain is in a closed confirmation

To directly observe the effects of mutation and ligand binding on the P450_{BM3} structure, X-ray crystallography was conducted on WT and PM P450_{BM3} proteins. Though the conditions of crystallization differ from the experimental conditions, crystallization is helpful to understand the lowest energy conformations of the P450_{BM3} variants. The C-terminal His-tagged proteins used in this study failed to crystallize under conditions reported in previous structural studies.^{2, 165} However, crystals of a unique hexagonal crystal form grew under conditions of nickel and low molecular weight polyethylene glycol (PEG). Refinement of the WT X-ray crystal structure was performed against diffraction data at a limit of 2.76 Å resolution and resulted in a model with excellent stereochemistry (4ZFA). The structure revealed that, in this hexagonal crystal form, P450_{BM3} exhibits the closed conformation that is typically observed in substrate-bound complex models (Figure 2.4A). Movement between the open and closed conformations involves *en bloc* rotation of a segment composed roughly of amino acids 168 to 267 that encompass helices F - I, as well as the loops that join them (Figure 2.4B). Helices F and G, along with helix B', form the lid domain of the substrate

access channel, which is lined by the F/G loop on one side and the 3₁₀ helix (residues 16–20) and β -sheet 1 on the other (Figures 2.4C and 2.4D).

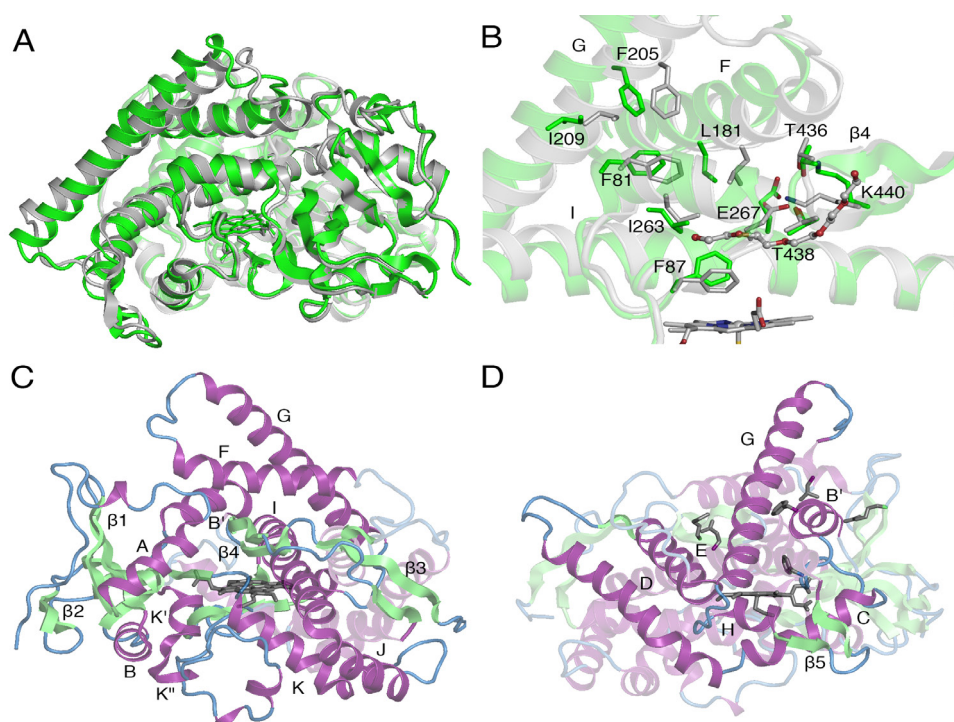


Figure 2.4. Crystal structures of substrate-free (open conformation) and substrate-bound (closed conformation) WT P450_{BM3}. The protein is shown in cartoon representation and the heme and residues of interest are shown in stick. (A) The closed conformation, represented by 4ZFA is shown in gray while the fully open conformation is represented by 1BU7², molecule B (green). (B) Helices F, G, and I undergo significant displacement upon substrate binding. A PEG molecule found in the substrate channel of 4ZFA is shown in ball-and-stick. E267 forms a salt bridge with K440 in both conformations and hydrogen bond with T438 in the closed conformation. F81 forms contacts with L181, F205, I209, and I263, which rearrange upon substrate binding. (C) and (D) The region nomenclature and mutated residues in PM P450_{BM3} are illustrated to aid in discussion. R47 is located in β -sheet 1, F81 in helix B', F87 between helices B' and C, L188 in helix F, and E267 in helix I. Crystal structure solved by W.E. Rogers, T. Othman, and T. Huxford.

Crystal packing is mediated by a nickel ion that is coordinated by amino acid residues D338 and E348 and the N-terminal threonine at the interface between crystallographic neighbors along the six-fold screw axis. However, besides slight changes to the side chain geometries, this interaction does little to perturb the local

structure relative to either the open- or closed-conformation P450_{BM3} crystallographic models (1BU7,² molecule B and 1FAG,¹⁶⁵ respectively). Similarly, coordination of a nickel ion by the side chains of H138 and H426 appears to do little more than change these surface-exposed residues to alternate rotamers. H285 rotates to contact a surface-exposed nickel ion. Even less change is observed due to nickel ion binding at H236. Therefore, the involvement of nickel in mediating crystal packing does not appear to be responsible for the closed conformation observed in the substrate-free WT model.

Analysis of the heme does not reveal any differences from previously reported P450_{BM3} crystal structures. What is evident within proximity of the enzyme's active site, however, is a strong peak of electron density that occupies the space previously observed to house palmitoleic acid in the complex X-ray co-crystal structure (1FAG). The ligand density refines best as a PEG fragment that is five ethylene glycol units in length (Figures 2.5 A, B). As in the previously reported P450_{BM3}:palmitoleic acid complex model, the bound ligand displaces R47, F87, and L188, as well as I263 and L437. Therefore, it is apparent that binding of the linear PEG molecule at a distance of $> 8 \text{ \AA}$ from the heme iron within the base of the substrate access channel casts the WT P450_{BM3} crystal structure in its closed conformation. The structure also contains an ethylene glycol molecule bound at the active site where a water molecule is typically found (Figure 2.5 C, D).

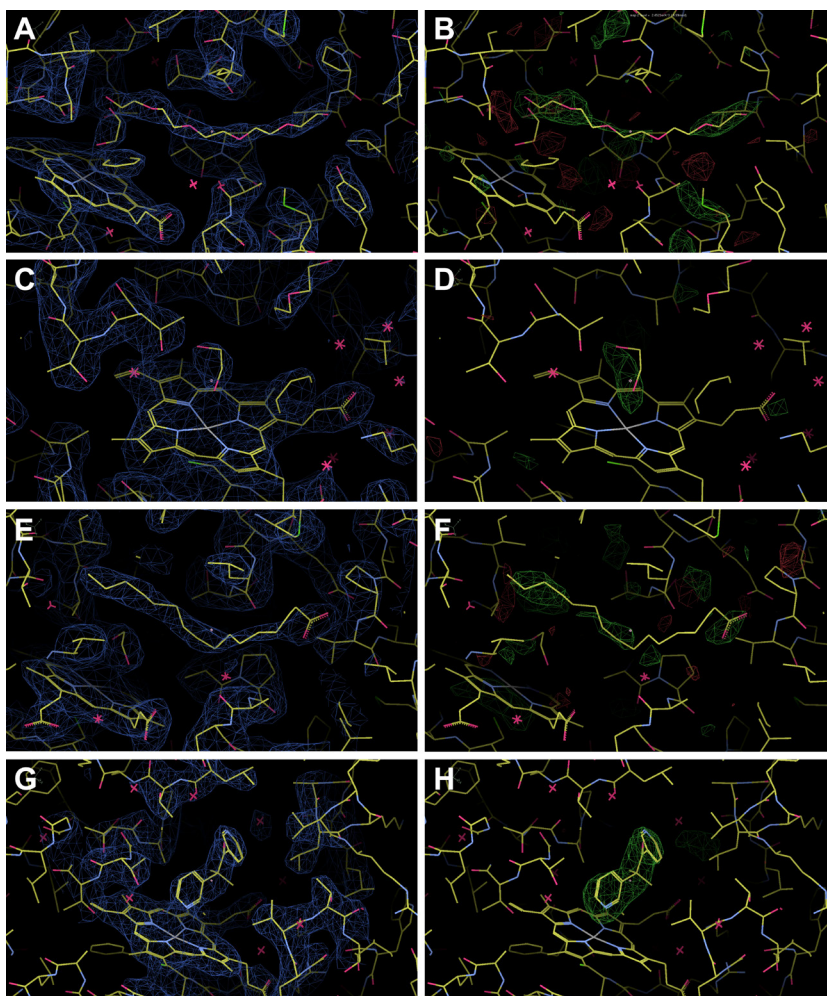


Figure 2.5 Omit maps for bound ligands in WT and PM P450_{BM3} x-ray crystal structures. (A) $2F_o-F_c$ difference electron density map for the crystallographic model of WT (4ZFA) contoured at 2.0σ showing the heme and PEG. (B) F_o-F_c omit map contoured at 7.0σ and calculated for a modified final WT model lacking only the PEG shown covering the same portion of the final refined model. (C) A portion of the final refined $2F_o-F_c$ difference electron density map (blue) for the WT model contoured at 2.0σ with the corresponding portion of the final refined model containing the heme and bound ethylene glycol (yellow carbon atoms). (D) F_o-F_c omit map (green/red) contoured at 9.0σ and calculated for a modified final WT model lacking only the ethylene glycol molecule shown covering the same portion of the final refined model. (E) $2F_o-F_c$ difference electron density map for the crystallographic model of PM bound to palmitic acid (4ZFB) contoured at 2.0σ showing the heme and palmitic acid. (F) F_o-F_c omit map contoured at 7.0σ and calculated for a modified final PM:palmitic acid complex model lacking only the palmitic acid shown covering the same portion of the final refined model. (G) $2F_o-F_c$ difference electron density map for the crystallographic model of PM bound to metyrapone (4ZF8) contoured at 2.0σ showing the heme bound to metyrapone. (H) F_o-F_c omit map contoured at 9.0σ and calculated for a modified final PM:metyrapone complex model lacking only the metyrapone shown covering the same portion of the final refined model. Crystal structure solved by W.E. Rogers, T. Othman, and T. Huxford.

2.3.4 The X-ray crystal structure of PM P450_{BM3} is similar to that of WT

Crystals of the PM P450_{BM3} formed in the same space group as the WT protein, and X-ray diffraction data of nearly identical quality were obtained for both crystals. Independent solution and refinement of the PM P450_{BM3} X-ray crystal structure revealed that it also adopts the closed conformation (4ZF6), with a PEG molecule positioned within the normally solvent-filled base of the substrate access channel.

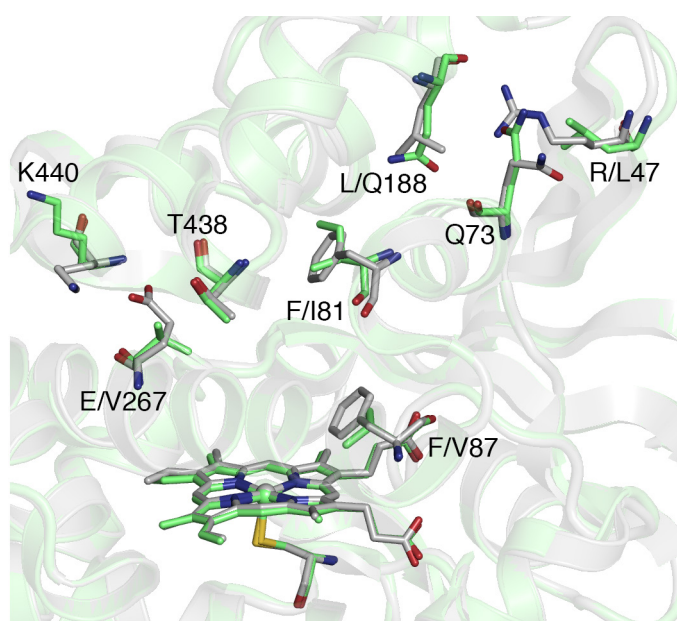


Figure 2.6 Crystal structures of WT (4ZFA, gray) and PM (4ZF6, green) BM3. The protein is shown in cartoon representation and the heme and mutated residues are shown in stick. The PEG molecule in the channel is not shown for clarity. E267 forms interactions with T438 and K440, which are lost upon mutation to valine. Q73 moves into the cavity left by the R47L mutation and could potentially interact with Q188. Crystal structure solved by W.E. Rogers, T. Othman, and T. Huxford.

Though the replacement of five amino acid side chains in PM does not significantly influence the fold or conformation of the P450_{BM3} protein, there are a few notable differences (Figure 2.6). Replacement of R47 with leucine (R47L) creates a cavity into which the side chain of Q73 moves, positioning it for interaction with Q188, which occupies the same position in WT near the end of the bound PEG. The E267V

mutation eliminated the interaction with the T438 and K440 side chains observed in the WT closed conformation model.

Mutation of F87 to valine (F87V) creates space above the heme porphyrin ring system adjacent to the O₂ binding site. The effect of this mutation on the environment at the O₂ binding site is evidenced by the severe change in orientation of the proximally bound ethylene glycol molecule relative to its position in the WT structure. Moreover, replacement with valine obviates the need for movement of the longer F87 side chain upon substrate binding. That movement, together with similar rearrangement of the I263 side chain, creates a hydrophobic cavity into which the hydrocarbon tail of long-chain fatty acids can anchor themselves. Therefore, the F87V mutation expands the active site, which would allow closer approach of substrates to the heme.

Comparison of the crystal structures of the PM:PEG complex (4ZF6) and the substrate-free R47L/Y51F/F87V/E267V/I401I mutant (4RNS¹⁶⁶) (Figure A4 A) suggests that the predominant form of PM in the absence of a ligand in the channel would be the closed conformation. Among the common substitutions of the two mutants, only L47 differed significantly in side chain position. Additionally, the neighboring Q73 side chain points outward unlike in PM (Figure A4 B).

2.3.5 X-ray co-crystal structures of WT and PM P450_{BM3} with substrate or inhibitor

Complexes of PM P450_{BM3} with the ligands palmitic acid (substrate) and metyrapone (inhibitor) were crystallized in the same crystal form as the WT and PM proteins described previously, and X-ray co-crystal structures were refined to 2.84 Å (4ZFB) and 2.77 Å (4ZF8), respectively. The PM:palmitic acid complex model is similar to the WT P450_{BM3} structure in complex with palmitoleic acid. In both, the carboxylate group of the substrate forms a hydrogen bond with the hydroxyl group of

Y51. However, the PM enzyme also involves the side chain of Q188 in anchoring the substrate. At the opposite end, the F87V mutation leaves a hydrophobic pocket that is amenable to accommodating the hydrocarbon tail without requiring movement of the phenylalanine side chain. In general, PM P450_{BM3} appears to be better suited to stably enfold its substrate, palmitic acid, in its binding site (Figure 2.5 E, F).

The PM:metyrapone complex crystal structure reveals a clear density for the inhibitor ligand at the active site and no evidence of elongated electron density in the vicinity of the fatty acid/PEG binding site (Figure 2.5 G, H). The pyridine nitrogen of metyrapone coordinates with the heme iron, as observed in complexes of P450_{cam} and CYP3A4.^{167, 168} The Fe–N distance in the P450_{BM3} PM:metyrapone complex is 2.62 Å. The average error in coordinate positions throughout the model as estimated by the maximum likelihood target function is 0.4 Å. The F87V mutation allows for metyrapone binding since the F87 side chain in either the substrate-bound or unbound conformation of WT would collide with metyrapone as it appears in the refined PM:metyrapone crystallographic model. This provides direct evidence of how mutating residues near the heme active site can significantly alter both the activity and specificity of the P450_{BM3} enzyme toward substrates and inhibitors.

In addition to these differences at the site of the heme, the lack of a fatty acid or PEG molecule within the enzyme causes the leucine side chain that substitutes for R47 in the PM enzyme to move into a solvent-exposed position. It is unclear what stabilizes this conformation. However, it appears that the absence of a fatty acid or its analogue allows for conformational flexibility within this region. None of the remaining mutated residues, F81I, L188Q, or E267V, appear to change relative to their positions in the PM and PM:palmitic acid complex crystallographic models.

2.3.6 Molecular dynamic simulations.

Simulations at 300 K were performed primarily to predict the native contacts in each system. Several interesting structural changes were also observed during the simulations. In substrate free WT, E267V, and L188Q (modeled from IBU7, molecule B), helix A and β -sheets 1-1 (residues 38-44) and 1-2 (residues 47-53) moved closer to the core of the protein, resulting in a partially closed substrate channel (Figure A5 A and Table A1) similar to IBU7 (molecule A). Helices D – H and β -sheet 4 were also shifted in position in E267V because of the elimination of the salt bridge with K440. Structural changes in R47L, F81I, and F87V were relatively less significant and mainly occurred in helices F and G (Table A1). On the other hand, the lid domain of substrate-free PM opened from the initial closed conformation (4ZF6) during the 300 K simulation (Figure A5 B). For the substrate-bound enzymes, larger backbone rmsds, with respect to the crystal structure, were observed for PM:palmitic acid (1.5 Å) and PM:metyrapone (1.1 Å) complexes. In addition to the movement of helix F to the N-terminal end of helix I, the substrates also changed in position in the PM active site. Palmitic acid moved closer to the heme, with its carboxylate group within hydrogen bonding distance of S72 (Figure A5 C). Metyrapone rotated slightly, bringing the uncoordinated pyridine ring in close contact with V87, T260, and I263 (Figure A5 D).

The unfolding of substrate-free and substrate-bound WT and PM was simulated using high-temperature (550 K) MD to rationalize the biochemical results. Simulations of the individual mutations R47L, F81I, F87V, L188Q, and E267V were also conducted to isolate the effect of each mutation on stability. As a technique, the thermally induced unfolding of these proteins provides mechanistic insights into regions of relative instability, which are identified by monitoring the native contacts of each residue. Native contact plots, averaged over three simulations, for helices F and G [residues

171-226 (Figure A6)] and the Cys ligand loop [residues 393-400 (Figure A7)] of substrate-free WT and PM are provided in the appendix as examples. Approximately 50% of the contacts were lost at the end of the 50-ns run for all simulations of substrate-free and substrate-bound enzymes.

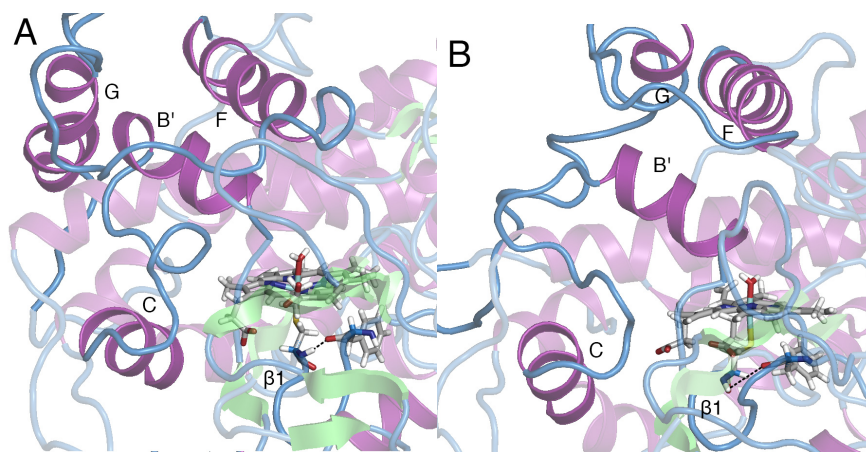


Figure 2.7 Snapshots at 25 ns from the 550 K simulations of substrate-free (A) WT and (B) PM viewed through the channel entrance. The protein is shown in cartoon representation, with helices colored purple, β -sheets green, and loops blue. The heme, bound water molecule, Cys ligand, and F393 at the other end of the loop are shown as sticks. The hydrogen bond distance between the Cys amide H and F393 carbonyl O (d_{O-H}) is represented by a dashed line. The Cys ligand loop is still intact in WT ($d_{O-H} = 1.75 \text{ \AA}$), but has begun to unfold in PM ($d_{O-H} = 3.98 \text{ \AA}$). MD simulations performed by I. Geronimo.

The different regions of P450_{BM3} are illustrated in panels C and D of Figures 2.4 to aid in the discussion of the results. Loss of contacts in substrate-free WT began at 3 ns in β -sheet 3, particularly those at the C-terminal end of the enzyme (Figure A5). A few contacts at helix B' were broken at 4 ns, followed by those of helix G residues near the F/G loop at 6 ns (Figure A6 A). In all simulations, the F/G loop and helix B' continue to unfold, along with β -sheet 1 and the N-terminal end, exposing the substrate channel (Figure 2.7 A and Figure A8 A, B).

The total number of native contacts in substrate-free PM is lower (659) compared to WT (680), which could explain the loss of PM stability. The increase in backbone rmsd within the first 10 ns was slightly faster than in WT (Figure A9 A, B). In addition to helix G, contacts were also lost in helices C and F (Figures A6 B), the Cys ligand loop [a β -bulge segment below the heme (Figure A7 B)], and β -sheet 1 within the first 5 ns (Figure A6). This was followed by helix K' and β -sheet 2, which are connected to the latter, and helix D. The unfolding process in all simulations is similar to that of WT, but with helices D and E unfolding concurrently (Figure 2.7 B and Figure A8 C, D). Among the single mutants, early loss of contacts in the β -sheets was also observed with L188Q, helix D with L188Q and E267V, and the Cys ligand loop with F81I, L188Q, and E267V. Surprisingly, F87V and R47L did not exhibit significant unfolding in the first 10 ns, although the increase in backbone rmsd was similar to those of the other mutants (Figure A9 C–G).

The unfolding of metyrapone-bound WT also began at β -sheet 3 albeit earlier in the simulation (1 ns). Unlike the substrate-free enzyme, the Cys ligand loop started to unfold after 4 ns, followed by helices C, F and G, and β -sheet 4 (5–6 ns). The latter is inserted into the channel and forms close contacts with the substrate. Shortly thereafter, the other side of the channel (β -sheets 1–2 and helix A) unfolded as well (7 ns). In comparison, fewer regions unfolded in the PM:metyrapone complex within the first 10 ns. Helix B' lost contacts first (2 ns) followed closely by helices F and G (3–4 ns), and then, β -sheet 1 (6 ns). As with the substrate-free and metyrapone-bound WT, helix G (3 ns) and β -sheet 3 (5 ns) in the WT:palmitic acid complex were involved in the early stages of unfolding. For the PM:palmitic acid complex, loss of contacts began at β -sheet 1 (3 ns), followed by β -sheet 3 (4 ns), helices G and H (5 ns), the Cys ligand loop (5 ns), β -sheet 4 (7 ns), and helix J' (8 ns). Generally, the substrate-bound variants

displayed the same unfolding process as the substrate-free ones (Figures A10 and A11). Each side of the substrate access channel continued to unfold, with the destruction of helices F and G extending to β -sheet 5 and, in some cases, even to part of helix I. The unfolding of the other portion of the lid domain (helix B') also extended to helix C, which consequently allowed the solvent to enter the active site. In contrast, a few strands of β -sheet 1 on the other side of the channel remained intact at the end of the simulation. For all substrate-bound enzymes, the hierarchy of unfolding in each trial simulation is essentially similar. However, the rate at which each side unfolds usually differs after ~ 10 ns (Figure A12); hence, the extent of damage to the channel at the end of the 50 ns simulation was not the same.

2.4 Discussion

The effects of mutations in the substrate access channel (R47L, F81I, F87V, L188Q, and E267V) and binding of the ligands palmitic acid and metyrapone on protein conformation and stability were analyzed using experimental and computational methods. Pulse proteolysis, which probes the global stability of a protein, indicated that PM is less stable than WT P450_{BM3}. Subsequent studies of WT by pulse proteolysis and UV-VIS indicate that it may not follow traditional unfolding described by most thermodynamic models ($N \leftrightarrow I \rightarrow U$), as biphasic unfolding was apparent. We hypothesize that there are either two populations present unfolding at different rates, or an intermediate state that exists long enough to be detected. Further studies will be discussed in chapter four elucidating the most likely mode of WT unfolding.

The crystal structures of WT and PM provide a possible explanation of how the mutations destabilize the enzyme. At the entrance of the channel, mutation of 188 in helix F from the nonpolar leucine to the polar asparagine can impact its interaction with

Q73 in helix B'. Previous studies have shown that variants with substitution at or near this residue (L188P, F162I/K187E, F162I/K187E/M237I, and F162I/K187E/L188P/M237I) are less stable.^{169, 170} Within the channel, the mutation of E267 to valine, in helix I eliminated the salt bridge with K440 in β -sheet 4, which would account for the 1 M decrease in the C_m of E267V. However, its effect on global stability appears to be less significant when combined with R47L, F87V, and L188Q mutations, as the similar C_m of TM and QM indicates. Residue F81, located in the lid domain (helix B'), is within contact distance of L181 in helix F, F205 and I209 in helix G, and I263 in helix I. Its mutation to the smaller isoleucine would therefore affect hydrophobic packing in this region, although pulse proteolysis of F81I suggests that this has a relatively minor effect on stability compared to the other mutations.

The chemical denaturation stabilities could be correlated to high-temperature simulations demonstrating the effect of mutations on the unfolding process. A linear correlation between C_m and T_m determined from heat inactivation curves of CO binding difference spectra was observed for P450_{BM3}.¹²⁹ A MD study of chymotrypsin inhibitor 2 also indicated that the overall unfolding mechanisms of chemical denaturation with urea and thermal denaturation are similar, in that key residues in the hydrophobic core are exposed first.¹⁷¹ Monitoring the decrease in the number of native contacts per residue over time revealed that the most labile regions of substrate-free WT P450_{BM3} are helices B' and G in the lid domain and β -sheet 3 in the C-terminal end of the protein. Hydrophobic contacts in the lid domain, aside from those observed in the crystal structure, include F205 (helix G)–A180 (helix F) and V211/M212 (helix G)–F173 (helix F) contacts.

As a biophysical technique to investigate global protein structure, pulse proteolysis is advantageous in that it doesn't require expensive instrumentation, and

can be done relatively quickly. Pulse proteolysis uses a protease, thermolysin, to determine the proteolytic susceptibility of a partially denatured protein. Using this technique, concentration midpoint (C_m) values can be determined and compared for various proteins with and without ligands bound. By first incubating the protein of choice in urea, it is assumed that after a set period of time there will be an equilibrium between the folded and unfolded populations of the enzyme. Thermolysin can then digest the unfolded regions of the protein that have been partially denatured. Thermolysin is an ideal protease for this application as it can work under a wide range of temperatures, pH, and denaturant concentrations.¹⁷² Though relatively small, given its mass of approximately 35 kDa,¹⁷³ thermolysin is not small enough to access the interior of a larger protein that is properly folded. As thermolysin preferentially cleaves at the N-terminus of hydrophobic residues (though there is evidence of broader specificity in several proteins),¹⁷² this implies that the hydrophobic core must be exposed to solvent for cleavage to occur.

Importantly, for this method to be successful, protein cleavage must be faster than protein unfolding while it is incubated with thermolysin, allowing for discrimination between the folded and unfolded populations. Determining the length of the pulse is essential. Park and Marqusee showed that when the urea concentration is below 7 M and thermolysin is in excess,^{137, 174} a pulse of 1 min is effective for cleavage of the unfolded protein.^{137, 139} As thermolysin is a zinc metalloenzyme that also requires calcium,¹⁷⁵ addition of EDTA will quickly inhibit activity, so the pulse can be timed exactly.¹⁷⁶ For our experiments, the thermolysin concentration was approximately 10 times that of the P450_{BM3} concentration, and the denaturant concentration was kept below 7 M. In addition, when P450_{BM3} was pulsed with thermolysin without first being incubated in urea, generally there was no indication of fragmentation on the gel.

Fragmentation would be expected if the enzyme had been cleaved, which indicates thermolysin wasn't able to cut P450_{BM3} when it is fully folded. Hydrogen/deuterium exchange (H/D exchange) coupled to mass spectrometry is another commonly used technique to monitor global structure stability of proteins. Unlike pulse proteolysis, which takes a snapshot of the protein at one set time, H/D exchange can monitor dynamics over a wide time scale taking place from 10 s⁻¹ to days.¹⁷⁷ Though this may be preferable for some applications, H/D exchange mass spectrometry is often prohibitively costly, requires specialized equipment and training, and data analysis is time consuming.

Protein conformational dynamics occur on different time scales, depending on the type of motion. Side chain rotations occur on a picosecond to nanosecond time scale.¹⁷⁸ This is opposed to proline isomerization which is known to be slow, on the order of tens to thousands of seconds.¹⁷⁹ Thus, observations of different kinetic phases by a slow technique such as pulse proteolysis suggests results are due to large conformational changes that occur over a 2 hr time frame, and cannot be due to rearrangement of residues.

Additional regions were shown to unfold earlier in PM, notably β -sheet 1 and the Cys ligand loop. Early unfolding of the Cys ligand loop is consistent with CD data indicating that the heme environment of substrate-free PM is less stable than that of WT. L188Q similarly lost contacts early in both regions, suggesting that this mutation has a significant contribution to destabilization. Simulations of the single-point mutants at 300 K showed that the L188Q mutation caused the most significant structural change, based on backbone rmsd at the N-terminal end up to β -sheet 1 of the substrate-free enzyme (Table A1), which is presumably destabilizing and might have affected the Cys ligand loop. On the basis of analysis of time-correlated atomic motions, these two

regions were assigned to the same protein domain, which implies that they move cooperatively and cohesively during structural transitions of the protein.¹⁸⁰

As for E267, simulations support the importance of its salt bridge with K440, as it was maintained even at high temperature in WT. The concurrent unfolding of helices D and E with sections of the substrate channel in PM may also be attributed to the E267V mutation, which disrupted hydrophobic contacts such as L150 (helix E)–H266 (helix I) and I122 (helix D)–L148 (helix E) contacts. R47L did not exhibit significant unfolding during the early stages of high-temperature simulations, despite the elimination of a salt bridge with another β -sheet 1 residue, E352 (Table A2). This may be explained by the fact that leucine is a better β -sheet-former.¹⁸¹ F87V was also relatively stable during the simulations, which is inconsistent with differential scanning calorimetry data showing that its melting temperature is lower by $\sim 4^\circ\text{C}$ than that of WT.¹⁶⁴ The discrepancy may be attributed to the difficulty in accurately predicting slight differences in stability in the case of conservative (in terms of hydrophobicity) substitutions such as F81I and F87V using MD simulations, which is exacerbated by the lack of available crystallographic evidence; initial coordinates for single-point mutant and WT simulations were all derived from 1BU7 (molecule B), which may not be adequately representative of the F87V structure.

Substrate binding generally stabilizes an enzyme.^{137, 182} However, pulse proteolysis and CD data demonstrated that this was not the case with the WT:metyrapone complex. This finding suggests a mismatch in complementarity between the ligand and enzyme. High-temperature simulations showed that additional regions, particularly the Cys ligand loop, unfolded early, which is consistent with the observed decrease in C_m for the heme environment. In contrast, the stability of the heme region of PM was enhanced by metyrapone, although it is not certain whether this can

be attributed to covalent bonding with the heme iron because simulations of P450_{cam} in complex with 4-phenylimidazole (Fe–N bond length of 2.21 Å in the crystal structure¹⁶⁷) showed instability of the Cys ligand loop.¹⁵¹ However, a new salt bridge, E380–K312, formed during the simulation (Table A2), and its proximity to the heme might contribute to the stabilization of PM. On the other hand, the stability of WT and PM was not significantly affected by the presence of palmitic acid, as indicated by pulse proteolysis. This finding implies that enzyme conformation of the palmitic acid bound and substrate free enzyme are similar with little change to overall structure with ligand bound. Computationally it was discovered that though the labile regions in the palmitic acid-bound complex of WT and PM are different from the corresponding substrate-free enzyme, the unfolding process was observed to be similar. The Cys ligand loop unfolded early in both forms of PM but was relatively stable in both forms of WT.

Increasing the stability of PM is advantageous if it is to be used as a starting point to develop more promiscuous variants for biotechnical applications. The lid domain, β -sheet 1, and Cys ligand loop would be the logical targets for mutation based on the hypothesis that delaying the unfolding of the most labile regions would increase the global stability of the protein. On the basis of analysis of physical factors that differentiate (hyper)thermophilic proteins from mesophilic ones,¹⁸³⁻¹⁸⁵ several approaches for protein stabilization have been attempted such as introducing salt bridges,¹⁸⁶ increasing structural rigidity,¹⁸⁷ and improving hydrophobic core packing.¹⁸⁸

The latter method is promising for P450_{BM3} on the basis of a previous study on the 21B3 variant of this enzyme.¹³⁵ Five of the eight mutations introduced through directed evolution, resulted in an increase of 15°C in T₅₀, happened to conserve hydrophobicity. Residues L52I (β -sheet 1) and A184V (helix F) are buried, while L324I (helix K), V340M (β -sheet 2), and I366V (helix K'') are located on the surface. The

authors hypothesized that these stabilizing mutations counteracted structural perturbations caused by previously introduced activity-enhancing mutations given the proximity of some residues in the two sets of mutations.¹³⁵ Interestingly, most of the stabilizing mutations are located at or near the labile regions identified in this study. Packing interactions in PM P450_{BM3} can be enhanced by introducing substitutions at the hydrophobic patches in the (a) lid domain, consisting of I81, A180, L181, F173, F205, I209, V211, M212, and I263, and (b) heme region, including W367, F379, and F390. This cluster of aromatic residues presumably stabilizes the Cys ligand loop, as is the case in the thermophilic CYP119.¹⁵¹

Salt bridges contribute to the stability of thermophilic P450s at elevated temperatures through hydration effects.¹⁸⁹ For instance, CYP175A1 ($T_m = 88^\circ\text{C}$), whose closest homologue is P450_{BM3} (26% sequence identity), has eight salt bridge networks (i.e., one that involves more than two charged residues).¹⁹⁰ MD simulations of P450_{BM3} variants showed that there are only three networks in substrate-free WT (R323/E320/R378/D370, K3/E344/R56/E38, and K94/E247/K98) and four in PM (R375/D370/R378, K3/E344/R56/E38, K94/E247/K98/D250, and E292/R296/E293). At the N-terminal end of P450_{BM3}, T339 (β -sheet 2) can be mutated to Asp to form an extended network with R66 (β -sheet 1) and E60 (helix B). New salt bridges in the other labile regions can also be introduced, for example, the D388 (mutated from His)-K391 salt bridge in the loop region near the heme, and the K445 (mutated from Val)-E140 salt bridge in β -sheet 3.

Pulse proteolysis, CD spectroscopy, x-ray crystallography, and MD simulations elucidated how mutations that destabilize P450_{BM3} impart affinity for nonnative substrates such as metyrapone. The method-dependent variation in stability measurements indicates that use of global, secondary structure, and active site

characterizing methods is necessary to effectively evaluate the effects of mutation on P450_{BM3} stability. Utilizing multiple techniques, when using a chemical denaturant, to probe various aspects of protein stability is important as denaturants effect various structures differently. In general, more urea was necessary for secondary structure unfolding than for global and active site unfolding. This may be due to the fact that hydrophobic contacts that keep the global structure together are easier to disrupt than the hydrogen bonding of the secondary structure.

Our models suggest that destabilization generally arose from disruption of important salt bridges and hydrophobic contacts and unfolding of the Cys ligand loop connected to the heme. The identification of the conserved Cys ligand loop as a key contributor to instability suggests that some findings may be generalizable to other CYP102A subfamily fatty acid hydroxylases.¹⁹¹ A commonly held view among the protein design community is that increasing the promiscuity of an enzyme comes with a requisite expense of protein stability. However, Arnold, *et al.* demonstrated that this is not necessarily the case, as more thermostable variants have been produced through further directed evolution of an existing mutant without compromising enzyme activity.^{129, 135, 136}

2.5 Conclusions

Biochemical techniques that used chemical denaturation as well as structural and computational methods were used to probe the thermodynamic stability of P450_{BM3}, a model system for human CYPs and a candidate for biotechnical applications. From the biochemical results it was evident that mutations that increase promiscuity, destabilize enzyme stability, but in some cases this stability can be recovered when substrates are bound. Though, the crystal structures of WT and PM were globally similar, mutations

at position 188 and 267 were most detrimental to enzyme stability. MD simulations further parsed the differences that lead to a decrease in stability. Primarily, these differences are a loss of contacts in PM, and early unfolding of β -sheet 1 and the Cys-ligand loop.

Studies of the role of the Cys ligand loop for protein stability were undertaken; particularly the role of residue I401 was investigated. I401 is directly next to the cysteine ligated to the heme and was mutated to a proline, which is the naturally occurring residue in some CYPs.^{192, 193} Disruption of the Cys ligand loop by P401 in P450_{BM3} leads to the enzyme being in a naturally high spin state, but also has further reaching consequences in that it changes the residue contacts in the I-helix of the enzyme, causing it to be more open. This openness leads to a more promiscuous but less stable enzyme, similar to PM. More discussion of this mutation will be included in chapter four. Additionally, this study and subsequent work demonstrated the possibility of biphasic unfolding of WT P450_{BM3} which will also be discussed in chapter four.

The characterization of the unfolding process of the P450_{BM3} variants presented herein provides fundamental knowledge that could be used to rationally design stability upon an enhanced specificity platform as well as understand the role in stability in promiscuous CYPs. Regions involved in the early stages of unfolding are potential targets for mutation to develop thermostable variants of the promiscuous PM P450_{BM3}.

CHAPTER 3. MOLECULAR DETERMINANTS OF SMALL MOLECULE AFFINITY AND ENZYME ACTIVITY OF A CYTOCHROME P450_{BM3} VARIANT.

Chapter adapted from: Geronimo, I., Denning, C. A., Heidary, D. K., Glazer, E. C., Payne, C. M. (2018). "Molecular Determinants of Substrate Affinity and Enzyme Activity of a Cytochrome P450_{BM3} Variant." *Biophysical Journal* **115**(7): 1251-1263.

Author Contributions: IG, CAD, ECG, and CMP designed the study, analyzed the data, and wrote the manuscript. IG performed the molecular dynamics simulations. CAD and DKH conducted the experiments and analyzed the data.

3.1 Introduction

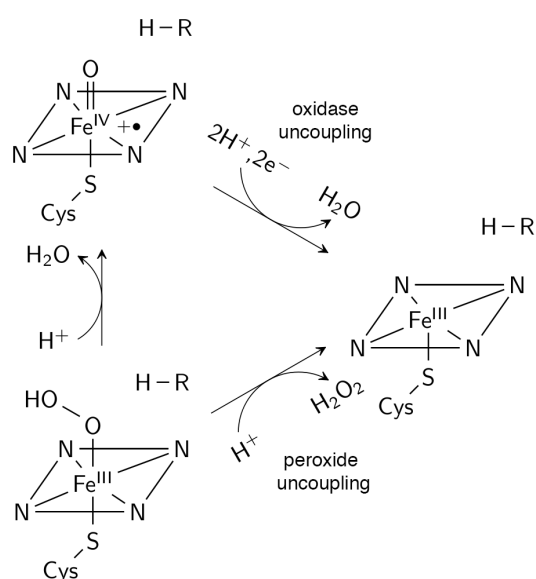


Figure 3.1 Peroxide and oxidase uncoupling pathways. The substrate is represented by R-H.

Characterization of the metabolite profile of a drug candidate is a crucial part of the drug discovery and development process. Drug metabolites, largely produced by hepatic cytochrome P450 enzymes (P450s), are needed as reference compounds and

reactive intermediates for assessing toxicity, drug-drug interactions, and biological activity.^{194, 195} For the preparative-scale synthesis of human drug metabolites, CYP102A1 (P450_{BM3}), a fatty acid hydroxylase from *Bacillus megaterium*, is considered an ideal biocatalyst because it has the highest known monooxygenase activity among P450s, is relatively stable compared to human P450s, and can be expressed at high levels in *Escherichia coli*.^{97, 134, 196} Wild-type (WT) P450_{BM3} has been shown to catalyze the oxidation of nifedipine, propranolol, and chlorzoxazone, which are substrates of the human P450s CYP3A4, CYP2D6, and CYP2E1, respectively.¹⁹⁷ To take full advantage of P450_{BM3} in an industrial setting, much research has been devoted to further expanding its substrate promiscuity and chemical reactivity through protein engineering.^{122, 125, 127, 166, 196, 198, 199} However, the molecular factors responsible for the stability of substrate binding and potential consequences of introducing nonnative substrates on the activity and coupling efficiency (i.e., ratio of substrate reacted to NAD(P)H cofactor consumed³⁴) of P450_{BM3} have yet to be determined. Peroxide or oxidase uncoupling (Figure 3.1) is of particular concern because it prevents product formation, thereby wasting reducing equivalents from the expensive NAD(P)H cofactor.^{33, 200} Furthermore, the production of these oxygen species can do further damage to the enzyme itself, causing it to unfold.

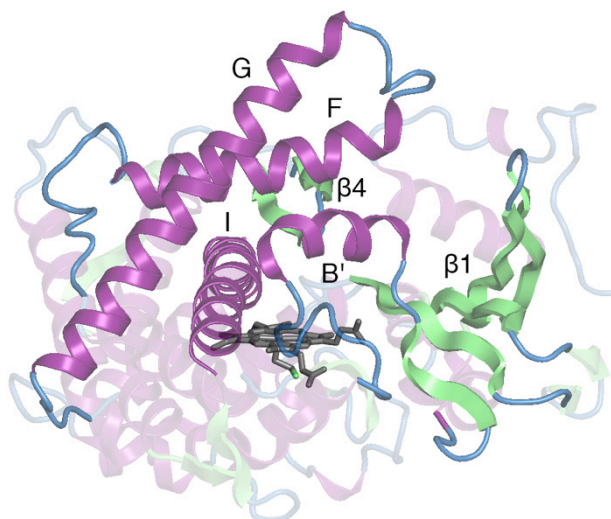


Figure 3.2 P450_{BM3} structure. Regions involved in substrate binding, including the lid domain (helices B', F, and G), are labeled in the figure. The heme is shown as sticks.

Interestingly, the P450_{BM3} variants developed to metabolize additional drug classes (e.g., nonsteroidal anti-inflammatory drugs (NSAIDs) like diclofenac, ibuprofen, and naproxen), including D251G/Q307H^{120, 201}, RP/FV/EV/FW¹⁶⁶, RT2/AP/FW¹⁶⁶, M11^{127, 198, 199}, and W7D8¹²² (Table 3.1), do not all share common substitutions. However, the mutations, generally located far from the heme active site, appear to have a similar functional effect of increasing the flexibility of the lid domain (helices B', F, and G, Figure 3.2), as revealed by the unresolved (or very high B factors of) lid domain residues in the crystal structures of the substrate-free variants.^{122, 164, 166, 199, 201, 202} Molecular dynamics simulations of R47L/F87V/L188Q/E267V/F81I pentuple mutant (PM) showed that the lid domain is, indeed, highly labile, and consequently, one of the regions that first unfolds at high temperature¹. In the case of D251G/Q307H (PDB ID: 5DYP²⁰¹), M11 (PDB ID: 5E9Z¹⁹⁹), and RP/FV/EV (PDB ID: 4RSN¹⁶⁶), the cause of increased flexibility is evident; D251 and E267 are part of the region that moves during the opening and closing of the substrate channel and form

salt bridges with K224 and K440, respectively, in WT.^{191, 203} The higher flexibility of the lid domain would account for the ability of P450_{BM3} variants to accept a broader range of substrates.^{122, 164} Additionally, many of these mutations are made in, or close to, substrate recognition sites (SRS) which are regions of high variability in bacterial and eukaryotic CYPs thought to be responsible for substrate binding.²⁰⁴ Mutations in these regions can easily impact enzyme promiscuity. At least three of the six possible SRS are associated with the main ingress/egress pathway way (pw2a) of P450_{BM3} as demonstrated by replica-exchange molecular dynamics (REMD) simulations and thermal motion pathway (TMP) analysis of published P450_{BM3} crystal structures.^{205, 206} The crystal structures further showed that substrate-free variants adopt the closed conformation characteristic of substrate-bound WT instead of the open conformation. This shift to the catalytically ‘ready’ conformation caused by mutation results in a more positive heme reduction potential. Consequently, the rate of the first electron transfer (believed to be the rate-limiting step²⁰⁷) increases, improving the oxidative activity of P450_{BM3} toward nonnative substrates.^{120, 166, 201, 202, 208}

Table 3.1. List of mutations in functional BM3 variants.

Variant	Mutations
RP/FV/EV ¹⁶⁶	R47L/Y51F/F87V/E267V/I401P
RP/FV/EV/FW ¹⁶⁶	RP/FV/EV/F81W
RT2/AP/FW ¹⁶⁶	R47L/Y51F/A191T/N239H/I259V/A276T/L353I/A330P/ F81W
M01 ¹²⁵	R47L/F87V/L188Q/E267V/G415S
M02 ¹²⁵	R47L/L86I/F87V/L188Q/N319T/A964V
M05 ¹²⁵	M01/F81I/G1049E
M11 ^{127, 198, 199}	M01/E64G/F81I/E143G/Y198C/H285Y
MT35 ¹²⁷	M11/L437S
W7D8 ¹²²	L52I/I58V/L75R/L86L/F87A/H100R/S106R/F107L/Q109L/ A135S/E140G/F162I/A184V/N239H/S274T/L324I/V340M/ I366V/K434E/E442K/V446I
9-10A ¹⁹⁶	V78A/H138Y/T175I/V178I/A184V/H236Q/E252G/R255S/A 290V/A295T/L353V/Y138H/I178V/F205C/S226R/A290V/ R47C/K94I/ P142S

The only crystal structures of drug-bound P450_{BM3} variants that have been reported thus far are A82F and A82F/F87V with omeprazole (PDB IDs: 4KEW and 4KEY¹⁶⁴), A82F/F87V with esomeprazole (PDB ID: 4O4P¹²¹), antifungals tioconazole, voriconazole, fluconazole and clotrimazole (PDB IDs: 6H1L, 6H1O, 6H1S, and 6H1T²⁰⁹), as well as PM with metyrapone (PDB ID: 4ZF8¹). In all structures, the

conformation is notably similar to that of the WT-fatty acid complex (PDB ID: 1FAG¹⁶⁵), raising two important questions: (1) What interactions stabilize a structurally different and highly polar drug molecule in the largely hydrophobic active site? (2) How would the lack of structural and electrostatic complementarity between substrate and enzyme affect activity and coupling efficiency? This study aims to address these key mechanistic questions by investigating the binding of a set of drugs of varying size, charge, polar surface area, and human P450 affinity. PM P450_{BM3} was chosen as the model system because it serves as a good platform to develop biocatalysts for the synthesis of drug metabolites, as well as for diversification of lead compounds; this was demonstrated by a study in which a library of mutants containing the PM mutations was able to metabolize 77% of the 43 commercial drugs tested by more than 20%.¹²⁷

The binding free energies of CYP2C9 (diclofenac, naproxen, *S*-warfarin), CYP2D6 (astemizole, dextromethorphan, 3,4-methylenedioxymethamphetamine or MDMA), and CYP2A6 (nicotine, cotinine) substrates, CYP2C9 inhibitors (lovastatin, *R*-warfarin), and metyrapone (Table 3.3, Table B1) were determined using spectroscopic binding titrations and supported by calculations using free energy perturbation with Hamiltonian replica-exchange molecular dynamics (FEP/ λ -REMD). To gain insight on the nature of the interaction that enables the binding of nonnative small molecules in the P450_{BM3} mutant, the calculated free energy was further decomposed into repulsive, dispersive, and electrostatic contributions. Residues that play a role in substrate binding were identified by analyzing hydrogen bond, ionic, and van der Waals interactions from the molecular dynamics (MD) trajectories. The possibility of reduced heme oxidizing ability and uncoupling, caused by the binding of nonnative substrates, was assessed by examining electrostatic interactions and water density in the active site.

Table 3.2 Drug molecules used in this study with function and CYP chemistry.

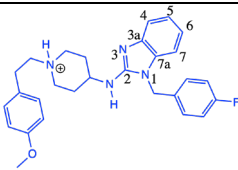
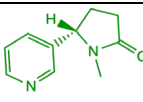
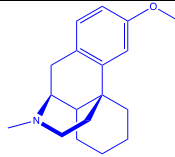
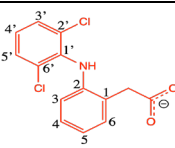
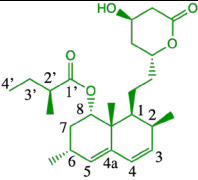
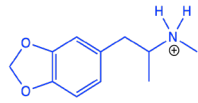
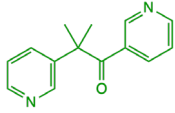
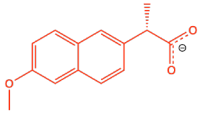
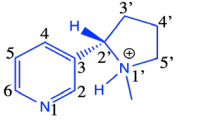
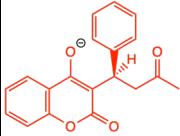
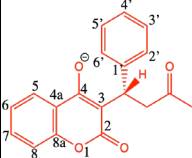
Compound Name	Chemical Structure ^a	Drug Class	CYP Chemistry
Astemizole		Antifungal	O-demethylation, N-demethylation, Hydroxylation ²¹⁰
Cotinine		Nicotine metabolite	N-demethylation, Hydroxylation, Oxidation ²¹¹
Dextromethorphan		Cough suppressant	O-demethylation, N-demethylation ²¹²
Diclofenac		NSAID	Hydroxylation ²¹³
Lovastatin		Statin	Hydroxylation, Desaturation ²¹⁴
MDMA		Stimulant, Hallucinogen	N-demethylation, O-demethylation ²¹⁵
Metyrapone		Inhibitor of 11β- hydroxylase	Inhibitor
Naproxen		NSAID	O-demethylation ²¹⁶
Nicotine		Stimulant	N-demethylation, Hydroxylation, Desaturation, Oxidation ²¹¹

Table 3.2 (continued)

R-Warfarin		Anticoagulant	Hydroxylation ²¹⁷
S-Warfarin		Anticoagulant	Hydroxylation ²¹⁷

- a. Color of each structure represents polarity at physiological pH, where green is neutral, blue is positively charged, and red is negatively charged.

3.2 Experimental procedures

3.2.1 Biochemical procedures

3.2.1.1 Chemicals for spectroscopic binding titrations

Dextromethorphan hydrobromide monohydrate, metyrapone, and sodium palmitate (palmitic acid) were purchased from Sigma Aldrich. (-)-Cotinine, lovastatin, and naproxen sodium were purchased from Alfa Aesar. Nicotine and warfarin sodium were purchased from TCI America.

3.2.1.2 Cloning and site-directed mutagenesis of P450_{BM3}

The heme domain of P450_{BM3} (Thr 1-Thr 463) with a C-terminal 6xHis tag was cloned into the pCWori plasmid. Mutations for generating PM P450_{BM3} were incorporated using QuikChange site-directed mutagenesis (Stratagene). The polymerase chain reaction product was DpnI treated, transformed into XL-Gold ultracompetent cells, and selected on carbenicillin Luria Broth-Agar plates. Colonies were grown in 5 mL of LB with 100 µg/mL ampicillin, followed by plasmid isolation

using the E.Z.N.A.® Plasmid Mini Kit (Omega Bio-tek®). All mutations were confirmed by sequence analysis.

3.2.1.3 Expression and purification of PM P450_{BM3}

The pCWori vector containing the PM P450_{BM3} heme domain was transformed in *E. coli* BL21(DE3) cells. Colonies were grown overnight in 5 mL LB with 100 µg/mL ampicillin in a shaking incubator set to 190 rpm and 37 °C before being transferred to 1 L Terrific Broth supplemented with 8 mL of 80% glycerol and 100 µg/mL ampicillin. The cells were grown until an OD₆₀₀ of 0.7–0.8 was reached. Expression of PM P450_{BM3} was induced upon addition of isopropyl β-D-1-thiogalactopyranoside (IPTG) at a final concentration of 0.5 mM. Cells were harvested after approximately 16 h by centrifugation at 4 °C and 3000 xg for 15 min. The cell pellets were stored at -80 °C until purification.

Cell pellets were resuspended in 30 mL lysis buffer (50 mM NaH₂PO₄, 300 mM NaCl, 10 mM imidazole, 0.1 mM EDTA, pH 8.0) with 0.1 mM phenylmethylsulfonyl fluoride. Cells were lysed on ice for 15 min by a microtip sonifier with output control of 3 and duty cycle of 50% (Branson Sonifier 250). The lysate was centrifuged at 4 °C and 17000 xg for 1 h, the supernatant decanted, and filtered through a 0.45 µM polytetrafluoroethylene syringe filter.

The clarified lysate was loaded onto a His-Trap column (GE Healthcare) equilibrated with Buffer A (50 mM NaH₂PO₄, 300 mM NaCl, 10 mM imidazole), and the protein was eluted with a linear gradient using Buffer B (50 mM NaH₂PO₄, 300 mM NaCl, 200 mM imidazole), where the concentration increased from 10 to 200 mM imidazole. Fractions containing PM P450_{BM3} were collected and concentrated to approximately 2 mL at 4500 xg and 4 °C with Ultracel-30K Millipore centrifugal units.

The concentrated protein was loaded onto a Hi-Prep 26/60 Sephacryl S200 HR size exclusion column equilibrated with 20 mM Tris and 150 mM NaCl buffer at pH 8.0. Fractions containing PM P450_{BM3} were analyzed by absorbance spectroscopy, and all fractions with a spectrophotometric index (A_{420}/A_{280}) above 1.2 were combined and concentrated. The protein concentration was determined by CO binding ($\epsilon = 91,000 \text{ M}^{-1} \text{ cm}^{-1}$)¹³⁸. Glycerol was added to approximately 50%, with the final protein concentration between 15 and 20 mg/mL. The protein was aliquoted, snap-frozen in a dry ice ethanol bath, and stored at -80 °C until use.

3.2.1.4 Binding constant determination by spectroscopic titration

Dextromethorphan hydrobromide monohydrate, naproxen sodium, nicotine, and warfarin sodium stock solutions were prepared in 18.2 MΩ water. (-)-Cotinine, lovastatin, metyrapone, and palmitic acid were prepared in dimethyl sulfoxide. UV/Visible absorption spectra were recorded using an Agilent 8453 spectrophotometer. Titrations were carried out in 2 mL of 100 mM KH₂PO₄ (pH 7.4) in a 1-cm optical path length cuvette, with protein concentrations between 0.15 and 0.25 mg/mL. All titrations were carried out with the organic solvent concentration kept below 1%.

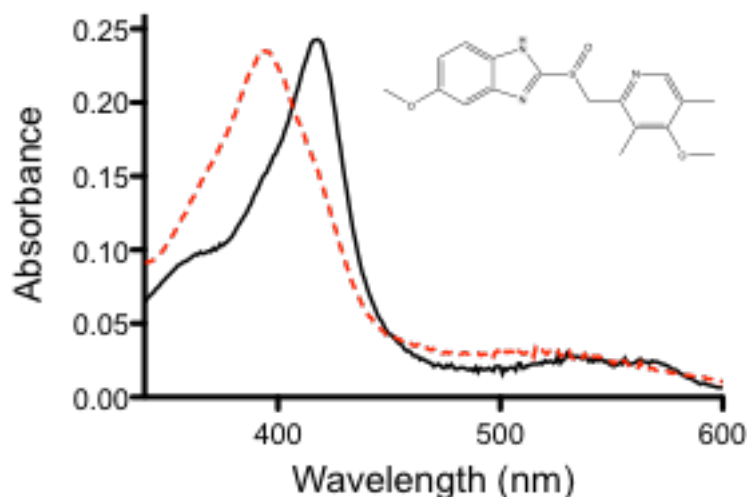


Figure 3.3 Comparison of a full type I spectral shift to the water bound resting state. Omeprazole bound (red dashed line) is 100% high spin, compared to the water bound state (black line). Saturation of PM P450_{BM3} (0.15 mg/ml) with omeprazole in 2 mL of 100 mM KPi pH 7.4 at room temperature in a 1 cm quartz cuvette.

Difference spectra were generated by subtracting the absorption spectrum at each concentration point in the titration from the original compound-free P450_{BM3} absorption spectrum. The wavelength where the maximum change occurred was identified and used to determine the binding dissociation constant (K_d), which was calculated in GraphPad Prism version 6 by fitting the data for the ligand-induced absorbance changes in the difference spectra ($A_{\max} - A_{\min}$) vs. ligand concentration to a one-site total binding equation. The ΔG_b value was determined using the equation $\Delta G_b = RT \ln K_d$, where $R = 1.99 \times 10^{-3} \text{ kcal K}^{-1} \text{ mol}^{-1}$ and $T = 298.15 \text{ K}$. A full spin shift was obtained using omeprazole as the substrate. For all other ligands, the percentage of protein in the high-spin state was calculated based on the assumption that water-bound PM P450_{BM3} is 100% low spin, and PM P450_{BM3} fully bound to omeprazole is 100% high spin (Figure 3.3).

3.2.1.5 5-Ethoxyresorufin-O-deethylase activity assay

Inhibition of PM P450_{BM3} was detected via a turnover assay for nicotine, cotinine, and metyrapone. Each compound was added to 2.5 μ M PM P450_{BM3} in 1x phosphate buffered saline (PBS, pH 7.5). The concentration of compound used was 10 x K_d . The compound and enzyme were incubated for 5 min at RT before 5-ethoxyresorufin was added to a final concentration of 5 mM. The solution was allowed to incubate for another 5 min before 0.1 M H₂O₂ was added. The Greiner clear bottom 96 well plate was immediately placed in a Tecan Spectrafluor plus microplate reader for 5 min. Fluorescence was monitored as a function of time with excitation 525 nm and emission 595 nm.

3.2.2 Computational procedures

3.2.2.1 Molecular dynamics (MD) simulations

Initial coordinates for the PM-metyrapone complex were obtained from the crystal structure PDB ID: 4ZF8.¹ The other enzyme-substrate complexes were prepared by ligand docking using AutoDock 4.2.²¹⁸ The structure of the solvent-free target protein (including the heme) was taken from the last point of the 100-ns, fully atomistic simulation of the PM-metyrapone complex performed in a previous study.¹ The charges used for the protein atoms were the same as the ones used in the MD simulation, while ligand charges were calculated using the Restrained Electrostatic Potential (RESP) method (*vide infra*).²¹⁹ The size of the grid box, centered on the Fe atom, was 60 Å × 60 Å × 60 Å, with a spacing of 0.250 Å. During the docking simulations, the protein was kept rigid while all rotatable dihedrals in the ligands were allowed to move freely. The Lamarckian genetic algorithm was used to search for low-energy ligand poses that

will yield the metabolites known to be produced by human P450s and/or P450_{BM3} mutants containing the PM mutations.

Preparation of the enzyme-substrate complexes for MD simulations, including assignment of the protonation state of titratable residues, has been described in detail in reference.¹ The solvated ligand system was prepared by neutralizing the ligand with Na⁺ or Cl⁻ and solvating it in a truncated octahedron box of TIP3P water¹⁴⁷ with a buffer distance of 25 Å between each wall and the closest atom in each direction. The AMBER ff14SB force field¹⁴⁶ was used to describe the protein. Force field parameters and partial charges for the high-spin, pentacoordinate ferric form of the heme active site (characteristic of substrate-bound P450_{BM3}¹⁹¹) were taken from literature.⁷² These parameters have been tested for stability and consistency with the expected heme geometry in implicit and explicitly solvated MD simulations of the heme active site alone and CYP3A4. Moreover, the use of the partial charges in docking calculations reproduced the experimentally observed metabolism of raloxifene by CYP3A4.⁷² Ligands parameters were calculated using *antechamber*¹⁴⁸ at the HF/6-31G* level to be consistent with the GAFF force field.¹⁴⁹ Periodic boundary conditions were applied using the Particle Mesh Ewald method¹⁵⁹ with a non-bonded cutoff of 10 Å. Energy minimization was performed in four stages: (1) protein and ligand were restrained with a harmonic force constant of 5.0 kcal/mol/Å² to allow water and ions to relax, (2) residues within 5 Å of the docked ligand were released from the restraint, (3) the whole protein was again restrained while the ligand was allowed to relax, and (4) the restraint was removed. At each stage, 1000 steps of steepest descent minimization was performed, followed by 1000 steps of conjugate gradient minimization.

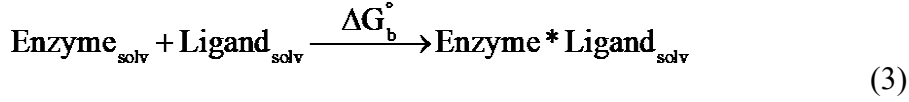
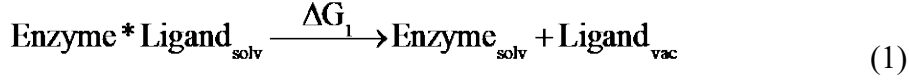
The system was then heated from 0 to 300 K for 50 ps using NMR weight restraints to linearly increase the temperature (≈ 6 K/ps) in order to avoid instabilities in

the simulation. C α atoms were restrained with a harmonic force constant of 5.0 kcal/mol/Å² during heating. Bonds involving hydrogen were constrained using the SHAKE algorithm¹⁶⁰, and a 2-fs time step was used for time integration. The temperature was controlled using Langevin dynamics¹⁶¹ with a collision frequency of 1.0 ps⁻¹. The system was equilibrated at constant pressure over a 200-ps period, during which the force constant was incrementally reduced (5.0, 2.0, 1.0, and 0.5 kcal/mol/Å²). Isotropic position scaling was used to maintain the pressure at 1 atm, with a relaxation time of 2 ps. Equilibration of the unrestrained system was then continued for 2 ns. Production MD simulations in the *NVT* ensemble were performed at 300 K for 100 ns using the same parameters as equilibration. During production, a harmonic restraint of 10 kcal/mol/Å was applied to the distance between the heme Fe and protonated nitrogen of dextromethorphan and MDMA to prevent large displacement of the substrate due to strong ionic interaction with heme propionate A.

Minimization, heating, and equilibration were run using Amber 14²²⁰ and production using nanoscale molecular dynamics (NAMD).²²¹ Residue-ligand interaction energies were calculated using NAMD (Table B1, B2, and B3). Hydrogen bond occupancy (i.e., fraction of time that the bond is present in each trajectory) and water density around the ligand and heme were calculated using the *cpptraj* module of Amber 2015.^{155, 222} The distance and angle cutoffs for the hydrogen bond are 3.0 Å and 135° (Table B4 and B5). The grid dimensions of the ligand + heme region used in the water density calculation were determined using the *bounds* command (grid spacing = 0.5 Å). The water density was visualized with PyMOL¹³³ using a contour level of 3.0 and mesh width of 0.5.

3.2.2.2 Free energy perturbation with Hamiltonian replica-exchange molecular dynamics (FEP/ λ -REMD)

In the FEP/ λ -REMD method²²³, the binding process is divided according to the thermodynamic cycle, wherein the bound ligand is decoupled from the enzyme (Eq. 1) and the solvated ligand is decoupled from bulk solution (Eq. 2). The free energy for the overall process (Eq. 3) is $\Delta G_b^\circ = \Delta G_2 - \Delta G_1$.



The ligand is decoupled from the binding pocket or bulk solution in three stages using the thermodynamic coupling parameters λ_{rep} , λ_{disp} , and $\lambda_{\text{elec}} \in [0,1]$ (Eqs. 4–6), giving the repulsive (ΔG_{rep}), dispersive (ΔG_{disp}), and electrostatic (ΔG_{elec}) contributions, respectively.

$$U(\lambda_{\text{rep}} = 0, \lambda_{\text{disp}} = 0, \lambda_{\text{elec}} = 0, \lambda_{\text{rstr}} = 1) \rightarrow U(\lambda_{\text{rep}} = 1, \lambda_{\text{disp}} = 0, \lambda_{\text{elec}} = 0, \lambda_{\text{rstr}} = 1) \quad (4)$$

$$U(\lambda_{\text{rep}} = 1, \lambda_{\text{disp}} = 0, \lambda_{\text{elec}} = 0, \lambda_{\text{rstr}} = 1) \rightarrow U(\lambda_{\text{rep}} = 1, \lambda_{\text{disp}} = 1, \lambda_{\text{elec}} = 0, \lambda_{\text{rstr}} = 1) \quad (5)$$

$$U(\lambda_{\text{rep}} = 1, \lambda_{\text{disp}} = 1, \lambda_{\text{elec}} = 0, \lambda_{\text{rstr}} = 1) \rightarrow U(\lambda_{\text{rep}} = 1, \lambda_{\text{disp}} = 1, \lambda_{\text{elec}} = 1, \lambda_{\text{rstr}} = 1) \quad (6)$$

For the decoupling of the bound ligand from the enzyme, an additional parameter, λ_{rstr} , is used to control the translational and orientational restraints (Eq. 7) and gives ΔG_{rstr} .

$$U(\lambda_{\text{rep}} = 1, \lambda_{\text{disp}} = 1, \lambda_{\text{elec}} = 1, \lambda_{\text{rstr}} = 1) \rightarrow U(\lambda_{\text{rep}} = 1, \lambda_{\text{disp}} = 1, \lambda_{\text{elec}} = 1, \lambda_{\text{rstr}} = 0) \quad (7)$$

The initial structure for the enzyme-substrate complex was taken from the 25-ns snapshot of the production MD simulation, while that for the solvated ligand was taken from the last point of the equilibration. The same simulation parameters outlined above were used except for the time step, which was reduced to 1 fs. Nonbonded forces were evaluated every step and full electrostatic forces every other step. A harmonic restraint was applied with a force constant of 10.0 kcal/mol/Å² to maintain the center-of-mass distance between the ligand and enzyme. 128 replicas (72 repulsive, 24 dispersive, and 32 electrostatic) were used with an exchange frequency of 1/100 steps. Sequential 0.1-ns simulations were performed until the calculation has converged (at least 2 ns), as evaluated from the fluctuation in the absolute free energy of the system over time (Figure B2). Repulsive, dispersive, and electrostatic contributions were determined using the Multistate Bennett Acceptance Ratio method.²²⁴ The average and standard deviation of the binding free energy were calculated using the last 1 ns of data.

3.3 Results and discussion

3.3.1 Experimental and calculated binding free energies

Substrate binding displaces the water molecule coordinated to the sixth position of the heme iron, resulting in a type I shift in the absorption spectrum, with the peak at approximately 390 nm in the difference spectra.²²⁵ The native substrate, palmitic acid, as well as diclofenac, naproxen, warfarin (the racemic mixture), lovastatin, and dextromethorphan exhibited a type I spectral shift upon binding (Figures 3.4 and 3.5). In the case of warfarin, the type I binding observed is presumably that of S-warfarin, as the R enantiomer is known to be inhibitory and would bind in a nonproductive manner that does not lead to metabolism.²²⁶

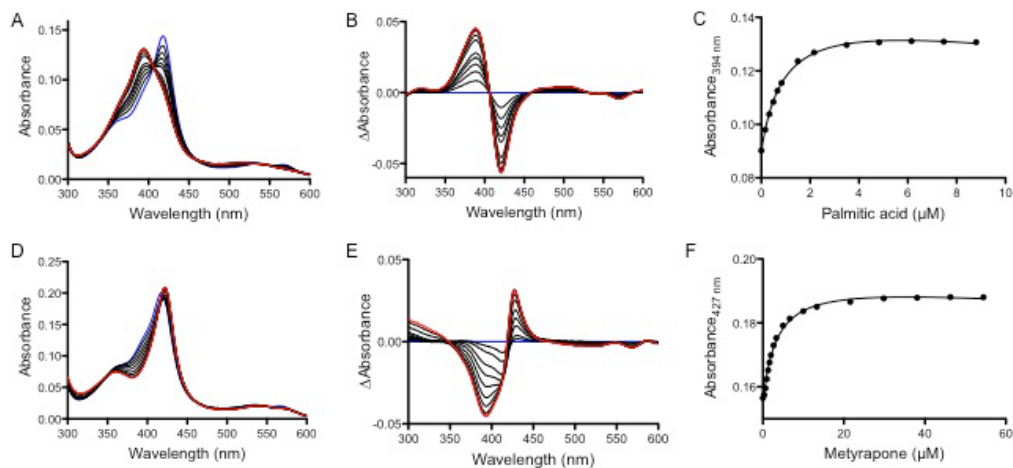


Figure 3.5 Spectral titration of PM BM3 with the native substrate palmitic acid (A–C) and inhibitor metyrapone (D–F). The red curve corresponds to the ligand-saturated enzyme, and the blue curve indicates the ligand-free enzyme. Palmitic acid exhibited a type I spectral shift, characterized by λ_{max} at 394 nm and trough around 420 nm (B), while metyrapone exhibited a type II spectral shift, characterized by λ_{max} at 427 nm and trough around 390 nm (E). The dissociation constant (K_d) was calculated by plotting the absorbance at λ_{max} as a function of ligand concentration (C, F). Plots were fit with a one-site total equation in GraphPad Prism. All titrations were done in a 1 cm quartz cuvette with 2 mL of 100 mM KPi, pH 7.4 buffer with protein at a concentration between 0.15 – 0.25 mg/ml. Concentrated compound was titrated in 1 – 5 μ L increments, with DMSO concentration kept below 1%.

Displacement of the water ligand changes the iron spin state from low to high spin and, consequently, alters the redox potential of the heme.²²⁷ The population of the high spin state for PM P450_{BM3} upon drug binding was lower than that observed with palmitic acid (Table 3.3), suggesting that the drug molecules possibly bind in the active site without displacing the water ligand in a fraction of the protein.²²⁸ A type II spectral shift occurred with metyrapone, nicotine, and cotinine, as evidenced by the absorption shift to about 430–455 nm (Figures 3.4 and 3.5).²²⁵ The type II shift indicates that these compounds directly coordinated the heme iron through the pyridine nitrogen. Generally, the type II shift is associated with enzyme inhibition; nevertheless, with nicotine or cotinine bound, the enzyme was active, as metabolism was observed using

the fluorescence-based 7-ethoxyresorufin-O-deethylase (EROD) activity assay (Figure 3.6).¹²³

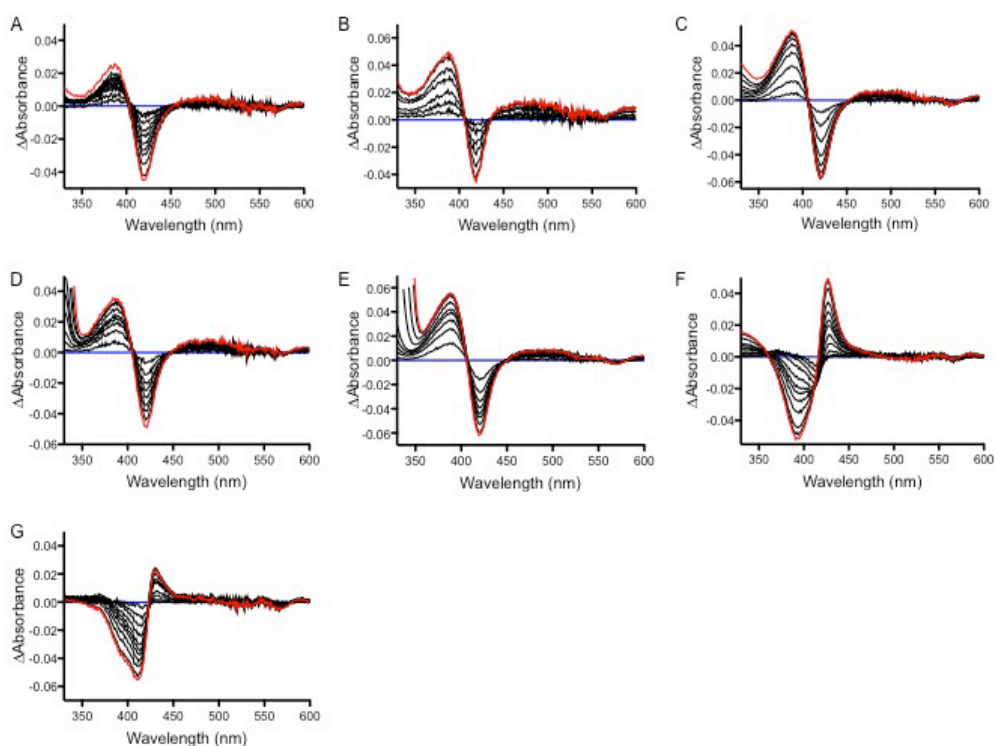


Figure 3.6 Difference spectra of all compounds bound to PM P450_{BM3} studied experimentally. The blue line is PM P450_{BM3} in which no compound is present, and the red line is fully saturated. (A) Dextromethorphan, (B) diclofenac, (C) lovastatin, (D) naproxen, and (E) racemic warfarin exhibit a type I spectral shift. (F) Cotinine and (G) nicotine exhibit a type II spectral shift. All titrations were done in a 1 cm quartz cuvette in 2 mL of 100 mM KPi pH 7.4 buffer at RT. Protein was kept at a concentration between 0.15 – 0.25 mg/mL. Concentrated compound was titrated in 1 – 5 μ L increments, with DMSO concentration kept below 1%.

The binding affinity of various drug molecules for PM P450_{BM3} was determined upon titrating small molecules and quantifying the change in absorption to obtain their K_d values. Based on predicted titration curves, diclofenac, naproxen, and warfarin are acidic; dextromethorphan and nicotine are basic; and cotinine, lovastatin, and metyrapone are neutral at physiological pH (Table B1). All substrates have negative ΔG_b° , indicating that binding to PM P450_{BM3} is stable, regardless of the type of drug

(acidic, basic, or neutral) (Table 3.3). Moreover, the binding affinities of naproxen, warfarin, dextromethorphan, and lovastatin are comparable to that of palmitic acid. Cotinine was the weakest binder, as indicated by the largest K_d value ($415 \pm 11 \mu\text{M}$), about 20x higher than that of nicotine ($23.5 \pm 6.3 \mu\text{M}$). The two molecules have the same ring systems but, unlike nicotine, cotinine has an additional carbonyl group and is neutral. The binding free energies calculated using FEP/ λ -REMD agree with experimental data for diclofenac, lovastatin, and dextromethorphan (Table 3.3). *S*-warfarin has a six-fold higher affinity than its enantiomer, and the calculated ΔG_b° is closer to the experimental value for the racemic mixture. On the other hand, the calculated ΔG_b° of naproxen is much more negative than the experimental value, possibly due to overestimation of the electrostatic contribution. As nicotine and cotinine are subject to metabolism by P450_{BM3}, the productive binding modes leading to metabolism were modeled instead of the inhibitory type II binding mode indicated by the absorbance spectra. Cotinine was predicted to bind with higher affinity than its parent compound with this orientation, unlike the case observed via spectroscopic titration determined for the type II binding mode. The ΔG_b° of the basic substrates, MDMA and astemizole, were also calculated to compare the free energies of different binding poses. The binding poses leading to N- and O-dealkylation have comparable ΔG_b° . A much more positive ΔG_b° was obtained when astemizole is positioned for C–H hydroxylation at C6.

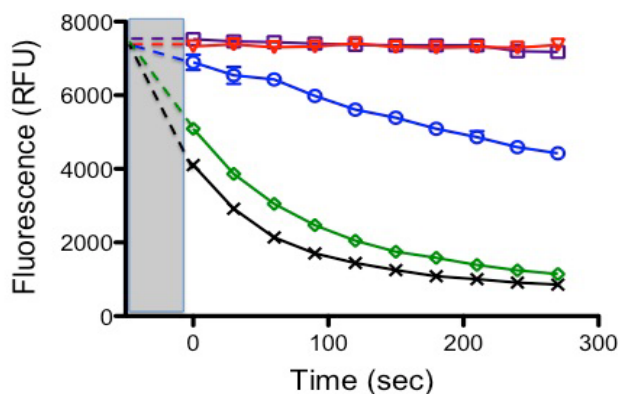


Figure 3.7 A 7-ethoxyresorufin-O-deethylase (EROD) activity assay was performed to determine if compounds that induced a type II spectral shift efficiently inhibited metabolism of the fluorescent substrate. PM P450_{BM3} (2.5 μ M in 1x PBS pH 7.5 buffer); fluorescence was monitored by excitation at 535 nm and emission at 595 nm. Saturating concentrations of compounds were incubated with protein for 5 min before 5 mM of 7-ethoxyresorufin was added, followed by 5 min incubation before H₂O₂ was added. The gray box indicates the dead time of the instrument, and the dashed lines are projected emissions during that time (approximately 50 seconds). The black crosses indicate metabolism of 7-ethoxyresorufin when PM P450_{BM3} was not inhibited. In contrast, the red triangles indicate the response when 7-ethoxyresorufin is not metabolized. Metyrapone-bound PM P450_{BM3} (purple squares) was fully inhibited, whereas when cotinine was bound (green diamonds), activity was barely impacted. Interestingly, nicotine (blue circles) had an inhibitory effect on 7-ethoxyresorufin metabolism, but activity was still observed.

The repulsive, electrostatic, and dispersive energy contributions are illustrated in Figure B3. The repulsive contribution is unfavorable (positive net energy) for the large ligands, astemizole, *S*-warfarin, and lovastatin, which could be attributed to expulsion of water and displacement of residues in the active site upon insertion of the ligand.²²⁹ On the other hand, smaller ligands, such as metyrapone, nicotine, and cotinine, have slightly favorable repulsive contribution since their small size allows binding without causing steric clashes. As expected, the electrostatic contribution generally become unfavorable as the ligand moves from bulk solution to the hydrophobic active site because of the loss of ligand-solvent hydrogen bonding interactions.²²⁹ Only the two acidic substrates, naproxen and *S*-warfarin, have negative

net electrostatic energies. Thus, the binding of nonnative substrates in PM is mainly facilitated by dispersion interactions. This contribution correlates with molecular size and compensates for the unfavorable repulsive contribution, particularly in the binding of astemizole and lovastatin.

Table 3.3 High spin fractions, dissociation constants (K_d), and binding free energies (ΔG_b) of palmitic acid and various drug molecules in PM BM3. Theoretical values calculated by I. Geronimo.

Substrate	%High spin	K_d (μM)	ΔG_b (kcal/mol)	
			Experimental	Theoretical
palmitic acid	94 ± 10	1.3 ± 0.9	-8.1 ± 0.4	-
diclofenac	83 ± 4	64.9 ± 3.9	-5.7 ± 0.1	-4.95 ± 0.62
naproxen	80 ± 2	4.6 ± 2.9	-7.4 ± 0.4	-15.20 ± 0.77
<i>S</i> -warfarin	75 ± 3	0.7 ± 0.4	-8.4 ± 0.3	-11.44 ± 0.68
<i>R</i> -warfarin				-1.84 ± 0.68
lovastatin	77 ± 3	3.3 ± 1.5	-7.5 ± 0.3	-6.15 ± 0.78
dextromethorphan	74 ± 5	3.7 ± 1.2	-7.4 ± 0.2	-6.89 ± 0.64
MDMA	-	-	-	-6.76 ± 0.57^a
				-6.21 ± 0.42^b
astemizole	-	-	-	-10.68 ± 0.91^a
				-8.57 ± 0.88^b
				-3.17 ± 0.53^c
nicotine ^d	-	23.5 ± 6.3	-6.3 ± 0.2	-4.60 ± 0.66^e
cotinine ^d	-	415 ± 11	-4.6 ± 0.1	-7.07 ± 0.60^e
metyrapone ^d	-	3.6 ± 0.6	-7.4 ± 0.1	-9.09 ± 0.41

^a Positioned for N-dealkylation. ^b Positioned for O-dealkylation. ^c Positioned for C–H hydroxylation. ^d Type II binding mode. ^e Calculated using productive binding mode.

3.3.2 Protein-ligand interactions in the PM BM3 active site

Residues that facilitate the binding of nonnative substrates were identified from analysis of the MD trajectories. The calculated average structures of the

different enzyme-substrate complexes are shown in Figures 3.7, 3.8, and 3.9. The discussion of the different drug molecules is divided below by the human P450s primarily responsible for their metabolism.

3.3.2.1 CYP2C9 substrates and inhibitors

CYP2C9 metabolizes ~15% of clinical drugs and exhibits selectivity toward lipophilic anions, including the NSAIDs diclofenac and naproxen and anticoagulant *S*-warfarin.²³⁰ Diclofenac yields 4'-hydroxydiclofenac upon oxidation by CYP2C9²³¹; this metabolite was also obtained using P450_{BM3} variants containing some or all of the mutations found in PM (e.g., RP/FV/EV¹⁶⁶, M11¹⁹⁸, and MT35¹²⁷, Table 3.1). When bound to the PM P450_{BM3} binding site, diclofenac has hydrophobic interactions with L75, V87, L437, and T438 (Figure 3.7, Table B2). Docking calculations predicted that the carboxylate group is hydrogen bonded to T438; however, the substrate changed position after ~12 ns of the simulation to form a hydrogen bond with S72 (Table B5). Both orientations place the C4' atom above the heme iron, though the orientation with the S72 hydrogen bond is presumably more stable. Naproxen undergoes O-demethylation by CYP2C9 to form desmethylnaproxen.²³² The RP/FV/EV variant also metabolized naproxen but at a lower conversion rate (58%) compared to diclofenac (91%).¹⁶⁶ The naproxen hydrophobic contacts in PM are L75, V87, and A330 (Figure 3.7, Table B2.). As in the diclofenac complex, the carboxylate group faces the substrate channel entrance and forms not only hydrogen bonds with the hydroxyl group and backbone nitrogen of S72 and backbone nitrogen of S332, but also a salt bridge with K69 (Table B5). This facilitates a binding orientation that positions the methoxy group over the heme for O-demethylation.

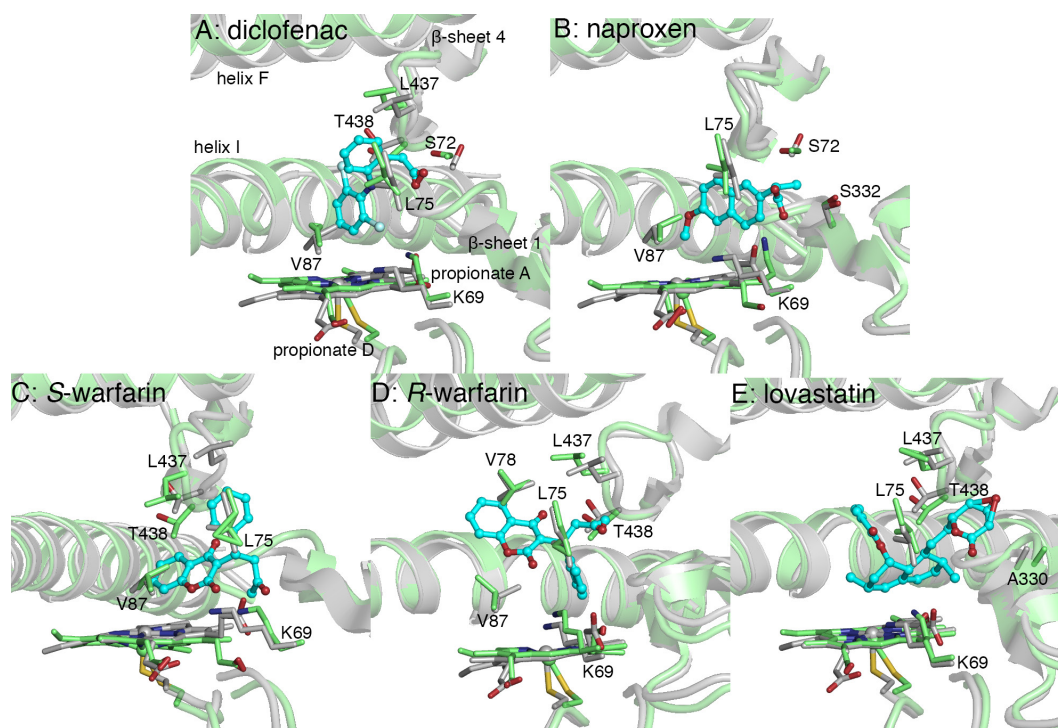


Figure 3.8 MD-averaged structures (green) superimposed on the PM-palmitic acid crystal structure (PDB ID: 4ZFB¹, gray). Naproxen is positioned for O-dealkylation, while diclofenac, S-warfarin, R-warfarin, and lovastatin are positioned for C–H hydroxylation at C4', C7, C4', and C6, respectively. MD simulations done by I. Geronimo.

S-warfarin is an acidic molecule under physiological conditions ($pK_a = 4.94$) due to the resonance stabilization of the anion and ketone-enol tautomerization that results in delocalization of charge between O2 and O4 of the benzopyran ring. It is hydroxylated at C7 by CYP2C9.²³³ In PM, it is positioned for reaction at C7 due to hydrophobic interaction primarily with L75, V87, and L437 (Figure 3.7, Table B2), while the oxo substituent in the benzopyran ring also forms a hydrogen bond with K69 (Table B5). There was no interaction with S72. The less potent R-warfarin is known to competitively inhibit the metabolism of its enantiomer.²²⁶ It is positioned for C4' attack in PM, which will yield the observed CYP2C9 product.²¹⁷ Unlike its enantiomer, R-warfarin does not form hydrogen bonds with substrate channel residues; its interactions

are primarily hydrophobic, specifically with L75, V78, L437, and T438 (Figure 3.7, Table B2).

Statins (or 3-hydroxy-3-methyl-glutaryl-CoA reductase inhibitors) such as lovastatin are substrates of CYP3A4 but are competitive inhibitors themselves of CYP2C9.²³⁴ Oxidation of lovastatin can occur at C6 or C3²³⁵, but only the hydroxylated product, 6 β -hydroxy lovastatin, and oxidized product, 6-exomethylene lovastatin, were obtained using PM/E143G and PM/E143G/E64G variants.¹⁶³ Unlike the other drugs discussed in this section, lovastatin is neutral at physiological pH. Its hydrophobic contacts in PM include L75, A330, L437, and T438 (Figure 3.7, Table B2). Hydrogen bonding of the hydroxyl substituent in the lactone ring with S72 was short lived (~22 ns), as it eventually formed interactions with solvent molecules. These interactions were also observed in the shorter (5 ns) MD simulations of lovastatin complexes of PM/E143G and PM/E143G/E64G.¹⁶³ This suggest that this hydrogen bonding interaction may not play a significant role in defining ligand binding orientation or affinity.

The MD simulations suggest that, for acidic drug molecules, residues S72 in helix B' and K69 in β -sheet 1 in P450_{BM3} generally play a role in substrate recognition and product regiospecificity, analogous to R108 in CYP2C9.²³⁶ The crystal structure of CYP2C9 in complex with a similar substrate, flurbiprofen (PDB ID: 1R9O²³⁶), has the carboxylate group buried within the active site cavity and held by a salt bridge with R108, which is located in the B–C loop (equivalent to helix B' in P450_{BM3}). Unfortunately, the crystal structure of *S*-warfarin in complex with CYP2C9 (PDB ID: 1OG5²³³) provides no information on the active site residues critical to the binding of this drug class, because the substrate is bound in a nonproductive position (C7 is more than 10 Å from the oxygen binding site). The interactions with either S72 or K69

identified by this current simulation would account for the favorable net electrostatic energy that contributes to the negative ΔG_b° for naproxen and *S*-warfarin binding in PM (Figure B3).

3.3.2.2 CYP2D6 substrates

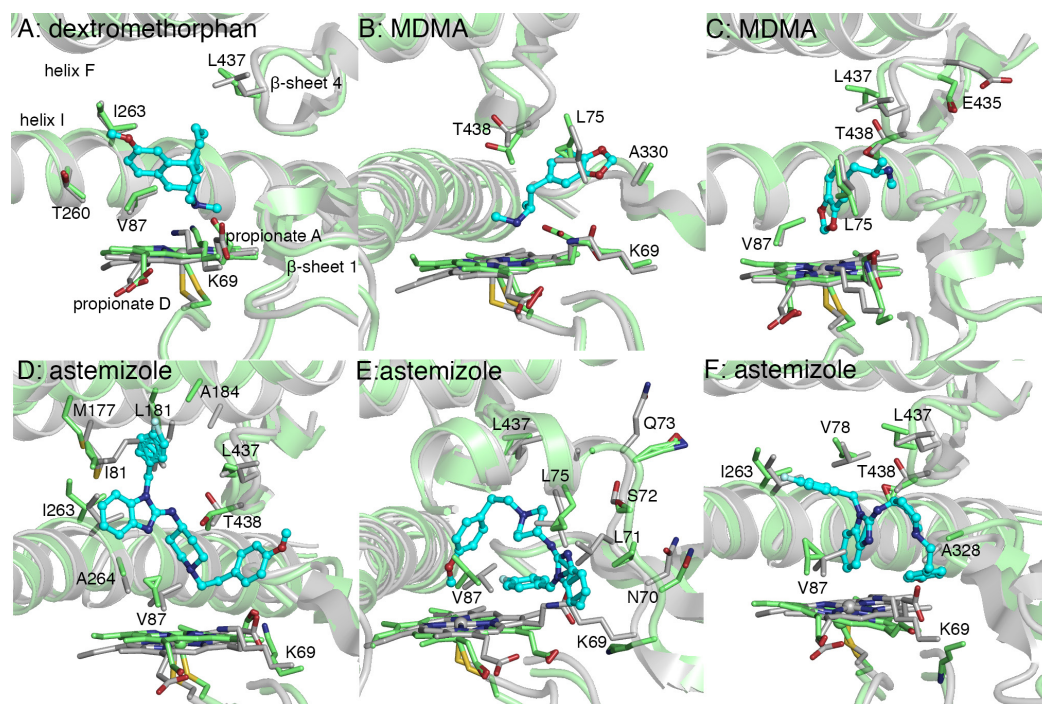


Figure 3.9 MD-averaged structures (green) superimposed on the PM-palmitic acid crystal structure (PDB ID: 4ZFB¹, gray). The substrates are positioned for N-dealkylation in *A*, *B*, and *D*, O-dealkylation in *C* and *E*, and C–H hydroxylation (C6) in *F*. MD simulations done by I. Geronimo.

CYP2D6 is responsible for the metabolism of ~25% of clinical drugs despite constituting <2% of hepatic CYPs.²³⁷ Typical substrates, such as antihistamines and amphetamines, contain a protonated basic nitrogen at physiological pH, and planar aromatic ring.^{237, 238} The major pathway for metabolism for these classes of molecules is O-dealkylation.²³⁹⁻²⁴¹ Two negatively charged residues in the active site, E216 and D301, are responsible for substrate specificity and product regioselectivity.^{242, 243}

In the absence of such residues in the P450_{BM3} active site, the protonated nitrogen of dextromethorphan, MDMA, and astemizole forms an ionic interaction with heme propionate A. This positions the substrates for N-dealkylation, a reaction mainly catalyzed by a different human P450, CYP3A4²⁴⁴; N-demethylation is the second main metabolic pathway for these three molecules. Experiments confirm that 3-methoxymorphinan and 3,4-methylenedioxyamphetamine are the major metabolites for dextromethorphan and MDMA, respectively, from oxidation by P450_{BM3} variants containing some or all of the PM substitutions such as M01, M02, and M05 (Table 3.1).¹²⁵ The N-dealkylation product of astemizole, norastemizole, is a minor product of CYP3A4 metabolism^{241, 245} and has only been obtained so far using chimeras of P450_{BM3} with other enzymes from the CYP102A subfamily.¹⁹⁶ Hydrophobic contacts in the active site are V87, T260, I263, and L437 for dextromethorphan; L75, A330, and L437 for MDMA; and V87, L181, I263, A264, L437, and T438 for astemizole (Figure 3.8, Table B3). A pronounced structural rearrangement was observed in the case of astemizole; helix F (M177, L181, A184) moved away from the protein core to accommodate the fluorophenyl ring. This would also account for the large repulsive contribution to the binding free energy (Figure B3). A suitable orientation for N-demethylation was not observed in the simulation.

The substrate-binding pose leading to O-dealkylation was found for MDMA and astemizole (Figure 3.8). The protonated nitrogen of MDMA forms a hydrogen bond with the backbone oxygen of L437 (Table B5), bringing it closer to E435 for ionic interaction. On the other hand, the benzimidazole ring of astemizole extends toward the loop connecting β -sheet 1-5 and helix B', causing a slight distortion in this region (residues 69–74) and breaking the heme propionate A-K69 salt bridge at different points during the simulation. MDMA forms favorable hydrophobic contacts with L75,

V87, L437, and T438, and astemizole mainly with L75, V87, and L437 (Table B3). In modeling the formation of another metabolite obtained with CYP2D6, 6-hydroxyastemizole²⁴¹, astemizole is forced into a folded conformation within the PM active site. The methoxyphenyl ring displaced the entire β -sheet 1, causing the heme propionate A-K69 salt bridge to break as well (Figure 3.8). Hydrophobic contacts of astemizole in this binding pose include V78, V87, I263, A328, L437, and T438 (Table B3). CYP2D6 metabolites of astemizole (desmethyastemizole and 6-hydroxyastemizole; note that these reactions occur at aromatic rings at opposite ends of the large drug molecule) have been obtained with the 9-10A/A78F and 9-10A/A78F/A82G/A328F variants of P450_{BM3} (Table 3.1).⁵ The A78F and A82G substitutions, presumably conferred greater flexibility to helix B', allowing the enzyme to easily accept this large drug molecule in different binding orientations without causing the disruption of structure observed in simulations of PM.

3.3.2.3 CYP2A6 substrates.

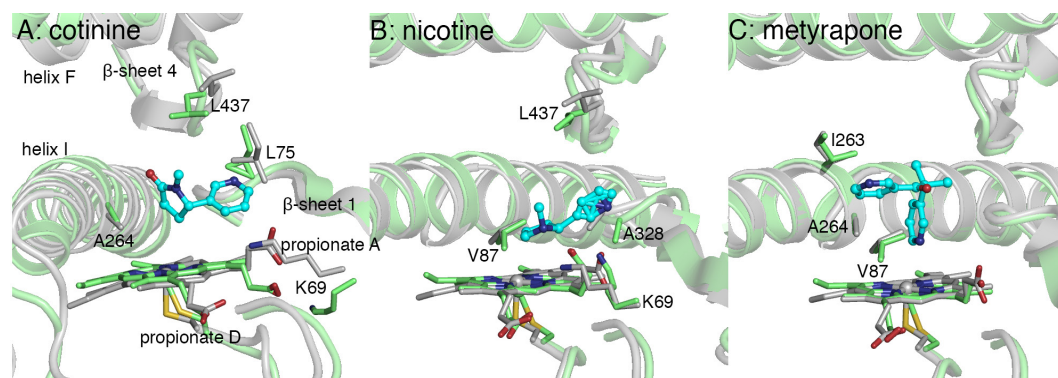


Figure 3.10 MD-averaged structures (green) of superimposed on the PM-palmitic acid crystal structure (PDB ID: 4ZFB¹, gray). Cotinine and nicotine are positioned for oxidation at C5' and C3'/C4', respectively. Metyrapone acts as an inhibitor by forming a covalent bond with the heme iron. MD simulation done by I. Geronimo.

CYP2A6 has relatively narrow substrate specificity but has gained interest due to its involvement in the metabolism of toxic and procarcinogenic compounds.²⁴⁶ The

crystal structure of the nicotine complex of CYP2A6 (PDB ID: 4EJJ²⁴⁷) indicates that F209 and I300 play a role in substrate orientation within the active site. However, nicotine does not form hydrogen bond interactions with any active site residues; its pyridine nitrogen is too far from N297, a conserved residue in CYP2A enzymes. In the PM P450_{BM3} active site, the protonated nitrogen of nicotine forms an ionic interaction with heme propionate A (Figure 3.9), similar to the CYP2D6 substrates. Significant hydrophobic contacts of nicotine include V87, A328, and L437 (Table B4). The major metabolite of nicotine, cotinine, is positioned for 3'- or 4'-hydroxylation in the active site (Figure 3.9). Cotinine is known to be further metabolized to trans-3'-hydroxycotinine, the major urinary metabolite of nicotine, by CYP2A6 and CYP2A13.^{248, 249} In the simulation, cotinine is held by hydrophobic interactions with L75, A264, and L437 (Table B4), which orient it for reaction. Unlike nicotine and cotinine, the P450 inhibitor metyrapone, which also contains a pyridine ring, interacts primarily through formation of a coordinative bond to the heme iron. This binding mode is consistent with its role as a P450 inhibitor specifically of 11 β -hydroxylase²⁵⁰ though off-target affects are known.^{251, 252} Metyrapone is not subject to oxidative metabolism by P450s; rather, it undergoes reductive metabolism to form the alcohol, metyrapole, before glucuronide conjugation.²⁵³

3.3.3 Factors contributing to uncoupling.

Low turnover number and coupling efficiency are often observed with oxidation of nonnative substrates by P450_{BM3} variants. This may be attributed to catalytic uncoupling.^{33, 34} The two major pathways for this alternative reaction pathway are (1) protonation of the proximal oxygen in the ferric hydroperoxide complex to release H₂O₂ (peroxide uncoupling) and (2) two-electron reduction and deprotonation of oxygen in

the oxo-ferryl porphyrin radical intermediate (Compound I) to yield a second water molecule (oxidase uncoupling; Figure 3.1).²⁰⁰

An experimental study of the mechanisms of the different uncoupling modes in P450_{cam} indicates that excess water in the active site plays an important role in both pathways by acting as a proton source. Moreover, for peroxide uncoupling, charge separation at Fe during dissociation of HOO⁻ is favored by the increased polarity of the environment. Water is also thought to destabilize the ferric hydroperoxide complex by disrupting its putative hydrogen bond with a threonine residue in the active site (T268 in P450_{BM3}).²⁵⁴ Figure 3.10 shows high water density in the substrate channel when dextromethorphan, MDMA, astemizole, diclofenac, or warfarin is bound, in contrast to when palmitic acid is bound (Figure B4). This may be attributed to the positioning of hydrophilic groups of these molecules deep within the cavity. Moreover, high water density near T268, where the hydroperoxo ligand would be bound, was observed when dextromethorphan, MDMA, and astemizole are oriented for N-dealkylation. This would be consistent with the relatively low fraction of high-spin protein found with the PM-dextromethorphan complex (Table 3.3), which indicates that there is room for excess water around the heme iron even in the presence of this large substrate.

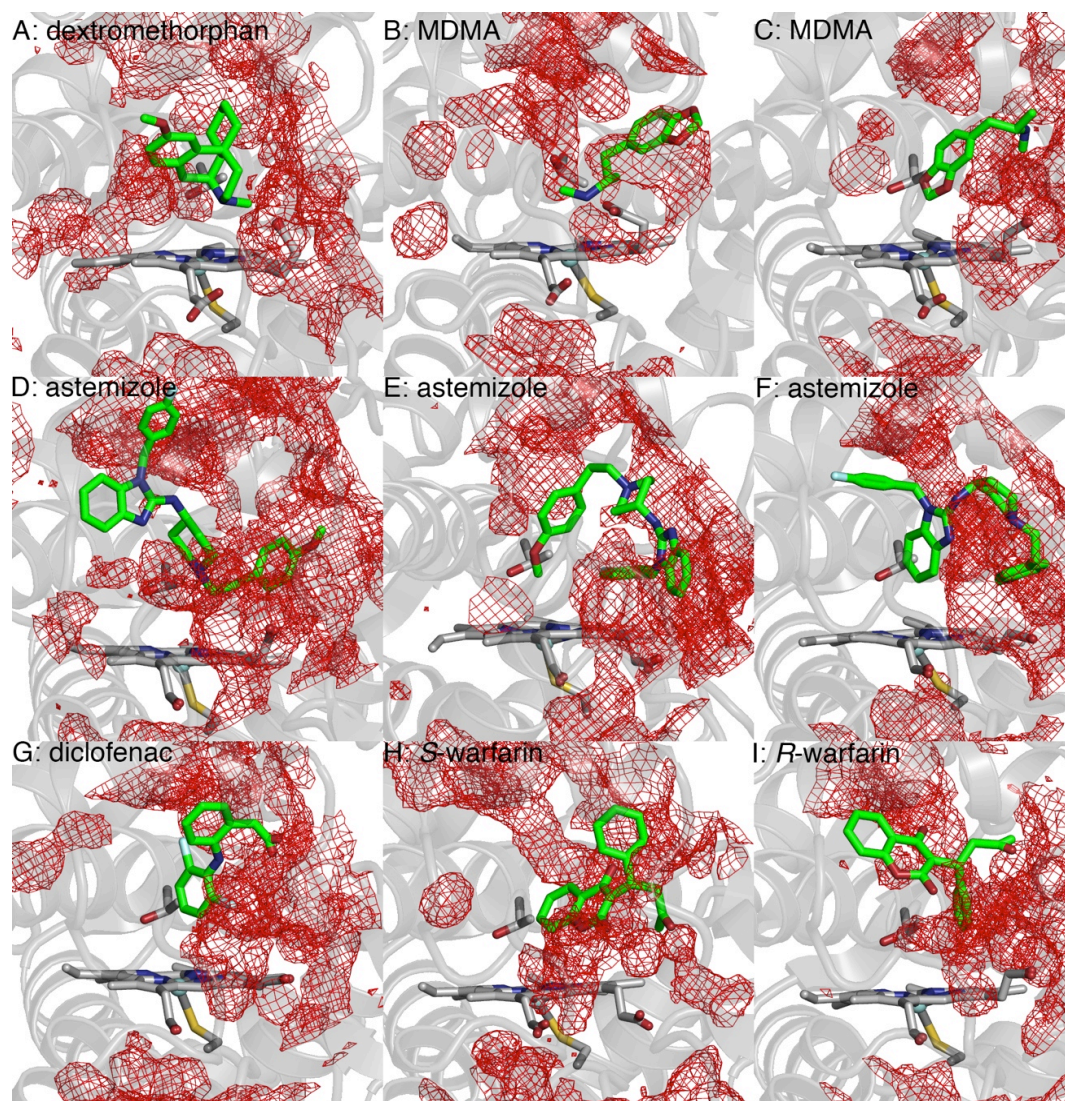


Figure 3.11 Water density at the PM P450_{BM3} substrate channel, with the reference structure averaged from the MD simulation. MDMA is positioned for N- and O-dealkylation in *B* and *C*. Astemizole is positioned for N- and O-dealkylation in *D* and *E*, and C–H hydroxylation in *F*. T268, located at the distal side of the heme (helix I) and believed to play a role in proton delivery and oxygen activation, is also shown. Water density is relatively lower in the presence of palmitic acid, naproxen, lovastatin, nicotine, and cotinine (Figure B4). MD simulation done by I. Geronimo.

In oxidase uncoupling, electron transfer to Compound I competes with substrate oxidation. This likely occurs if the substrate is too mobile and/or the reacting atom is too distant from the oxidizing species, a consequence associated with lack of complementarity within the active site.⁹³ The MD-averaged structures show that the

shape of the PM P450_{BM3} active site, meant to accommodate long-chain fatty acids, is essentially unaltered in the presence of drug molecules (Figures 3.7–3.9). Thus, small substrates or those that do not form stable ionic/hydrogen bond interactions with active site residues would be highly mobile during the simulations, as was the case with astemizole, diclofenac, lovastatin, cotinine, and *R*-warfarin (Figure B5).

Reducing substrate mobility and water access to the active site can be achieved by substituting smaller active site residues with leucine, isoleucine, methionine, or phenylalanine.²⁵⁴ β -sheet 1-4 (residues 329–336) offers a promising mutation site for P450_{BM3} because substitution with large residues would not hinder substrate access to the oxidizing heme intermediate. For example, variants containing tryptophan at position 330 within β -sheet 1-4 had high conversion rates for chlorzoxazone and lidocaine.¹⁶⁶ On the other hand, the A330P mutation (PDB ID: 3M4V²⁰⁸) was found to reduce the size of the cavity by displacing the side chain of the adjacent P329 into the active site. A330P-containing variants exhibited improved coupling efficiencies for the oxidation of small alkanes and aromatic compounds²⁰⁸ and high conversion rates for naproxen, chlorzoxazone, and amitriptyline.¹⁶⁶ The key is combining structural flexibility to allow for promiscuity with sufficient water exclusion to increase catalytic efficiency.

3.3.4 Heme interactions affecting oxidizing ability.

Heme propionate groups not only play the structural role of anchoring the heme, but may also be involved in regulating electrostatic interactions that are key to the catalytic reaction.^{255, 256} Propionate A forms a salt bridge with K69, while propionate D forms a salt bridge with R398 and a hydrogen bond with W96 in P450_{BM3}. The binding of acidic and basic ligands, but not neutral ligands, disrupted these interactions. With

dextromethorphan, MDMA, and nicotine oriented for N-dealkylation, propionate A bent toward the active site (dihedral angle of $\approx 60^\circ$) during the simulations (Figures 3.8, 3.9 and B6), while maintaining interaction with K69 (Table B6). Propionate bending also occurred in the M01, M02, and M05 variants (substrate-free and in complex with dextromethorphan and MDMA) based on Resonance Raman and MD simulations.¹²⁸ Hydrogen bonding between propionate A and the protonated nitrogen was observed for nicotine and MDMA, which would facilitate electron transfer from the substrate to the porphyrin π -cation radical and then to Fe(IV) of Compound I.²⁵⁶ Thus, basic functional groups that can interact directly with heme propionates do not seem to jeopardize catalytic reactivity.

In contrast, as discussed earlier, the acidic drugs *S*-warfarin and naproxen interact with K69 (Figure 3.7), thus competing with propionate A (Table B5) for interaction with this residue. In the PM-naproxen complex, the interaction with K69 was broken during the simulation and propionate A, instead, forms a hydrogen bond with the backbone nitrogen of N395 (Table B6). This may reduce the oxidizing ability of Compound I, which depends on the spin density localized on the porphyrin ring.²⁵⁶ Density functional theory calculations indicated that the salt bridge formed by heme propionates with Arg or Lys stabilizes the cationic porphyrin radical by weakening charge donation from the carboxylate group.^{255, 257} Interaction with K69 could explain the low activity of most P450_{BM3} variants toward acidic substrates.^{122, 166} Introducing another hydrogen-bond-forming residue in the active site to interact with acidic substrates would therefore improve activity, as appears to be the case with the MT35 variant (Table 3.1), which contains the L437S substitution.¹²⁷

3.4 Conclusions

P450_{BM3} variants are capable of metabolizing a wide variety of nonnative substrates, and have been the subject of extensive protein engineering efforts. The resulting enzymes typically contain mutations far from the active site that increase the flexibility of the lid domain and SRS without significantly altering the active site architecture. In order to better understand the features that regulate binding, key molecular interactions that impact substrate positioning, and factors that impact catalytic efficiencies, we performed an investigation combining experimental and computational analyses of diverse small molecules that bind to P450_{BM3}.

Structurally different and highly polar human P450 substrates and inhibitors were chosen for the analysis. These molecules contain acidic, basic, and polar groups, aromatic and aliphatic ring systems, and range in molecular weight from 162.2 to 458.6 AMU (Table 3.2). Despite the chemical diversity, all molecules nevertheless exhibit affinity for PM P450_{BM3} and bind with negative ΔG_b° primarily due to dispersion interactions, specifically with L75 in helix B', I263 in helix I, L437 and T438 in β -sheet 4, A328, and V87 (Figure 3.2). In addition, acidic drug molecules form electrostatic interactions with S72 in helix B' and K69 in β -sheet 1, and basic drug molecules engage with heme propionate A. However, the lack of structural and electrostatic complementarity between nonnative substrates and the active site would have an impact on the turnover number and coupling efficiency of P450_{BM3} variants. The resulting increase in substrate mobility and water access to the active site could lead to uncoupling reactions. Substrate interaction with K69, which forms an important salt bridge with the heme, could lessen the oxidizing ability of the enzyme. Protein engineering efforts to develop more active and efficient P450_{BM3} variants should therefore focus on reducing these effects.

CHAPTER 4. CORRELATIONS BETWEEN THE PROMISCUITY OF CYTOCHROME P450_{BM3} VARIANTS AND OXIDATION STATE DEPENDENT STABILITY

4.1 Introduction

Cytochrome P450s (CYPs) are cysteine-ligated heme monooxygenases that incorporate molecular oxygen into C-H bonds. In humans, CYPs play a fundamental role in steroidogenesis and xenobiotic metabolism, and exhibit some variation in selectivity for their substrates. CYPs active in xenobiotic metabolism interact with a wide variety of diverse substrates. The prime example of this is CYP3A4, which metabolizes approximately 50% of known drugs.^{65, 258} This is facilitated by the fact that CYP3A4 has a highly flexible conformation in which diverse substrates are able to reach the deeply buried active site.⁶⁷ In comparison, aromatase (CYP19A1) plays a key role in estrogen synthesis, and is a very selective enzyme that only converts androstenedione and testosterone into estrone and estradiol respectively.²⁵⁹ Thus, while CYPs are similar in global structure and utilize the same catalytic cycle, they have evolved to range from selective to promiscuous based on their function.

In order to investigate properties related to promiscuity, Cytochrome P450_{BM3} (CYP102A1), a bacterial enzyme isolated from *Bacillus megaterium*, was used as a model system. P450_{BM3} is a good candidate to examine a variety of questions relating to P450 behavior as it is soluble and can be easily expressed and purified. Most importantly for investigating how enzyme promiscuity either arises or the impact it has on a protein is the range of selectivity that can be incorporated. Wild type P450_{BM3} (WT) is relatively selective, preferentially binding medium to long chain fatty acids. Five residues (R47L/F81I/F87V/L188Q/E267V, the “Pentuple mutant”, PM) can be made to the WT to

become more promiscuous, and able to interact with drug-like molecules similar to xenobiotic metabolizing CYPs.¹²⁸ Previous studies have documented that although the PM is more promiscuous, this comes at the cost of stability. We have shown that the global structure of the PM unfolds with a urea concentration midpoint of 2.7 ± 0.2 M compared to WT at 5.4 ± 0.5 M by pulse proteolysis.²⁶⁰ In addition, this change in stability can be significantly attenuated by the presence of native and non-native substrates and inhibitors.²⁶⁰

As a follow-up study, we are interested in determining how the iron oxidation state impacts enzyme stability, and if correlations can be made to the overall selectivity of the enzyme. This is of particular importance as it was shown that both Fe(III) and Fe(II) states are present in cells without substrate bound for P450cam, P450cin, and five human xenobiotic- metabolizing CYPs.¹⁴ This finding contradicts the established model, which presupposes that CYPs are in a low-spin (LS) Fe(III) water bound state at rest, and do not become reduced until after substrate has bound and the enzyme is converted to the high spin state. It would be expected that a population of enzyme in the ferrous state in the absence of substrate would lead to an increased rate of uncoupled catalysis, thus increasing reactive oxygen species (ROS). While this study did not find a decrease in P450 content as a result of ROS production,¹⁴ they did not investigate the stability of the enzymes trapped in the Fe(III) or Fe(II) states.

Several studies have investigated the stability of Cytochrome *c* (cyt *c*) as a function of iron oxidation state.²⁶¹⁻²⁶⁵ Cyt *c* is similar to CYPs as it is a heme enzyme, though it is bis-ligated to histidine and methionine. Unlike CYPs, whose main function is to catalyze insertion of oxygen into a substrate, cyt *c*'s main role is electron transfer. The stability of

cyt *c* is higher in the ferrous state (C_m of ~ 5 M guanidium hydrochloride, as determined by tryptophan fluorescence) than the ferric state (C_m of ~ 2.5 M guanidium hydrochloride).²⁶⁴ Interestingly, when the methionine-heme ligation was broken and replaced with cysteine, this relationship inverted, so that the ferric state was more stable than the ferrous. This change in iron state stability was also accompanied by a dramatic decrease in the reduction potential (290 mV vs. -390 mV), indicating the ease of electron transfer from NAD(P)H.²⁶⁶ In theory, replacing the methionine-heme ligation to a cysteine should make cyt *c* more adept at catalysis rather than electron transfer.

We aim to discover the role of promiscuity in regulating the relationship between the ferrous and ferric states in CYPs. To do this, UV/Vis spectroscopy, circular dichroism (CD), and pulse proteolysis were used to probe active site, secondary structure, and global structure of the enzyme to achieve a comprehensive view of oxidation state. As CYPs play a vital role in health and exhibit potential biotechnical applications, understanding the relationship between promiscuity, oxidation state, and stability is essential. This is especially relevant for further understanding of how these enzymes function as well as how they differ from other heme-bound proteins.

4.2 Experimental procedures

4.2.1 Cloning and site-directed mutagenesis of P450_{BM3}

The heme domain (Thr 1 to Thr 463) of P450_{BM3} containing a C-terminal 6xHis tag was cloned into the pCWori vector. All point mutations were incorporated into the heme domain through site-directed mutagenesis using the Quikchange kit (Stratagene). The ligation mixture was transformed into Top10 competent cells and screened for ampicillin

resistance. Colonies were selected and grown in Luria Broth, followed by plasmid isolation and digestion with AgeI and BseRI. Plasmids containing the heme portion of the gene were sequenced for verification (Eurofins Genomics).

4.2.2 Expression and purification

P450_{BM3} variants were expressed in BL21(DE3) *E. coli* cells which were grown in 1 L Terrific Broth at 37°C while shaking at 180 rpm until an OD₆₀₀ of 0.7 to 0.8 was reached. Protein expression was induced upon addition of IPTG to a final concentration of 0.5 mM. Cells grew for another 20 h before harvested by centrifugation (Beckman Avanti™ J-25 I) at 2,975 xg and 4 °C. Cell pellets were stored at -80 °C for further use.

For purification, the cells were resuspended in lysis buffer (50 mM NaH₂PO₄, 300 mM NaCl, 10 mM imidazole, and 0.1 mM EDTA, pH 8.0) with 0.1 mM phenylmethylsulfonyl fluoride (PMSF) added. Afterwards, cells were lysed by sonication on ice for 15 min using a microtip (Branson Sonifier 250) with output control of 3 and duty cycle of 50%. This was followed by centrifugation at 20,000 xg for 1 h at 4 °C. The supernatant was decanted and passed through a 0.45 μM polytetrafluoroethylene syringe filter before being loaded onto a His-Trap column (GE Healthcare) equilibrated in Buffer A (50 mM NaH₂PO₄, 300 mM NaCl, 20 mM imidazole). Protein was eluted as the imidazole gradient gradually increased from 20 mM to 200 mM upon the addition of Buffer B (50 mM NaH₂PO₄, 300 mM NaCl, 200 mM imidazole) by an Äkta explorer. The protein containing fractions were collected based on absorbance at 420 nm and concentrated to approximately 2 ml using Amicon Ultracel-30K Millipore centrifugal units. Protein was then loaded onto a Hi-Pre 26/60 Sephacryl S200 HR column equilibrated in gel filtration buffer (20 mM Tris, 150 mM NaCl, pH 8.0). Fractions with a 420/280 absorbance ratio

>1.4 for WT, and >1.2 for F81I, I401P, and PM were concentrated to below 20 mg/ml. Co-binding was used to determine concentration.²⁶⁷ Glycerol was added to approximately 20%; aliquots were made, snap-frozen, and stored at -80 °C until use.

4.2.3 Pulse proteolysis

The pulse proteolysis procedure was adapted from work by Park and Marqusee.¹³⁷ The enzyme was diluted to 0.75 mg/ml in various concentrations of urea from 0 – 6.8 M made in pulse buffer (20 mM Tris, 10 mM CaCl₂, and 20 mM NaCl, pH 7.4). After a 2 h incubation at room temperature, 10 mg/ml thermolysin was added and vortexed. After 1 min, the reaction was stopped by addition of EDTA to a final concentration of 37 mM and samples were immediately placed on ice. β -laemmlli was added to each sample, which were subsequently placed in a hot block for 1 min at 95 °C. Denatured protein was then loaded and run on a 4-12% tris-glycine gel for 1 h at 120 volts. Gels were stained in Coomassie blue for approximately 2 h and left overnight in destain (45% water, 45% methanol, 10% acetic acid). The next day gels were imaged using a ChemiDoc™ MP with Image Quant software (Biorad). Concentration midpoint (C_m) values were determined using Graphpad Prism graphing software. Data was normalized to fraction folded and fit with either a sigmoidal or biphasic equation. For Fe(III)-4-cyanopyridine (CNPy) systems, substrate was added to enzyme before dilution in urea for approximately 5 min. Excess CNPy was also added to each urea concentration. For Fe(II)-CO systems, all buffer and urea was CO-saturated before use. Fresh dithionite at a concentration of 2 mM was added to enzyme before dilution and was also present in each urea sample. For Fe(II)-CNPy systems, enzyme was reduced with 2 mM dithionite and CNPy was immediately added. After a 5 min incubation reduced and bound enzyme was diluted in urea with excess dithionite and

CNPy added. All states were checked by UV/VIS to ensure they were in the proper state before the experiment was performed.

4.2.4 Circular dichroism (CD)

CD spectroscopy was performed to investigate the unfolding of protein secondary structure by following the signal at 222 nm. The protein was diluted to a concentration of 0.1 mg/ml in urea ranging from 0 - 6.8 M made in 100 mM KPi buffer, pH 7.4. After a 2 h incubation, spectra were obtained using a Jasco J-815 CD spectrometer. The settings were as follows: sensitivity – standard, bandwidth – 1.00 nm, D.I.T – 0.5 sec, measure range 260-200 nm, scanning speed – 50 nm/min, and 2 accumulations. Enzyme in various iron states was prepared as written in the pulse proteolysis section. Data was plotted using Graphpad Prism software. Ellipticity (mdeg) at 222 nm was plotted versus urea concentration, and a sigmoidal regression equation was applied to determine the C_m value.

4.2.5 UV/Vis spectroscopy

Absorbance spectra were taken to examine the direct consequences of unfolding on the heme environment. The protein was diluted to 0.15 mg/ml in varying concentration of urea from 0 – 6.8 M made in 100 mM KPi buffer, pH 7.4. After a 2 h incubation, absorbance spectra were obtained using an Agilent 8453 UV-visible spectrometer. Results were plotted using Graphpad Prism. To determine which wavelength experienced the greatest change as a result of unfolding, difference spectra were produced. The C_m value was found by plotting the normalized absorbance of λ_{max} versus urea concentration. For the various iron states studied, the enzyme was prepared as described for pulse proteolysis.

4.2.6 Determination of reduction potential

Reduction potentials of P450_{BM3} variants were estimated using a modified procedure from Ost et al.²⁶⁸ The enzyme was diluted in 100 mM KPi, pH 7.4 to 0.15 mg/ml in a 3 mL quartz cuvette. A few granules of dithionite were added to the cuvette followed by CNPy to saturation. An absorbance spectrum was taken once the enzyme was fully reduced and CNPy bound. Data was plotted using Graphpad Prism, with an emphasis on the metal-to-ligand charge transfer absorption band (MLCT) from 600-700 nm. The λ_{max} was determined in the MLCT region, and using the equation, $E_{\text{MLCT}} = (3.53 \times E_m) + 17,005 \text{ cm}^{-1}$,²⁶⁸ the reduction potential was estimated. Each experiment was performed in triplicate.

4.3 Results

4.3.1 Selectivity of P450_{BM3} can be modulated by strategic mutations.

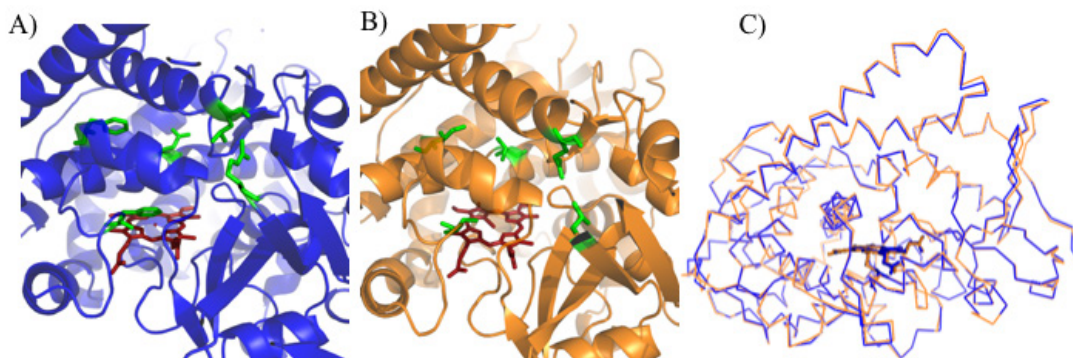


Figure 4.1 Crystal structures of the active site of A) WT (PDB ID: 4ZFA) and B) PM P450_{BM3} (PDB ID: 4ZF6). Residues highlighted by green denote location and orientation of mutations. A ribbon diagram of WT (blue) and PM (orange) overlaid is depicted in panel C) indicating a similarity in global structure.

For this study, four variants of P450_{BM3} were chosen that exhibit a range of promiscuity. This study includes the wild type (WT), F81I, I401P, and pentuple mutant (R47L, F81I, F87V, L188Q, E267V; PM), (Figure 4.1). The mutation in the first of these variants, F81I, is also present in PM. The residue is located in the B'-helix, and though the side chain is not directly in the active site, it is oriented to the interior, allowing for interactions with amino acids in the F-helix, specifically L181. According to van Vugt-Lussenburg et al., though the I81 mutation only has a subtle shift in position compared to F81, it subsequently changes the location of L181. This leads to a conformational change in the active site that impacts how the ligand fits into the hydrophobic interior.²⁶⁹ Additionally, a further study using MD simulations indicated that the F81I mutation shifts the B'-helix slightly further away from other helices in the interior, leading to a widening of the access channel to the active site.¹²⁸ It was also shown that inclusion of I81 to PM increases the rate of dextromethorphan and MDMA turnover by 3 to 5 fold.¹²⁸ Our examination of the F81I P450_{BM3} enzyme indicates that it has behavior similar to WT in regards to binding of substrates. Specifically, in that binding of several substrates (ie. metyrapone, Figure C1) is not observable by typical type I or II spectral shifts.

The I401P P450_{BM3} mutant was first published by Whitehouse et al. in 2009.²⁷⁰ Isoleucine is a hydrophobic residue located beside the cysteine proximally ligated to the Fe-heme. Though prolines are thought to be disruptive residues, for select heme-Cys ligated enzymes this position is naturally a proline.^{192, 193} Distinct changes are seen to the overall protein structure based on this single mutation (Figure C2 A). The most obvious change is the spin state of the heme in the resting state. Unlike WT P450_{BM3}, the I401P P450_{BM3} mutant was mostly in the high spin state¹⁵⁹, which is typically seen upon substrate

binding. In addition, a broad metal to ligand transition (MLCT) band appeared from 600 – 700 nm as shown in Figure C2. The I-helix experiences the impact of this mutation, with the positions of G265 and H266 being slightly altered. These changes lead to a loosening of contacts as they prevent intrahelical hydrogen bond formation.²⁷⁰ These structural changes lead to an enzyme that is in its catalytically active state in the *absence* of substrate, allowing it to avoid the conformational changes other P450_{BM3} variants must go through before catalysis can occur. It is not clear if the structure enjoys added flexibility, but if it does, this may be one of the reasons why I401P P450_{BM3} is able to turnover a more diverse substrate class than WT. The I401P P450_{BM3} mutant is able to metabolize a large class of substrates, such as fluorene, toluene, 3-methylpentane, and (+)- α -piene, but it has the same high reactivity as WT P450_{BM3}.^{270, 271} It was determined by GC/MS that oxidation of lauric acid by both the WT and I401P P450_{BM3} enzymes yielded three major products, where the ω -1, ω -2, or ω -3 carbon was hydroxylated at a ratio of approximately 30% each.²⁷⁰ This trend was also replicated with palmitic acid.²⁷¹

PM P450_{BM3} is an extremely promiscuous P450_{BM3} variant that is able to turnover drug-like molecules such as dextromethorphan,²⁶⁹ MDMA,²⁶⁹ amitriptyline,^{272, 273} and buspirone.^{272, 273} The decrease in selectivity for this variant is also accompanied by a decrease in stability as compared to WT P450_{BM3}, which can be attributed to the cumulative impact of the five mutations made to PM P450_{BM3}.²⁶⁰ As mentioned above, changing a larger hydrophobic residue to a smaller residue for the F81I mutation impacts hydrophobic contacts of the lid domain. The E267V and R47L mutations both eliminate salt bridges that provide important contributions to protein stability. When L188 is mutated to the polar glutamine residue, it causes a negative interaction with Q73, decreasing

stability. While these mutations decrease stability, their combination causes a closed conformation of the enzyme that increases its catalytic activity towards non-native substrates.

Table 4.1 Concentration midpoint (C_m) values of P450_{BM3} variants determined by UV/Vis spectroscopy.^a

	Fe(III)- H ₂ O	Fe(III)-CNPy	Fe(II)-CNPy ^b	Fe(II)-CO ^b
WT	4.0 ± 0.4, 5.6 ± 0.3 ^c	5.5 ± 0.1	4.2 ± 0.2 (426 nm) 4.9 ± 0.2 (445 nm)	3.0 ± 0.2, 5.6 ± 0.1 (420 nm) ^c 3.1 ± 0.1, 5.6 ± 0.1 (450 nm) ^c
F81I	5.3 ± 0.1	-	-	3.6 ± 0.1 (420 nm) 3.1 ± 0.1, 5.1 ± 0.2 (450 nm)
I401P	3.6 ± 0.1	-	-	3.6 ± 0.1 (420 nm) 3.4 ± 0.1, 5.1 ± 0.2 (450 nm)
PM	2.3 ± 0.2, 3.9 ± 0.2 ^c	3.1 ± 0.1	3.4 ± 0.1 (426 nm) 2.9 ± 0.1 (445 nm)	2.2 ± 0.1 (420 nm) 2.3 ± 0.1 (450 nm)

^a. All values are in molar urea. ^b. Two values are listed for ferrous states as two separate unfolding events occurred. ^c. Two values separated by a comma indicate biphasic unfolding.

4.3.2 Changes in active site stability are observed by UV/Vis spectroscopy.

UV/Vis spectroscopy is a robust technique to evaluate the protein environment around chromophores.²⁷⁴ As P450s have a heme porphyrin ligated to a cysteine thiol, absorbance methods can be used to examine how the active site environment is perturbed by various factors, including effects on the distal and proximal faces, along with hydrogen bonding interactions with the heme propionates. Conformational rearrangements are

associated with reduction of the iron heme, so the impact of the oxidation state of the iron was evaluated in the different variants.

Four states were studied for comparison purposes for the two extreme variants, WT and PM P450_{BM3} were examined while F81I and I401P P450_{BM3} were examined as intermediates. While the water-bound and carbon monoxide-bound states are commonly used as the resting state and a model for the Fe(II)-O₂ state,²⁷⁵ 4-Cyanopyridine (CNPy) was chosen as it binds to both the Fe(II) and Fe(III) states (Figure C3). This ligand is bound to the Fe-heme via the nitrogen pyridine as previously shown for P450_{BM3}²⁶⁸ and P450cam.²⁷⁶ Binding dissociation constants (K_d) for CNPy were found for WT and PM P450_{BM3} in the Fe(III) and Fe(II) states (Figure C3, Table C1). Consistent with literature²⁶⁸, tighter binding was observed for the ferrous states as opposed to the ferric states (Table C1). Thus, the states compared were Fe(III)-H₂O, Fe(III)-CNPy, Fe(II)-CNPy and Fe(II)-CO. For the two single point variants, only the resting Fe(III)-H₂O and Fe(II)-CO states were investigated, as to simplify analysis. All concentration midpoint values are shown in Table 4.1.

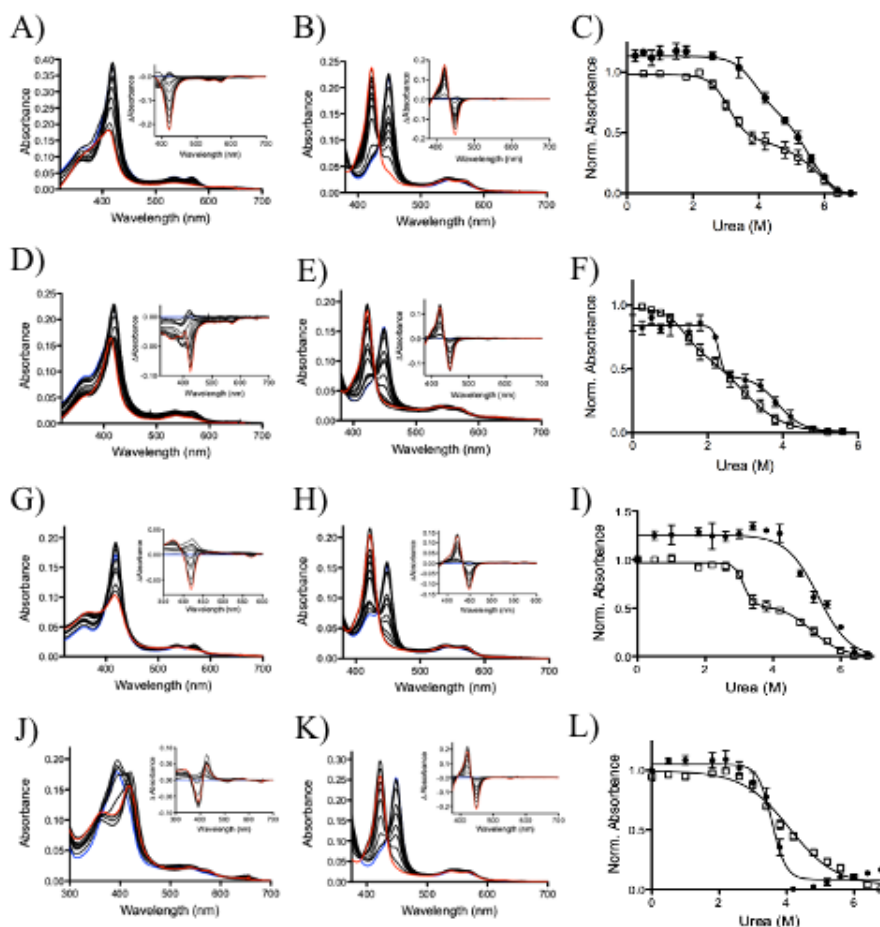


Figure 4.2 Reduction of P450_{BM3} variants impacts stability as detected by UV/Vis spectroscopy. In each case, the left absorbance spectra is the Fe(III)-H₂O state, monitored over 0 – 6.8 M urea; the middle absorbance spectra is the Fe(II)-CO state monitored over 0 – 6.8 M urea. Insets show difference spectra, where the blue line = 0 urea, and the red line is the last urea addition. The fits to the data on the right are the normalized absorbance of Fe(III)-H₂O P450_{BM3} at 418 nm (closed circles) and Fe(II)-CO P450_{BM3} at 450 nm (open squares), which were used to determine C_m for both states. A-C) WT P450_{BM3}. D-F) PM P450_{BM3}. G-I) F81I P450_{BM3}. J-L) I401P P450_{BM3}. Studies were performed in 100 mM KPi pH 7.4 buffer with protein at a concentration between 0.15 – 0.25 mg/mL. All experiments were done in a 1-cm quartz cuvette. Concentrated urea was made in 100 mM KPi pH 7.4 buffer before dilution. For CO-bound studies, KPi buffer was first saturated with CO. Sodium dithionite was made immediately before use and dissolved in CO-saturated 100 mM KPi pH 7.4 buffer. All samples were incubated for 2 hr at RT before absorbance spectra were taken. For results with one transition, data was fit on Graphpad prism with the sigmoidal dose-response (variable slope) equation. For results with two unfolding transitions data was fit with a biphasic nonlinear fit equation.

Unfolding of the WT Fe(III)-H₂O state was demonstrated by a decrease in absorbance of the Soret band at 418 nm and the q-bands from 500 - 600 nm (Figure 4.2A) as the urea concentration was increased. The WT Fe(III)-H₂O state was best fit by a biphasic equation as opposed to a monophasic equation as shown by residual plots (Figure C5). It was the most stable state, exhibiting a C_m of 4.0 ± 0.4 M for the first unfolding event and 5.6 ± 0.1 M for the second. This biphasic fit hinged on one point around 4 M urea, but was observed consistently through three separate experiments. Unfolding of the WT Fe(II)-CO state was observed optically by a disappearance of the P450 state and a rise of the P420 state as denaturant increased (Figure 4.2B). As two distinct processes occurred, two C_m values are reported, 3.0 ± 0.2 M and 5.6 ± 0.1 M for the process at 420 nm and 3.1 ± 0.1 M and 5.6 ± 0.1 M for the process at 450 nm (Figure 4.3, Table 4.1). For the P450 state, a majority of the protein (60%) was denatured during the first unfolding event (3.1 ± 0.1 M) and 40% unfolded over 2 M later, with a C_m of 5.6 ± 0.1 M shown in Figure 4.2C. The WT Fe(III)-CNP_y state exhibited a decrease in absorbance of the slight red shifted Soret band with very little change to the q-bands (Figure C6). Similarly to the Fe(II)-CO state, the WT Fe(II)-CNP_y state unfolded by two processes- disappearance of the properly ligated state at 445 nm and appearance of the misligated state²⁷⁷ at 426 nm. There was also a slight blue shift of the q-bands as the active site unfolded (Figure C6). Unlike the water and carbon monoxide states, the CNP_y bound states unfolded monophasically with a C_m of 5.5 ± 0.1 M for the ferric state and 4.2 ± 0.2 M (426 nm) and 4.9 ± 0.2 M (445 nm) for the ferrous state (Figure 4.3, Table 4.1). The stability of the WT ferrous states were, in general, lower than the WT ferric states. The most obvious example is of the Fe(II)-CO state compared to

the WT Fe(III)-H₂O state where there is over a two molar unit difference in stability (Figure C7).

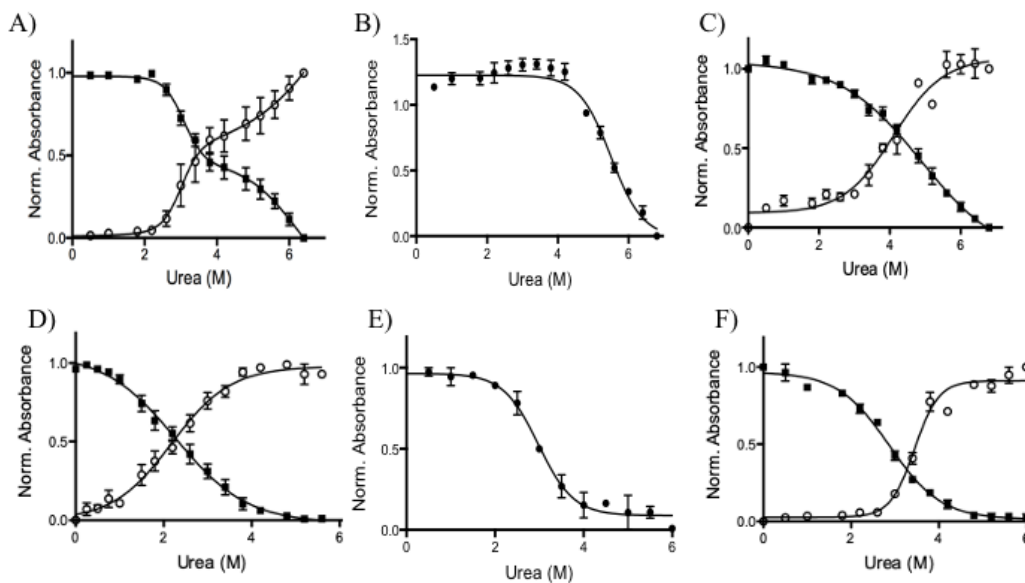


Figure 4.3 Unfolding of WT and PM P450_{BM3} as detected by UV/Vis spectroscopy. A) and D) the Fe(II)-CO state; B) and E) the Fe(III)-CNP_y state; C) and F) the Fe(II)-CNP_y state. A) through C) WT P450_{BM3}; D) through F) PM P450_{BM3}. For the ferrous states the open circles represent the appearance of the inactive state (420 nm for the Fe(II)-CO state and 426 nm for the Fe(II)-CNP_y state) and the closed circles are disappearance of the active state (450 nm for the Fe(II)-CO state and 445 nm for the Fe(II)-CNP_y state).

The PM P450_{BM3} species studied were less stable than the same WT P450_{BM3} species by UV/Vis. All four states unfolded optically similar to the WT species with the exception of the Fe(II)-CNP_y state (Figure C6). The extinction coefficient for the 426 nm state for the PM P450_{BM3} species was observably higher than that of the WT, shown by the higher absorbance of the 426 state compared to the 445 state. The PM P450_{BM3} Fe(III)-H₂O state studied by UV/Vis (Figure 4.2D) was the only PM P450_{BM3} state that displayed biphasic unfolding by any technique. The first phase had a $C_m = 2.3 \pm 0.2$ M and contributed approximately 50% to the overall unfolding event. The second higher C_m was

3.9 ± 0.2 M (Table 4.1). The C_m values of the Fe(II)-CO transitions were similar to the first unfolding event for the water bound state, with C_m values of 2.2 ± 0.1 M (420 nm) and 2.3 ± 0.1 M (450 nm). Similar values were also found between the CNPy bound PM P450_{BM3} states, in fact one of the ferrous transitions exhibited a higher C_m than the ferric state, 3.4 ± 0.1 (426 nm) for the Fe(III) state vs 3.1 ± 0.1 M for the Fe(II) state (Figure 4.3, Table 4.1).

Unfolding of the F81I P450_{BM3} species occurred similarly to the corresponding WT and PM P450_{BM3} states. For the water bound state this meant a decrease in the Soret band and for the Fe(II)-CO state a decrease in the P450 state with an increase of the P420 state (Figure 4.2G,H). Concentration midpoint values were comparable to WT, though not biphasic for the water bound state ($C_m = 5.3 \pm 0.1$ M). C_m values for the Fe(II)-CO transitions were 3.6 ± 0.1 M (420 nm) and 3.1 ± 0.1 M, 5.1 ± 0.2 M (450 nm) as seen in Table 4.1. As the I401P P450_{BM3} is naturally high spin in the resting state, it unfolded differently than all other variants. Upon denaturation, the Soret band red shifted from the HS resting state at 395 nm to an inactive state at 420 nm. As the urea concentration continued to increase, the absorbance at 420 nm decreased, indicating a loss of the heme from the active site. This shift in absorbance was accompanied by the appearance of a large shoulder at the HS position and a decrease in absorbance of the MLCT band (Figure 4.2J). The C_m for the water bound state was between that of PM and WT P450_{BM3} with a C_m of 3.6 ± 0.1 M (Table 4.1). When reduced and CO-bound, the I401P P450_{BM3} variant shows the typical red shift expected to approximately 450 nm. Upon denaturation by urea, this peak shifts to an inactive species at approximately 425 nm (Figure 4.2K). As compared to the Fe(III)-H₂O state, unfolding of the Fe(II)-CO state unfolds more rapidly evidenced

for the steepness of the slope of the unfolding plot (Figure 4.2L). The C_m values at both 425 nm and 450 nm were close to those observed for CO bound ferrous WT P450_{BM3} with a biphasic unfolding pattern apparent at 450 nm. Though close in stability, for WT P450_{BM3}, the ΔC_m between the resting state and the Fe(II)-CO bound state is 0.4 – 0.9 M for the first transitions. For I401P P450_{BM3}, this difference is only 0.1-0.2 M. The smaller difference in ΔC_m is similar to the pattern seen for PM P450_{BM3} in which the ferrous and ferric states are closer in stability as seen in Table 4.1.

Besides the presence of biphasic unfolding, other interesting observations were made for the various BM3 variants. Of the Fe(II)-CO states, WT and PM P450_{BM3} unfolding occurred synergistically meaning both the P420 and P450 C_m values were within error. Additionally, for WT P450_{BM3} this was surprising as both states unfolded via biphasic mechanisms. For all the variants in the resting state (Fe(III)-H₂O for WT and F81I, Fe(III) HS for I401P), except PM P450_{BM3}, an initial compaction event was evident upon unfolding. This initial compaction may be due to urea displacing water around the enzyme by an indirect mechanism,²⁷⁸⁻²⁸⁰ placing a force on the enzyme that allows it to constrict. As PM P450_{BM3} is already significantly destabilized it is likely that urea was more readily able to reach the hydrophobic core than the other P450_{BM3} variants.

4.3.3 Circular dichroism monitored changes in α -helical content.

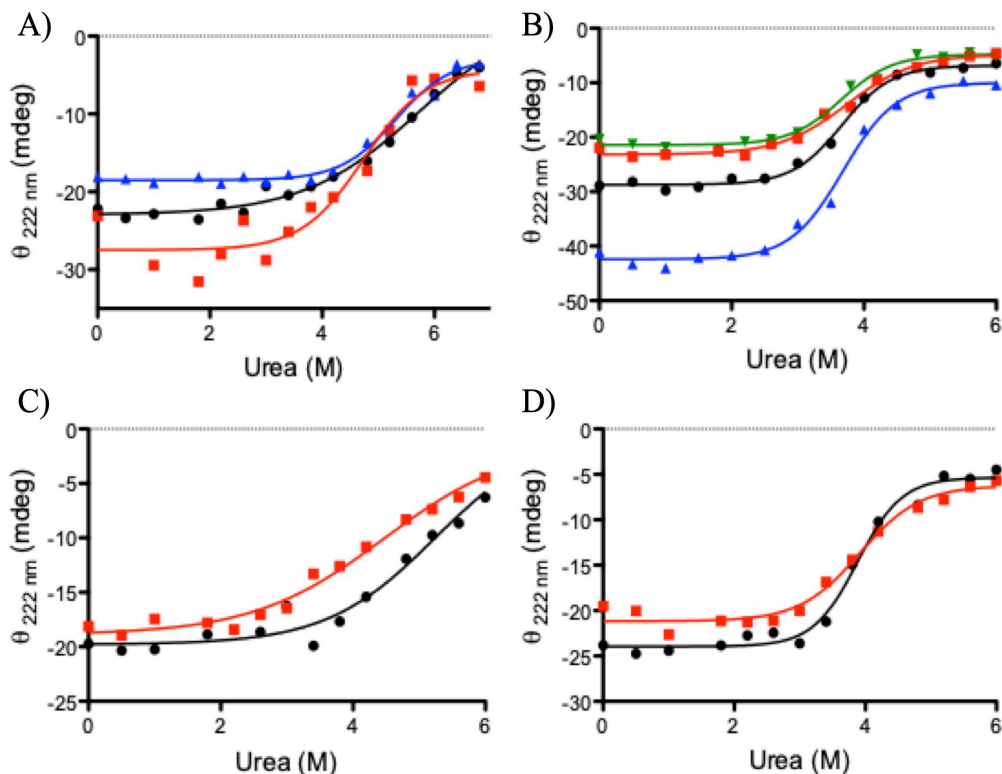


Figure 4.4 Reduction from Fe(III) to Fe(II) states of selective and promiscuous variants has an opposing effect on secondary structure stability. Change in ellipticity at 222 nm as a function of urea concentration for A) WT P450_{BM3}, B) PM P450_{BM3}, C) F81I P450_{BM3}, and D) I401P P450_{BM3}. In all panels, black circles are the water bound resting state, blue triangles represent the ferric CNPY state, green triangles the ferric CNPY state, and the red squares represent the ferrous CO-bound state.

The denaturation of the α -helical content of WT, F81I, I401P, and PM P450_{BM3} variants was investigated by Circular Dichroism spectroscopy (CD) in the far-UV region, as shown in Figure 4.8 and Table 4.2. In general, an increase of the denaturant concentration was correlated with a decrease in α -helical content as shown by a decrease in ellipticity at 222 nm (Figure C8). Of the four WT P450_{BM3} species studied, the most stable was the resting state, Fe(III)-H₂O, which exhibited a C_m of 5.6 ± 0.2 M; the ferric CNPY state was within error of this value at 5.5 ± 0.2 M (Table 4.2). The Fe(II)-CO state

was approximately 1 M less stable, exhibiting a C_m of 4.4 ± 0.4 M. Results for the ferrous CNPy bound state were not included due to signal interference.

Table 4.2 Concentration midpoint (C_m) values of P450_{BM3} variants by circular dichroism spectroscopy.^a

	Fe(III)- H₂O	Fe(III)-CNPy	Fe(II)-CNPy	Fe(II)-CO
WT	5.6 ± 0.2	5.5 ± 0.2	-	4.4 ± 0.4
F81I	5.2 ± 0.1	-	-	4.4 ± 0.1
I401P	3.9 ± 0.1	-	-	3.9 ± 0.1
PM	3.7 ± 0.2	3.6 ± 0.1	3.7 ± 0.2	3.8 ± 0.1

^a. All C_m values are molar urea.

In marked contrast, the four PM P450_{BM3} states had similar C_m values within error of each other ranging from 3.6 ± 0.1 M to 3.8 ± 0.1 M (Table 4.2). The same trend followed for the I401P P450_{BM3} variant as for PM P450_{BM3} in which the ΔC_m between the Fe(III) and Fe(II) states is negligible or non-existent. The C_m values for both the resting state and Fe(II)-CO bound I401P P450_{BM3} variant are within error of the PM P450_{BM3} values, with stability in the high 3 M range. Interestingly, as seen by UV/Vis spectroscopy for the I401P P450_{BM3} variant, the slope of the unfolding curve for the Fe(II)-CO state is steeper than that of the Fe(III)-H₂O state (Figure 4.4D). As the I401P P450_{BM3} variant parodies PM P450_{BM3}, so does F81I P450_{BM3} to WT P450_{BM3}. There is a larger gap in stability for the two selective water bound states, than for the two promiscuous variants (ΔC_m of 0.4 M for the selective variants vs ΔC_m of 0.2 M for the promiscuous variants), but they are still overall much more stable than their counterparts. For F81I P450_{BM3}, there is a noticeable drop in stability for the Fe(II)-CO bound state when compared to the resting state of almost 1 M, similar to what is seen with WT P450_{BM3} ferric and ferrous states.

4.3.4 Pulse proteolysis uses a protease to investigate global structure stability.

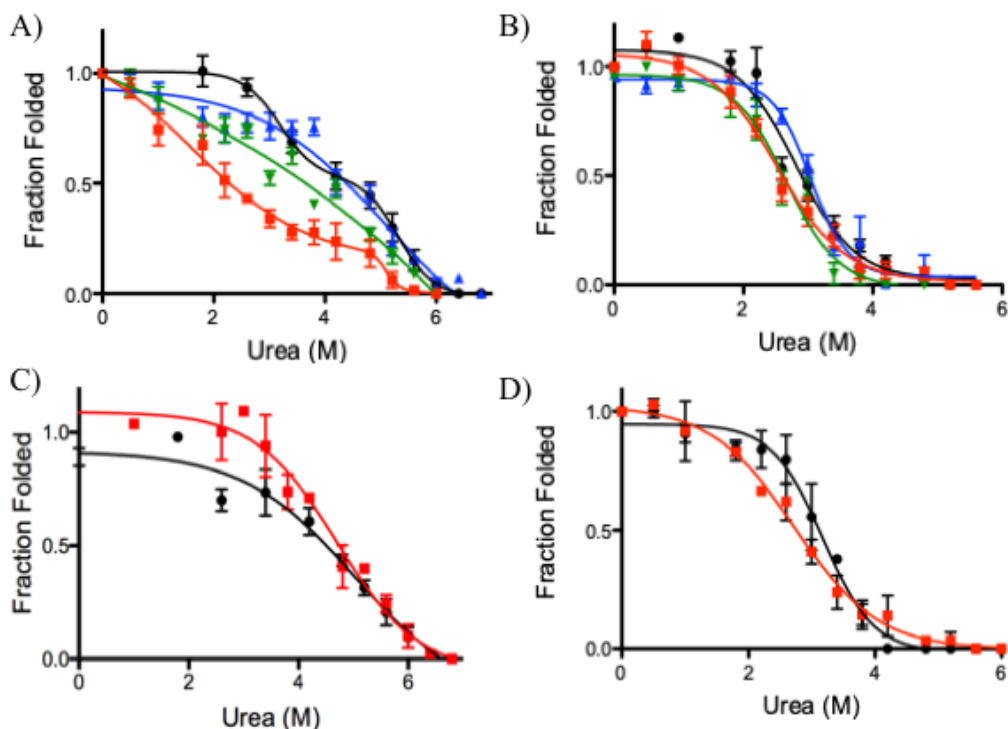


Figure 4.5 A greater disparity in stability of the global structure occurred as a function of iron oxidation state for selective P450_{BM3} variants. A) WT P450_{BM3} stability monitored by pulse proteolysis in which a decrease in protein content was observed. B) PM P450_{BM3} and D) I401P P450_{BM3} are promiscuous variants whereas C) F81I P450_{BM3} is more selective. In all panels, black circles represent the ferric H₂O state, blue triangles the ferric CNPy bound state, green triangles the ferrous CNPy bound state, and red squares represent the ferrous CO bound state.

Pulse proteolysis was first described by Park and Marqusee as a method to investigate the stability of global protein structure.¹³⁷ In this technique, the protein is first denatured by urea subsequently, cleaved by the protease thermolysin and then run on a 4-12% bis-tris protein gel. The more unstable the protein, the more denatured it will become by urea and therefore, more exposed to thermolysin. Concentration midpoints (C_m) are calculated in which the protein is 50% unfolded (Figure 4.5, Table 4.3). An example of a gel is shown in Figure C10.

Table 4.3 Concentration midpoint (C_m) values of P450_{BM3} variants by pulse proteolysis.^a

	Fe(III)-H ₂ O	Fe(III)-CNP _y	Fe(II)-CNP _y	Fe(II)-CO
WT	3.2 ± 0.2, 5.3 ± 0.1 ^b	4.5 ± 0.1	3.6 ± 0.2	2.2 ± 0.4, 5.0 ± 0.2 ^b
F81I	4.6 ± 0.1	-	-	4.7 ± 0.2
I401P	3.3 ± 0.1	-	-	2.7 ± 0.1
PM	2.9 ± 0.1	3.0 ± 0.1	2.7 ± 0.1	2.1 ± 0.1

^a. All C_m values are molar urea. ^b. Two values separated by a comma indicate biphasic unfolding.

As measured by pulse proteolysis, WT P450_{BM3} Fe(III)-H₂O exhibited biphasic unfolding and was the most stable of the four WT P450_{BM3} species studied, exhibiting a C_m of 5.3 ± 0.1 M for the second transition (Table 4.3). Residual plots indicating the suitability of biphasic fits are shown in Figure C11. For the water bound state, the biphasic transition split the population in half; approximately 50% of the enzyme was unfolded at the first C_m of 4.0 ± 0.4 M and 50% at the higher (Figure 4.5A). If reflecting on the total population as a whole, the Fe (III)-CNP_y state could be considered more stable than the Fe (III)-H₂O as the C_m for the Fe(III)-CNP_y state was 4.5 ± 0.1 M. The WT P450_{BM3} Fe(II)-CO state also displayed biphasic unfolding but with a much lower initial C_m . Unlike the water bound state, the ferrous CO bound state exhibited an immediate drop-off in stability when exposed to urea with a C_m of 2.2 ± 0.4 M. Approximately 90% of the enzyme unfolded in this first phase, and 10% in the last phase with a C_m of 5.0 ± 0.2 M (Figure 4.5A). This small portion of the enzyme population could represent molecules that reverted to the Fe(III)-H₂O state as this C_m value is within error of the higher value for that system, 5.3 ± 0.1 M. Unlike the Fe(III)-H₂O and Fe(II)-CO states, both the WT P450_{BM3} ferric and

ferrous CNPy bound states exhibited monophasic unfolding, although the ferric state was more stable by approximately 1 M with a C_m of 4.5 ± 0.1 M vs 3.6 ± 0.2 M, respectively (Table 4.3).

Unlike the WT P450_{BM3} species, none of the other P450_{BM3} variants exhibited biphasic unfolding profiles. Of the four PM P450_{BM3} states studied, the HS Fe(III)-CNPy state was the most stable, however, the stability of the Fe(III)-H₂O and Fe(II)-CNPy states were also comparable. The biggest difference observed was for the Fe(II)-CO state, which had the lowest C_m of 2.1 ± 0.1 M (Table 4.3). Compared to the other techniques, pulse proteolysis shows the greatest difference in stability for the PM and I401P P450_{BM3} ferric vs ferrous states. In both cases the ferrous states are less stable than the ferric, the most drastic example is the ΔC_m (0.8 M) between the resting state and ferrous CO-bound state for PM P450_{BM3} (Figure C12). This gap is a bit smaller for I401P P450_{BM3} with a ΔC_m of 0.6 M. Though, these ΔC_m values are larger than expected, they are still smaller than those seen for WT P450_{BM3}.

4.3.5 Promiscuous P450_{BM3} variants have a more positive reduction potential than more selective variants

To determine if there was a relationship between stability and ease of reduction, the reduction potential of all four P450_{BM3} variants was calculated. A method first published by Ost *et al.* was used in which MLCT between the iron heme and CNPy ligand was related to reduction potential using the equation $E_{MLCT} = (3.53 \times E_M) + 17,005 \text{ cm}^{-1}$ where E_M is the reduction potential and E_{MLCT} is the wavelength of the maximum absorbance of the MLCT band in cm^{-1} .²⁶⁸ In short, after the enzyme was reduced with sodium dithionite, CNPy was added to saturation and the maximum wavelength of the MLCT band (600-700 nm) was

determined by UV/Vis spectroscopy (Figure C13). Using the above equation, reduction potential was calculated and corrected based on previously published values for WT and I401P P450_{BM3}. As expected, WT P450_{BM3} exhibited the lowest reduction potential of -429 ± 8 mV. Values from literature for reduction potential of WT P450_{BM3} vary from -449 to -368 mV,^{268, 270, 271, 281-284} placing our value within agreement. Also in agreement with literature, is our calculated reduction potential for I401P P450_{BM3} of -284 ± 28 mV as compared to -303 mV.²⁷⁰ Reduction potentials for F81I and PM P450_{BM3} were determined to be -429 ± 8 mV and -341 ± 23 mV, respectively.

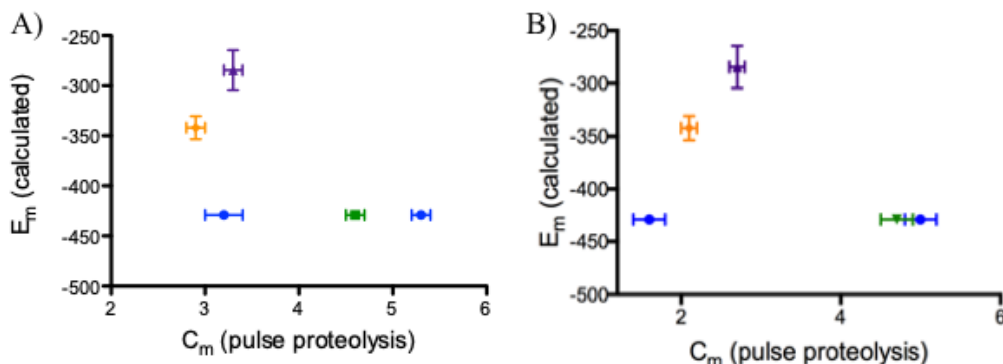


Figure 4.6 Redox potential is correlated to iron state stability of selective vs. promiscuous P450_{BM3} variants. A) Concentration midpoints as determined by pulse proteolysis for ferric water bound P450_{BM3} variants are plotted against calculated reduction potential. B) Ferrous CO-bound P450_{BM3} variants in relation to calculated reduction potentials. In both panels, blue circles represent WT P450_{BM3}, and two data points are shown as both ferrous and ferric states exhibited biphasic unfolding by pulse proteolysis. Green circles show F81I P450_{BM3}, orange diamonds show I401P P450_{BM3}, and purple circles are PM P450_{BM3}. The reduction potential was calculated by determining the λ_{max} of the MLCT band (600 – 700 nm) of the ferric-CNP_y bound species. All UV/Vis experiments were done in a 1-cm pathlength quartz cuvette with 0.15 mg/ml protein diluted in 100 mM Kpi pH 7.4 buffer at RT. The enzyme was reduced with freshly made sodium dithionite made in 100 mM Kpi pH 7.4 buffer. CNP_y was used at saturating concentrations.

Not surprisingly, the more promiscuous the variant, the higher the reduction potential, implying an ease of reduction by NADPH (-320 mV)²⁸⁵ as compared to the more selective variants. In addition, there seems to be a correlation between stability of the global structure as determined by pulse proteolysis and reduction potential. Upon comparing the C_m of the resting state (Fe(III)-H₂O for WT, F81I, and PM P450_{BM3} variants and Fe(III)-HS for I401P P450_{BM3}) to reduction potential, there are two clusters apparent, one consisting of the WT and F81I P450_{BM3} variants and another of the PM and I401P P450_{BM3} variants, indicating a similarity in behavior (Figure 4.6A). The same is obvious for the correlation between C_m of the Fe(II)-CO state with reduction potential (Figure 4.6B). As WT P450_{BM3} unfolds biphasically by pulse proteolysis, both C_m values are included.

4.4 Discussion

Though PM and I401P P450_{BM3} are more promiscuous, this loss of selectivity comes at the cost of stability. By all three methods – pulse proteolysis, CD, and UV/Vis spectroscopy, WT and F81I P450_{BM3} were in general 1-2 M more stable than PM and I401P P450_{BM3} when exposed to increasing concentrations of urea. Generally, as compared to the WT and F81I P450_{BM3} species investigated, the stability of the states studied for PM and I401P BM3 were very similar regardless of oxidation state, summarized in Figure 4.7. The general trend for WT P450_{BM3} states studied was that the ferric states were more stable than the ferrous states. Comparing just the oxidized and reduced WT-CNP_y bound states, the smallest ΔC_m was 0.9 M urea by pulse proteolysis and the greatest ΔC_m was 1.3 M urea by UV/Vis spectroscopy. In contrast, for the PM P450_{BM3} ferric and ferrous forms bound to CNP_y the greatest ΔC_m was 0.3 M, observed by both pulse proteolysis and UV/Vis spectroscopy.

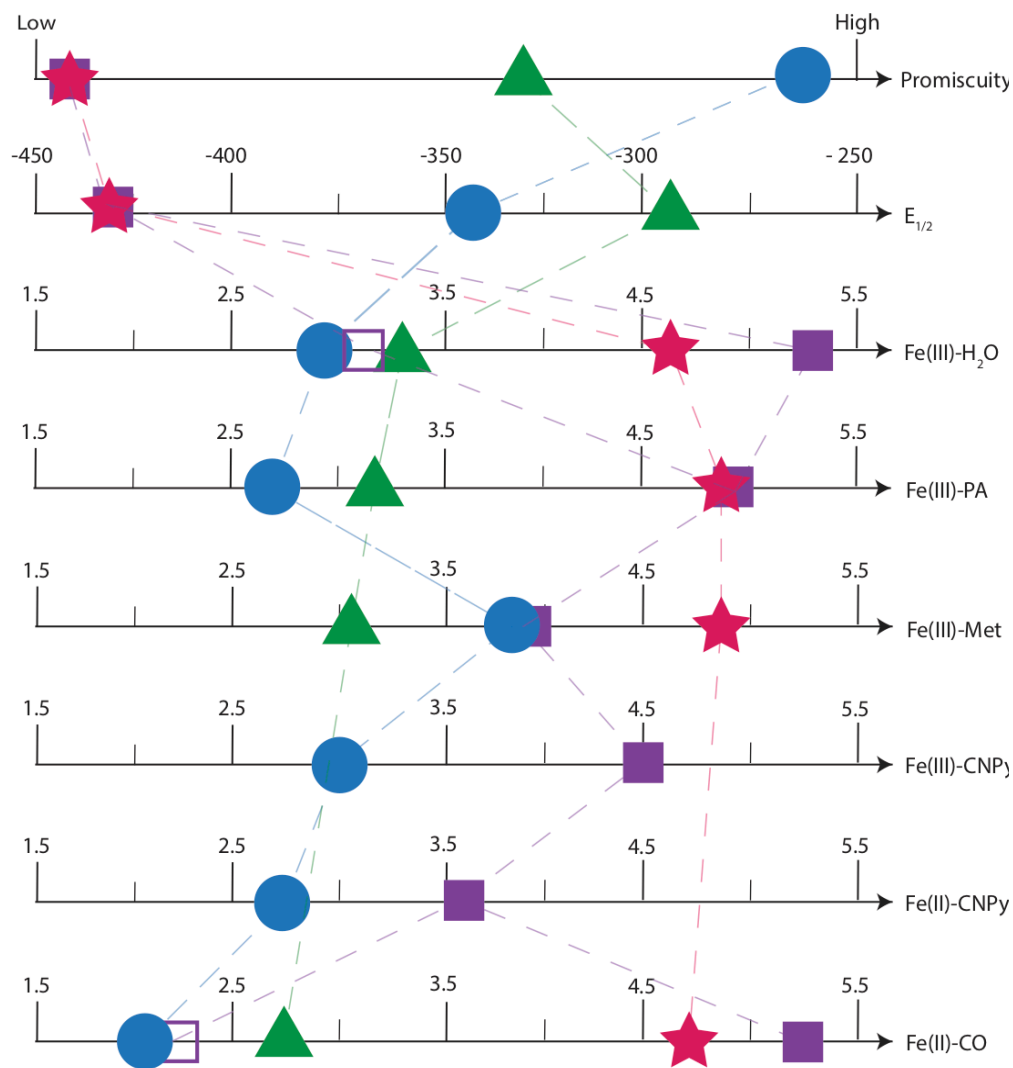


Figure 4.7 Change in concentration midpoint (C_m) of all tested variants by pulse proteolysis. The C_m is compared to an estimation of promiscuity and the reduction potential. Purple squares represent WT, green triangles are I401P, pink stars are F81I, and blue circles are PM. Open purple squares and filled purple squares indicate a biphasic unfolding, in which the open square is the lower C_m value and the closed square is the higher C_m value.

The similarity in stability between the oxidized and reduced states of PM and I401P P450_{BM3} variants indicates structural regularity between the two states. For the selective P450_{BM3} variants to undergo turnover there must be a larger rearrangement in overall

structure as there is a greater difference in stability. In essence, the energy barrier between the Fe(III) and Fe(II) state is greatly reduced for the promiscuous P450_{BM3} variants as opposed to the more selective P450_{BM3} variants. In addition, the increase in positivity of the reduction potential of the promiscuous variants indicates they can more readily accept an electron from their reductase partner. As the rate limiting step of P450 catalysis is the first electron transfer to the substrate bound HS Fe(III) state,²⁰⁷ this finding is extremely important. Because non-native substrates disrupt natural contacts in the active site, the quicker rearrangement in protein structure between the Fe(III) and Fe(II) states may help account for why promiscuous P450s are able to successfully turnover a plethora of diverse substrates.

A) One population (N) via an intermediate (I) to an unfolded state (U).



B) Two different populations (N_A and N_B) denatured to an unfolded state.

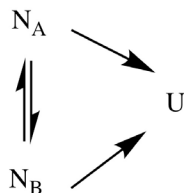


Figure 4.8 Possible pathways for biphasic unfolding. In both depictions, “N” represents the native population and “U” the unfolded population. “N_A” and “N_B” represent the possibility of two native states.

Though all variants exhibited biphasic unfolding for particular states, it was more ubiquitous for WT P450_{BM3}. Biphasic unfolding was apparent for both the resting state and the Fe(II)-CO state by UV/Vis spectroscopy and pulse proteolysis. This is in contrast to

biphasic unfolding only occurring for F81I and I401P P450_{BM3} for the Fe(II)-CO state and the Fe(III)-H₂O state for PM P450_{BM3} by UV/Vis spectroscopy. Two-stage unfolding could be occurring via two separate pathways expressed in Figure 4.8. Panel A depicts a scenario in which biphasic unfolding occurs via an intermediate which indicates a metastable form of the enzyme appears as it unfolds. Panel B in contrast, depicts a situation in which biphasic unfolding occurs as the result of two native populations (N_A and N_B), in equilibrium with each other, unfold at different rates. If the true unfolding pathway is attributed to the later, it could be rationalized that the presence of two native states could be an artifact of protein purification. This line of reasoning is unlikely as biphasic unfolding for WT P450_{BM3} has been observed in previous studies in which protein was purified using a different method.¹³²

If biphasic unfolding occurred due to the presence of an intermediate, for the Fe(II)-CO state it would be expected that the C_m values for the appearance of the P420 state and disappearance of the P450 state are similar. This is consistent for WT P450_{BM3} in which the C_m values at 420 nm are 3.0 ± 0.2 and 5.6 ± 0.1 M and are 3.1 ± 0.1 and 5.6 ± 0.1 M at 450 nm (Table 4.1). Unfortunately, this trend does not follow for F81I and I401P P450_{BM3} in which only the P450 state unfolds via a biphasic mechanism.

A third possibility for biphasic unfolding is especially relevant for the WT P450_{BM3} Fe(II)-CO state as detected by pulse proteolysis. It is possible that a small population of the enzyme reverted from the ferrous-CO bound state to the ferric water bound state as 90% unfolded at 2.2 ± 0.4 M and 10% later at 5.0 ± 0.2 M (Table 4.3). The higher C_m of 5.0 ± 0.2 M is within error of the higher C_m for the water bound state (5.3 ± 0.1 M) which lends credence to this hypothesis. It is possible that all three mechanisms discussed are

relevant to biphasic unfolding of the various P450_{BM3} states. Work is currently being done utilizing single molecule pulsed interleaved excitation-forster resonance energy transfer (PIE-FRET) to parse which hypothesis is more accurate for the systems investigated in this study.

degradation of xenobiotics, and thus, play a central role in drug metabolism and deactivation. One problematic issue is that their substrates include many anticancer agents, decreasing the effective drug concentration in the body. Compounding this problem, some P450s are found specifically in tumors, where they are over expressed and play a direct role in cancer initiation, progression, and drug resistance. For example, CYP1B1 has been shown to metabolize procarcinogens to carcinogens to initiate DNA damage, and subsequently induce resistance to DNA damaging chemotherapeutics.²⁸⁶⁻²⁸⁸ Alternatively, CYP19A (aromatase) converts androgens to estrogens, and is an important target in the treatment of estrogen driven cancers.²⁸⁹⁻²⁹³ CYP17A1 is responsible for androgen synthesis, and abiraterone is a first-in-class steroidal inhibitor of this enzyme used in late-stage prostate cancer.²⁹⁴⁻²⁹⁷

Currently, P450 inhibitors have been used as treatments for the inhibition of steroid biosynthesis, as for breast and prostate cancer, and for other indications, such as Cushing's disease.²⁹⁸⁻³⁰⁰ The dangers associated with clinical use of P450 inhibitors is that they are generally not isoform selective ($<10^3$ difference in K_d), and long-term systemic inhibition of P450s can result in adverse drug interactions and altered hormone levels.^{301, 302} An alternative approach to avoid these consequences would be to develop agents that can be activated to selectively inhibit desired P450 enzymes in a spatially and temporally regulated manner. In the context of anti-cancer agents, inhibition of P450s in cancerous tissues is also a rational strategy to sensitize the cells to DNA damaging agents,²⁸⁶ while reducing the bioactivation of procarcinogens as a cancer driver. Furthermore, if the inhibition of the P450 could occur concurrently with the local administration of a cytotoxic agent only within the tumor, deactivation of the drug by hepatic P450s could be avoided.

Accordingly, we have synthesized dual action Ru(II) complexes as pro-drugs that can be triggered with light to simultaneously release a P450 inhibitor and a DNA damaging metal center.

Photocaging is a well-established means to selectively release biologically active agents with temporal and spatial control.³⁰³ Metal complexes have been used as photocaging groups with great success, with pioneering work by Etchenique,³⁰⁴⁻³⁰⁶ Franz,³⁰⁷⁻³⁰⁹ and Kodanko.³¹⁰⁻³¹² Our approach differed slightly from traditional photocaging, however, as the metal complex is intended to act as a caging group that would transform into an active biological effector in its own right, in addition to the ligand that it protected in the intact complex form.

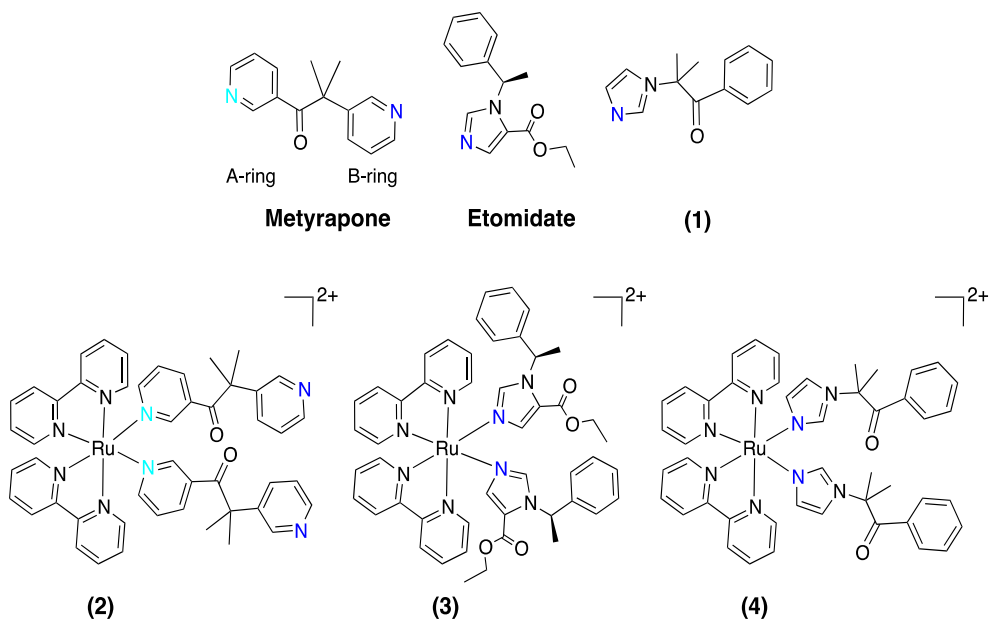


Figure 5.2 Structures of P450 inhibitors and Ru(II) complexes. Complexes synthesized by A. Zamora.

In order to test this strategy, three P450 inhibitors were chosen that could be coordinated to Ru(II) complexes. These compounds all contain nitrogen heterocycles, and

thus are able to directly ligate both the Ru(II) center and, after photorelease, the iron heme in P450s. Metyrapone and etomidate have been primarily used to inhibit P450 11B1, also known as steroid 11-beta-monooxygenase.³¹³ Both compounds appear to bind similarly to the binding site of CYP11B1, where the N-heterocycle is capable of ligating the catalytic heme iron while the other ring interacts with Arg110 and Phe130 via π -stacking.³¹⁴ A third, novel small molecule, compound **1**, was synthesized;³¹⁵ it has the metyrapone molecular skeleton with etomidate features: imidazole and benzene rings (Figure 5.2).

5.2 Experimental Procedures

5.2.1 Materials and instrumentation

Chemicals used for synthesis were purchased from VWR or Fisher Scientific and used without further purification. *cis*-Dichlorobis(2,2'-bipyridine)ruthenium(II) dihydrate was purchased from Strem chemicals. Human liver microsomes were purchased from Sekisui Xenotech.

A Varian Mercury spectrometer was used to obtain ¹H NMR (400 MHz) and ¹³C (100 MHz) spectra. Chemical shifts are reported relative to the solvent peak (CD₃CN – δ 1.94 or CDCl₃ – δ 7.24 for ¹H NMR; CD₃CN – δ 1.39 for ¹³C NMR). Electrospray ionization (ESI) mass spectra were obtained using a Varian 1200L mass spectrometer at the University of Kentucky Environmental Research Training Laboratory (ERTL). Absorption spectra for the extinction coefficient determination, acetonitrile photoejection and binding constant (K_d) determination for ligands were obtained on a Cary 60 UV/Vis spectrophotometer. Full spectrum absorbance readings to study the photoejection for complexes **1–3** in different aqueous media were obtained using a BMG Labtech FLUOstar

Omerga microplate reader. Binding saturation studies for each compound as well as K_d determination for irradiated complexes **1–3** were completed using an Agilent 8453 UV/Vis spectrometer. Compound purity was determined with an Agilent 1100 Series HPLC using a previously reported method.³¹⁶ Light activation for photoejection experiments was achieved using a 470 nm LED array from Elixia. An Indigo LED array from Loctite was used for light activation for the enzyme assays. A Tecan SPECTRAFluorPlus Plate Reader was used to determine change in fluorescence for the enzyme activity assay and IVTT assay. Agarose gels were digitally imaged using a BioRad ChemiDoc System.

5.2.2 Compound synthesis, characterization, and ion exchange

2-(1-Imidazolyl)-2-methyl-1-phenyl-2-propanone (**1**) was synthesized following a previously published procedure.⁵² All metal complexes were synthesized under low ambient light and were protected using aluminum foil throughout each step of synthesis, isolation, and characterization. Silver salts were used to facilitate ligand exchange; the choice of the specific salts in the different reactions was due only to reagent availability.

5.2.2.1 $[\text{Ru}(\text{bpy})_2(\text{Met})_2](\text{PF}_6)_2$ (**2**)

$[\text{Ru}(\text{bpy})_2\text{Cl}_2] \cdot 2 \text{H}_2\text{O}$ (125 mg, 0.240 mmol) was dissolved in water (7 mL) under N_2 at 80 °C. To this 2-methyl-1,2-di-3-pyridil-1-propanone (136 mg, 0.6 mmol) was added, and the red solution was stirred overnight at 80 °C. The resulting solution was cooled to room temperature (RT) and extracted into CH_2Cl_2 (3x10 mL) to remove the excess free ligand. The complex was precipitated out of the aqueous phase with 1–2 mL of a saturated aqueous KPF_6 solution and extracted with $\text{CH}_2\text{Cl}_2/\text{MeCN}$ (3x10 mL). The crude complex

was purified by column chromatography using H₂O:MeCN:KNO₃ as eluent (from 0:100:0 to 12:87.2:0.8). The product was obtained in 38% yield (104 mg) as an orange solid. ESI MS C₄₈H₄₄N₈O₂Ru: m/z calcd [M]²⁺ 433.13, found 433.2 [M]²⁺. Purity by HPLC: 99.3 % by area; UV/Vis in CH₃CN, λ_{max} (ε M⁻¹ cm⁻¹) = 290 (43200), 345 (12100), 445 (8400). Note: NMR was not completed due to the compound containing a mixture of isomers.

5.2.2.2 [Ru(bpy)₂(Eto)₂](PF₆)₂ (**3**)

Silver triflate (99 mg, 0.384 mmol) was added to a suspension of [Ru(bpy)₂Cl₂]₂·H₂O (100 mg, 0.192 mmol) in water (15 mL) and the mixture was stirred overnight at RT. The solution was filtered under N₂. Etomidate (94 mg, 0.384 mmol) and 15 mL of EtOH were added to the solution, which was then stirred at 85 °C under N₂ for 24 hr. After cooling the reaction, the solution was concentrated, 1-2 mL of a saturated aqueous KPF₆ solution was added, and the precipitate was extracted into CH₂Cl₂ (3x15 mL). The crude was purified by column chromatography using H₂O:MeCN:KNO₃ as eluent (from 0:100:0 to 20:80:0.4). The product was obtained in 47% yield (108 mg) as a crystalline red solid. ¹H NMR (CD₃CN, 400 MHz): δ 9.03 (d, *J* = 5.6 Hz, 1H), 8.97 (d, *J* = 5.2 Hz, 1H), 8.35 (d, *J* = 8.4 Hz, 2H), 8.27 (d, *J* = 8.0 Hz, 1H), 8.24 (d, *J* = 8.4 Hz, 1H), 8.12 (q, *J* = 8.4 Hz, 2H), 8.00 (d, *J* = 5.2 Hz, 1H), 7.87 (m, 3H), 7.70 (m, 3H), 7.49 (s, 1H), 7.37-7.19 (m, 10H), 6.88 (d, *J* = 6.4 Hz, 2H), 6.72 (d, *J* = 7.2 Hz, 2H), 6.29 (q, *J* = 7.0 Hz, 1H), 6.19 (q, *J* = 7.2 Hz, 1H), 4.15 (m, 4H), 1.75 (d, *J* = 7.2 Hz, 3H), 1.71 (d, *J* = 7.2 Hz, 3H), 1.19 (m, 6H); ¹³C NMR (CD₃CN, 100 MHz): δ 159.57, 159.48, 159.01, 158.96, 158.47, 158.37, 154.10, 154.00, 153.96, 153.83, 142.93, 142.82, 141.88, 141.52, 138.42, 138.35, 138.16, 138.10, 129.90, 129.23, 129.09, 128.46, 128.10, 128.03, 126.95, 126.63, 126.10, 126.05, 124.70, 124.48, 62.41, 57.86, 57.62, 22.35, 22.12, 14.46, 14.42 ppm; ESI MS C₄₈H₄₈N₈O₄Ru: m/z

calcd $[M]^+ PF_6^-$ 1047.25, $[M]^{2+}$ 451.14, found 1047.1 $[M]^+ PF_6^-$, 451.1 $[M]^{2+}$. Purity by HPLC: 98.3 % by area; UV/Vis in CH_3CN , λ_{max} ($\epsilon M^{-1} cm^{-1}$) = 235 (50900), 290 (53900), 325 (8900), 475 (8200).

5.2.2.3 $[Ru(bpy)_2(1)_2(PF_6)_2$ (**4**)

Silver nitrate (65.2 mg, 0.384 mmol) was added to a suspension of $[Ru(bpy)_2Cl_2] \cdot 2 H_2O$ (100 mg, 0.192 mmol) in water (15 mL), and the mixture was stirred overnight at RT. The solution was filtered under N_2 . 2-(1-Imidazolyl)-2-methyl-1-phenyl-2-propanone; compound **1** (102.8 mg, 0.480 mmol) and 15 mL of EtOH were added to the solution, which was stirred at 85 °C under N_2 for 24 hr. After cooling the reaction, the solution was concentrated, 1–2 mL of a saturated aqueous KPF_6 solution was added and the precipitate was extracted into CH_2Cl_2 (3x15 mL). The crude was purified by column chromatography using $H_2O:MeCN:KNO_3$ as eluent (from 0:100:0 to 10:90:0.2). The product was obtained in 73% yield (158 mg) as a crystalline red solid. 1H NMR (CD_3CN , 400 MHz): δ 8.66 (d, $J = 5.2$, 2H), 8.22 (d, $J = 8.0$ Hz, 2H), 8.08 (d, $J = 8.0$ Hz, 2H), 7.99 (t, $J = 8.0$ Hz, 2H), 7.75 (m, 4H), 7.53 (m, 4H), 7.29 (s, 2H), 7.25 (s, 2H), 7.17 (m, 6H), 7.06 (d, $J = 7.6$ Hz, 4H), 6.53 (s, 2H), 1.78 (s, 12H); ^{13}C NMR (CD_3CN , 100 MHz): δ 158.67, 158.16, 153.58, 153.25, 139.57, 137.97, 137.54, 135.15, 134.23, 130.68, 129.61, 128.80, 128.12, 127.76, 124.54, 124.26, 120.71, 67.75, 30.99, 27.54, 27.26 ppm; ESI MS $C_{46}H_{44}N_8O_2Ru$: m/z calcd $[M]^+ PF_6^-$ 987.23, $[M]^{2+}$ 421.13, found 987.4 $[M]^+ PF_6^-$, 421.1 $[M]^{2+}$. Purity by HPLC: 97.5 % by area; UV/Vis in CH_3CN , λ_{max} ($\epsilon M^{-1} cm^{-1}$) = 245 (41200), 290 (50400), 335 (8200), 485 (8300).

Compounds **2–4** were converted to Cl⁻ salts by dissolving 5–20 mg of product in 1–2 mL methanol. The dissolved product was loaded onto an Amberlite IRA-410 chloride ion exchange column, eluted with methanol, and the solvent was removed *in vacuo*.

The purity of each Ru(II) complex was analyzed using the method in Table D1 (mobile phases of 0.1% formic acid in dH₂O and 0.1% formic acid in HPLC grade CH₃CN). Samples of each Ru(II) complex were prepared in dH₂O and protected from light before injection on the HPLC.

5.2.3 Photoejection studies

5.2.3.1 MeCN photoejection studies

Photoejection studies were performed on the PF₆⁻ salts of **2–4** (30 μM) in 3 mL of acetonitrile in a 1 cm pathlength quartz cuvette placed 12 inches below a 470 nm LED array in duplicate. Each sample was prepared from the dissolution of the pure solid in acetonitrile and diluting it to the above final concentration. The samples were protected from ambient light until irradiated with the LED array. Ligand ejection was monitored by taking absorption spectra after specific time points until the spectra ceased to evolve. The half-life ($t_{1/2}$) of photoejection was determined by plotting the difference in absorbance between two points around the isosbestic point versus time using Graphpad Prism software.

5.2.3.2 Aqueous photoejection studies

Photoejection studies using the Cl⁻ salts of **2–4** in aqueous media (water, 1X PBS and Opti-MEM with 1% FBS) were performed in triplicate using a Greiner UV clear half-area 96-well plate. The kinetics for ligand ejection were determined for **2–4** (40 μM) with

a final volume of 200 μ L. The well plate was positioned 12 inches below a 470 nm LED array, and full spectra were collected after set time points of light exposure for a total of 5 hrs. The change in absorbance was plotted using the same method as described for acetonitrile.

5.2.4 Expression and purification of P450_{BM3}

The pCWori vector containing the gene for the heme domain (Thr 1–Thr 463) of P450_{BM3} with five mutations incorporated (R47L, F81I, F87V, L188Q, E267V, “PM BM3”) was transformed into BL21(DE3) cells. After transformation, cells were grown overnight on 50 μ g/ml carbenicillin plates at 37 °C.

Small 5 mL growths in Luria Broth (LB) with 100 μ g/mL ampicillin were grown overnight and then added to 1 L of Terrific Broth (TB) with 100 μ g/mL ampicillin and 0.4% glycerol. Cells were grown at 180 rpm and 37 °C until an OD₆₀₀ of 0.6–0.8 was reached. Protein production was induced by addition of 0.5 mM isopropyl β -D-1 thiogalactopyranoside (IPTG). Temperature and shaking were decreased to 30 °C and 150 rpm, respectively. After 16-20 hrs, the cells were harvested by centrifugation at 4,000 rpm for 15 min at 4 °C. The supernatant was decanted, and the cell pellet was resuspended in lysis buffer (50 mM NaH₂PO₄, 300 mM NaCl, 10 mM imidazole, 0.1 mM EDTA, and 0.1 μ M phenylmethylsulfonyl fluoride (PMSF), pH 8.0). The resuspended pellet was sonicated on ice using a Branson Sonifer 250 microtip, for 15 min with output control of 3 and duty cycle of 50%. The lysate was then centrifuged for 1 hr at 17,000 x g and 4 °C.

The supernatant was decanted, and syringe filtered with a 0.45 μ m polytetrafluoroethylene filter prior to addition to a His-Trap column (GE Healthcare)

equilibrated in buffer A (50 mM NaH₂PO₄, 300 mM NaCl, and 20 mM imidazole, pH 8.0). PM BM3 was eluted using a linear gradient of 20 mM to 200 mM imidazole with buffer B (50 mM NaH₂PO₄, 300 mM NaCl, and 200 mM imidazole, pH 8.0). Fractions were collected based on color and absorbance at 420 nm and 280 nm. PM BM3 containing fractions were then concentrated using Ultracel-30K Millipore centrifugal units at 4500 x g and 4 °C. Protein was further purified by loading onto a Hi-Prep 26/60 Sephacryl S200 HR (GE Healthcare) sizing column equilibrated with gel filtration buffer (20 mM Tris, 150 mM NaCl, pH 8.0).

All fractions with a 420/280 nm ratio above 1.2 were concentrated using Ultracel-30K Millipore centrifugal units. For storage, glycerol was added to give a final concentration of 50%, the protein was aliquoted, snap frozen, and stored at -80 °C.

Prior to using PM BM3, glycerol was removed, and the buffer was exchanged to assay buffer (20 mM Tris, 20 mM NaCl, 10 mM CaCl₂, pH 7.4) using a PD-10 desalting column (GE Healthcare). To determine protein concentration, a CO binding assay was used as previously described.¹³⁸

5.2.5 P450_{BM3} binding affinity

To determine if the inhibitors could saturate PM BM3, the protein was added to a 3 mL 1 cm pathlength quartz cuvette at a final concentration of 2.5 μM. UV/Vis spectra were taken before and after the addition of compound. Ligands were tested at 10 μM, whereas Ru(II) complexes were tested at 25 μM in the dark and after 1 min irradiation. After the addition of compound, the samples were incubated at RT for 30 sec before data collection.

Absorbance binding titrations of ligands and light activated complexes **2–4** were performed in a 1 cm pathlength quartz cuvette with 2.5 μM protein and a total volume of 3 mL. The absorbance was measured after each ligand or Ru(II) addition from 0–64.0 μM (metyrapone), 0–30.3 μM (etomidate and **1**), 0–64.7 μM (**2**), 0–54.2 μM (**3**) and 0–45.8 μM (**4**). The Ru(II) only absorbance was measured and blanked in parallel. Binding constants were determined by plotting the change in absorbance at 425 nm vs. concentration of ligand or Ru(II). Data was plotted using Graphpad Prism software and fit using a one site-total binding equation.

5.2.6 Enzyme inhibition assay

5.2.6.1 Inhibition assay with purified PM BM3

An enzymatic turnover assay was utilized to determine the inhibition of resorufin ethyl ether metabolism by PM BM3 in the presence of added compound. Each compound was added to 250 nM PM BM3 in 1X PBS (phosphate buffered saline, pH 7.5) at varying concentrations between 0–10 μM in Greiner clear 96 well plates and incubated for 10 min. Ru(II) complexes were tested in the presence and absence of light, where stock solutions were irradiated for 1 min prior to incubation with PM BM3. Following incubation with compound, 5 μM resorufin ethyl ether was added and incubated at RT for 5 min. To initiate enzymatic turnover, 5 mM hydrogen peroxide was added, and changes in fluorescence of resorufin ethyl ether were monitored over 5 min using a Tecan Spectrafluor plus microplate reader at excitation 535 nm and emission 595 nm.

5.2.6.2 Inhibition assay with Human liver microsomes (HLMs)

An enzymatic turnover assay was utilized to determine the inhibition of resorufin ethyl ether metabolism by enzymes responsible for first-pass metabolism in pooled human liver microsomes (HLMs) in the presence of added compound. 125 μM of **1** or **4** was added to 20 mg/mL HLM to a final concentration of 100 μM in 100 mM KH_2PO_4 , 10 mM MgCl_2 buffer, pH 7.5. After incubation with compound for 10 min, 5 μM resorufin ethyl ether was added followed by 1.3 mM NADPH to initiate enzymatic turnover. Changes in fluorescence of resorufin ethyl ether were monitored over 30 min using a Tecan spectrafluor plus microplate reader at the same settings as above. Compound **4** was incubated with HLMs in the dark and after 1 min irradiation with the Indigo LED.

5.2.7 *In vitro* transcription and translation

A 1-Step Human Coupled IVT Kit–DNA (Thermo Scientific) was used to carry out the experiment.³¹⁷ For each reaction, 0.5 μg of the pCFE-GFP plasmid and 5–20 μM **4** was used. Complex **4** was either irradiated for 1 min with the Indigo LED or kept in the dark. Prior to carrying out the IVT reaction, **4** was incubated with the plasmid overnight in the presence or absence of PM BM3 (0.5 μg). All IVT reactions were scaled to 12.5 μL total volume. Following the completion of the IVT reaction, the GFP emission was read in a Greiner-Bio One 384-well small volume plate on a Tecan SPECTRAFluorPlus Plate Reader with 485 nm excitation and 535 nm emission filters.

5.2.8 DNA gel electrophoresis

Compounds were mixed with 40 $\mu\text{g/mL}$ pUC19 plasmid in 10 mM potassium phosphate buffer, pH 7.4. To determine the effect of light, samples were irradiated with a 470 nm LED for 1 hr. Samples were then incubated for 12 hr at 37 $^\circ\text{C}$ in the dark. Single

and double-strand DNA break controls were prepared, and the DNA samples were resolved on agarose gels, as described previously.³¹⁸

In brief, samples were resolved on a 1% agarose gels prepared in tris-acetate buffer with 0.3 μg of plasmid/lane. The gels were stained with 0.5 $\mu\text{g}/\text{mL}$ ethidium bromide in tris-acetate buffer at RT for 40 min, destained with tris-acetate buffer, and imaged on a ChemiDoc MP System (Bio-Rad).

5.2.9 Singlet oxygen assay

Compounds were serially diluted in 96 well plates in extracellular solution (10 mM HEPES pH 7.5, 145 mM NaCl, 10 mM glucose, 1.2 mM CaCl_2 , 1.2 mM MgCl_2 , 3.3 mM KH_2PO_4 , 0.8 mM K_2HPO_4 , 50 U mL^{-1} penicillin and 50 mg mL^{-1} streptomycin). To this was added Singlet Oxygen Sensor Green (SOSG) reagent to give a final concentration of 5 μM . The plates were read on a SpectraFluor Plus plate reader with an excitation filter of 485 nm and emission of 535 nm both pre- and post- irradiation with the Loctite Indigo LED for 1 min. The relative values of the SOSG emission were plotted as a function of compound concentration to give a dose response.

5.3 Results and Discussion

5.3.1 Light triggered P450 inhibitors were synthesized from $\text{Ru}(\text{bpy})_2\text{Cl}_2$.

Ruthenium complexes **2–4** (Figure 5.2) were synthesized by refluxing the respective inhibitors with $\text{Ru}(\text{bpy})_2\text{Cl}_2$ (bpy = 2,2'-bipyridine) or the corresponding bis-aqua $\text{Ru}(\text{bpy})_2(\text{OH}_2)_2$ in EtOH/ H_2O (1:1) while protected from light. Abstraction of the chlorides was carried out with a silver salt in order to diminish the percentage of the

undesired monocoordinate complexes, $[\text{Ru}(\text{bpy})_2\text{LCI}]^+$, which complicated the purification. All complexes were formed in good yields (38–73% yield) and exhibited moderately intense metal-to-ligand charge transfer (MLCT) bands centered around 450–490 nm. Not surprisingly, compound **2** was isolated as a mixture of the possible coordination isomers, as either pyridyl ring in the asymmetric ligand (A- or B-ring, as shown in Figure 5.2) can coordinate to the Ru(II) center.

Light-triggered release of the coordinated ligands was monitored under different solvent conditions by UV/Vis absorption spectroscopy, HPLC, and mass spectrometry. All complexes were able to cleanly release both monodentate ligands in acetonitrile (MeCN) after irradiation with blue light (470 nm). A biphasic blue-shift was observed in their spectra (Figures D6 - D8), and a common final 425 nm band was found for **2–4**, which indicated the formation of a unique product, $[\text{Ru}(\text{bpy})_2(\text{MeCN})_2]^{2+}$, after the release of the corresponding inhibitors.

The photoproducts formed in aqueous solution were identified using HPLC and mass spectrometry analysis (Figures D9-D14). The chromatograms showed the appearance of new signals in irradiated samples, which corresponded to the free inhibitor and the mono-aqua Ru(II) complex. This was confirmed by the mass spectrum of the solution, with peaks corresponding to $[\text{Ru}(\text{bpy})_2\text{L}(\text{H}_2\text{O})]^{2+}$, $[\text{Ru}(\text{bpy})_2\text{L}]^2$ and $[\text{L}+\text{H}]^+$ (Figures D10, D12, D14). It is to be noted that the UV/Vis profile of the products for **3** and **4** did not differ significantly from that of the complex protected from light. The extent of the photoejection reaction varied from 40 to 65%. This observation is consistent with other $[\text{Ru}(\text{bpy})_2\text{L}_2]^{2+}$ and $[\text{Ru}(\text{phen})_2\text{L}_2]^{2+}$ complexes, where substitution of the second N-monodentate ligand,

L, requires much longer irradiation times or does not occur.^{304 310, 319-322} Finally, in the dark, all complexes were stable at room temperature and at 37 °C (Figure D5).

5.3.2 Complex 2-4 bind and inhibit P450_{BM3} and human liver microsomes (HLMs) after light irradiation.

In order to directly investigate the interactions of the metal complexes with a P450, cytochrome P450_{BM3} (CYP102A1), a soluble bacterial P450, was chosen as a model system. A mutant form of P450_{BM3} has been shown to recapitulate the activity of mammalian drug metabolizing P450s,³²³ which has made P450_{BM3} a commonly used experimental system.³²⁴ Importantly, while mammalian P450s are generally membrane associated, which complicates analysis, P450_{BM3} is soluble and thus amenable to various spectroscopic investigations as well as enzyme turnover assays. Furthermore, the *in vitro* system was chosen due to the intrinsic complications of studying P450 inhibition in cells or cell lysates, due to the need to create cell lines that overexpress the enzyme and reductase partners, and to provide exogenous reductants such as NADPH.

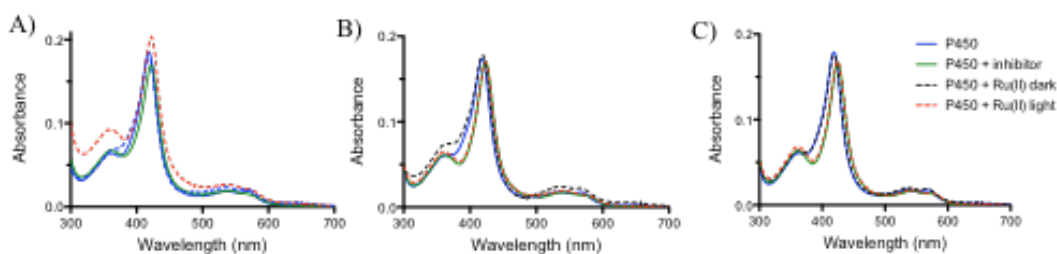


Figure 5.3 Absorption spectrum of P450_{BM3} inhibitor saturated and Ru(II) dark and light systems: 2 (A), 3 (B), 4 (C). The ratio used was 2.5 μ M P450: 25 μ M Complex (1:10) and 2.5 μ M P450: 10 μ M Ligand (1:4) for each of the respective ligands used to generate the complexes. Experiments were carried out in a 3 mL 1 cm pathlength quartz cuvette at RT.

As all three free P450 inhibitors directly ligate the heme iron, either through a pyridyl or imidazole ring, a type II spectra shift was observed upon inhibitor binding (Figure 5.3). A 7 nm red-shift in the heme Soret was observed for metyrapone, etomidate, and compound **1**, with the appearance of a second minor peak around 360 nm, where a shoulder is observed in the free enzyme. Difference spectra for all compounds show a trough maxima around 410 nm (Figure D17). Significant shoulders are observed on the troughs at 390 nm, consistent with a mixture of type IIa and type IIb spectra³²⁵⁻³²⁷ (type IIa spectra are observed when the enzyme is in the high-spin state in the absence of ligand; type IIb is seen when the enzyme is in the low-spin state).³²⁷ The ΔA_{\max} between the peak and trough and the intensity of the shoulder varied as a function of the nitrogen containing coordinating ligand, as previously reported.³²⁵

Upon exposure to an Indigo LED array (28 J/cm²), each complex induced the same type IIa and IIb spectral shift observed with the free inhibitors. Conversely, when the Ru(II) complexes **3** and **4** were kept in the dark there was little or no observed change in the P450_{BM3} absorption spectra, indicating that the complexes function as pro-drugs and do not directly affect the active site of the enzyme. Complex **2**, containing the pendant metyrapone, did exhibit a slight change in absorption profile, suggesting the intact complex containing the pendant pyridyl ligand was capable of interacting with the enzyme enough to perturb the absorption spectra. While unexpected, previous structural studies have shown that small molecules that are tethered to large fluorophores³²⁸⁻³³⁰ or even metal complexes³³¹⁻³³⁵ can bind P450s and induce opening of the substrate channel. Interestingly, the difference spectrum (Figure D17 A) indicates a different binding mode than either free metyrapone or the light-activated **2** complex, and appears to be more a type I spectrum,

consistent with displacement of water from the heme, but with no direct ligation of a coordinating nitrogen.³²⁷

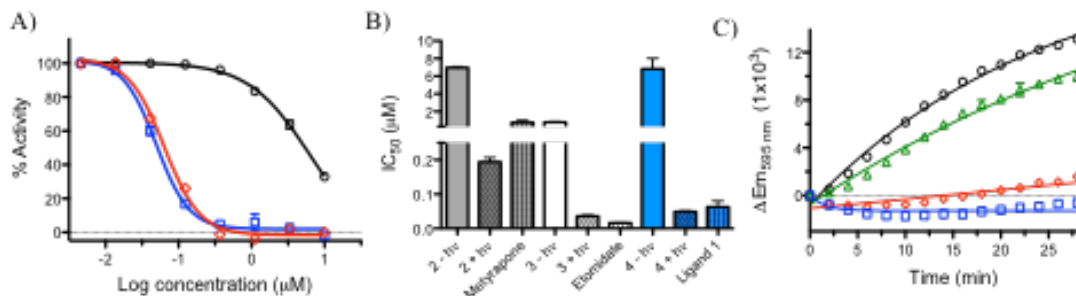


Figure 5.4 (A) Relative activity of 250 nM P450_{BM3} in the presence of 0-10 μM **1** (red diamonds) and **4** in the dark (black circles) and following irradiation (blue squares) in 1X PBS pH 7.5 buffer. 5 mM H₂O₂ was added to initiate turnover. B) IC₅₀ values for all three complexes and the respective free ligands. C) Inhibition of CYPs in 20 mg/mL HLMs by 125 μM free ligand **1** (red circles) and 125 μM complex **4** (blue squares) after irradiation compared to no compound (black circles) and **4** in the dark (green triangles). HLM experiments were done in 100 mM KPi, 10 mM MgCl₂ pH 7.5 buffer with 1.3 mM NADPH added to initiate turnover. All experiments were carried out in a Greiner clear 96 well plate. Fluorescence of 5 μM resorufin ethyl ether was monitored over a length of 5 min for P450_{BM3} and 30 min for HLMs at 37 °C at excitation 535 nm and emission of 595 nm by a Tecan spectralfluor plus microplate reader.

Enzyme inhibition was tested using resorufin ethyl ether as a substrate in a fluorescence based assay.^{336, 337} Each of the free ligands exhibited inhibition of enzyme activity (Figure 5.4 and Figure D18). As anticipated, the three Ru(II) complexes all demonstrated triggerable enzyme inhibition. Compound **4** gave the largest window for dark vs. light activity (Figure 5.4), with IC₅₀ values for enzyme inhibition of 6.8 and 0.05 μM, respectively. This compound thus provides a 136-fold difference between activity in the dark and the light. The IC₅₀ value for the free ligand **1** was 0.06 μM, in excellent agreement with the activity of the complex in the light. Each light activated system displayed very

similar activity to the free inhibitor (Figure 5.4B; compound **2** IC_{50} = 0.19 μ M vs. 0.75 μ M for metyrapone; compound **3** IC_{50} = 0.04 μ M vs. 0.02 μ M for etomidate).

To extend the investigation to a medically validated, commonly used experimental system, pooled human liver microsomes (HLMs) were used to study the light-triggered inhibition of enzyme turnover. HLMs contain membrane-bound human CYPs which play major roles in first pass metabolism of xenobiotics.^{338, 339} Incubation of HLMs with compound allows study of how these compounds impact activity of multiple CYPs at once, and in a membrane environment. This provides a good model for human CYPs. Compound **4** exhibited the largest window for light-mediated enzyme inhibition for P450_{BM3}, so it was tested along with the free ligand **1**. In the dark, at 100 μ M, compound **4** was found to minimally inhibit CYPs in HLMs, but complete inhibition was observed after irradiation (Figure 5.4C). A similar trend was seen with free ligand **1**, with nearly complete inhibition of enzyme turnover.

5.3.3 DNA damage is induced by complex **2-4** after light irradiation.

Having confirmed the utility of the light active compounds for inhibition of cytochrome P450 activity, DNA damage was investigated using agarose gel electrophoresis. Dose responses were performed with compound **2-4** with pUC19 plasmid, and the solutions were either protected from light or irradiated for 1 or 3 h (60.4 or 181.4 J/cm^2) before incubation at 37 °C for 12 h (Figure 5.5). No effect was seen for any of the intact pro-drug forms of the complexes, but all induced DNA damage upon light activation. DNA damage was visualized by reduced mobility of DNA, consistent with direct adduct

formation, as demonstrated in classical experiments on cisplatin³⁴⁰⁻³⁴² and more recently with analogous light-activated ruthenium compounds.^{318, 343}

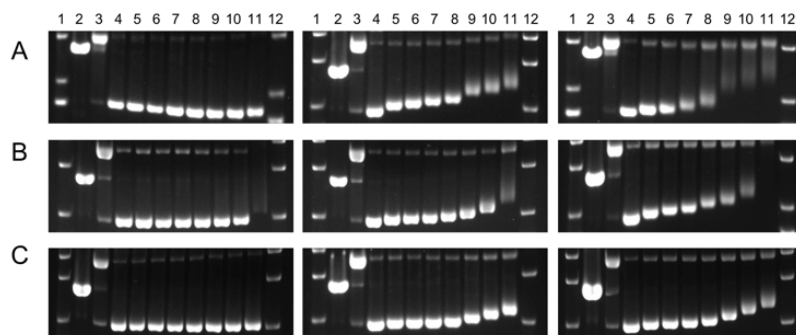


Figure 5.5 Agarose gels showing the dose response of 2 (A), 3 (B), and 4 (C) with 40 $\mu\text{g/mL}$ pUC19 plasmid with and without irradiation ($\lambda > 470$ nm). Dark, left; 1 hr irradiation, middle; 3 hr irradiation, right. Lane 1 and 12: DNA ladder; Lane 2: EcoRI; Lane 3: Cu(OP)_2 ; Lanes 4–11: 0, 7.8, 15.6, 31.3, 62.5, 125, 250, 500 μM (500 μM corresponds to a metal center:base ratio of 4:1). EcoRI and Cu(OP)_2 are used as controls for linear and relaxed circular DNA. EtBr was used to visualize the DNA. DNA damage gels performed by A. Zamora.

Very little relaxed circular DNA was observed, but what was formed likely resulted from single strand breaks induced by singlet oxygen ($^1\text{O}_2$). Ligand ejection proceeds from an excited state that is populated from the $^3\text{MLCT}$ state, which also generates $^1\text{O}_2$; thus, there is a competition in relaxation pathways, and complexes that have longer $t_{1/2}$ values have been found to induce more single strand breaks. We^{318, 344} and others³⁴⁵ have thus observed that the combination of the different relaxation pathways makes these agents capable of “dual photoreactivity” independent of the biological activity of the released ligands. However, little $^1\text{O}_2$ was detected, as shown in Figure D19, consistent with the DNA damage study and relaxation primarily through ligand ejection. Finally, all the free ligands

were tested as controls, and as anticipated, they had no impact on the plasmid DNA (Figure D20).

5.3.4 Transcription and translation in the presence of P450_{BM3} and complex 2-4 after light irradiation is inhibited.

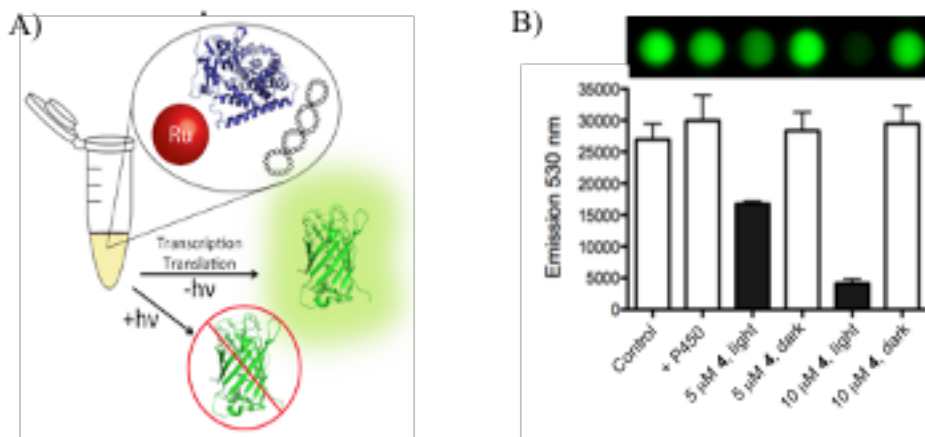


Figure 5.6 (A) An *in vitro* transcription and translation experiment allows for detection of DNA damage that results in inhibition of GFP production. Compound 4 was incubated in the presence of both plasmid and P450_{BM3} at equal concentrations. (B) GFP production was unaffected by the addition of P450_{BM3} (+ P450; lane 2) and the protein had no impact on the ability of compound 4 to damage DNA upon light activation (lanes 3–6). IVTT assay carried out by L. Nease and D. Heidary.

The ultimate experiment was to investigate if the light activated metal complexes were able to inhibit DNA function in the presence of the P450 enzyme. Accordingly, an *in vitro* transcription and translation experiment³¹⁷ was performed, as shown in Figure 5.6A. A plasmid coding for green fluorescent protein (GFP) was incubated with compound 4 in the dark or following activation with light. The experiment was also performed in the presence of P450_{BM3}. No impact on GFP production was observed for 4 in the dark, while a dose dependent inhibition of

protein production was found following activation with light as shown in Figure 5.6B. The addition of P450_{BM3} had no impact on GFP transcription or translation in the absence of the Ru(II) complex, or in its presence. Thus, the P450_{BM3} enzyme does not serve as a “sink” for the activated metal center and does not interfere with the DNA damage mechanism. This validates that the Ru(II) center can target DNA while the released ligands target the P450 enzyme.

5.4 Conclusions

The three complexes described in this report serve as proof-of-concept systems for single agent “drug cocktails” and demonstrate that, upon light activation, the metal center is able to damage DNA while the liberated ligand acts as a cytochrome P450 inhibitor. The best system, compound **4**, exhibited a 136-fold difference in protein inhibition when irradiated with light as compared to in the dark, with an IC₅₀ of 0.05 μM upon activation. In the absence of irradiation, the complexes did not damage or interfere with its function, as indicated by gel electrophoresis and activity in a transcription and translation assay. Upon light activation, protein production was inhibited with an IC₅₀ between 5 and 10 μM in the light. Furthermore, the metal center damages the DNA even in the presence of protein, indicating that DNA is the preferred target.

The choice to inhibit P450 enzymes is a key feature in the design of these prodrugs. The targeting of enzymes implicated in drug resistance could result in synergistic activity for DNA damaging agents in cancer cells and tissues, though more involved studies in cancer cell lines engineered and optimized to detect P450 activity and inhibition will be required for full validation of this potential therapeutic approach. However, the clear

inhibition of P450 activity and the DNA damage and suppression of transcription and translation *in vitro*, combined with the well-established cytotoxicity of light activated, ligand deficient Ru(II) complexes in cells are strongly promising. This is also, to the best of our knowledge, the first report of photocaged P450 inhibitors. These compounds may be useful for basic research applications as tools that provide spatial and temporal control over P450 inhibition and could answer several open questions in the role that P450s play in malignant cell transformation and drug resistance. Single mode of action photocaged systems, which do not damage DNA, are also under development to allow for the triggered control of P450 activity without complications from the activity of the metal center.

CHAPTER 6. CONCLUSIONS

The central dogma of biology is a simple yet elegant process that details how life is able to exist. DNA, which stores information, is transcribed into mRNA which is then translated into proteins. Proteins are the “workhorse” of the cell and perform a majority of the actions that need to occur for life to be viable. Investigating protein function is key to understanding part of what makes us human, but also what allows for life to flourish. There are several variables that can be studied that impact protein function and stability, including, but not limited to, cell localization, solubility, substrate preference, impact of residues, and if a metalloprotein, the impact of charge and electron transfer systems.

Cytochrome P450s (CYPs) are a family of heme enzymes present in almost all forms of life that use oxygen to make hydrophobic substrates more hydrophilic. In humans this means they are crucial for steroidogenesis and xenobiotic metabolism^{346, 347} while in plants they are necessary for defense,^{348, 349} and they aid in antifungal resistance in some fungi.³⁵⁰⁻³⁵² We used CYP102A1 (P450_{BM3}), a bacterial CYP, as a model system to understand particular properties of human CYPs. Using a variety of biophysical techniques, we investigated the role of specific residues in increasing promiscuity, how native and non-native substrates can bind favorably, and how iron oxidation state impacts stability.

By investigating the above three variables, we elucidated some requirements of promiscuity, but also some of its costs, which are important for any possible biotechnical applications incorporating these enzymes. The main cost is that increased promiscuity translates to increased flexibility of the enzyme. Though flexibility is necessary for binding of non-native substrates, it leads to a decrease in stability and increase in uncoupled catalysis. The consequences are an increase in ROS generation, accelerated degradation of

the enzyme, and limited function. In theory, mutating smaller residues external to the active site to bulkier residues should help alleviate the stress caused by promiscuity without impacting the openness of the interior. Though we have not studied this in-depth, it would make a good follow-up study to this work. From studying the role of promiscuity on oxidation state it has become clear that there is a relationship between the energy barrier needed to move between various iron oxidation states and ligand selectivity. Promiscuous CYPs are more likely to have a lower energy barrier between initial steps in their catalytic cycles as compared to more selective variants. This was expressed by a similarity in stability between the ferrous and ferric states as well as an increase in reduction potential of the more promiscuous enzymes.

George E. P. Box was a famous statistician, (if modern mathematicians can be considered famous) who is perhaps most known for saying, “All models are wrong, but some are useful.”³⁵³ This dissertation is a detailed study of using P450_{BM3} as a model for human CYPs. Of the several variables that impact CYP function and stability that can be studied, three were investigated. These variables were: the role of residues in selectivity, substrate specificity of native and non-native substrates, and the impact of promiscuity on iron oxidation state. Work is currently on-going to elucidate the mechanism of biphasic unfolding for P450_{BM3}, as well as research initially started by the Ru(II) dual mechanism project. Further studies would use rational mutagenesis to make our promiscuous mutant more stable, determine methods or models to study more states of the catalytic cycle, and incorporate a larger body of biophysical methods such as electron paramagnetic resonance (EPR).

Appendix A: Chapter 2 Additional Figures and Tables

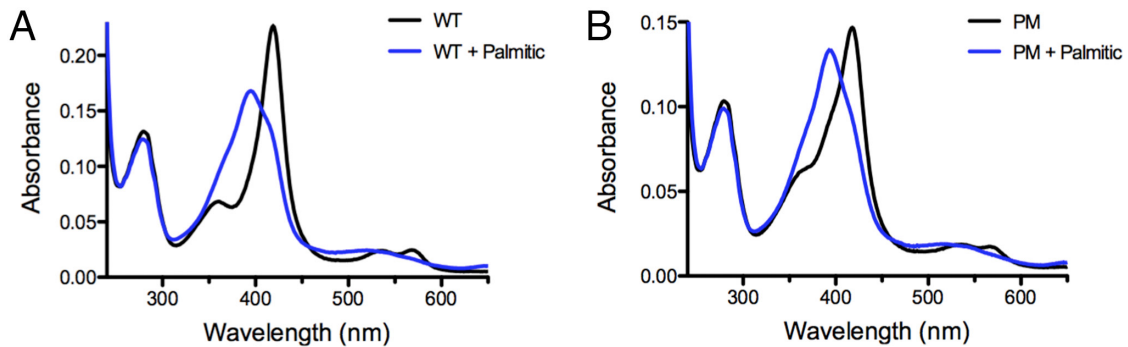


Figure A1. UV-Vis spectra of purified P450_{BM3} oxidase domain. (A) WT oxidase spectra is in the water-bound form after gel filtration chromatography with a peak at 418 nm (black line) and undergoes a spin shift to 394 nm when bound to the substrate, palmitic acid (blue line). (B) The behavior of the purified PM oxidase is similar to the WT oxidase domain indicating that the purified form is water-bound and undergoes a spin shift with palmitic acid.

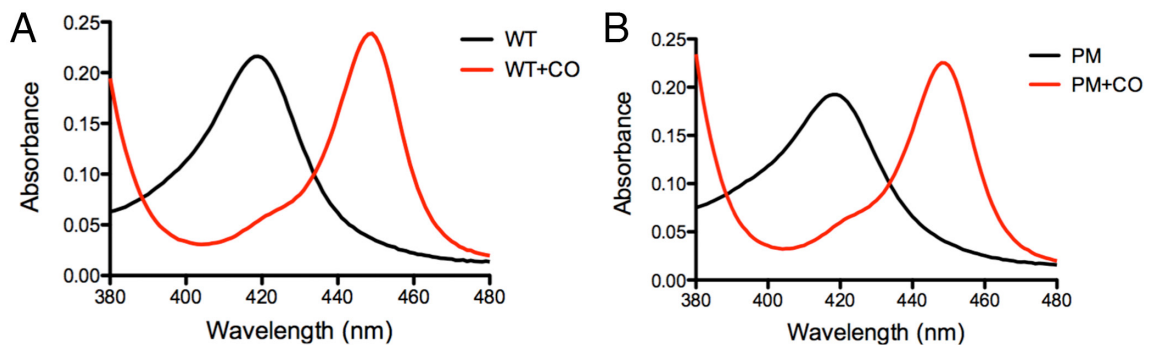


Figure A2. UV-Vis spectra of WT and PM spin shift from 418 nm to 450 nm upon carbon monoxide binding. (A) WT oxidase domain absorption spectra in the water-bound form (black line) and after CO coordination to the heme (red line). (B) The PM oxidase domain undergoes the same absorption change as WT.

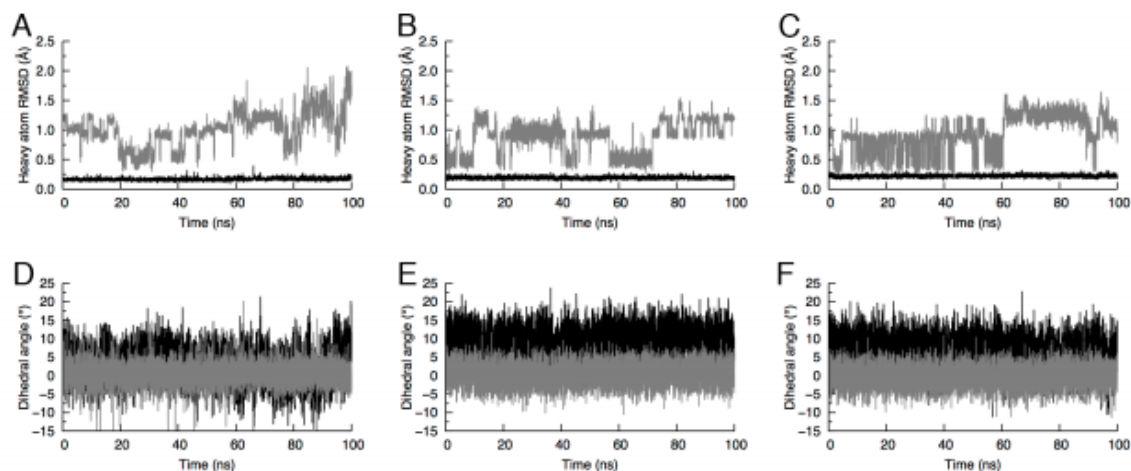


Figure A3. RMSD of heme heavy atoms in (A) substrate-free WT, (B) WT:metyrapone, and (C) WT: palmitic acid during the 300-K simulations. Ring atoms are shown in black lines, while propionate and vinyl atoms are shown by gray lines. Planarity of heme in (D) substrate-free WT, (E) WT:metyrapone, and (F) WT:palmitic acid during the 300-K simulations. The dihedral angle between the carbon atoms connecting the four pyrrole subunits is shown in black lines, while that between the pyrrole nitrogen atoms are shown in gray lines.

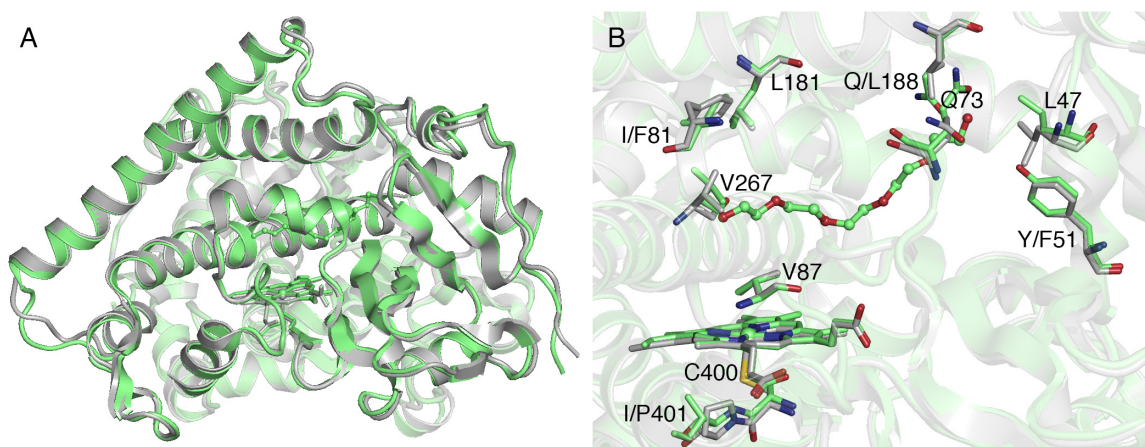


Figure A4. Crystal structures of PM in the presence of polyethylene glycol (4ZF6, green) and substrate-free R47L/Y51F/F87V/E267V/I401P mutant (4RNS, gray). The heme and residues of interest are shown in stick and polyethylene glycol in ball-and-stick. (A) Overall structure. (B) Substrate channel. Among the common mutations, only L47 differed significantly in side chain position, The Q73 side chain also points outward unlike in PM.

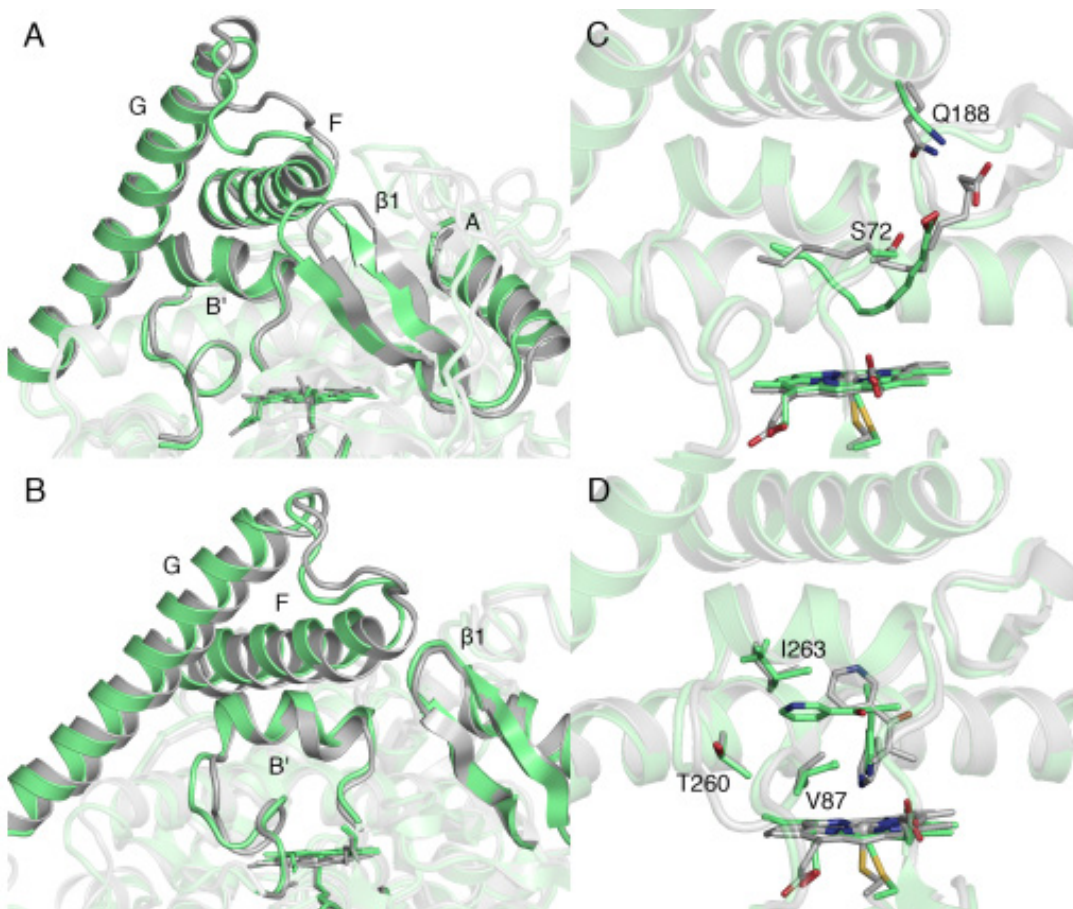


Figure A5. Comparison of crystal (gray) and MD-averaged (green) structures. (A) Substrate-free L188Q and IBU7 (molecule B). Helix A and β -sheet 1 of L188Q moved closer to the protein core during the 300-K simulation, partially closing the channel. This was also observed in the MD-averaged structures of substrate-free WT and E267V. (B) Substrate-free PM and 4ZF6. Helices F and G moved away from the protein core during the 300-K simulation, partially opening the channel. (C) PM:palmitic acid and 4ZFB. Palmitic acid moved closer to the heme and formed a hydrogen bond with S72 during the 300-K simulation. (D) PM:metyrapone and 4ZF8. Metyrapone rotated during the 300-K simulation, bringing the unbound pyridine ring in close contact with V87, T260, and I263. MD simulations performed by I. Geronimo.

Table A1. Backbone RMSD (Å) of average structures with respect to wild-type P450_{BM3} (IBU7, molecule B). MD simulations performed by I. Geronimo.

Region	R47L	F81I	F87V	L188Q	E267V
Helix					
A	1.07	0.95	0.92	1.28	1.16
B	0.80	0.58	0.44	1.25	0.98
B'	0.95	0.77	0.62	1.08	0.63
C	0.83	0.58	0.80	0.69	0.80
D	0.47	0.33	0.45	0.59	0.50
E	0.64	0.61	0.55	0.79	0.86
F	0.79	0.80	0.71	0.88	0.84
G	1.14	1.01	0.92	1.43	1.27
H	1.26	0.88	1.12	1.02	0.87
I	0.74	0.70	0.68	0.72	0.82
J	0.40	0.36	0.55	0.60	0.73
J'	0.54	0.39	0.59	1.00	0.82
K	0.52	0.45	0.43	0.75	0.57
K'	0.37	0.32	0.39	0.72	0.49
K''	0.30	0.43	0.47	0.57	0.53
L	1.07	0.83	0.90	2.23	1.21
β-sheet					
1	0.79	0.62	0.44	1.03	0.86
2	0.64	0.66	0.56	0.65	0.53
3	1.06	0.95	1.08	1.47	1.41
4	0.72	0.79	0.86	0.69	1.32
5	0.35	0.44	0.47	0.59	0.51
Cys loop	1.97	0.46	0.65	0.92	0.61

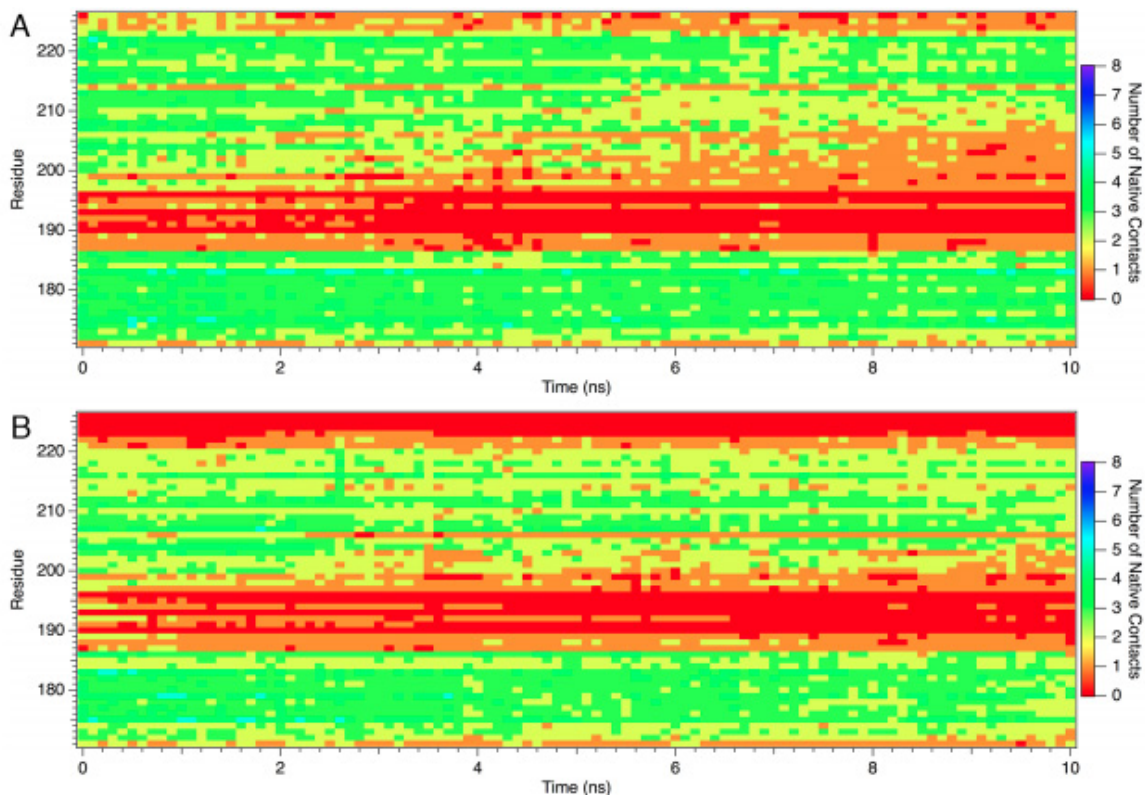


Figure A6. Plot of native contacts of residues in helices F (171-190) and G (197-226) of substrate-free (A) WT and (B) PM as a function of simulation time at 550 K. The number of contacts is the average from three independent simulations. MD simulations performed by I. Geronimo.

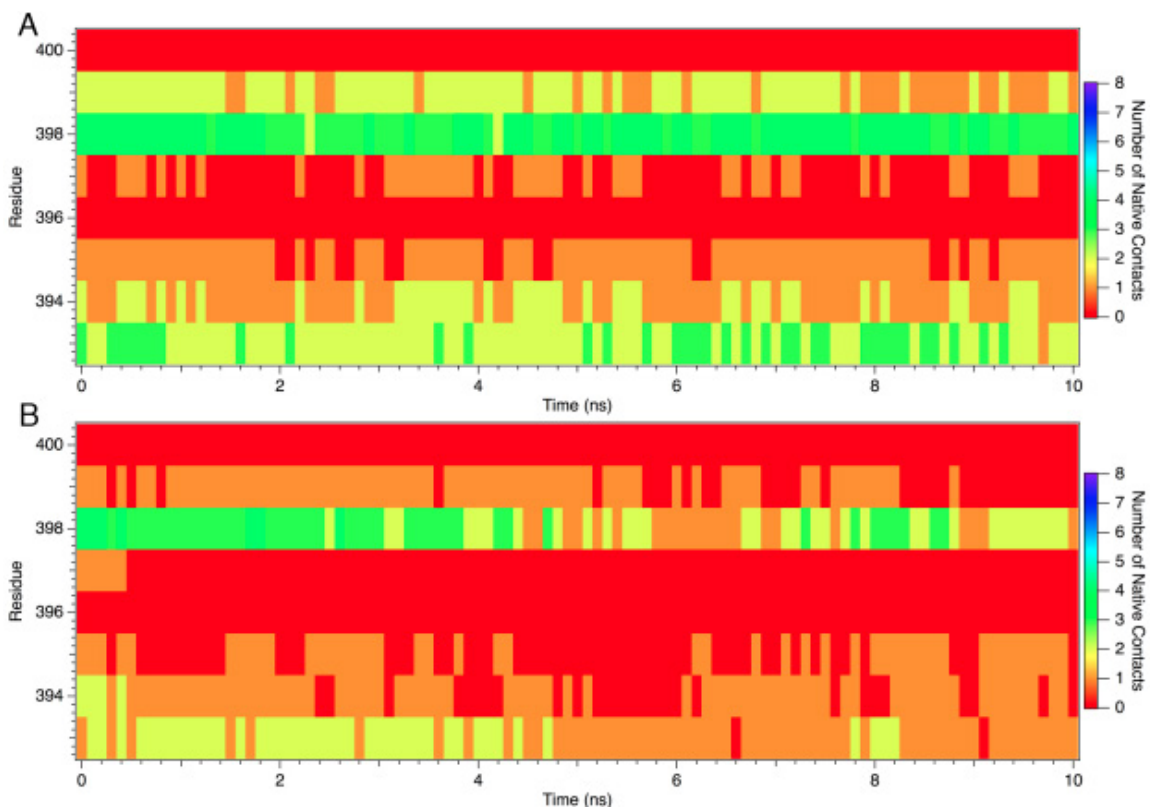


Figure A7. Plot of native contacts of residues in the Cys ligand loop of substrate-free (A) WT and (B) PM as a function of simulation time at 550 K. The number of contacts is the average from three independent simulations. MD simulations performed by I. Geronimo.

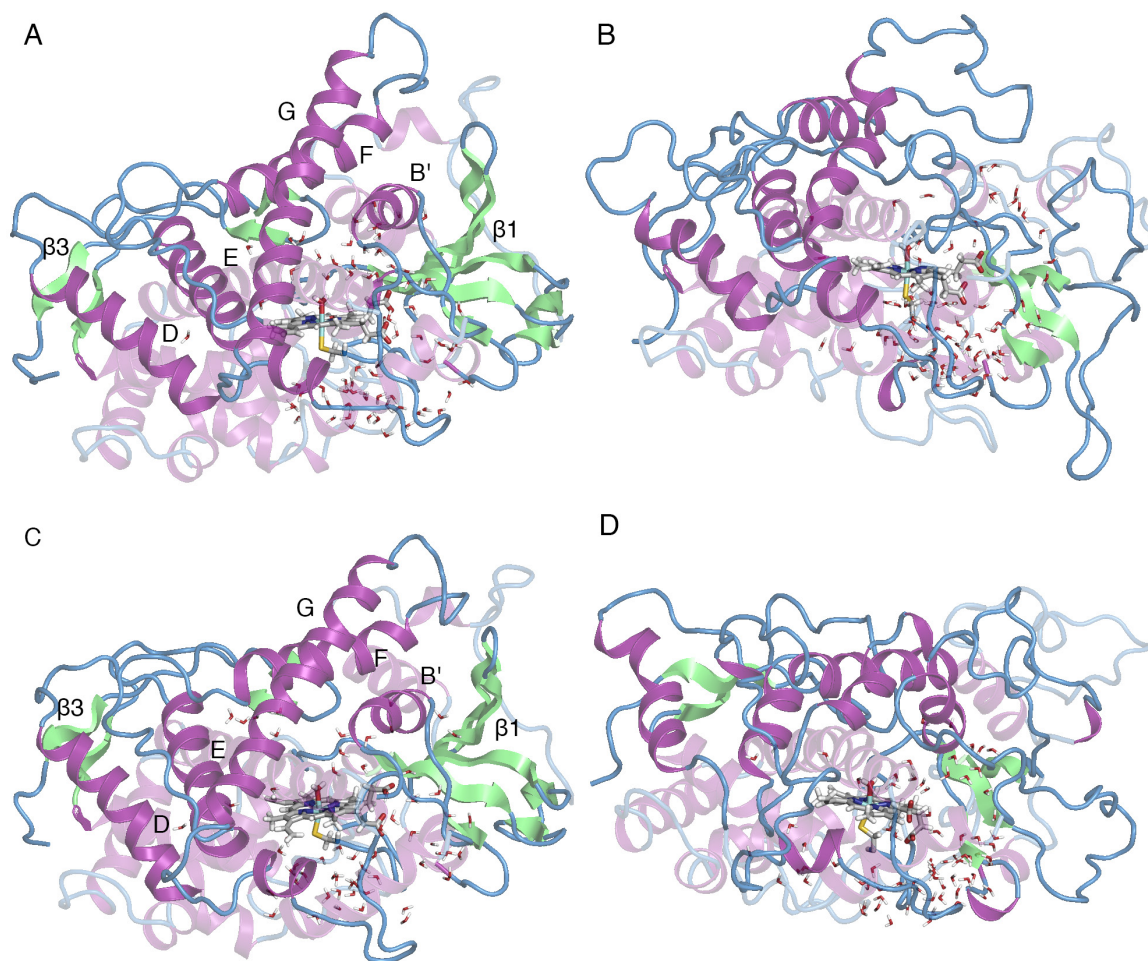


Figure A8. High-temperature (550 K) simulations of substrate-free P450_{BM3} variants (cartoon representation). The heme, cys ligand, bound water, and water within 10 Å of the heme are shown in stick. Snapshots of WT at (A) 0 ns and (B) 50 ns. Snapshots of PM at (C) 0 ns and (D) 50 ns. Helices D and E of PM unfolded concurrently with sections of the substrate channel unlike in WT. MD simulations performed by I. Geronimo.

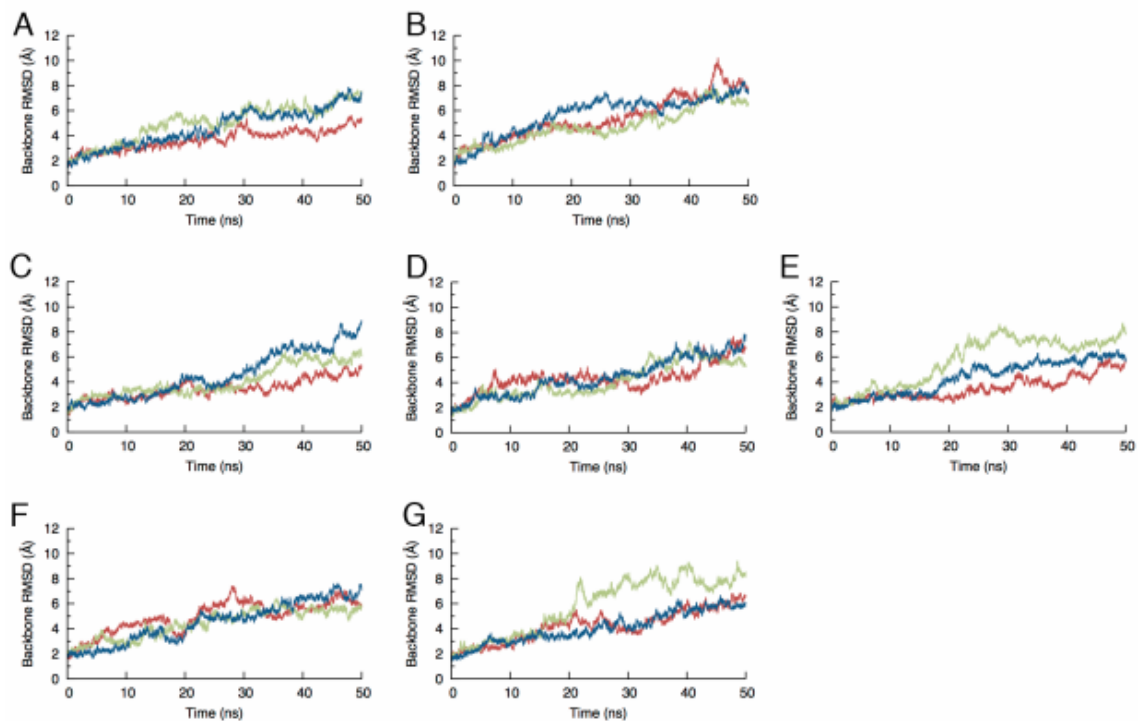


Figure A9. RMSD of backbone atoms in substrate-free (A) WT, (B) PM, (C) R47L, (D) F81I, (E) F87V, (F) L188Q, and (G) E267V. Three independent simulations at 550 K were performed for each system. MD simulations performed by I. Geronimo.

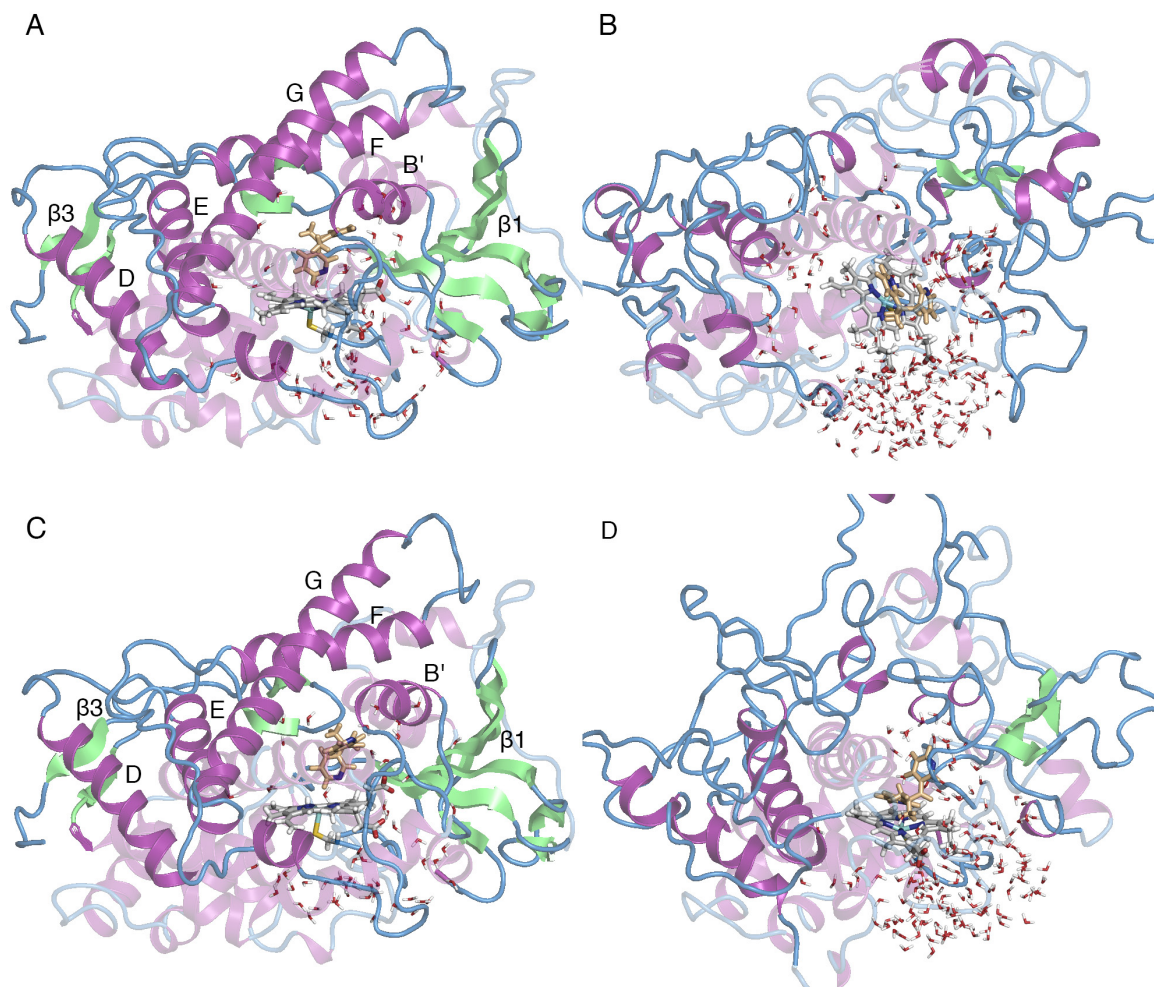


Figure A10. High-temperature (550 K) simulations of P450_{BM3} variants with metyrapone (cartoon representation). The heme, Cys ligand, metyrapone, and water within 10 Å of the heme are shown in stick. Snapshots of WT at (A) 0 ns and (B) 50 ns. Snapshots of PM at (C) 0 ns and (D) 50 ns. The heme region of both enzymes is destroyed at the end of simulation. MD simulations performed by I. Geronimo.

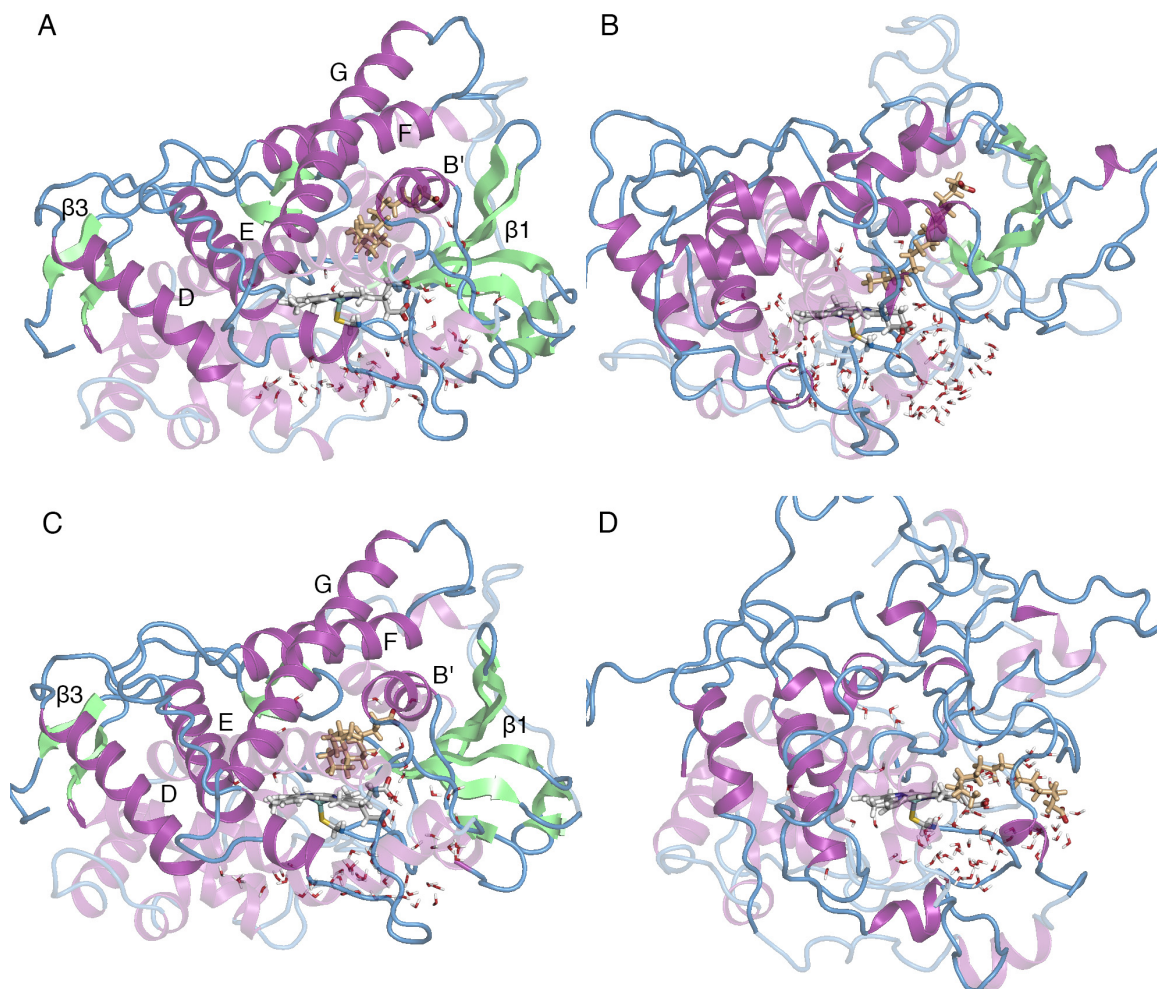


Figure A11. High-temperature (550 K) simulations of P450_{BM3} variants with palmitic acid (cartoon representation). The heme, Cys ligand, metyrapone, and water within 10 Å of the heme are shown in stick. Snapshots of WT at (A) 0 ns and (B) 50 ns. Snapshots of PM at (C) 0 ns and (D) 50 ns. MD simulations performed by I. Geronimo.

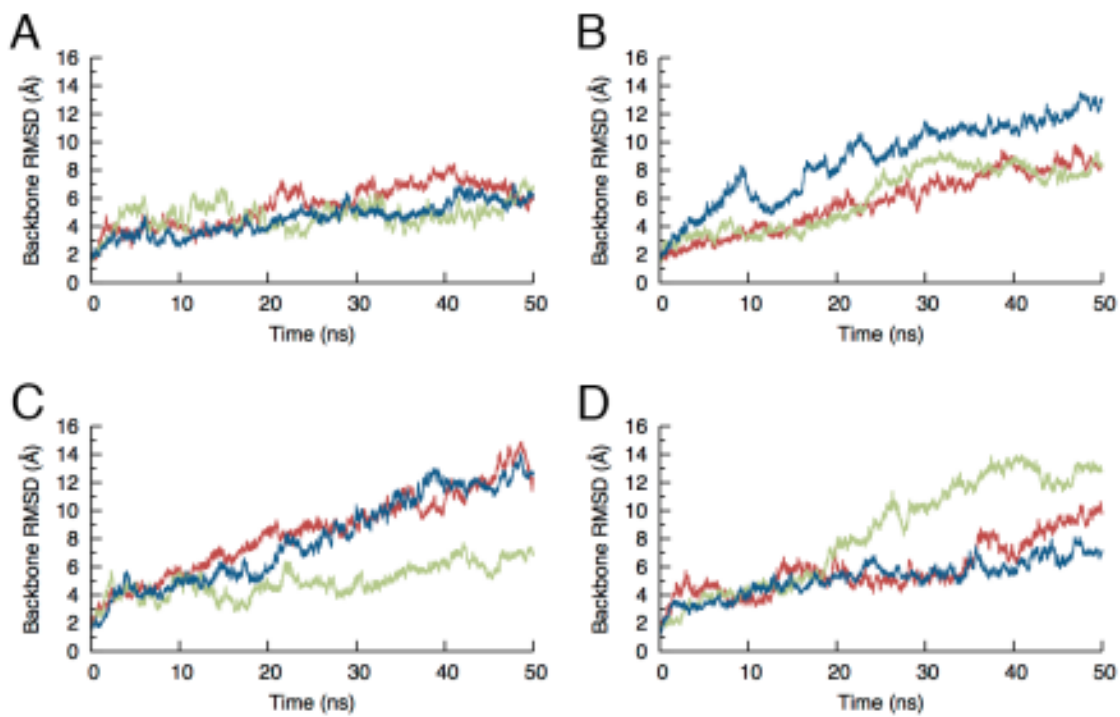


Figure A12. RMSD of backbone atoms in (A) WT:palmitic acid, (B) WT:metyrapone, (C) PM: palmitic acid, and (D) PM:metyrapone complexes. Three independent simulations at 550 K were performed for each system. MD simulations performed by I. Geronimo.

Table A2. Salt bridge occupancies calculated from the 300-K MD simulation.^{a,b} MD simulations performed by I. Geronimo.

Salt bridge	WT-SF	WT-MYT	WT-PLM	PM-SF	PM-MYT	PM-PLM
E38-R56	0.949	0.907	0.839	0.921	0.914	0.953
E60-R66	0.828	0.741	–	0.722	0.723	0.806
D68-H92	–	–	0.631	–	–	–
D84-R79	–	–	0.947	–	–	0.805
E93-R79	1.000	1.000	–	0.861	1.000	–
D121-R161	0.925	0.880	0.638	0.984	0.946	0.904
D144-K129	0.985	0.984	0.679	0.908	0.910	0.859
E183-R190	0.995	0.999	0.657	1.000	1.000	0.999
E200-R203	0.618	0.566	0.552	–	0.526	0.606
E207-K210	0.563	–	–	–	–	–
D208-R179	0.933	0.925	0.941	0.917	0.937	0.943
D214-K210	–	0.572	–	–	0.549	–
D217-R255	0.816	0.894	0.539	0.985	0.702	0.666
D222-K218	0.572	0.681	–	–	–	0.781
D232-R223	1.000	1.000	0.995	0.974	1.000	1.000
E247-K94	0.717	–	0.567	0.524	–	–
E247-K98	0.801	0.693	0.749	0.765	0.675	–
D250-K98	–	0.529	0.683	0.694	0.676	–
D251-K224	0.934	–	–	–	–	–
E267-K440 ^c	0.783	0.969	0.987			
E292-R296	–	0.746	–	0.836	–	–
E293-R296	0.845	0.522	0.577	0.699	–	–
E320-R323	0.955	0.875	0.823	0.964	0.885	0.887
E320-R378	0.711	0.623	0.689	–	0.667	0.835
E344-K3	0.720	0.692	0.712	0.656	0.627	0.694
E344-R56	0.960	0.974	0.931	0.915	0.954	0.962
D351-R50	0.557	–	0.589	0.571	–	–
E352-R47 ^d	0.812	0.650	–			
D370-R375	–	0.916	0.688	0.877	0.682	–
D370-R378	0.653	–	–	0.946	–	0.969
E372-R362	–	0.557	0.707	0.761	0.701	0.558

Table A2 (continued)

E377-K289	–	–	0.539	–	0.728	0.705
E380-K312	–	–	–	–	0.573	–
D425-K282	0.867	0.705	0.535	0.729	–	–
D432-K24	0.744	0.640	0.513	0.538	0.861	–
E442-K434	–	–	0.610	–	–	–

^a Salt bridge defined as interaction between O atom of Asp/Glu and protonated N atom of Arg/Lys/His within a distance cutoff of 4.0 Å. “–” indicates that the occupancy is < 0.5 ^b SF, substrate-free; MYT, metyrapone; PLM, palmitic acid ^c Residue 267 is Val in PM ^d Residue 47 is Leu in PM

Appendix B: Chapter 3 Additional Figures and Tables

Table B1. Predicted protonation states of substrates at physiological pH.^a Predictions determined by I. Geronimo.

Substrate	Number of titratable atoms	Strongest acidic/basic pK _a	Charge at pH 7.4
diclofenac	2	4.00	-1.00
naproxen	1	4.19	-1.00
warfarin	1	5.56	-0.99
lovastatin	1	14.91	0.00
dextromethorphan	1	9.85	1.00
MDMA	1	10.14	1.00
astemizole	2	8.73	1.02
nicotine	2	8.58	0.94
cotinine	2	4.79	0.00
metyrapone	2	4.87	0.00

^a <https://chemicalize.com> (accessed April 2018)

Table B2. Van der Waals component of pairwise interaction energy (kcal/mol) for diclofenac (DIF), naproxen (NPS), S-warfarin (SWF), R-warfarin (RWF), and lovastatin (LVA) complexes. Mean and standard deviation were calculated by averaging over 5-ns blocks. MD simulations performed by I. Geronimo.

Residue	DIF	NPS	SWF	RWF	LVA
S72	0.14 ± 0.57	1.02 ± 0.20	-0.54 ± 0.12	-0.18 ± 0.15	-0.76 ± 0.25
A74	-1.23 ± 0.20	-0.44 ± 0.08	-1.17 ± 0.04	-0.77 ± 0.17	-1.18 ± 0.36
L75	-4.20 ± 0.72	-3.60 ± 0.16	-4.05 ± 0.14	-2.67 ± 0.15	-3.99 ± 0.18
V78	-0.98 ± 0.10	-0.15 ± 0.01	-1.04 ± 0.05	-3.86 ± 0.20	-1.64 ± 0.12
V87	-2.50 ± 0.32	-1.71 ± 0.22	-3.01 ± 0.10	-2.19 ± 0.21	-2.11 ± 0.13
L181	-0.63 ± 0.33	-0.05 ± 0.02	-0.08 ± 0.01	-0.96 ± 0.04	-1.29 ± 0.15
T260	-0.15 ± 0.01	-0.06 ± 0.01	-0.08 ± 0.01	-1.31 ± 0.27	-0.48 ± 0.13
I263	-1.21 ± 0.24	-0.27 ± 0.08	-0.19 ± 0.03	-2.07 ± 0.10	-1.31 ± 0.15
A264	-1.52 ± 0.22	-1.10 ± 0.16	-0.92 ± 0.06	-2.06 ± 0.28	-1.21 ± 0.08
V267	-0.73 ± 0.08	-0.41 ± 0.21	-0.38 ± 0.07	-0.73 ± 0.08	-1.05 ± 0.30
T268	-0.93 ± 0.07	-0.79 ± 0.09	-0.82 ± 0.02	-0.58 ± 0.07	-1.25 ± 0.12
A328	-0.55 ± 0.42	-1.50 ± 0.07	-1.62 ± 0.21	-1.21 ± 0.21	-1.04 ± 0.17
A330	-0.47 ± 0.25	-1.89 ± 0.04	-1.33 ± 0.03	-0.50 ± 0.11	-2.91 ± 0.19
M354	-0.09 ± 0.04	-0.93 ± 0.06	-0.33 ± 0.09	-0.05 ± 0.01	-1.24 ± 0.07
L437	-3.37 ± 0.64	-1.64 ± 0.17	-3.79 ± 0.13	-3.76 ± 0.10	-4.99 ± 0.54
T438	-2.32 ± 0.42	-1.26 ± 0.11	-0.94 ± 0.04	-2.47 ± 0.30	-3.30 ± 0.36

Table B3. Van der Waals component of pairwise interaction energy (kcal/mol) for DEX, MDMA, and AST complexes. Mean and standard deviation were calculated by averaging over 5-ns blocks. MD simulations performed by I. Geronimo.

Residue	DEX	MDMA ^a	MDMA ^b	AST ^a	AST ^b	AST ^c
S72	-0.01 ± 0.01	-0.64 ± 0.11	-0.19 ± 0.03	-0.20 ± 0.11	-1.71 ± 0.90	-0.70 ± 0.52
A74	-0.04 ± 0.01	-0.15 ± 0.02	-0.88 ± 0.07	-0.59 ± 0.12	-0.97 ± 0.63	-1.13 ± 0.46
L75	-1.48 ± 0.19	-2.24 ± 0.14	-2.02 ± 0.11	-1.48 ± 0.42	-3.86 ± 1.10	-2.40 ± 0.82
V78	-1.34 ± 0.27	-0.06 ± 0.01	-0.99 ± 0.11	-5.41 ± 0.38	-2.15 ± 0.40	-2.76 ± 0.45
V87	-3.78 ± 0.08	-1.22 ± 0.16	-2.06 ± 0.18	-1.82 ± 0.12	-5.37 ± 0.37	-3.22 ± 0.40
L181	-1.17 ± 0.34	-0.02 ± 0.01	-0.17 ± 0.06	-3.20 ± 0.41	-0.58 ± 0.29	-1.05 ± 0.16
T260	-2.20 ± 0.15	-0.04 ± 0.01	-0.13 ± 0.02	-1.71 ± 0.09	-0.27 ± 0.03	-1.12 ± 0.22
I263	-3.88 ± 0.45	-0.10 ± 0.01	-0.70 ± 0.18	-4.65 ± 0.32	-1.45 ± 0.29	-2.80 ± 0.34
A264	-1.35 ± 0.17	-0.83 ± 0.04	-1.71 ± 0.08	-3.02 ± 0.14	-1.73 ± 0.19	-2.53 ± 0.23
V267	-1.47 ± 0.55	-0.02 ± 0.01	-0.60 ± 0.14	-1.08 ± 0.09	-1.48 ± 0.53	-1.17 ± 0.08
T268	-1.59 ± 0.10	-1.10 ± 0.06	-1.12 ± 0.04	-1.54 ± 0.05	-1.37 ± 0.17	-1.15 ± 0.16
A328	-0.95 ± 0.21	-1.36 ± 0.05	-1.16 ± 0.34	-2.40 ± 0.09	-1.17 ± 0.25	-2.84 ± 0.53
A330	-0.12 ± 0.03	-2.39 ± 0.12	-0.38 ± 0.07	-1.57 ± 0.20	-0.57 ± 0.24	-1.25 ± 0.19
M354	0.00	-0.72 ± 0.05	-0.03 ± 0.01	-0.14 ± 0.03	-0.08 ± 0.05	-0.05 ± 0.01
L437	-2.33 ± 0.44	-2.65 ± 0.11	-1.94 ± 0.14	-5.22 ± 0.92	-2.60 ± 0.31	-3.86 ± 0.57
T438	-1.40 ± 0.28	-1.28 ± 0.03	-2.09 ± 0.08	-3.14 ± 0.11	-1.37 ± 0.21	-2.76 ± 0.61

^a positioned for N-dealkylation ^b positioned for O-dealkylation ^c positioned for C–H hydroxylation

Table B4. Van der Waals component of pairwise energy (kcal/mol) for nicotine (NCT), cotinine (CTN), and metyrapone (MYT) complexes. Mean and standard deviation were calculated by averaging over 5-ns blocks. MD simulations performed by I. Geronimo.

Residue	NCT	CTN	MYT
S72	-0.12 ± 0.04	-0.19 ± 0.05	-0.01 ± 0.01
A74	-0.04 ± 0.01	-0.10 ± 0.02	-0.04 ± 0.01
L75	-1.35 ± 0.16	-2.23 ± 0.10	-1.34 ± 0.09
V78	-0.07 ± 0.01	-0.40 ± 0.06	-1.40 ± 0.07
V87	-1.61 ± 0.12	-1.66 ± 0.05	-3.78 ± 0.08
L181	-0.04 ± 0.01	-0.08 ± 0.03	-0.91 ± 0.12
T260	-0.11 ± 0.01	-0.14 ± 0.02	-1.82 ± 0.04
I263	-0.41 ± 0.08	-1.11 ± 0.19	-2.91 ± 0.05
A264	-1.54 ± 0.06	-2.17 ± 0.17	-2.89 ± 0.07
V267	-0.11 ± 0.03	-0.20 ± 0.06	-1.15 ± 0.02
T268	-1.02 ± 0.03	-0.79 ± 0.19	-1.21 ± 0.03
A328	-1.77 ± 0.14	-1.78 ± 0.11	-0.68 ± 0.13
A330	-0.94 ± 0.15	-0.39 ± 0.04	-0.07 ± 0.01
M354	-0.05 ± 0.01	-0.02 ± 0.01	0.00
L437	-1.84 ± 0.23	-2.41 ± 0.20	-2.12 ± 0.08
T438	-1.55 ± 0.09	-1.60 ± 0.08	-1.46 ± 0.06

Table B5. Hydrogen bond occupancies of substrates. Occupancies determined by I. Geronimo.

Substrate	Residue	Occupancy (%)
diclofenac:O1	S72:OG	28
diclofenac:O2	S72:OG	12
naproxen:O1	S72:OG	98
naproxen:O1	S72:N	40
naproxen:O2	S332:N	87
naproxen:O2	K69:NZ	88
<i>S</i> -warfarin:O2	K69:NZ	73
MDMA:N	L437:O	61

Table B6. Hydrogen bond occupancies of heme propionate A oxygen atoms. Occupancies determined by I. Geronimo.

Substrate	Heme propionate O atom	Hydrogen bond donor	Occupancy (%)
dextromethorphan	O1A	K69:NZ	24
	O2A	K69:NZ	27
MDMA	O1A	K69:NZ	74
	O2A	MDMA:N	61
astemizole	O1A	K69:NZ	34
	O2A	K69:NZ	27
nicotine	O1A	K69:NZ	16
		nicotine:N	39
	O2A	nicotine:N	46
naproxen	O1A	N395:N	19
	O2A	N395:N	17
<i>S</i> -warfarin	O1A	K69:NZ	53
	O2A	K69:NZ	27

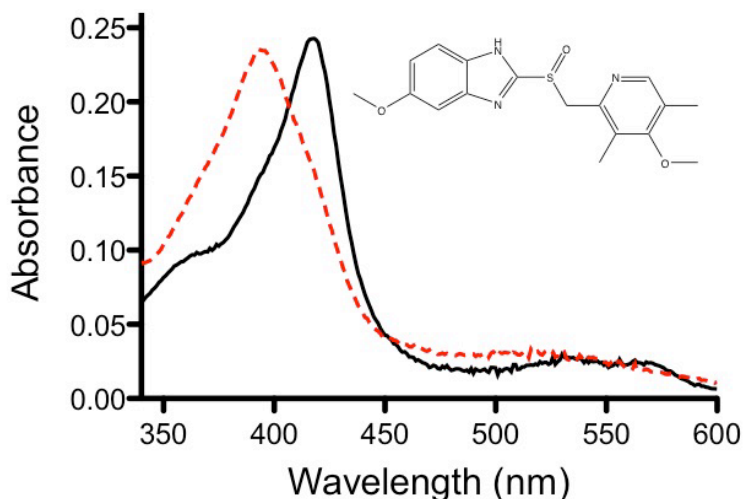


Figure B1. Absorption spectra of PM P450_{BM3} bound to omeprazole (inset). The black solid curve indicates the resting, low spin state when water is bound to ferric iron. The red dotted curve represents the 100% high spin state in which water is no longer bound and omeprazole is in the active site.

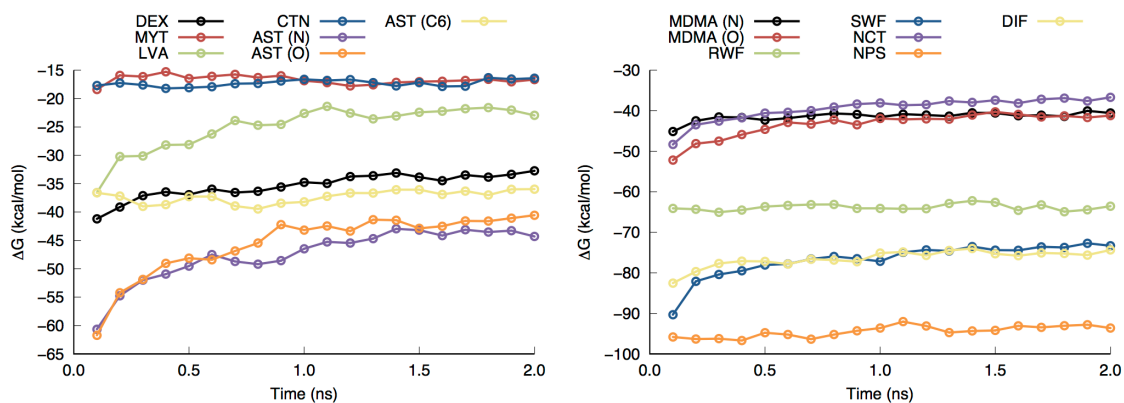


Figure B2. Gibbs free energy of the enzyme-substrate complexes during the last 2 ns of FEP/ λ -REMD. The substrates are dextromethorphan (DEX), metyrapone (MYT), lovastatin (LVA), cotinine (CTN), astemizole (AST), MDMA, *R*-warfarin (RWF), *S*-warfarin (SWF), nicotine (NCT), naproxen (NPS), and diclofenac (DIF). Different binding poses were modeled for MDMA and astemizole, including N-dealkylation (N), O-dealkylation (O) and C-H hydroxylation (C6). MD simulations performed by I. Geronimo.

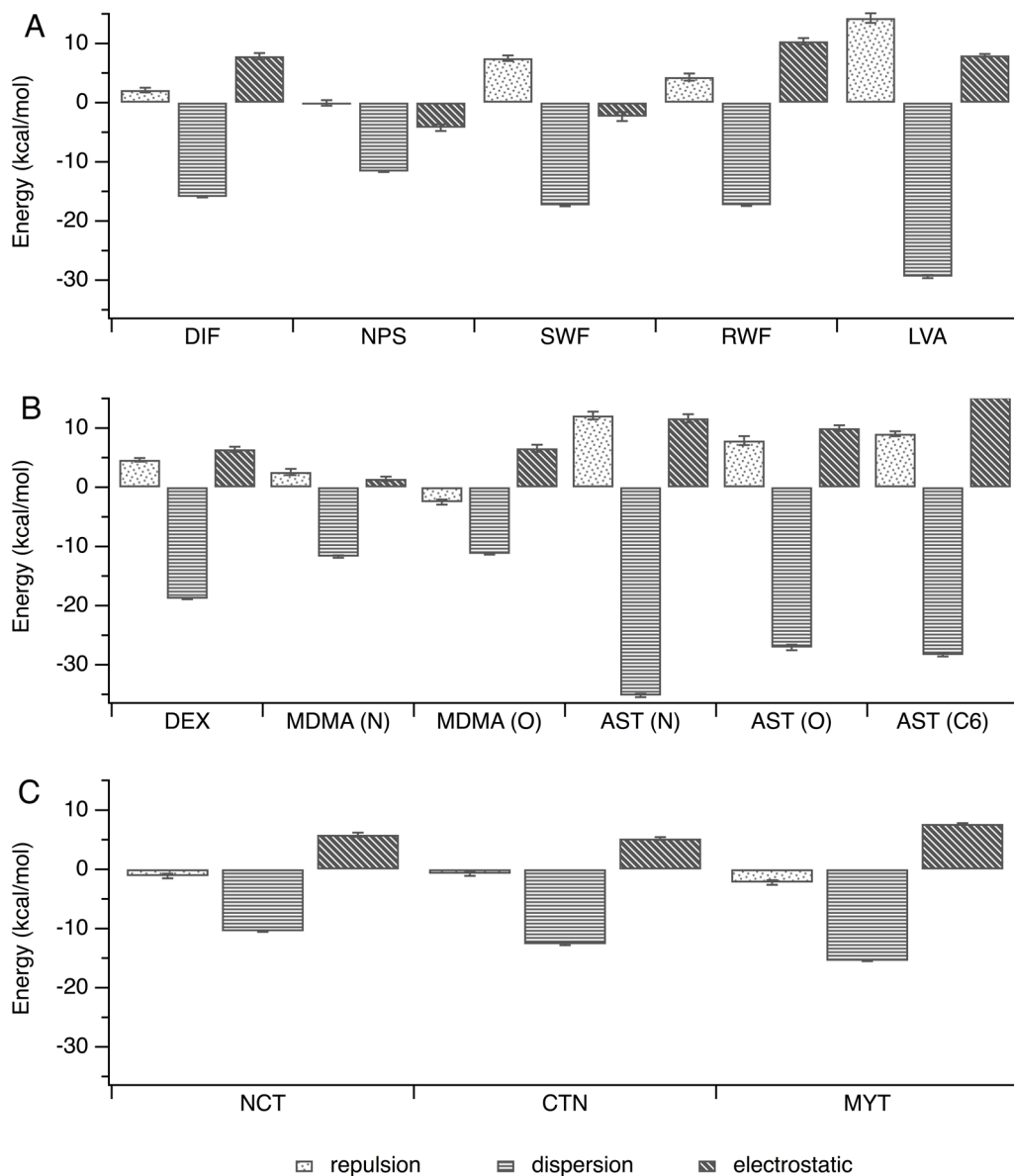


Figure B3. Repulsive, dispersive, and electrostatic energy contributions to the binding of (A) diclofenac (DIF), naproxen (NPS), S-warfarin (SWF), R-warfarin (RWF), lovastatin (LVA), (B) dextromethorphan (DEX), MDMA, astemizole (AST), (C) nicotine (NCT), cotinine (CTN), and metyrapone (MYT). Different binding poses were modeled for MDMA and astemizole including N-dealkylation (N), O-dealkylation (O), and C-H hydroxylation (C6). MD simulations performed by I. Geronimo.

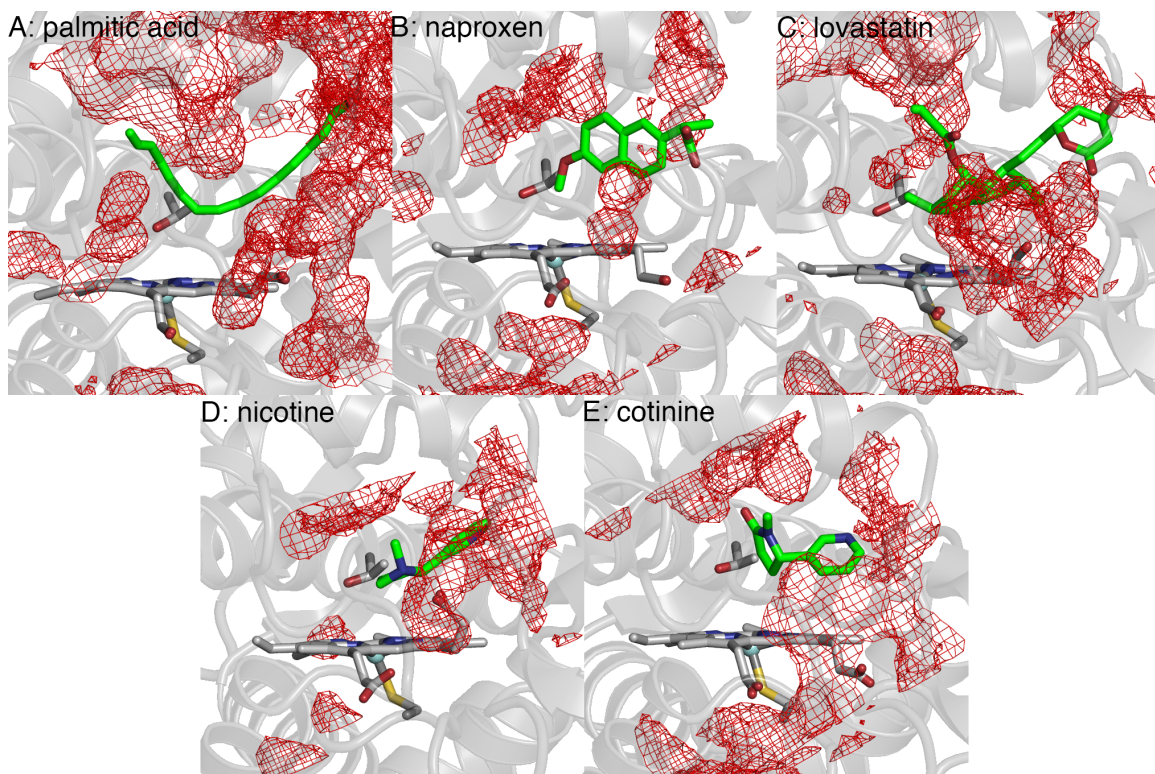


Figure B4. Water density at the PM P450_{BM3} substrate channel with the reference structure averaged from the MD simulation. T268, located at the distal side of the heme (helix I) and believed to play a role in proton delivery and oxygen activation, is also shown. MD simulations performed by I. Geronimo.

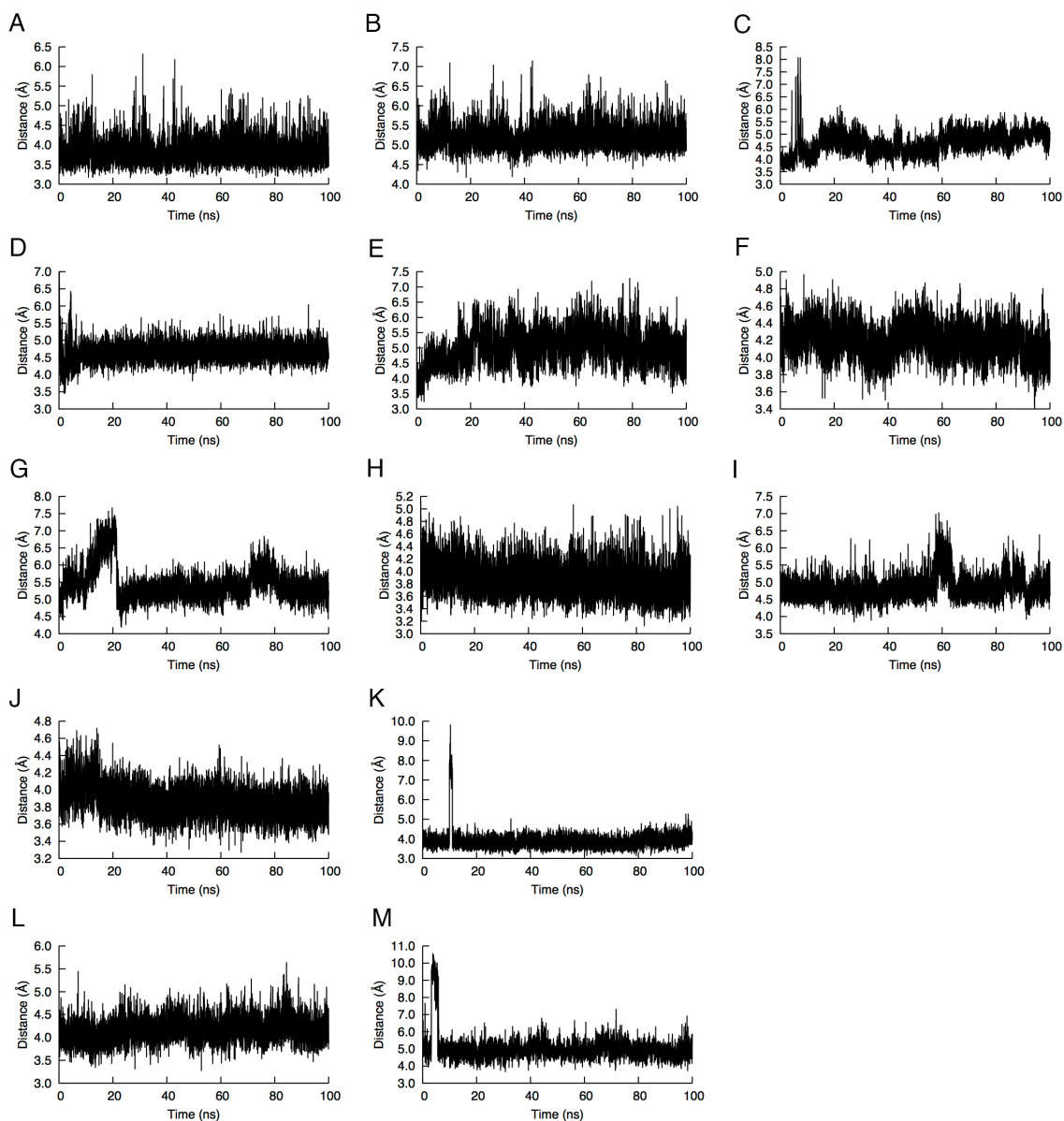


Figure B5. Plot of the distance between heme Fe and reacting atom of (A) diclofenac(C4'), (B) naproxen (methoxy C), (C) lovastatin (C6), (D) S-warfarin (C7), (E) R-warfarin (C4'), (F) dextromethorphan (protonated N), (G–I) astemizole (protonated N, methoxy C, C6), (J, K) MDMA (protonated N, C2), (L) nicotine (C5'), and (M) cotinine (C4'). MD simulations performed by I. Geronimo.

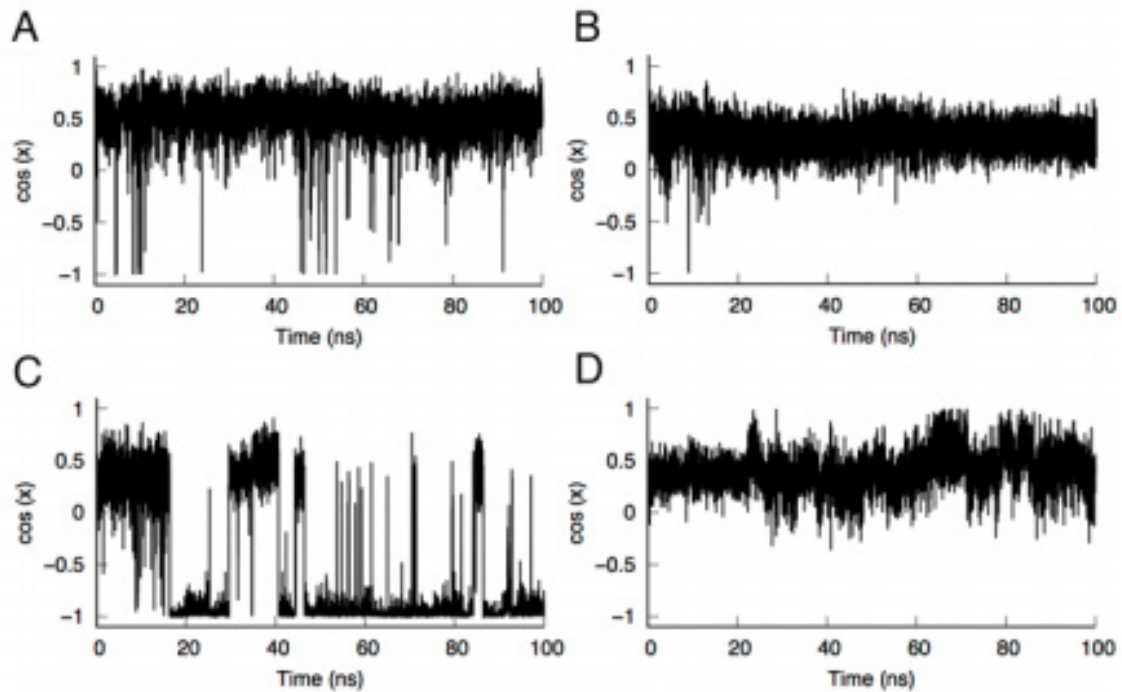


Figure B6. Plot of the cosine of the heme propionate A dihedral angle in (A) dextromethorphan, (B) MDMA, (C) astemizole, and (D) nicotine complexes of PM P450BM3. The cosine of the dihedral angle in the PM-palmitic acid crystal structure (PDB ID:4ZFB) is approximately -1. MD simulations performed by I. Geronimo.

Appendix C: Chapter 4 Additional Figures and Tables

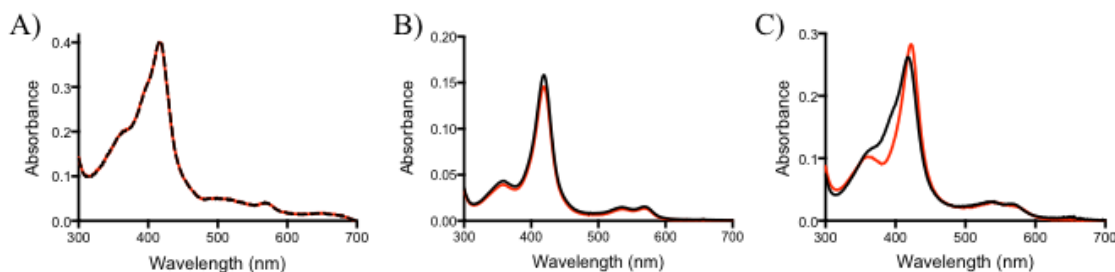


Figure C1. Binding of metyrapone to A) WT, B) F81I, and C) PM P450_{BM3} where the black line represents the Fe(III)-H₂O resting state and the red line indicates saturation with metyrapone. Metyrapone binds WT and F81I P450_{BM3} by a reverse type I mechanism while it binds PM P450_{BM3} via a type II mechanism.

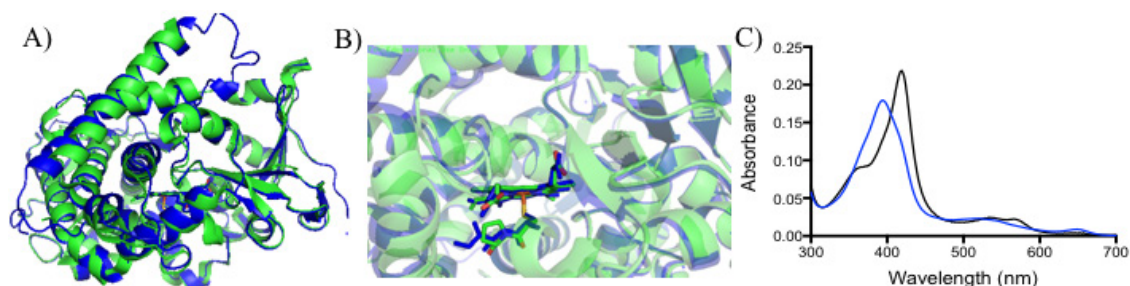


Figure C2. A) Overlay of WT (blue, PDB ID:4ZFA) and I401P P450_{BM3} (green, PDB ID:3hf2) showing differences to the overall global structure. B) Zoomed in view of the cysteine ligand loop depicting the I401P mutation in WT and the I401P P450_{BM3} variant. C) Absorbance of the I401P P450_{BM3} variant in the resting state (blue line) as compared to WT P450_{BM3} (black line). Unlike WT P450_{BM3} in its resting state (Fe(III)-H₂O), the I401P P450_{BM3} mutant was naturally high spin as shown by the Soret band at ~394 nm as opposed to 418 nm. In addition, for I401P P450_{BM3} the β -band appeared prominently with less definition between the α and β -bands as seen for WT P450_{BM3}. Lastly, the MLCT band was quite sharp for the I401P P450_{BM3} mutant.

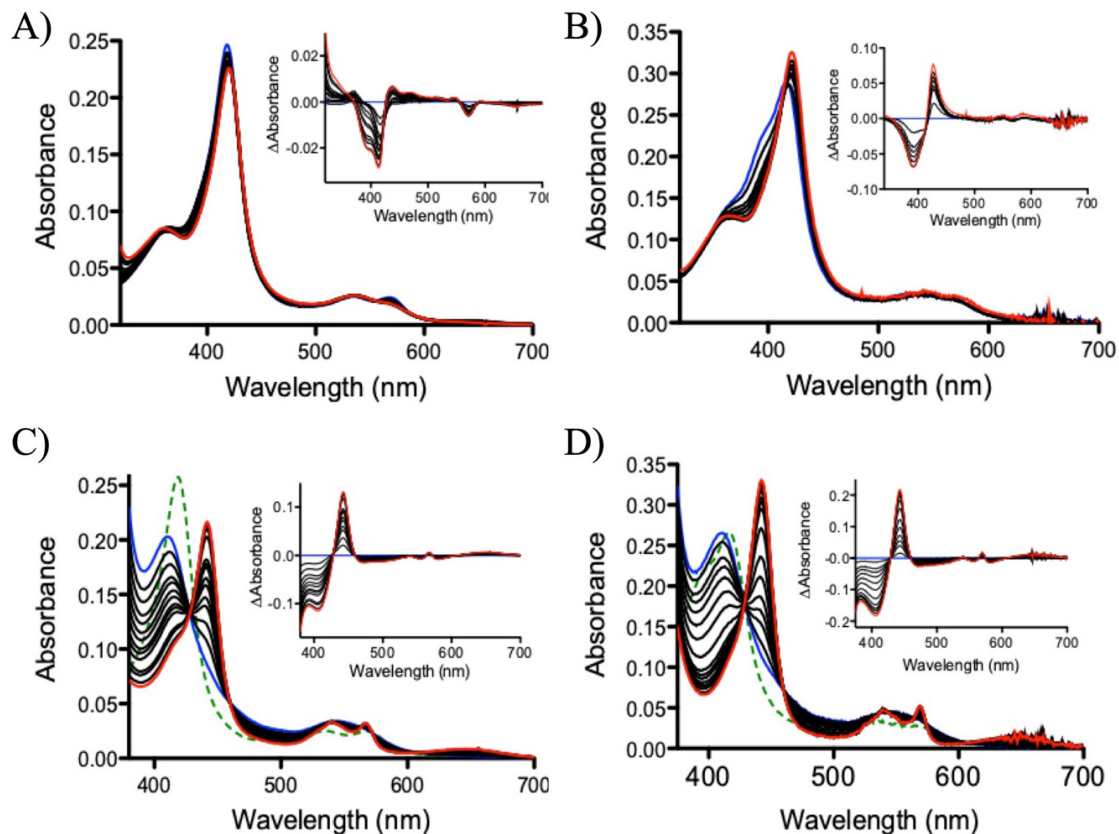


Figure C3. 4-Cyanopyridine (CNPy) had a higher binding affinity for the ferrous state than ferric state. A) Binding titration of CNPy to ferric WT P450_{BM3}. The inset is the Δ Absorbance plot in which maximum changes to the Soret, Q-, and MLCT bands were most apparent. The blue line is no substrate bound and the red line is CNPy saturation. B) Binding of CNPy to ferric PM P450_{BM3}, C) binding of CNPy to ferrous WT P450_{BM3}, D) CNPy bound to ferrous PM P450_{BM3}. The green dashed line in panels C) and D) represent the ferric state before reduction with dithionite.

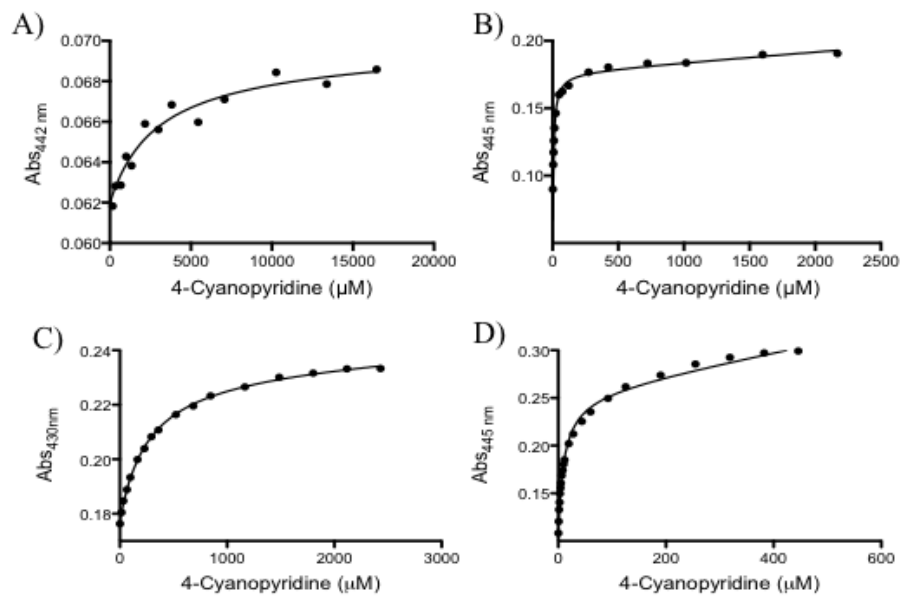


Figure C4. Plots of curves used to determine K_d of CNPY for WT and PM P450_{BM3}. A) WT Fe(III)-CNPY, B) WT Fe(II)-CNPY, C) PM Fe(III)-CNPY, and D) PM Fe(II)-CNPY.

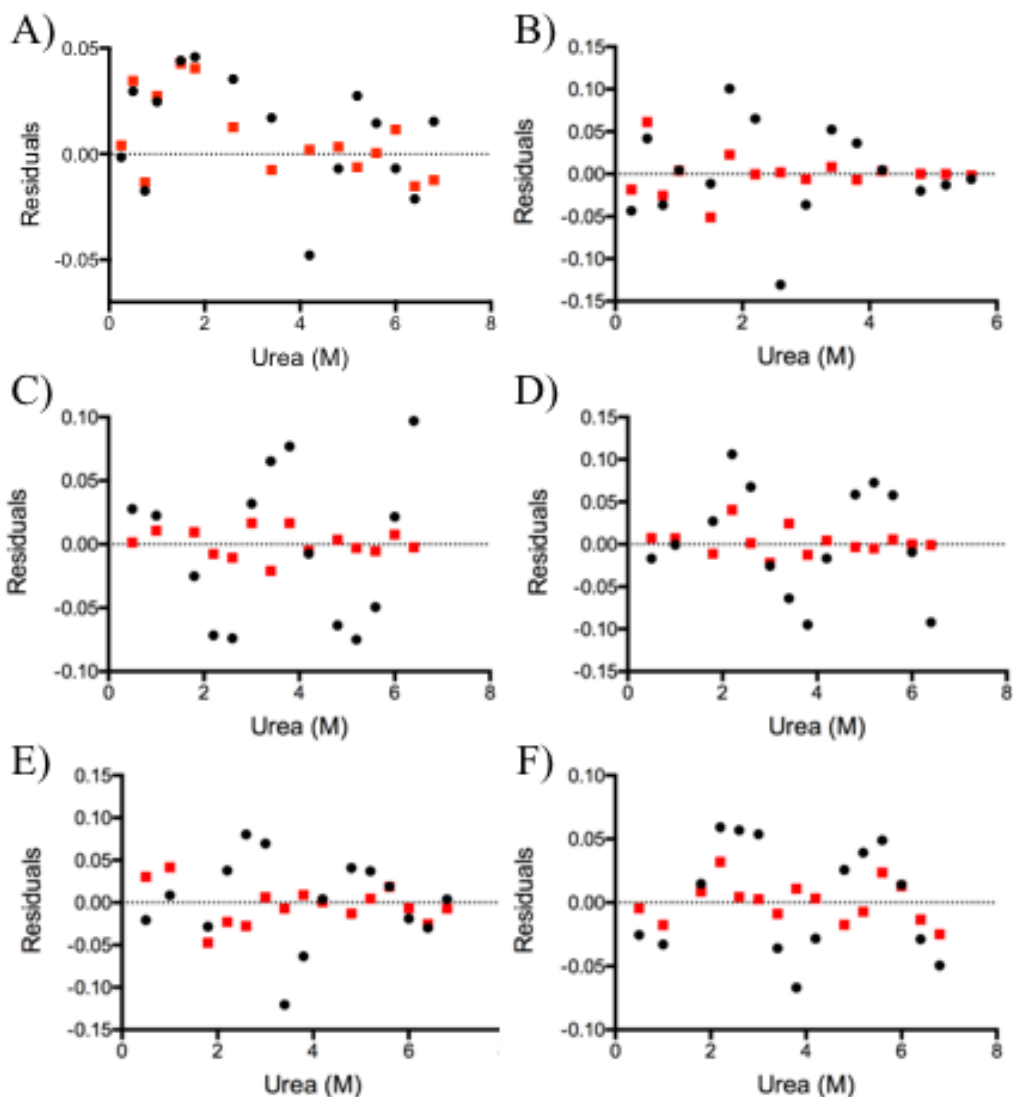


Figure C5. Residual plots of monophasic and biphasic fits for unfolding by UV/Vis spectroscopy. Black circles represent monophasic fit residuals and red squares represent biphasic fit residuals. For fits shown, smaller residuals were apparent for biphasic fits as compared to monophasic fits to determine C_m values. A) residual plot of WT Fe(III)-H₂O and B) residual plot of PM Fe(III)-H₂O. Residual plots of WT Fe(II)-CO bound are shown in C) and D) where C) indicates appearance of the inactive state at 420 nm and D) indicates disappearance of the P450 state. Residuals for the disappearance of the P450 for the F81I Fe(II)-CO state are shown in E). The P420 state is not included as a biphasic equation does not fit the data. Residuals for the disappearance of the P450 for the I401P Fe(II)-CO state are shown in F). As with the F81I P450_{BM3} variant, the P420 state is not included as a biphasic equation does not fit the data.

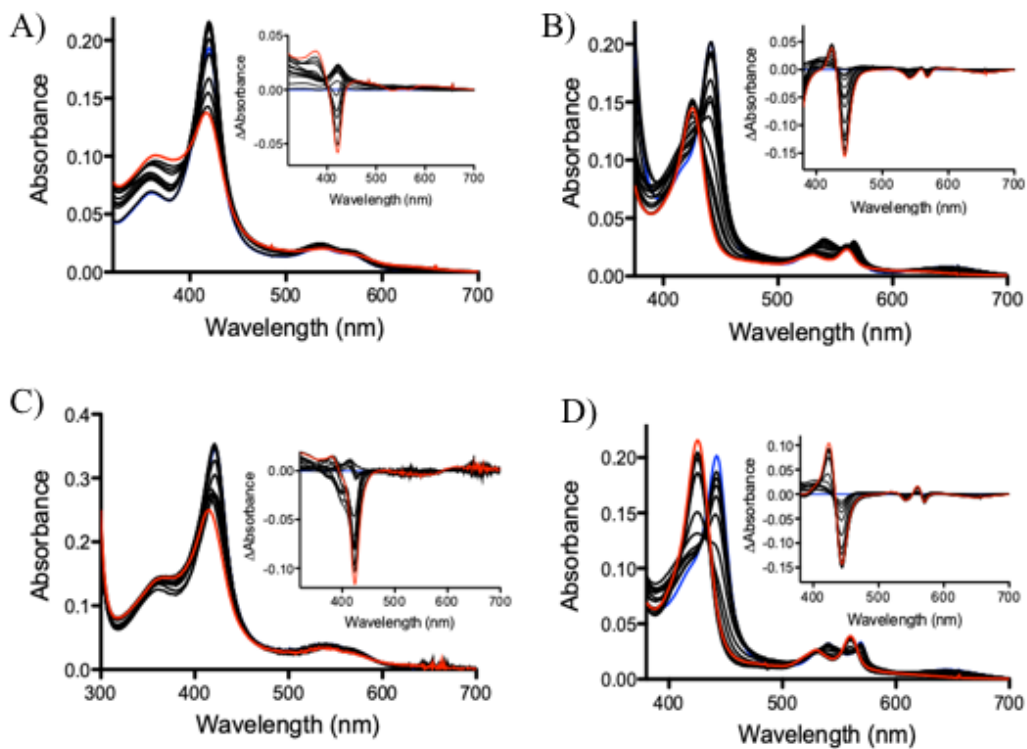


Figure C6. Active site stability of WT and PM P450_{BM3} was evident by changes to the Soret band for CNPy bound species. A) Urea titration of ferric WT P450_{BM3} with CNPy bound and B) ferrous WT P450_{BM3} with CNPy bound by UV/Vis spectroscopy in which the blue line is no urea, and the red is the final urea addition (6.8 M). C) and D) are PM P450_{BM3} species in the ferric and ferrous states CNPy bound, respectively. The insets are the Δ Absorbance plots indicating where maximum changes in absorbance occurred.

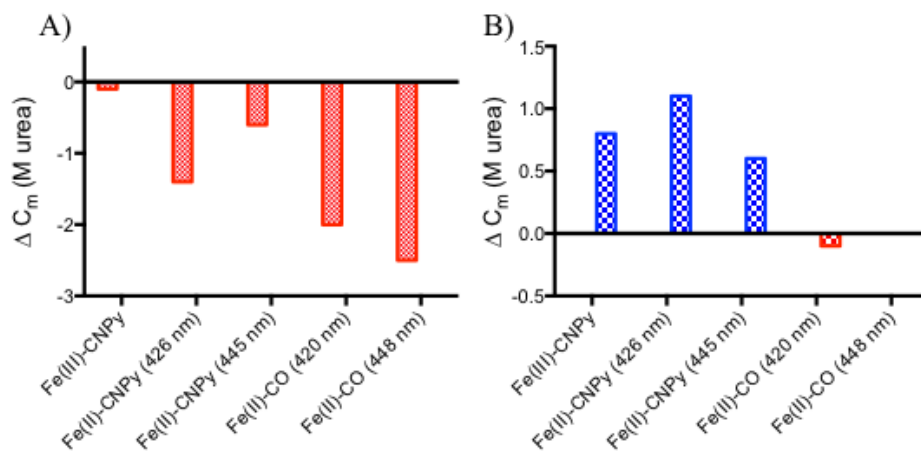


Figure C7. ΔC_m of unfolding for A) WT and B) PM P450_{BM3} as determined by UV/Vis spectroscopy. ΔC_m was calculated for WT P450_{BM3} by subtracting the C_m for the major water bound population (5.6 M) from the C_m for each specific state. ΔC_m for PM P450_{BM3} was calculated by subtracting the C_m for the major water bound population (2.3 M) from all other states. Blue represents states where the Fe(III)-H₂O state was less stable and red represents where the Fe(III)-H₂O state was more stable than the state the ΔC_m was determined for.

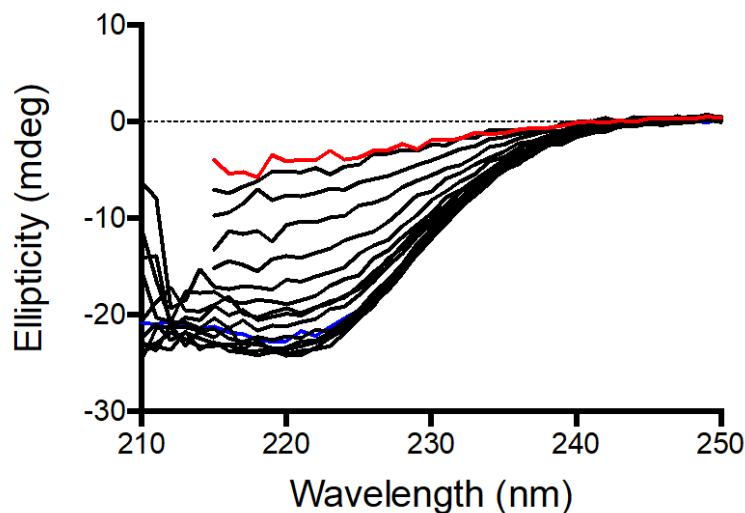


Figure C8. Example urea titration as monitored by Circular Dichroism spectroscopy. Plot shows unfolding of α -helical content for WT Fe(III)-H₂O. The blue line represents the properly folded state with no urea while the red line is with the maximum urea concentration of 6.8 M.

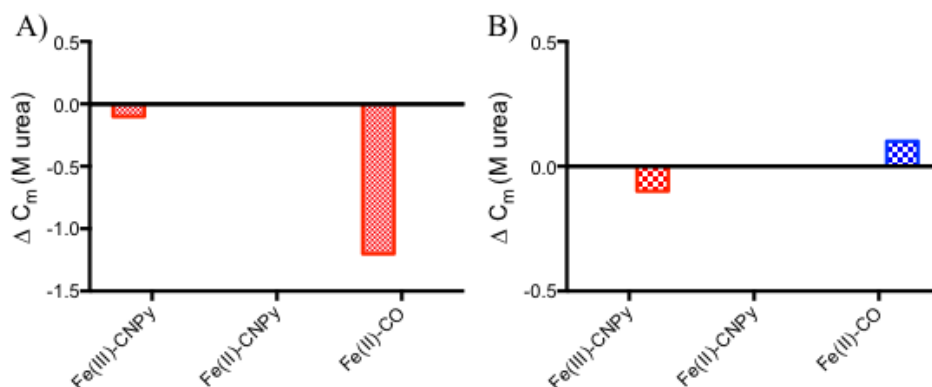


Figure C9. ΔC_m of unfolding for A) WT and B) PM P450_{BM3} as determined by CD. ΔC_m was calculated for WT P450_{BM3} by subtracting the C_m for the water bound population (5.6 M) from the C_m for each specific state. ΔC_m for PM P450_{BM3} was calculated by subtracting the C_m for the water bound population (3.7 M) from all other states. Blue represents states where the Fe(III)-H₂O state was less stable and red represents where the Fe(III)-H₂O state was more stable than the state the ΔC_m was determined for. Values were not included for the WT Fe(II)-CNPy because data was not included for this study. For the PM P450_{BM3} Fe(II)-CNPy state, the ΔC_m was zero.

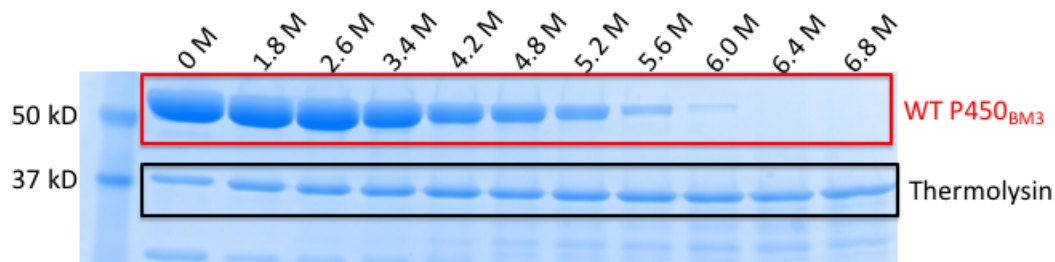


Figure C10. Pulse proteolysis gel of WT P450_{BM3} water bound. As the urea concentration increased, degradation of WT P450_{BM3} increased as shown by a decrease in the protein band at 50 kD. The protease used to cleave WT P450_{BM3}, thermolysin, is shown in the bands at 37 kD.

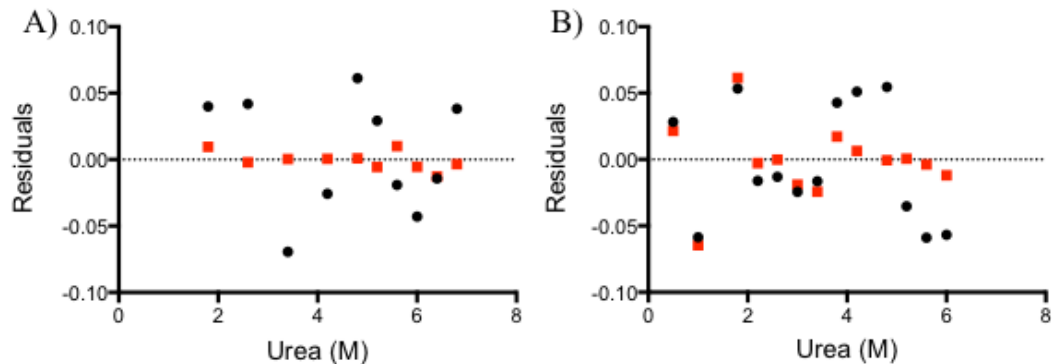


Figure C11. Residual plots of monophasic and biphasic fits for unfolding detected by pulse proteolysis. Black circles represent monophasic fit residuals and red squares represent biphasic fit residuals. A) residual plot of WT Fe(III)-H₂O and B) residual plot of WT Fe(II)-CO.

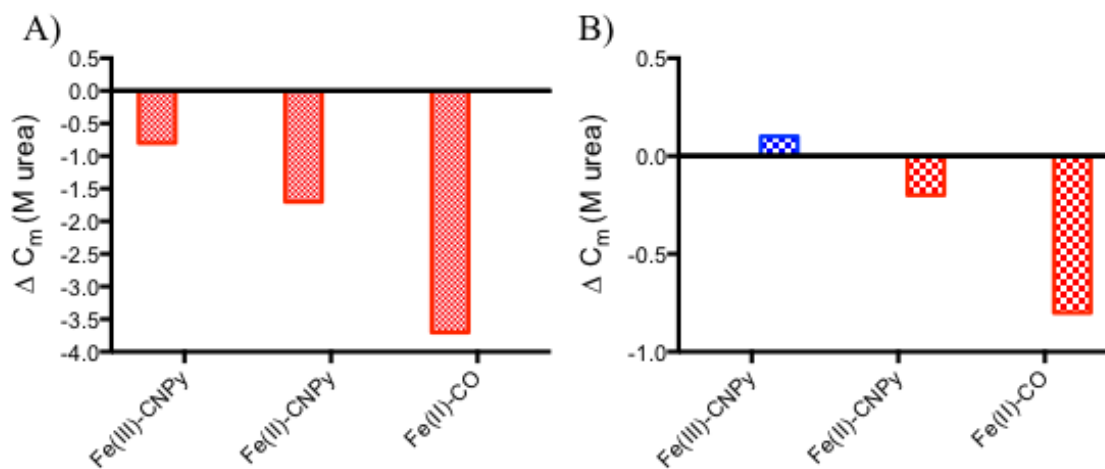


Figure C12. ΔC_m of unfolding for A) WT and B) PM P450_{BM3} as determined by pulse proteolysis. ΔC_m was calculated for WT P450_{BM3} by subtracting the C_m of the higher transition for the water bound population (5.3 M) from the C_m for each specific state. For the WT P450_{BM3} Fe(II)-CO state, the lower C_m value was used (2.2 M) as it is the major population (90%). ΔC_m for PM P450_{BM3} was calculated by subtracting the C_m for the water bound population (2.9 M) from all other states. Blue represents states where the Fe(III)-H₂O state was less stable and red represents where the Fe(III)-H₂O state was more stable than the state the ΔC_m was determined for.

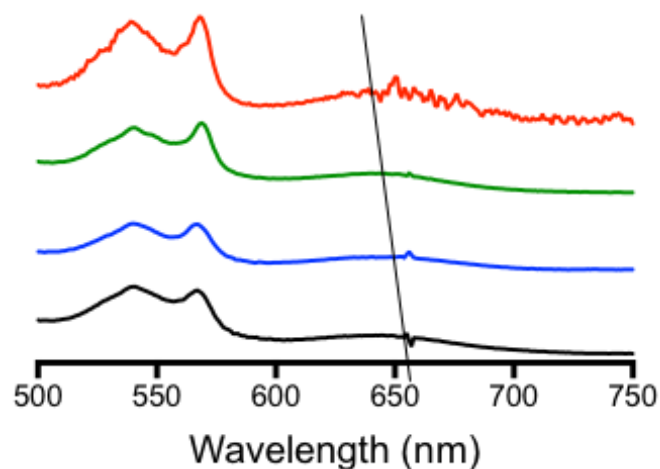


Figure C13. The MLCT region (600-700 nm) of the P450_{BM3} variants in the Fe(II)-CNPy state was used to calculate reduction potential. The black line represents WT P450_{BM3}, the blue line F81I P450_{BM3}, the green line I401P P450_{BM3}, and the red line PM P450_{BM3}.

Table C1. Binding dissociation constants (K_d) for the ferric and ferrous WT and PM P450_{BM3} states.

BM3 Variant	Fe(III)-CNPy (μM)	Fe(II)-CNPy (μM)
WT ^a	1130 \pm 45	1.80 \pm 0.7
WT ^b	2440 \pm 570	9.93 \pm 2.9
PM ^b	240 \pm 40	17.6 \pm 12.2

^a. Previously published data.²⁶⁸ ^b. Data from this study.

Appendix D: Chapter 5 Additional Figures and Tables

Table D1. HPLC method 1.

Time (min)	0.1% formic acid in dH ₂ O	0.1% formic acid in CH ₃ CN
0	98	2
2	95	5
5	70	30
15	70	30
20	40	60
30	5	95
35	98	2
40	98	2

Table D2. HPLC method 2.

Time (min)	0.1% formic acid in dH ₂ O	0.1% formic acid in CH ₃ CN
0	98	2
2	95	5
5	95	5
10	90	10
20	90	10
25	70	30
30	40	60
35	5	95
40	98	2
45	98	2

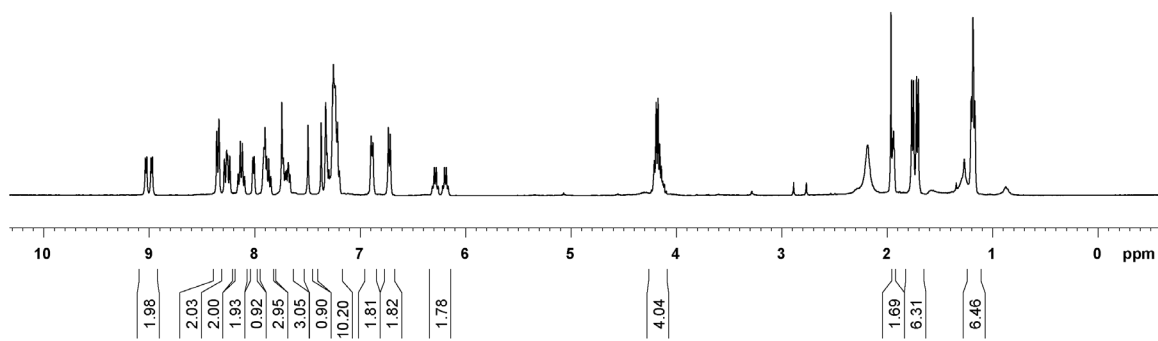
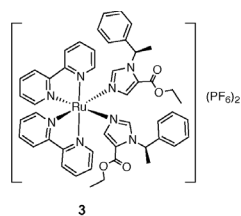


Figure D1. ¹H NMR spectrum of **3** (400 MHz, CD₃CN). Synthesis by A. Zamora.

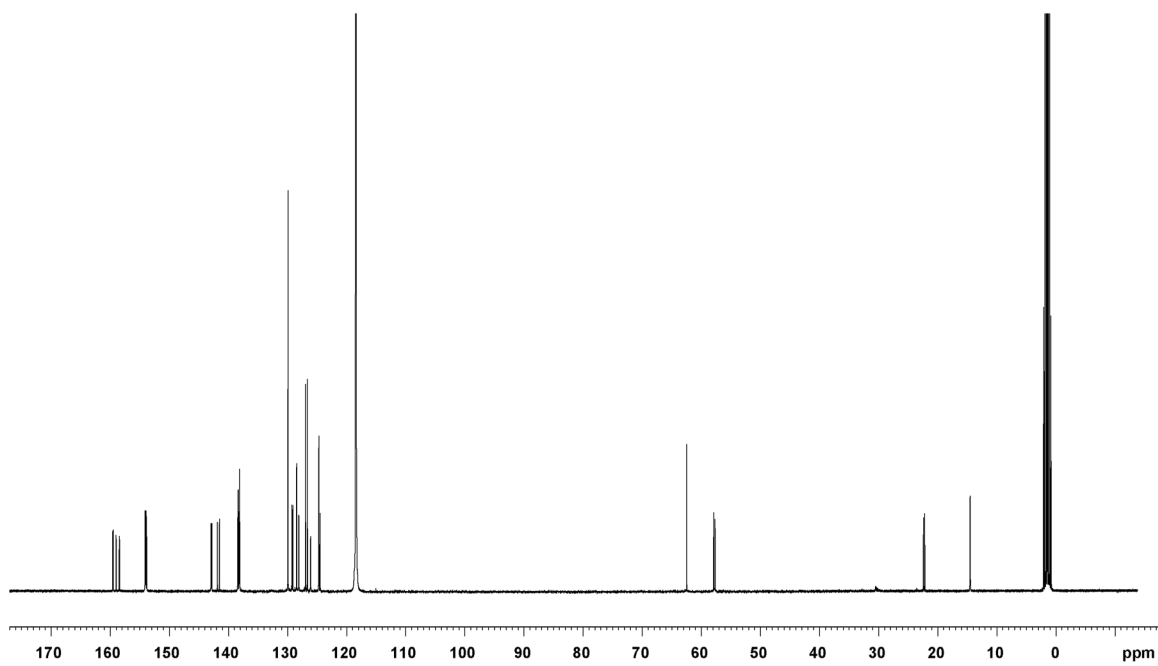


Figure D2. ¹³C NMR spectrum of **3** (100 MHz, CD₃CN). Synthesis by A. Zamora.

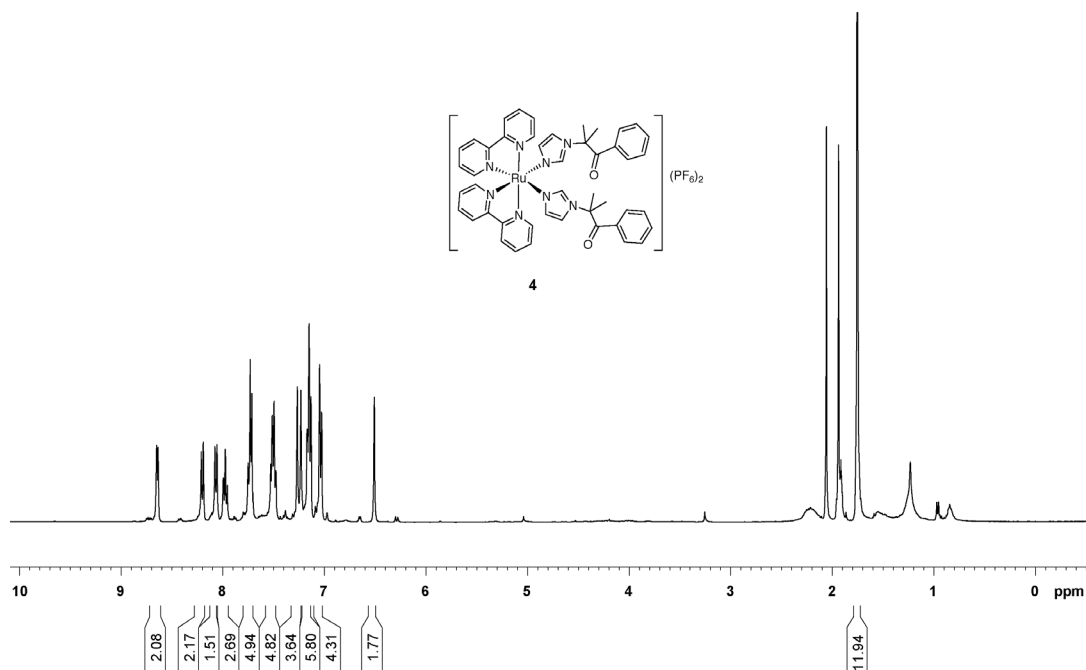


Figure D3. ^1H NMR spectrum of **4** (400 MHz, CD_3CN). Synthesis by A. Zamora.

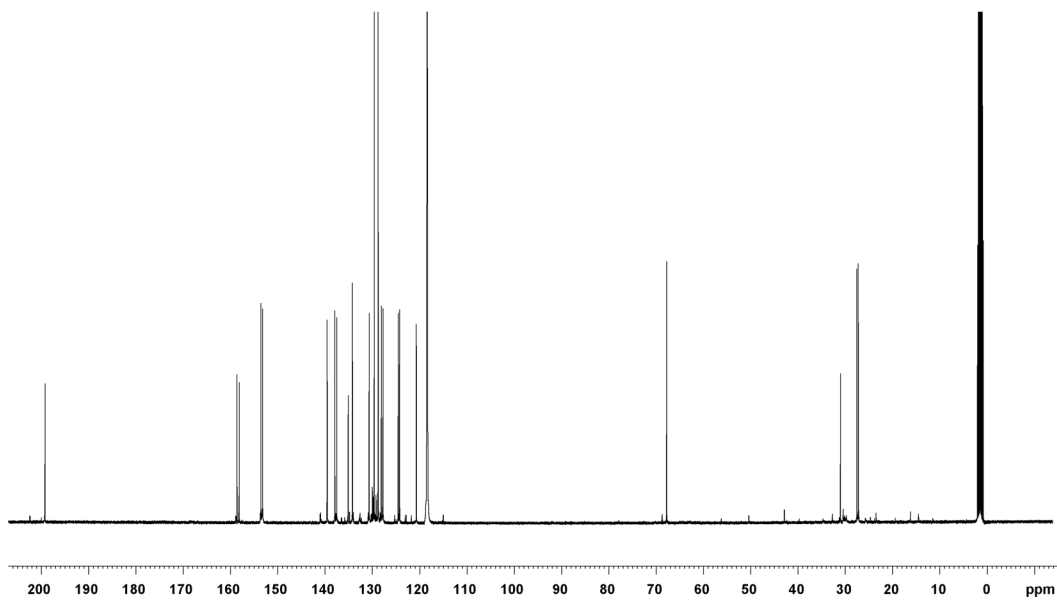


Figure D4. ^{13}C NMR spectrum of **4** (100 MHz, CD_3CN). Synthesis by A. Zamora.

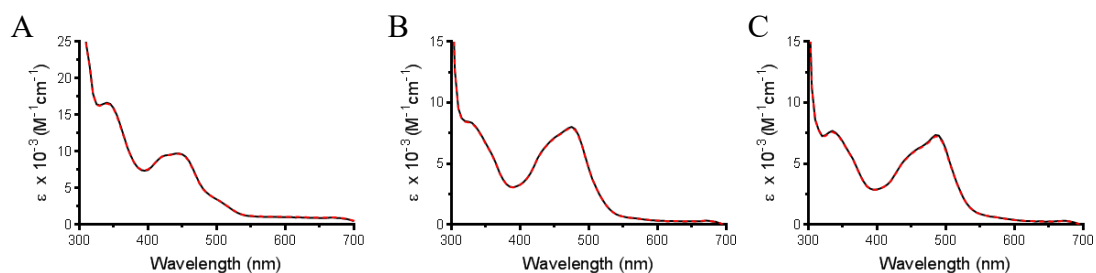


Figure D5. Thermal stability for complexes **2–4**. (A) **2**, (B) **3**, and (C) **4** at RT (–) and 37 °C (– –) after 30 min incubation in MeCN. Studies were also performed in H₂O over 48 hours at 37 °C, and no changes were observed. Studies by A. Zamora.

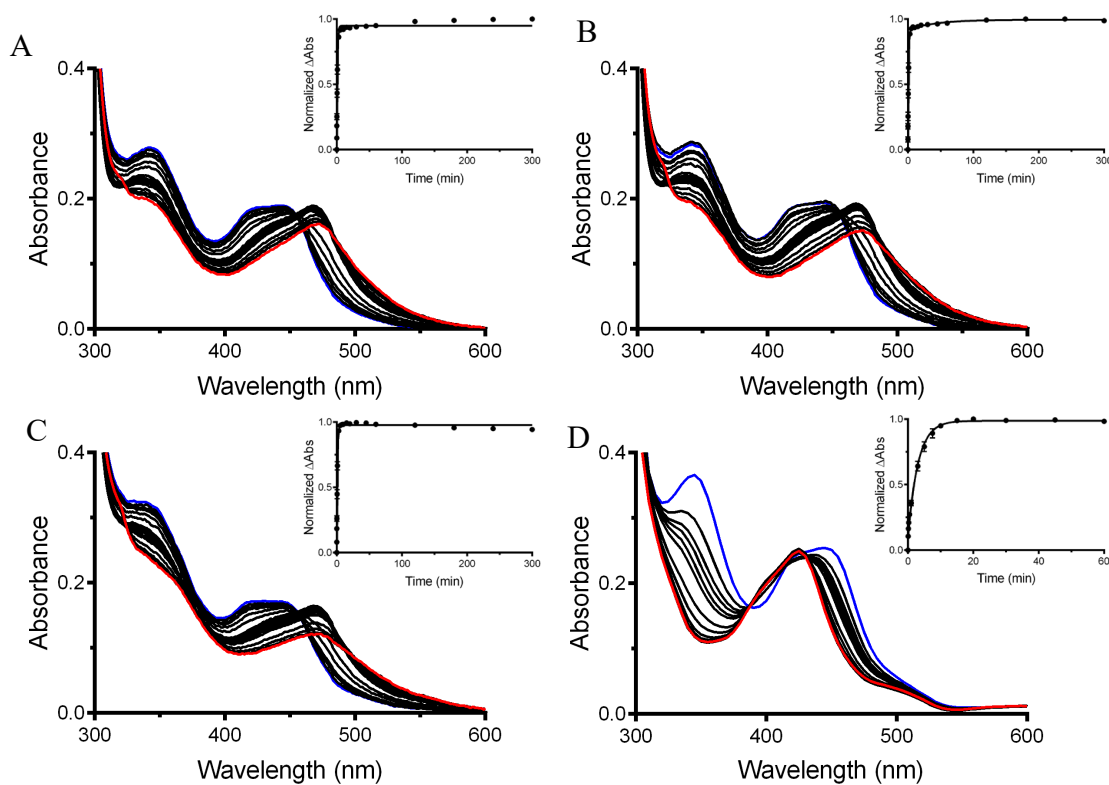


Figure D6. Photoejection of **2** (30 μM) followed by UV/Vis absorption spectroscopy in different media; (A) water, (B) 1X PBS, (C) Opti-MEM with 1% FBS, (D) CH₃CN. Studies by A. Zamora.

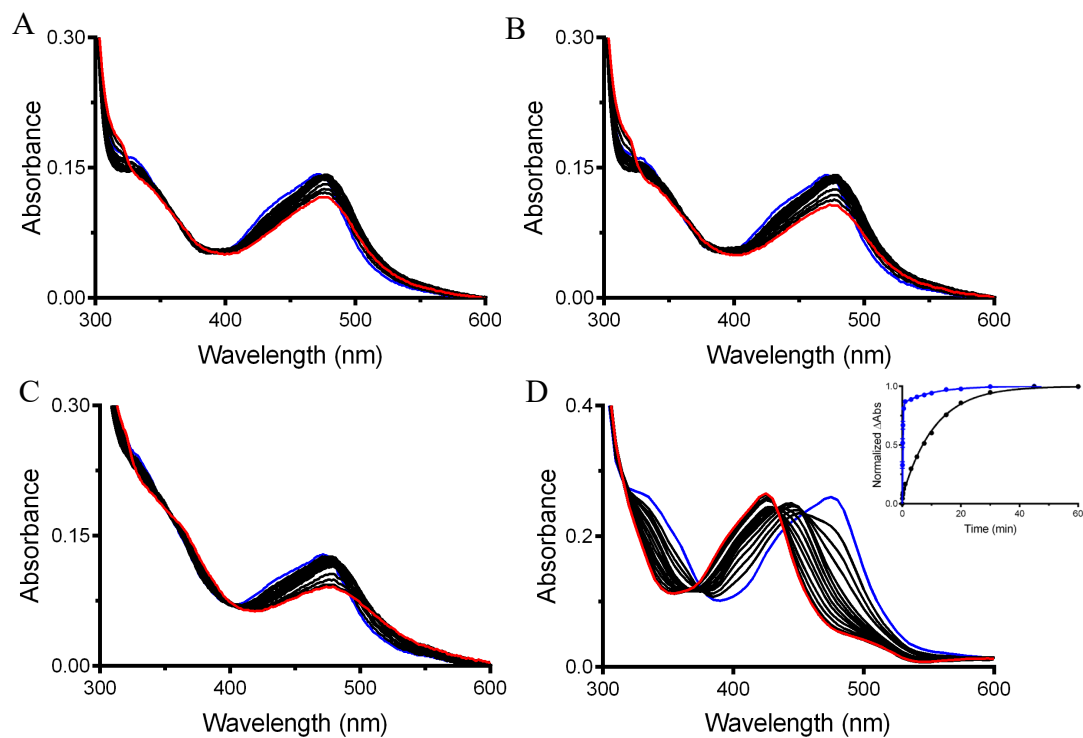


Figure D7. Photoejection of **3** (30 μM) followed by UV/Vis absorption spectroscopy in different media; (A) water, (B) 1X PBS, (C) Opti-MEM with 1% FBS, (D) CH_3CN . Studies by A. Zamora.

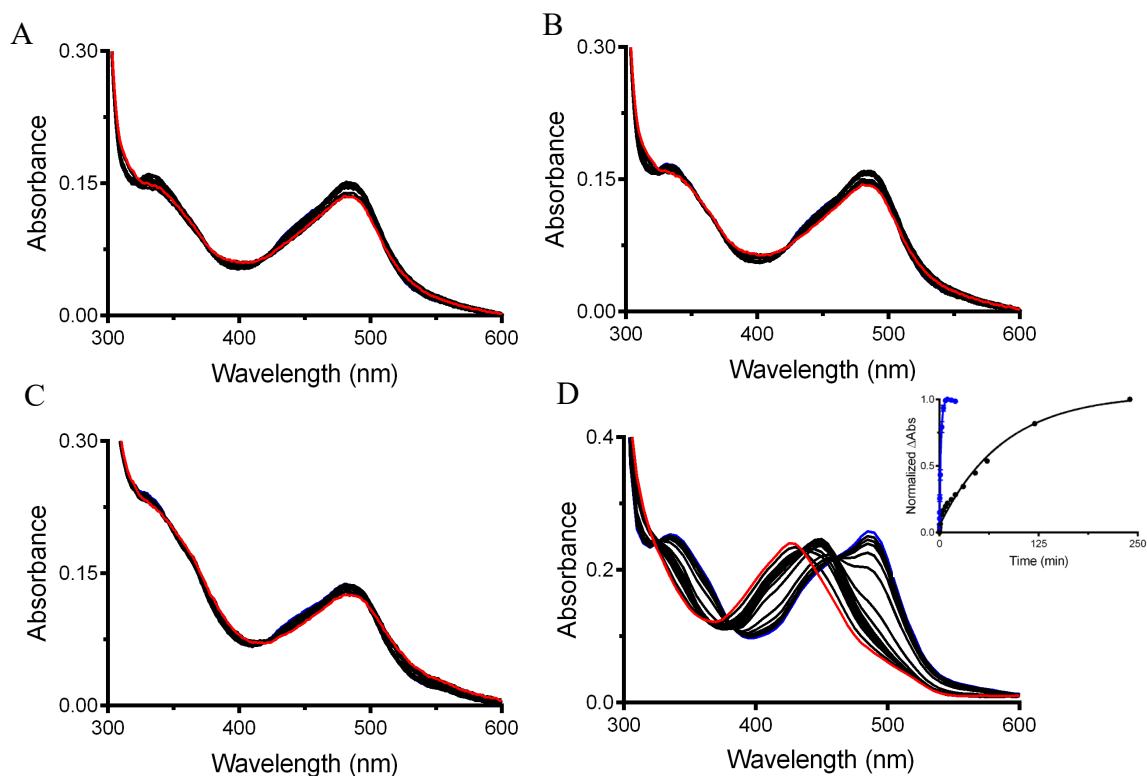


Figure D8. Photoejection of **4** (30 μ M) followed by UV/Vis absorption spectroscopy in different media; (A) water, (B) 1X PBS, (C) Opti-MEM with 1% FBS, (D) CH₃CN. The blue line is the initial and the red line is the final spectra. Inset: The kinetics curve was produced by monitoring the change in absorbance at 450-485 nm (blue) and 430-450 nm (black) and fit with a one phase decay equation using GraphPad Prism software. Studies by A. Zamora.

Table D3. Half-lives ($t_{1/2}$) for photoejection for **2**.^a

Condition	$t_{1/2}$ (min) ^b
Water	0.6 ± 0.1 and 58 ± 12
1X PBS	0.6 ± 0.1 and 32 ± 3
Opti-MEM with 1% FBS	0.6 ± 0.1
Acetonitrile	0.07 ± 0.02 and 2.5 ± 0.5

^aHalf-lives determined by A. Zamora. ^bKinetics were determined using the change in absorbance at 470-440 nm for aqueous conditions and 425-445 nm for acetonitrile and fit to a two phase decay except for Opti-MEM, which was fit to a one phase decay equation.

Table D4. Δ abs of photoejection for 3.^a

Condition	Δabs @ 470 nm
Water	0.028 ± 0.001
1X PBS	0.038 ± 0.002
Opti-MEM with 1% FBS	0.041 ± 0.006
Acetonitrile ^b	0.15 ± 0.02 and 7.8 ± 0.5

^aKinetics determined by A. Zamora. ^bKinetics were determined using the changes in absorbance at 475-440 nm for the initial fast phase and 425-440 nm for the slow phase and fit to a one phase decay.

Table D5. Δ abs of photoejection for 4.^a

Condition	Δabs @ 485 nm
Water	0.012 ± 0.001
1X PBS	0.013 ± 0.001
Opti-MEM with 1% FBS	0.012 ± 0.003
Acetonitrile ^b	1.3 ± 0.2 and 55.8 ± 0.3

^aKinetics determined by A. Zamora. ^bKinetics were determined using the changes in absorbance at 450-485 nm for the initial fast phase and 430-450 nm for the slow phase and fit to a one phase decay.

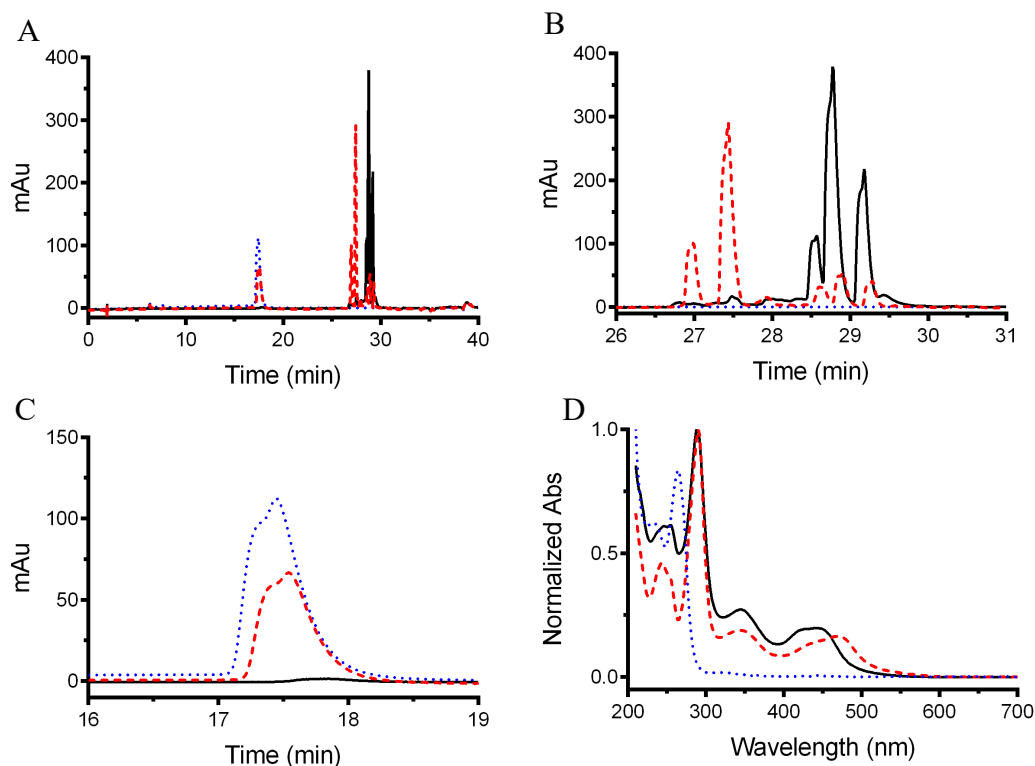


Figure D9. HPLC chromatograms of **2** in the dark and after 1 min irradiation with 470 nm light. For all graphs black (—): **2** in the dark, red (---): **2** after 1 min irradiation, blue (---): metyrapone. (A) Full HPLC chromatograms, where 17.5 min = free metyrapone, 26.5–27.8 min = **2** after 1 min irradiation, 28.5–29.5 min = **2**. Intact complex **2** has three peaks with the same absorption profiles due to the presence of the different isomers. (B) Ru(II) complex region of the HPLC chromatograms showing decreased signal for intact complex (26.5–27.8 min) and onset of shorter retention time products (28.5–29.5 min) following irradiation. (C) Metyrapone region of the HPLC chromatograms showing appearance of the signal in the irradiated sample. (D) UV/Vis absorption traces of the peaks showing a red-shifted MLCT band of **2** when irradiated with light. Extent of the photoejection reaction is 53%. HPLC performed by A. Zamora.

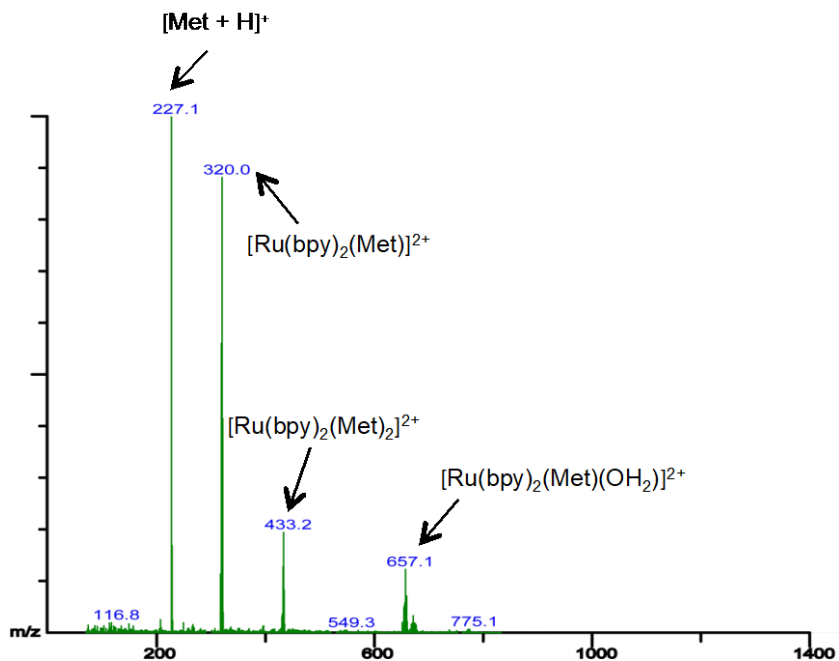


Figure D10. ESI-MS of **2** after being irradiated with 470 nm light. Ejection of one metyrapone ligand was confirmed by appearance of the peaks corresponding to free ligand and $[\text{Ru}(\text{bpy})_2(\text{Met})]^{2+}$ or $[\text{Ru}(\text{bpy})_2(\text{Met})(\text{H}_2\text{O})]^{2+}$, as well as the reduction in the signal of the intact complex. ESI-MS performed by A. Zamora.

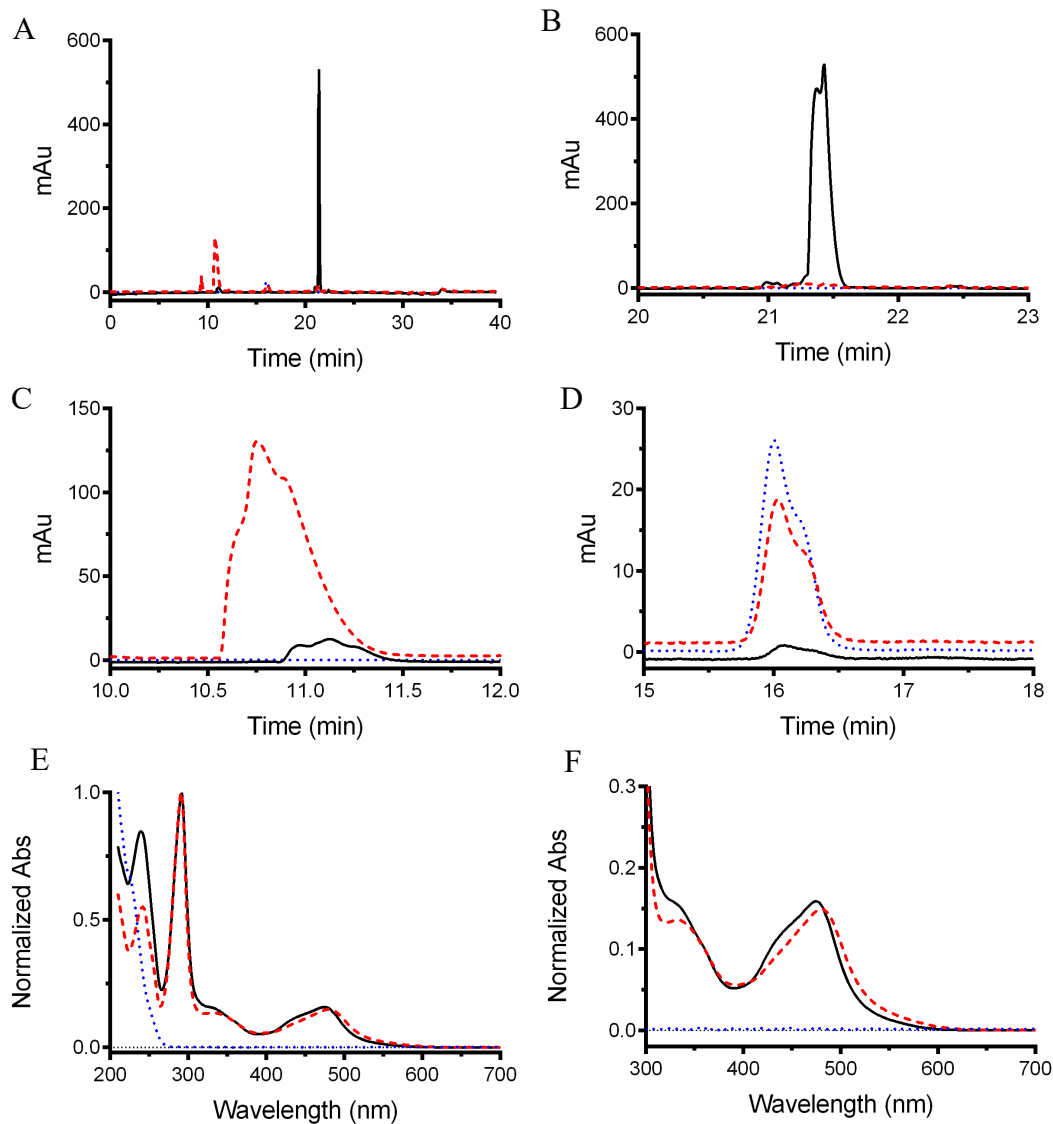


Figure D11. HPLC chromatograms of **3** in the dark and after 1 min irradiation with 470 nm light. For all figures black (—): **3** in the dark, red (---): **3** after 1 min irradiation, blue (---): etomidate. (A) Full HPLC chromatograms, where 11 min = **3** after 1 min irradiation, 16 min = free etomidate, 21.5 min = **3** in the dark. (B) Intact **3** region of the HPLC chromatograms showing decreased signal following irradiation. (C) Irradiated product region of the HPLC chromatograms showing increased signal following irradiation. (D) Etomidate region of the HPLC chromatograms showing appearance of free ligand following irradiation. (E) Full and (F) zoomed UV/Vis absorption traces of the peaks showing a slight red-shifted MLCT band of **3** when irradiated with light. Extent of the photoejection reaction is 65%. HPLC performed by A. Zamora.

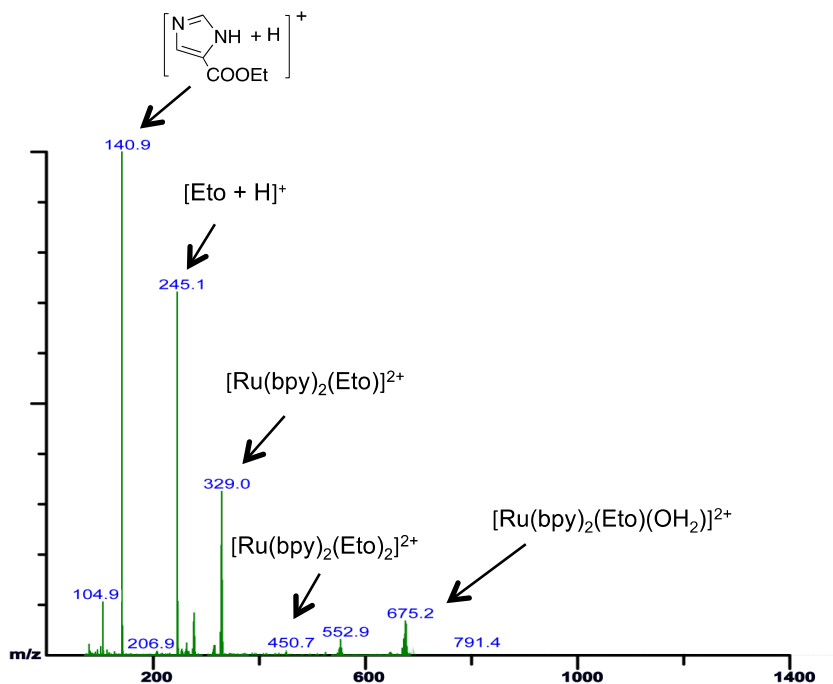


Figure D12. ESI-MS of **3** after being irradiated with 470 nm light. Ejection of one etomidate ligand was confirmed by appearance of the peaks corresponding to free ligand and $[Ru(bpy)_2(Eto)]^{2+}$ or $[Ru(bpy)_2(Eto)(H_2O)]^{2+}$, as well as the reduction in the signal of the intact complex. ESI-MS performed by A. Zamora.

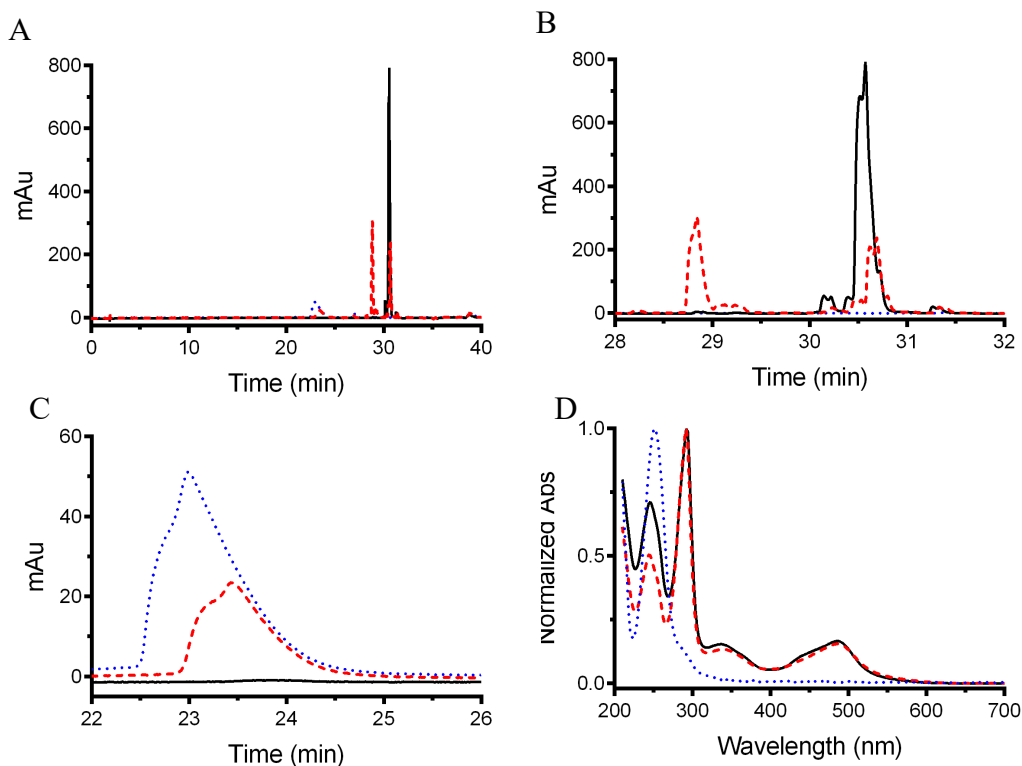


Figure D13. HPLC chromatograms of **4** in the dark and after 1 min irradiation with 470 nm light. For each figure black (—): **4** in the dark, red (— —): **3** after 1 min irradiation, blue (— —): **1**. (A) Full HPLC chromatograms, where 23 min = **1**, 28.8 min = **4** after 1 min irradiation, 30.6 min = **4** in the dark. (B) Ru(II) complex region of the HPLC chromatograms showing decreased signal for intact **4** and appearance of the Ru(II) product following irradiation. (C) Compound **1** region of the HPLC chromatograms showing the appearance of the signal following irradiation. (D) Full UV/Vis absorption traces of the peaks showing slight changes in the MLCT band of **4** when irradiated with light. Extent of the photoejection reaction is 40%. HPLC performed by A. Zamora.

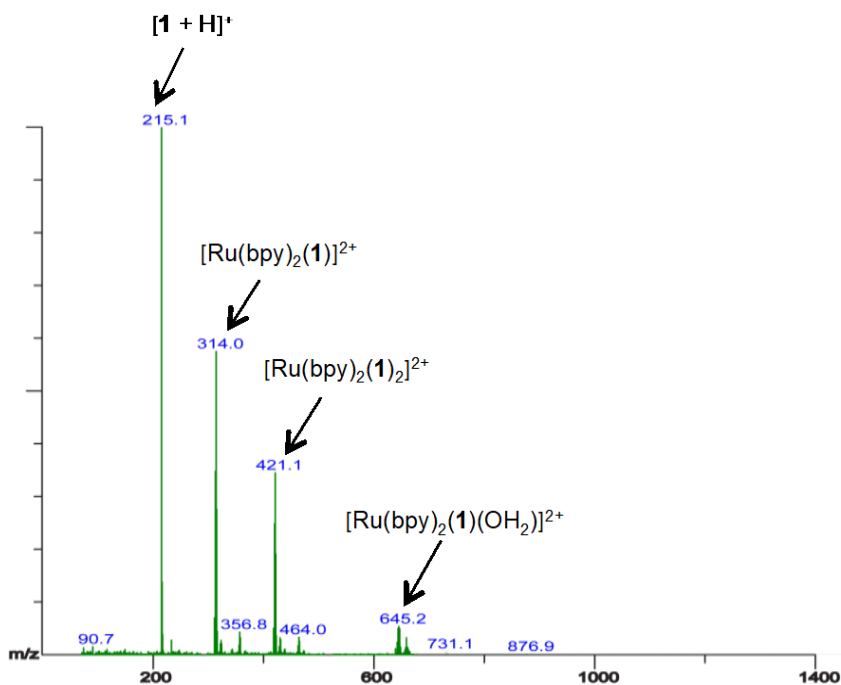


Figure D14. ESI-MS of **4** after being irradiated with 470 nm light. Ejection of one **1** ligand was confirmed by appearance of the peaks corresponding to free ligand and $[\text{Ru}(\text{bpy})_2(\mathbf{1})]^{2+}$ or $[\text{Ru}(\text{bpy})_2(\mathbf{1})(\text{H}_2\text{O})]^{2+}$, as well as the reduction in the signal of the intact complex. ESI-MS performed by A. Zamora.

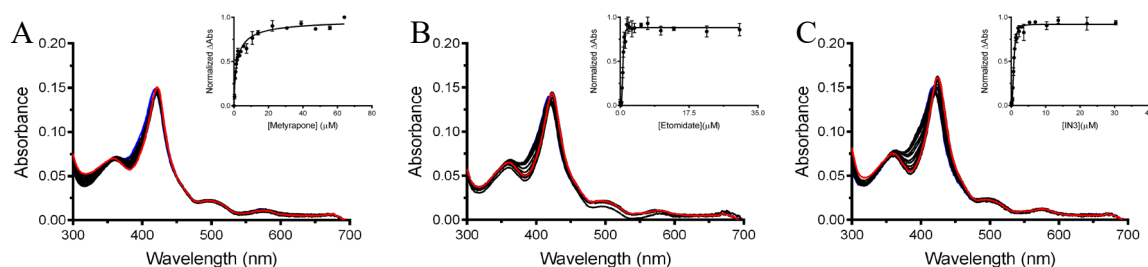


Figure D15. UV/Vis spectral traces of PM BM3 (2.5 μM) at RT in assay buffer with increasing ligand concentration: (A) metyrapone, (B) etomidate, (C) and **1**. The blue line is the initial and the red line is the final spectra. Inset: The binding curves were produced by monitoring the change in absorbance at 425 nm and fit with a one site-total non-linear equation using GraphPad Prism software.

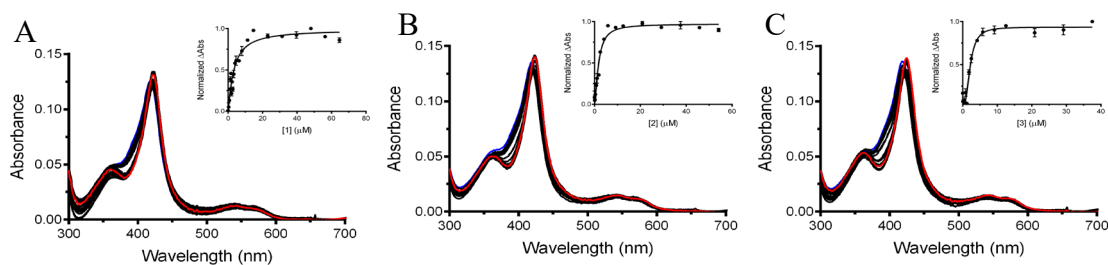


Figure D16. UV/Vis spectral traces of PM BM3 (2.5 μM) at RT in assay buffer with increasing concentration of complexes: (A) **2**, (B) **3**, and (C) **4** after irradiation with the Indigo LED. The blue line is the initial and the red line is the final spectra. Inset: The binding curves were produced by monitoring the change in absorbance at 425 nm and fit with a one site-total non-linear equation using GraphPad Prism software.

Table D6. K_d values for ligands and light-activated complexes.

Ligand	K_d (μM)	Complex	K_d (μM)
Metyrapone	1.09 ± 0.18	2	6.13 ± 1.46
Etomidate	0.83 ± 0.22	3	3.20 ± 0.59
1	0.93 ± 0.18	4	4.63 ± 1.75

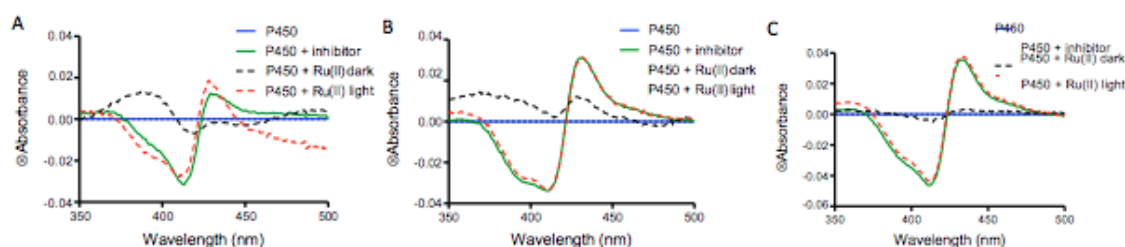


Figure D17. Difference spectra of P450_{BM3} inhibitor saturated and Ru(II) dark and light systems: **2** (A), **3** (B), **4** (C). The ratio used was P450: Complex (1:10) and P450: Ligand (1:4) for each of the respective ligands used to generate the complexes. The absolute spectra are shown in Figure 1.

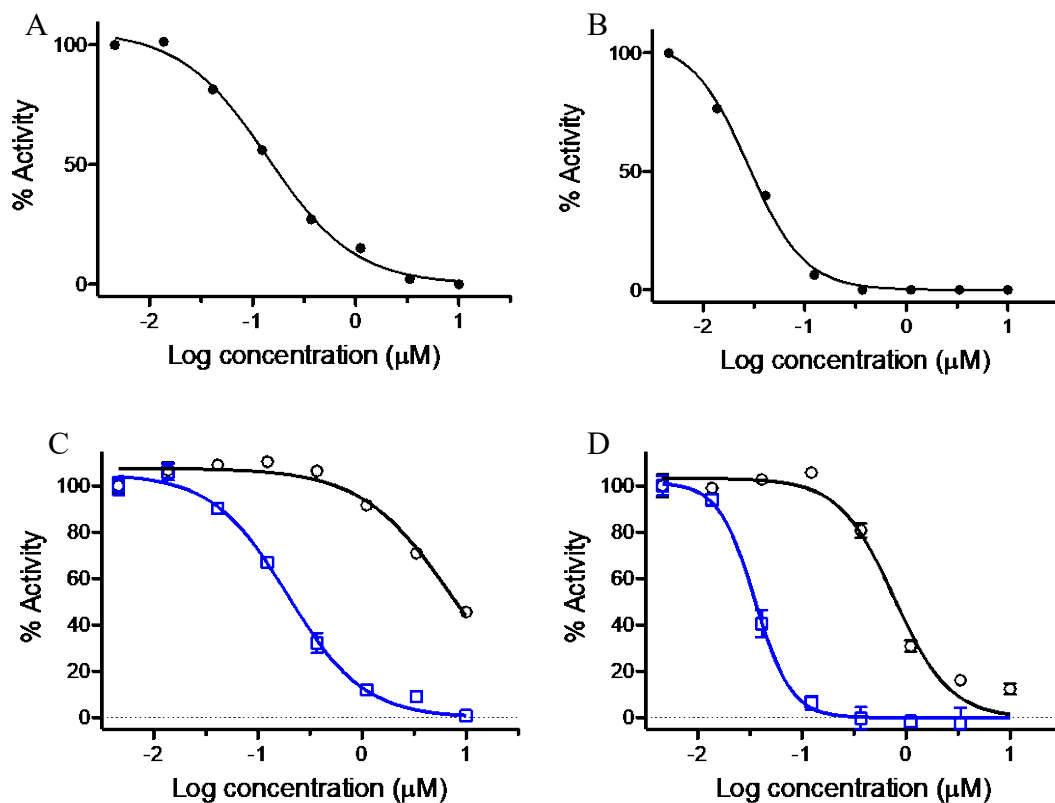


Figure D18. P450_{BM3} activity assay for (A) metyrapone, (B) etomidate, (C) **2** and (D) **3**. For (C) and (D), complexes **2** and **3** were tested in the absence of light (—) and following 1 min of irradiation with the Indigo LED (—)

Table D7. P450_{BM3} activity assay IC₅₀ values.

Ligand	IC ₅₀ (μM)	Complexes	IC ₅₀ (μM) ^a
Metyrapone	0.75 ± 0.43	2	0.19 ± 0.02 3.47 ± 0.74
Etodimate	0.02 ± 0.00	3	0.04 ± 0.01 0.61 ± 0.05
1	0.06 ± 0.03	4	0.05 ± 0.00 6.82 ± 2.06

^a Values listed first in black are light activated complexes. Values listed in blue are IC₅₀ values for complexes in the dark.

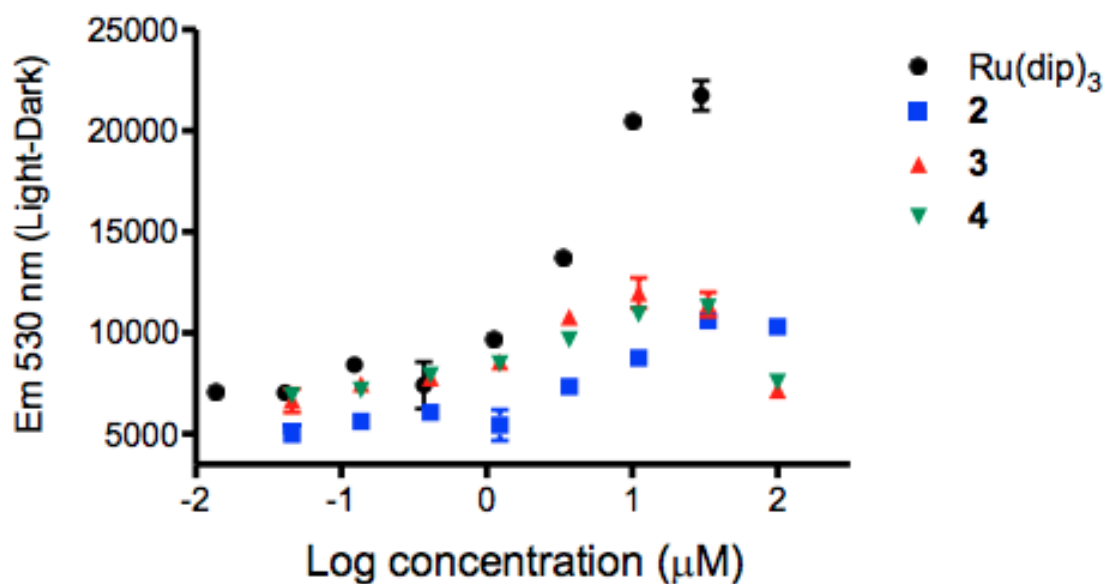


Figure D19. Singlet Oxygen Sensor Green detection of $^1\text{O}_2$ demonstrated low levels are produced by complexes **2-4**. Ru(dip)₃ (dip = bathophenanthroline) was used as a control. Assay performed by L. Nease and D. Heidary.

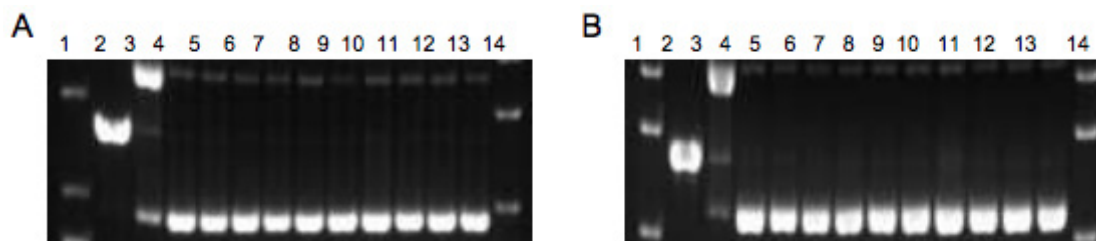


Figure D20. Agarose gels showing the dose response of ligands with 40 µg/mL pUC19 plasmid with and without irradiation (470 nm). (A) Dark and (B) 3 hr irradiation. Lane 1 and 14: DNA ladder; Lane 2: EcoRI; Lane 3: Cu(OP)₂; Lane 4: 0 mM, Lanes 5–7: 7.8, 62.5, 500 mM metyrapone; Lanes 8–10: 7.8, 62.5, 500 mM etomidate; Lanes 11–13: 7.8, 62.5, 500 mM **1**. EcoRI and Cu(OP)₂ are used as controls for linear and relaxed circular DNA, respectively. EtBr was used to visualize the DNA. Gels run by A. Zamora.

REFERENCES

- [1] Geronimo, I., Denning, C. A., Rogers, W. E., Othman, T., Huxford, T., Heidary, D. K., Glazer, E. C., and Payne, C. M. (2016) Effect of mutation and substrate binding on the stability of cytochrome P450BM3 variants, *Biochemistry* 55, 3594-3606.
- [2] Sevrioukova, I. F., Li, H., Zhang, H., Peterson, J. A., and Poulos, T. L. (1999) Structure of a cytochrome P450–redox partner electron-transfer complex, *Proceedings of the National Academy of Sciences of the United States of America* 96, 1863-1868.
- [3] Omura, T., and Sato, R. (1964) The Carbon Monoxide-Binding Pigment of Liver Microsomes. I. Evidence for Its Hemoprotein Nature, *J Biol Chem* 239, 2370-2378.
- [4] Gilardi, G., and Di Nardo, G. (2017) Heme iron centers in cytochrome P450: structure and catalytic activity, *Rend. Fis. Acc. Lincei*. 28, S159-S167.
- [5] Nebert, D. W., Wikvall, K., and Miller, W. L. (2013) Human cytochromes P450 in health and disease, *Philos Trans R Soc Lond B Biol Sci* 368, 20120431.
- [6] Gonzalez, F. J. (1988) The molecular biology of cytochrome P450s, *Pharmacol Rev* 40, 243-288.
- [7] Poulos, T. L., Finzel, B. C., Gunsalus, I. C., Wagner, G. C., and Kraut, J. (1985) The 2.6-Å crystal structure of *Pseudomonas putida* cytochrome P-450, *J Biol Chem* 260, 16122-16130.
- [8] Schlichting, I., Berendzen, J., Chu, K., Stock, A. M., Maves, S. A., Benson, D. E., Sweet, R. M., Ringe, D., Petsko, G. A., and Sligar, S. G. (2000) The catalytic pathway of cytochrome p450cam at atomic resolution, *Science* 287, 1615-1622.
- [9] Nagano, S., and Poulos, T. L. (2005) Crystallographic study on the dioxygen complex of wild-type and mutant cytochrome P450cam. Implications for the dioxygen activation mechanism, *J Biol Chem* 280, 31659-31663.
- [10] Rittle, J., and Green, M. T. (2010) Cytochrome P450 compound I: capture, characterization, and C-H bond activation kinetics, *Science* 330, 933-937.
- [11] Newcomb, M., Halgrimson, J. A., Horner, J. H., Wasinger, E. C., Chen, L. X., and Sligar, S. G. (2008) X-ray absorption spectroscopic characterization of a cytochrome P450 compound II derivative, *Proc Natl Acad Sci U S A* 105, 8179-8184.
- [12] Behan, R. K., Hoffart, L. M., Stone, K. L., Krebs, C., and Green, M. T. (2006) Evidence for basic ferryls in cytochromes P450, *J Am Chem Soc* 128, 11471-11474.
- [13] Jung, C., Schunemann, V., and Lendzian, F. (2005) Freeze-quenched iron-oxo intermediates in cytochromes P450, *Biochem Biophys Res Commun* 338, 355-364.
- [14] Johnston, W. A., Hunter, D. J., Noble, C. J., Hanson, G. R., Stok, J. E., Hayes, M. A., De Voss, J. J., and Gillam, E. M. (2011) Cytochrome P450 is present in both ferrous and ferric forms in the resting state within intact *Escherichia coli* and hepatocytes, *J Biol Chem* 286, 40750-40759.
- [15] Munro, A. W., Leys, D. G., McLean, K. J., Marshall, K. R., Ost, T. W., Daff, S., Miles, C. S., Chapman, S. K., Lysek, D. A., Moser, C. C., Page, C. C., and Dutton, P. L. (2002) P450 BM3: the very model of a modern flavocytochrome, *Trends Biochem Sci* 27, 250-257.
- [16] Imai, M., Shimada, H., Watanabe, Y., Matsushima-Hibiya, Y., Makino, R., Koga, H., Horiuchi, T., and Ishimura, Y. (1989) Uncoupling of the cytochrome P-450cam monooxygenase reaction by a single mutation, threonine-252 to alanine or valine:

- possible role of the hydroxy amino acid in oxygen activation, *Proc Natl Acad Sci U S A* 86, 7823-7827.
- [17] Martinis, S. A., Atkins, W. M., Stayton, P. S., and Sligar, S. G. (1989) A conserved residue of cytochrome P-450 is involved in heme-oxygen stability and activation, *Journal of the American Chemical Society* 111, 9252-9253.
- [18] Gerber, N. C., and Sligar, S. G. (1992) Catalytic mechanism of cytochrome P-450: evidence for a distal charge relay, *J Am Chem Soc* 114, 8742-8743.
- [19] Gerber, N. C., and Sligar, S. G. (1994) A role for Asp-251 in cytochrome P-450cam oxygen activation, *J Biol Chem* 269, 4260-4266.
- [20] Sundaramoorthy, M., Terner, J., and Poulos, T. L. (1995) The crystal structure of chloroperoxidase: a heme peroxidase--cytochrome P450 functional hybrid, *Structure* 3, 1367-1377.
- [21] Green, M. T. (2009) C-H bond activation in heme proteins: the role of thiolate ligation in cytochrome P450, *Curr Opin Chem Biol* 13, 84-88.
- [22] Dawson, J. H., and Sono, M. (1987) Cytochrome P-450 and Chloroperoxidase: Thiolate-ligated heme enzymes. Spectroscopic determination of their active site structures and mechanistic implications of thiolate ligation, *Chemical Reviews* 87, 1255-1276.
- [23] Ortiz de Montellano, P. R., (Ed.) (2005) *Cytochrome P450: Structure, Mechanism, and Biochemistry*, 3rd ed.
- [24] Cirino, P. C., and Arnold, F. H. (2003) A self-sufficient peroxide-driven hydroxylation biocatalyst, *Angewandte Chemie* 42, 3299-3301.
- [25] Gorsky, L. D., Koop, D. R., and Coon, M. J. (1984) On the stoichiometry of the oxidase and monooxygenase reactions catalyzed by liver microsomal cytochrome P-450. Products of oxygen reduction, *J Biol Chem* 259, 6812-6817.
- [26] Nordblom, G. D., and Coon, M. J. (1977) Hydrogen peroxide formation and stoichiometry of hydroxylation reactions catalyzed by highly purified liver microsomal cytochrome P-450, *Arch Biochem Biophys* 180, 343-347.
- [27] Sousa, R. L., and Marletta, M. A. (1985) Inhibition of cytochrome P-450 activity in rat liver microsomes by the naturally occurring flavonoid, quercetin, *Arch Biochem Biophys* 240, 345-357.
- [28] Stefek, M. (1993) In vitro studies on the interaction of the pyridoindole antioxidant stobadine with rat liver microsomal P450, *Xenobiotica* 23, 983-993.
- [29] Imai, Y., and Nakamura, M. (1989) Point mutations at threonine-301 modify substrate specificity of rabbit liver microsomal cytochromes P-450 (laurate (ω -1)-hydroxylase and testosterone 16 α -hydroxylase), *Biochem Biophys Res Commun* 158, 717-722.
- [30] Gruenke, L. D., Konopka, K., Cadieu, M., and Waskell, L. (1995) The stoichiometry of the cytochrome P-450-catalyzed metabolism of methoxyflurane and benzphetamine in the presence and absence of cytochrome b5, *J Biol Chem* 270, 24707-24718.
- [31] Hlavica, P. (1984) On the function of cytochrome b5 in the cytochrome P-450-dependent oxygenase system, *Arch Biochem Biophys* 228, 600-608.
- [32] Hlavica, P., and Lewis, D. F. (2001) Allosteric phenomena in cytochrome P450-catalyzed monooxygenations, *Eur J Biochem* 268, 4817-4832.
- [33] Fasan, R. (2012) Tuning P450 enzymes as oxidation catalysts, *ACS Catal.* 2, 647-666.

- [34] Jung, S. T., Lauchli, R., and Arnold, F. H. (2011) Cytochrome P450: Taming a wild type enzyme, *Curr. Opin. Biotechnol.* 22, 809-817.
- [35] Grinkova, Y. V., Denisov, I. G., McLean, M. A., and Sligar, S. G. (2013) Oxidase uncoupling in heme monooxygenases: human cytochrome P450 CYP3A4 in Nanodiscs, *Biochem Biophys Res Commun* 430, 1223-1227.
- [36] Zangar, R. C., Davydov, D. R., and Verma, S. (2004) Mechanisms that regulate production of reactive oxygen species by cytochrome P450, *Toxicol Appl Pharmacol* 199, 316-331.
- [37] Finkel, T. (1998) Oxygen radicals and signaling, *Curr Opin Cell Biol* 10, 248-253.
- [38] Khan, A. U., and Wilson, T. (1995) Reactive oxygen species as cellular messengers, *Chem Biol* 2, 437-445.
- [39] Lenaz, G. (1998) Role of mitochondria in oxidative stress and ageing, *Biochim Biophys Acta* 1366, 53-67.
- [40] Hrycay, E. G., and Bandiera, S. M. (2015) Involvement of Cytochrome P450 in Reactive Oxygen Species Formation and Cancer, *Adv Pharmacol* 74, 35-84.
- [41] Parke, D. V. (1994) The cytochromes P450 and mechanisms of chemical carcinogenesis, *Environ Health Perspect* 102, 852-853.
- [42] Shields, P. G., Ambrosone, C. B., Graham, S., Bowman, E. D., Harrington, A. M., Gillenwater, K. A., Marshall, J. R., Vena, J. E., Laughlin, R., Nemoto, T., and Freudenheim, J. L. (1996) A cytochrome P4502E1 genetic polymorphism and tobacco smoking in breast cancer, *Mol Carcinog* 17, 144-150.
- [43] Dennig, A., Lulsdorf, N., Liu, H., and Schwaneberg, U. (2013) Regioselective o-hydroxylation of monosubstituted benzenes by P450 BM3, *Angew Chem Int Ed Engl* 52, 8459-8462.
- [44] Le-Huu, P., Heidt, T., Claasen, B., Laschat, S., and Urlacher, V. B. (2015) Chemo-, Regio-, and stereoselective oxidation of the monocyclic diterpenoid b-cembrenediol by P450 BM3, *ACS Catal.* 5, 17772-11780.
- [45] Wang, Z. J., Renata, H., Peck, N. E., Farwell, C. C., Coelho, P. S., and Arnold, F. H. (2014) Improved cyclopropanation activity of histidine-ligated cytochrome P450 enables the enantioselective formal synthesis of levomilnacipran, *Angew Chem Int Ed Engl* 53, 6810-6813.
- [46] Hannemann, F., Bichet, A., Ewen, K. M., and Bernhardt, R. (2007) Cytochrome P450 systems--biological variations of electron transport chains, *Biochim Biophys Acta* 1770, 330-344.
- [47] Fukami, M., Shozu, M., Soneda, S., Kato, F., Inagaki, A., Takagi, H., Hanaki, K., Kanzaki, S., Ohyama, K., Sano, T., Nishigaki, T., Yokoya, S., Binder, G., Horikawa, R., and Ogata, T. (2011) Aromatase excess syndrome: identification of cryptic duplications and deletions leading to gain of function of CYP19A1 and assessment of phenotypic determinants, *J Clin Endocrinol Metab* 96, E1035-1043.
- [48] Shozu, M., Fukami, M., and Ogata, T. (2014) Understanding the pathological manifestations of aromatase excess syndrome: lessons for clinical diagnosis, *Expert Rev Endocrinol Metab* 9, 397-409.
- [49] Faustini-Fustini, M., Rochira, V., and Carani, C. (1999) Oestrogen deficiency in men: where are we today?, *Eur J Endocrinol* 140, 111-129.
- [50] Spector, A. A. (1999) Essentiality of fatty acids, *Lipids* 34 Suppl, S1-3.

- [51] Storlien, L. H., Hulbert, A. J., and Else, P. L. (1998) Polyunsaturated fatty acids, membrane function and metabolic diseases such as diabetes and obesity, *Curr Opin Clin Nutr Metab Care* 1, 559-563.
- [52] Connor, W. E. (2000) Importance of n-3 fatty acids in health and disease, *Am J Clin Nutr* 71, 171S-175S.
- [53] Kris-Etherton, P. M., Harris, W. S., Appel, L. J., and American Heart Association. Nutrition, C. (2002) Fish consumption, fish oil, omega-3 fatty acids, and cardiovascular disease, *Circulation* 106, 2747-2757.
- [54] Tapiero, H., Ba, G. N., Couvreur, P., and Tew, K. D. (2002) Polyunsaturated fatty acids (PUFA) and eicosanoids in human health and pathologies, *Biomed Pharmacother* 56, 215-222.
- [55] Nebert, D. W., and Russell, D. W. (2002) Clinical importance of the cytochromes P450, *Lancet* 360, 1155-1162.
- [56] Capdevila, J. H., Falck, J. R., and Harris, R. C. (2000) Cytochrome P450 and arachidonic acid bioactivation. Molecular and functional properties of the arachidonate monooxygenase, *J Lipid Res* 41, 163-181.
- [57] Oliw, E. H., Bylund, J., and Herman, C. (1996) Bisallylic hydroxylation and epoxidation of polyunsaturated fatty acids by cytochrome P450, *Lipids* 31, 1003-1021.
- [58] Roman, R. J. (2002) P-450 metabolites of arachidonic acid in the control of cardiovascular function, *Physiol Rev* 82, 131-185.
- [59] Konkel, A., and Schunck, W. H. (2011) Role of cytochrome P450 enzymes in the bioactivation of polyunsaturated fatty acids, *Biochim Biophys Acta* 1814, 210-222.
- [60] Funk, C. D. (2001) Prostaglandins and leukotrienes: advances in eicosanoid biology, *Science* 294, 1871-1875.
- [61] Wade, M. L., Voelkel, N. F., and Fitzpatrick, F. A. (1995) "Suicide" inactivation of prostaglandin I₂ synthase: characterization of mechanism-based inactivation with isolated enzyme and endothelial cells, *Arch Biochem Biophys* 321, 453-458.
- [62] Zou, M., Martin, C., and Ullrich, V. (1997) Tyrosine nitration as a mechanism of selective inactivation of prostacyclin synthase by peroxynitrite, *Biol Chem* 378, 707-713.
- [63] Nakayama, T., Soma, M., Rahmutula, D., Izumi, Y., and Kanmatsuse, K. (1997) Nonsense mutation of prostacyclin synthase gene in a family, *Lancet* 349, 1887-1888.
- [64] Rubin, L. J. (1995) Pathology and pathophysiology of primary pulmonary hypertension, *Am J Cardiol* 75, 51A-54A.
- [65] Anzenbacher, P., and Anzenbacherova, E. (2001) Cytochromes P450 and metabolism of xenobiotics, *Cell Mol Life Sci* 58, 737-747.
- [66] Johnson, E. F., and Stout, C. D. (2005) Structural diversity of human xenobiotic-metabolizing cytochrome P450 monooxygenases, *Biochem Biophys Res Commun* 338, 331-336.
- [67] Yano, J. K., Wester, M. R., Schoch, G. A., Griffin, K. J., Stout, C. D., and Johnson, E. F. (2004) The structure of human microsomal cytochrome P450 3A4 determined by X-ray crystallography to 2.05-Å resolution, *J Biol Chem* 279, 38091-38094.

- [68] Anzenbacherova, E., Bec, N., Anzenbacher, P., Hudecek, J., Soucek, P., Jung, C., Munro, A. W., and Lange, R. (2000) Flexibility and stability of the structure of cytochromes P450 3A4 and BM-3, *Eur J Biochem* 267, 2916-2920.
- [69] Guengerich, F. P., and Shimada, T. (1991) Oxidation of toxic and carcinogenic chemicals by human cytochrome P-450 enzymes, *Chem Res Toxicol* 4, 391-407.
- [70] Nebert, D. W., and Dalton, T. P. (2006) The role of cytochrome P450 enzymes in endogenous signalling pathways and environmental carcinogenesis, *Nat Rev Cancer* 6, 947-960.
- [71] Shimada, T., and Fujii-Kuriyama, Y. (2004) Metabolic activation of polycyclic aromatic hydrocarbons to carcinogens by cytochromes P450 1A1 and 1B1, *Cancer Sci* 95, 1-6.
- [72] Shahrokh, K., Orendt, A., Yost, G. S., and Cheatham, T. E., III. (2012) Quantum mechanically derived AMBER-compatible heme parameters for various states of the cytochrome P450 catalytic cycle, *Journal of computational chemistry* 33, 119-133.
- [73] Hayes, C. L., Spink, D. C., Spink, B. C., Cao, J. Q., Walker, N. J., and Sutter, T. R. (1996) 17 beta-estradiol hydroxylation catalyzed by human cytochrome P450 1B1, *Proc Natl Acad Sci U S A* 93, 9776-9781.
- [74] Spink, D. C., Spink, B. C., Cao, J. Q., DePasquale, J. A., Pentecost, B. T., Fasco, M. J., Li, Y., and Sutter, T. R. (1998) Differential expression of CYP1A1 and CYP1B1 in human breast epithelial cells and breast tumor cells, *Carcinogenesis* 19, 291-298.
- [75] Chun, Y. J., and Kim, S. (2003) Discovery of cytochrome P450 1B1 inhibitors as new promising anti-cancer agents, *Med Res Rev* 23, 657-668.
- [76] McFadyen, M. C., McLeod, H. L., Jackson, F. C., Melvin, W. T., Doehmer, J., and Murray, G. I. (2001) Cytochrome P450 CYP1B1 protein expression: a novel mechanism of anticancer drug resistance, *Biochem Pharmacol* 62, 207-212.
- [77] Rochat, B., Morsman, J. M., Murray, G. I., Figg, W. D., and McLeod, H. L. (2001) Human CYP1B1 and anticancer agent metabolism: mechanism for tumor-specific drug inactivation?, *J Pharmacol Exp Ther* 296, 537-541.
- [78] Ortiz de Montellano, P. R. (2013) Cytochrome P450-activated prodrugs, *Future Med Chem* 5, 213-228.
- [79] Brantley, E., Trapani, V., Alley, M. C., Hose, C. D., Bradshaw, T. D., Stevens, M. F., Sausville, E. A., and Stinson, S. F. (2004) Fluorinated 2-(4-amino-3-methylphenyl)benzothiazoles induce CYP1A1 expression, become metabolized, and bind to macromolecules in sensitive human cancer cells, *Drug Metab Dispos* 32, 1392-1401.
- [80] Mortimer, C. G., Wells, G., Crochard, J. P., Stone, E. L., Bradshaw, T. D., Stevens, M. F., and Westwell, A. D. (2006) Antitumor benzothiazoles. 26.(1) 2-(3,4-dimethoxyphenyl)-5-fluorobenzothiazole (GW 610, NSC 721648), a simple fluorinated 2-arylbenzothiazole, shows potent and selective inhibitory activity against lung, colon, and breast cancer cell lines, *J Med Chem* 49, 179-185.
- [81] Tan, B. S., Tiong, K. H., Muruhadas, A., Randhawa, N., Choo, H. L., Bradshaw, T. D., Stevens, M. F., and Leong, C. O. (2011) CYP2S1 and CYP2W1 mediate 2-(3,4-dimethoxyphenyl)-5-fluorobenzothiazole (GW-610, NSC 721648) sensitivity in breast and colorectal cancer cells, *Mol Cancer Ther* 10, 1982-1992.

- [82] Wang, K., and Guengerich, F. P. (2012) Bioactivation of fluorinated 2-arylbenzothiazole antitumor molecules by human cytochrome P450s 1A1 and 2W1 and deactivation by cytochrome P450 2S1, *Chem Res Toxicol* 25, 1740-1751.
- [83] Downie, D., McFadyen, M. C., Rooney, P. H., Cruickshank, M. E., Parkin, D. E., Miller, I. D., Telfer, C., Melvin, W. T., and Murray, G. I. (2005) Profiling cytochrome P450 expression in ovarian cancer: identification of prognostic markers, *Clin Cancer Res* 11, 7369-7375.
- [84] Karlgren, M., Gomez, A., Stark, K., Svard, J., Rodriguez-Antona, C., Oliw, E., Bernal, M. L., Ramon y Cajal, S., Johansson, I., and Ingelman-Sundberg, M. (2006) Tumor-specific expression of the novel cytochrome P450 enzyme, CYP2W1, *Biochem Biophys Res Commun* 341, 451-458.
- [85] Kumarakulasingham, M., Rooney, P. H., Dundas, S. R., Telfer, C., Melvin, W. T., Curran, S., and Murray, G. I. (2005) Cytochrome p450 profile of colorectal cancer: identification of markers of prognosis, *Clin Cancer Res* 11, 3758-3765.
- [86] Nishida, C. R., Lee, M., and de Montellano, P. R. (2010) Efficient hypoxic activation of the anticancer agent AQ4N by CYP2S1 and CYP2W1, *Mol Pharmacol* 78, 497-502.
- [87] Zamora, A., Denning, C. A., Heidary, D. K., Wachter, E., Nease, L. A., Ruiz, J., and Glazer, E. C. (2017) Ruthenium-containing P450 inhibitors for dual enzyme inhibition and DNA damage, *Dalton Trans* 46, 2165-2173.
- [88] Appleby, A. C. (1967) A soluble haemoprotein P 450 from nitrogen-fixing Rhizobium bacteroids, *Biochim Biophys Acta* 147, 399-402.
- [89] Nelson, D. R. (2011) Progress in tracing the evolutionary paths of cytochrome P450, *Biochim Biophys Acta* 1814, 14-18.
- [90] Kelly, S. L., Kelly, D. E., Jackson, C. J., Warrilow, A. G. S., and Lamb, D. C. (2005) The diversity and importance of microbial cytochromes P450, In *Cytochrome P450: Structure, Mechanism, and Biochemistry* (Ortiz de Montellano, P. R., Ed.) 3rd ed., p 689, Kluwer Academic/Plenum Publishers.
- [91] Kimata, Y., Shimada, H., Hirose, T., and Ishimura, Y. (1995) Role of Thr-252 in cytochrome P450cam: a study with unnatural amino acid mutagenesis, *Biochem Biophys Res Commun* 208, 96-102.
- [92] Raag, R., Martinis, S. A., Sligar, S. G., and Poulos, T. L. (1991) Crystal structure of the cytochrome P-450CAM active site mutant Thr252Ala, *Biochemistry* 30, 11420-11429.
- [93] Raag, R., and Poulos, T. L. (1991) Crystal structures of cytochrome P-450CAM complexed with camphane, thiocamphor, and adamantane: Factors controlling P-450 substrate hydroxylation, *Biochemistry* 30, 2674-2684.
- [94] Miura, Y., and Fulco, A. J. (1974) (Ω -2) hydroxylation of fatty acids by a soluble system from bacillus megaterium, *J Biol Chem* 249, 1880-1888.
- [95] Narhi, L. O., and Fulco, A. J. (1986) Characterization of a catalytically self-sufficient 119,000-dalton cytochrome P-450 monooxygenase induced by barbiturates in *Bacillus megaterium*, *J Biol Chem* 261, 7160-7169.
- [96] Narhi, L. O., and Fulco, A. J. (1987) Identification and characterization of two functional domains in cytochrome P-450BM-3, a catalytically self-sufficient monooxygenase induced by barbiturates in *Bacillus megaterium*, *J Biol Chem* 262, 6683-6690.

- [97] Noble, M. A., Miles, C. S., Chapman, S. K., Lysek, D. A., MacKay, A. C., Reid, G. A., Hanzlik, R. P., and Munro, A. W. (1999) Roles of key active-site residues in flavocytochrome P450 BM3, *Biochemical Journal* 339, 371-379.
- [98] Geronimo, I., Denning, C. A., Heidary, D. K., Glazer, E. C., and Payne, C. M. (2018) Molecular Determinants of Substrate Affinity and Enzyme Activity of a Cytochrome P450BM3 Variant, *Biophys J* 115, 1251-1263.
- [99] Bommarius, A. S., and Paye, M. F. (2013) Stabilizing biocatalysts, *Chemical Society Reviews* 42, 6534-6565.
- [100] Iyer, P. V., and Ananthanarayan, L. (2008) Enzyme stability and stabilization—Aqueous and non-aqueous environment, *Process Biochemistry* 43, 1019-1032.
- [101] Brissos, V., Gonçalves, N., Melo, E. P., and Martins, L. O. (2014) Improving kinetic or thermodynamic stability of an azoreductase by directed evolution, *PLoS One* 9, e87209.
- [102] Volkin, D., and Klibanov, A. (1989) Minimizing protein inactivation, In *Protein Function. A practical approach* (Creighton, T., Ed.), pp 1-24, IRL Press, Oxford.
- [103] Eijssink, V. G. H., Bjørk, A., Gåseidnes, S., Sirevåg, R., Synstad, B., Burg, B. v. d., and Vriend, G. (2004) Rational engineering of enzyme stability, *Journal of Biotechnology* 113, 105-120.
- [104] Alonso, D. O., and Dill, K. A. (1991) Solvent denaturation and stabilization of globular proteins, *Biochemistry* 30, 5974-5985.
- [105] Ghosh, K., and Dill, K. A. (2009) Computing protein stabilities from their chain lengths, *Proc Natl Acad Sci U S A* 106, 10649-10654.
- [106] Swint, L., and Robertson, A. D. (1993) Thermodynamics of unfolding for turkey ovomucoid third domain: thermal and chemical denaturation, *Protein Sci* 2, 2037-2049.
- [107] Ramprakash, J., Doseeva, V., Galkin, A., Krajewski, W., Muthukumar, L., Pullalarevu, S., Demirkan, E., Herzberg, O., Moul, J., and Schwarz, F. P. (2008) Comparison of the chemical and thermal denaturation of proteins by a two-state transition model, *Anal Biochem* 374, 221-230.
- [108] Wang, Q., Christiansen, A., Samiotakis, A., Wittung-Stafshede, P., and Cheung, M. S. (2011) Comparison of chemical and thermal protein denaturation by combination of computational and experimental approaches. II, *J Chem Phys* 135, 175102.
- [109] Agundez, J. A. (2004) Cytochrome P450 gene polymorphism and cancer, *Curr Drug Metab* 5, 211-224.
- [110] Rodriguez-Antona, C., and Ingelman-Sundberg, M. (2006) Cytochrome P450 pharmacogenetics and cancer, *Oncogene* 25, 1679-1691.
- [111] Fisher, C. D., Lickteig, A. J., Augustine, L. M., Ranger-Moore, J., Jackson, J. P., Ferguson, S. S., and Cherrington, N. J. (2009) Hepatic cytochrome P450 enzyme alterations in humans with progressive stages of nonalcoholic fatty liver disease, *Drug Metab Dispos* 37, 2087-2094.
- [112] George, J., Liddle, C., Murray, M., Byth, K., and Farrell, G. C. (1995) Pre-translational regulation of cytochrome P450 genes is responsible for disease-specific changes of individual P450 enzymes among patients with cirrhosis, *Biochem Pharmacol* 49, 873-881.

- [113] George, J., Murray, M., Byth, K., and Farrell, G. C. (1995) Differential alterations of cytochrome P450 proteins in livers from patients with severe chronic liver disease, *Hepatology* 21, 120-128.
- [114] Belmouden, A., Melki, R., Hamdani, M., Zaghoul, K., Amraoui, A., Nadifi, S., Akhayat, O., and Garchon, H. J. (2002) A novel frameshift founder mutation in the cytochrome P450 1B1 (CYP1B1) gene is associated with primary congenital glaucoma in Morocco, *Clin Genet* 62, 334-339.
- [115] Colomb, E., Kaplan, J., and Garchon, H. J. (2003) Novel cytochrome P450 1B1 (CYP1B1) mutations in patients with primary congenital glaucoma in France, *Hum Mutat* 22, 496.
- [116] Kakiuchi-Matsumoto, T., Isashiki, Y., Ohba, N., Kimura, K., Sonoda, S., and Unoki, K. (2001) Cytochrome P450 1B1 gene mutations in Japanese patients with primary congenital glaucoma(1), *Am J Ophthalmol* 131, 345-350.
- [117] Prosser, D. E., and Jones, G. (2004) Enzymes involved in the activation and inactivation of vitamin D, *Trends Biochem Sci* 29, 664-673.
- [118] Yang, C. S., Brady, J. F., and Hong, J. Y. (1992) Dietary effects on cytochromes P450, xenobiotic metabolism, and toxicity, *FASEB J* 6, 737-744.
- [119] Munro, A. W., Daff, S., Coggins, J. R., Lindsay, J. G., and Chapman, S. K. (1996) Probing electron transfer in flavocytochrome P-450 BM3 and its component domains, *European Journal of Biochemistry* 239, 403-409.
- [120] Tsotsou, G. E., Sideri, A., Goyal, A., Di Nardo, G., and Gilardi, G. (2012) Identification of mutant Asp251Gly/Gln307His of cytochrome P450 BM3 for the generation of metabolites of diclofenac, ibuprofen and tolbutamide, *Chemistry* 18, 3582-3588.
- [121] Butler, C. F., Peet, C., McLean, K. J., Baynham, M. T., Blankley, R. T., Fisher, K., Rigby, S. E., Leys, D., Voice, M. W., and Munro, A. W. (2014) Human P450-like oxidation of diverse proton pump inhibitor drugs by 'gatekeeper' mutants of flavocytochrome P450 BM3, *The Biochemical journal* 460, 247-259.
- [122] Rentmeister, A., Brown, T. R., Snow, C. D., Carbone, M. N., and Arnold, F. H. (2011) Engineered bacterial mimics of human drug metabolizing enzyme CYP2C9, *ChemCatChem* 3, 1065-1071.
- [123] Lussenburg, B. M. A., Babel, L. C., Vermeulen, N. P. E., and Commandeur, J. N. M. (2005) Evaluation of alkoxyresorufins as fluorescent substrates for cytochrome P450 BM3 and site-directed mutants, *Analytical Biochemistry* 341, 148-155.
- [124] van Vugt-Lussenburg, B. M., Damsten, M. C., Maasdijk, D. M., Vermeulen, N. P., and Commandeur, J. N. (2006) Heterotropic and homotropic cooperativity by a drug-metabolising mutant of cytochrome P450 BM3, *Biochem Biophys Res Commun* 346, 810-818.
- [125] van Vugt-Lussenburg, B. M. A., Stjerschantz, E., Lastdrager, J., Oostenbrink, C., Vermeulen, P. E., and Commandeur, J. N. M. (2007) Identification of critical residues in novel drug metabolizing mutants of cytochrome P450 BM3 using random mutagenesis, *Journal of Medicinal Chemistry* 50, 455-461.
- [126] Kim, D. H., Ahn, T., Jung, H. C., Pan, J. G., and Yun, C. H. (2009) Generation of the human metabolite piceatannol from the anticancer-preventive agent resveratrol by bacterial cytochrome P450 BM3, *Drug metabolism and disposition: the biological fate of chemicals* 37, 932-936.

- [127] Reinen, J., van Leeuwen, J. S., Li, Y., Sun, L., Grootenhuis, P. D. J., Decker, C. J., Saunders, J., Vermeulen, N. P. E., and Commandeur, J. N. M. (2011) Efficient screening of cytochrome P450 BM3 mutants for their metabolic activity and diversity toward a wide set of drug-like molecules in chemical space, *Drug metabolism and disposition: the biological fate of chemicals* 39, 1568-1576.
- [128] Stjerschantz, E., van Vugt-Lussenburg, B. M., Bonifacio, A., de Beer, S. B., van der Zwan, G., Gooijer, C., Commandeur, J. N., Vermeulen, N. P., and Oostenbrink, C. (2008) Structural rationalization of novel drug metabolizing mutants of cytochrome P450 BM3, *Proteins* 71, 336-352.
- [129] Bloom, J. D., Labthavikul, S. T., Otey, C. R., and Arnold, F. H. (2006) Protein stability promotes evolvability, *Proceedings of the National Academy of Sciences of the United States of America* 103, 5869-5874.
- [130] Tokuriki, N., and Tawfik, D. S. (2009) Stability effects of mutations and protein evolvability, *Current Opinion in Structural Biology* 19, 596-604.
- [131] Besenmatter, W., Kast, P., and Hilvert, D. (2007) Relative tolerance of mesostable and thermostable protein homologs to extensive mutation, *Proteins: Struct., Funct., Bioinf.* 66, 500-506.
- [132] Munro, A. W., Lindsay, J. G., Coggins, J. R., Kelly, S. M., and Price, N. C. (1996) Analysis of the structural stability of the multidomain enzyme flavocytochrome P-450 BM3, *Biochimica et Biophysica Acta (BBA) - Protein Structure and Molecular Enzymology* 1296, 127-137.
- [133] Eiben, S., Bartelmas, H., and Urlacher, V. B. (2007) Construction of a thermostable cytochrome P450 chimera derived from self-sufficient mesophilic parents, *Applied microbiology and biotechnology* 75, 1055-1061.
- [134] Eiben, S., Kaysser, L., Maurer, S., Kuhnel, K., Urlacher, V. B., and Schmid, R. D. (2006) Preparative use of isolated CYP102 monooxygenases — a critical appraisal, *J Biotechnol* 124, 662-669.
- [135] Salazar, O., Cirino, P. C., and Arnold, F. H. (2003) Thermostabilization of a cytochrome p450 peroxygenase, *Chembiochem : a European journal of chemical biology* 4, 891-893.
- [136] Fasan, R., Chen, M. M., Crook, N. C., and Arnold, F. H. (2007) Engineered alkane-hydroxylating cytochrome P450(BM3) exhibiting natively catalytic properties, *Angewandte Chemie* 46, 8414-8418.
- [137] Park, C., and Marqusee, S. (2005) Pulse proteolysis: a simple method for quantitative determination of protein stability and ligand binding, *Nature methods* 2, 207-212.
- [138] Omura, T., and Sato, R. (1964) The carbon monoxide-binding pigment of liver microsomes: II. Solubilization, purification, and properties, *Journal of Biological Chemistry* 239, 2379-2385.
- [139] Park, C., and Marqusee, S. (2006) Quantitative determination of protein stability and ligand binding by pulse proteolysis, In *Current Protocols in Protein Science*, pp 20.11.21-20.11.14, John Wiley & Sons, Inc.
- [140] Kabsch, W. (2010) Xds, *Acta crystallographica. Section D, Biological crystallography* 66, 125-132.
- [141] Adams, P. D., Afonine, P. V., Bunkoczi, G., Chen, V. B., Davis, I. W., Echols, N., Headd, J. J., Hung, L. W., Kapral, G. J., Grosse-Kunstleve, R. W., McCoy, A. J., Moriarty, N. W., Oeffner, R., Read, R. J., Richardson, D. C., Richardson, J. S.,

- Terwilliger, T. C., and Zwart, P. H. (2010) PHENIX: a comprehensive Python-based system for macromolecular structure solution, *Acta crystallographica. Section D, Biological crystallography* 66, 213-221.
- [142] Chen, V. B., Arendall, W. B., III, Headd, J. J., Keedy, D. A., Immormino, R. M., Kapral, G. J., Murray, L. W., Richardson, J. S., and Richardson, D. C. (2010) MolProbity: all-atom structure validation for macromolecular crystallography, *Acta crystallographica. Section D, Biological crystallography* 66, 12-21.
- [143] McCoy, A. J., Grosse-Kunstleve, R. W., Adams, P. D., Winn, M. D., Storoni, L. C., and Read, R. J. (2007) Phaser crystallographic software, *Journal of applied crystallography* 40, 658-674.
- [144] Emsley, P., Lohkamp, B., Scott, W. G., and Cowtan, K. (2010) Features and development of Coot, *Acta crystallographica. Section D, Biological crystallography* 66, 486-501.
- [145] Winn, M. D., Ballard, C. C., Cowtan, K. D., Dodson, E. J., Emsley, P., Evans, P. R., Keegan, R. M., Krissinel, E. B., Leslie, A. G., McCoy, A., McNicholas, S. J., Murshudov, G. N., Pannu, N. S., Potterton, E. A., Powell, H. R., Read, R. J., Vagin, A., and Wilson, K. S. (2011) Overview of the CCP4 suite and current developments, *Acta crystallographica. Section D, Biological crystallography* 67, 235-242.
- [146] Hornak, V., Abel, R., Okur, A., Strockbine, B., Roitberg, A., and Simmerling, C. (2006) Comparison of multiple Amber force fields and development of improved protein backbone parameters, *Proteins* 65, 712-725.
- [147] Jorgensen, W. L., Chandrasekhar, J., Madura, J. D., Impey, R. W., and Klein, M. L. (1983) Comparison of simple potential functions for simulating liquid water, *J. Chem. Phys.* 79, 926-935.
- [148] Wang, J., Wang, W., Kollman, P. A., and Case, D. A. (2006) Automatic atom type and bond type perception in molecular mechanical calculations, *Journal of molecular graphics & modelling* 25, 247-260.
- [149] Wang, J., Wolf, R. M., Caldwell, J. W., Kollman, P. A., and Case, D. A. (2004) Development and testing of a general amber force field, *Journal of computational chemistry* 25, 1157-1174.
- [150] Case, D. A., Babin, V., Berryman, J. T., Betz, R. M., Cai, Q., Cerutti, D. S., Cheatham, T. E., III, Darden, T. A., Duke, R. E., Gohlke, H., Goetz, A. W., Gusarov, S., Homeyer, N., Janowski, P., Kaus, J., Kolossváry, I., Kovalenko, A., Lee, T. S., LeGrand, S., Luchko, T., Luo, R., Madej, B., Merz, K. M., Paesani, F., Roe, D. R., Roitberg, A., Sagui, C., Salomon-Ferrer, R., Seabra, G., Simmerling, C. L., Smith, W., Swails, J., Walker, R. C., Wang, J., Wolf, R. M., Wu, X., Kollman, P. A. (2014) AMBER 14, University of California, San Francisco.
- [151] Meharena, Y. T., and Poulos, T. L. (2010) Using molecular dynamics to probe the structural basis for enhanced stability in thermal stable cytochromes P450, *Biochemistry* 49, 6680-6686.
- [152] Day, R., Bennion, B. J., Ham, S., and Daggett, V. (2002) Increasing temperature accelerates protein unfolding without changing the pathway of unfolding, *Journal of molecular biology* 322, 189-203.

- [153] Huang, X., and Zhou, H. X. (2006) Similarity and difference in the unfolding of thermophilic and mesophilic cold shock proteins studied by molecular dynamics simulations, *Biophys J* 91, 2451-2463.
- [154] Sham, Y. Y., Ma, B., Tsai, C. J., and Nussinov, R. (2002) Thermal unfolding molecular dynamics simulation of Escherichia coli dihydrofolate reductase: thermal stability of protein domains and unfolding pathway, *Proteins* 46, 308-320.
- [155] Roe, D. R., and Cheatham, T. E., III. (2013) PTRAJ and CPPTRAJ: software for processing and analysis of molecular dynamics trajectory data, *J. Chem. Theory Comput.* 9, 3084-3095.
- [156] Anandkrishnan, R., Aguilar, B., and Onufriev, A. V. (2012) H++ 3.0: automating pK prediction and the preparation of biomolecular structures for atomistic molecular modeling and simulations, *Nucleic Acids Res* 40, W537-541.
- [157] Gordon, J. C., Myers, J. B., Folta, T., Shoja, V., Heath, L. S., and Onufriev, A. (2005) H++: a server for estimating pKas and adding missing hydrogens to macromolecules, *Nucleic Acids Res* 33, W368-371.
- [158] H++.
- [159] Essmann, U., Perera, L., Berkowitz, M. L., Darden, T., Lee, H., and Pedersen, L. G. (1995) A smooth particle mesh Ewald method, *J. Chem. Phys.* 103, 8577-8593.
- [160] Ryckaert, J.-P., Ciccotti, G., and Berendsen, H. J. C. (1977) Numerical integration of the cartesian equations of motion of a system with constraints: Molecular dynamics of n-alkanes, *J. Comput. Phys.* 23, 327-341.
- [161] Pastor, R. W., Brooks, B. R., and Szabo, A. (1988) An analysis of the accuracy of Langevin and molecular dynamics algorithms, *Mol. Phys.* 65, 1409-1419.
- [162] Kim, D.-H., Kim, K.-H., Kim, D., Jung, H.-C., Pan, J.-G., Chi, Y.-T., Ahn, T., and Yun, C.-H. (2010) Oxidation of human cytochrome P450 1A2 substrates by Bacillus megaterium cytochrome P450 BM3, *J. Mol. Catal. B: Enzym.* 63, 179-187.
- [163] Kim, K. H., Kang, J. Y., Kim, D. H., Park, S. H., Park, S. H., Kim, D., Park, K. D., Lee, Y. J., Jung, H. C., Pan, J. G., Ahn, T., and Yun, C. H. (2011) Generation of human chiral metabolites of simvastatin and lovastatin by bacterial CYP102A1 mutants, *Drug. Metab. Dispos.* 39, 140-150.
- [164] Butler, C. F., Peet, C., Mason, A. E., Voice, M. W., Leys, D., and Munro, A. W. (2013) Key mutations alter the cytochrome P450 BM3 conformational landscape and remove inherent substrate bias, *J Biol Chem* 288, 25387-25399.
- [165] Li, H., and Poulos, T. L. (1997) The structure of the cytochrome p450 BM-3 haem domain complexed with the fatty acid substrate, palmitoleic acid, *Nature structural biology* 4, 140-146.
- [166] Ren, X., Yorke, J. A., Taylor, E., Zhang, T., Zhou, W., and Wong, L. L. (2015) Drug oxidation by cytochrome P450BM3: metabolite synthesis and discovering new P450 reaction types, *Chem. Eur. J.* 21, 15039-15047.
- [167] Poulos, T. L., and Howard, A. J. (1987) Crystal structures of metyrapone- and phenylimidazole-inhibited complexes of cytochrome P-450cam, *Biochemistry* 26, 8165-8174.
- [168] Williams, P. A., Cosme, J., Vinković, D. M., Ward, A., Angove, H. C., Day, P. J., Vonrhein, C., Tickle, I. J., and Jhoti, H. (2004) Crystal structures of human

- cytochrome P450 3A4 bound to metyrapone and progesterone, *Science* 305, 683-686.
- [169] Fasan, R., Meharena, Y. T., Snow, C. D., Poulos, T. L., and Arnold, F. H. (2008) Evolutionary history of a specialized p450 propane monooxygenase, *Journal of molecular biology* 383, 1069-1080.
- [170] Park, S. H., Kim, D. H., Kim, D., Kim, D. H., Jung, H. C., Pan, J. G., Ahn, T., Kim, D., and Yun, C. H. (2010) Engineering bacterial cytochrome P450 (P450) BM3 into a prototype with human P450 enzyme activity using indigo formation, *Drug metabolism and disposition: the biological fate of chemicals* 38, 732-739.
- [171] Bennion, B. J., and Daggett, V. (2003) The molecular basis for the chemical denaturation of proteins by urea, *Proceedings of the National Academy of Sciences of the United States of America* 100, 5142-5147.
- [172] Heinrikson, R. L. (1977) Applications of thermolysin in protein structural analysis, *Methods Enzymol* 47, 175-189.
- [173] Holmes, M. A., and Matthews, B. W. (1982) Structure of thermolysin refined at 1.6 Å resolution, *Journal of molecular biology* 160, 623-639.
- [174] Park, C., and Marqusee, S. (2004) Probing the high energy states in proteins by proteolysis, *Journal of molecular biology* 343, 1467-1476.
- [175] Latt, S. A., Holmquist, B., and Vallee, B. L. (1969) Thermolysin: a zinc metalloenzyme, *Biochem Biophys Res Commun* 37, 333-339.
- [176] Morihara, K., and Tsuzuki, H. (1966) Proteolytic substrate specificity and some elastolytic properties of a thermostable bacterial proteinase, *Biochim Biophys Acta* 118, 215-218.
- [177] Mearns, S. R., and Engen, J. R. (2010) Hydrogen exchange mass spectrometry: what is it and what can it tell us?, *Anal Bioanal Chem* 397, 967-972.
- [178] Dias, D. M., and Ciulli, A. (2014) NMR approaches in structure-based lead discovery: recent developments and new frontiers for targeting multi-protein complexes, *Prog Biophys Mol Biol* 116, 101-112.
- [179] Osvath, S., and Gruebele, M. (2003) Proline can have opposite effects on fast and slow protein folding phases, *Biophys J* 85, 1215-1222.
- [180] Arnold, G. E., and Ornstein, R. L. (1997) Molecular dynamics study of time-correlated protein domain motions and molecular flexibility: cytochrome P450BM-3, *Biophysical Journal* 73, 1147-1159.
- [181] Chou, P. Y., and Fasman, G. D. (1974) Prediction of protein conformation, *Biochemistry* 13, 222-245.
- [182] Cimperman, P., Baranauskiene, L., Jachimoviciute, S., Jachno, J., Torresan, J., Michailoviene, V., Matuliene, J., Sereikaite, J., Bumelis, V., and Matulis, D. (2008) A quantitative model of thermal stabilization and destabilization of proteins by ligands, *Biophys J* 95, 3222-3231.
- [183] Kumar, S., Tsai, C.-J., and Nussinov, R. (2000) Factors enhancing protein thermostability, *Protein Engineering* 13, 179-191.
- [184] Taylor, T. J., and Vaisman, I. I. (2010) Discrimination of thermophilic and mesophilic proteins, *BMC Structural Biology* 10, 1-10.
- [185] Radestock, S., and Gohlke, H. (2011) Protein rigidity and thermophilic adaptation, *Proteins: Struct., Funct., Bioinf.* 79, 1089-1108.

- [186] Chen, J., Yu, H., Liu, C., Liu, J., and Shen, Z. (2013) Improving stability of nitrile hydratase by bridging the salt-bridges in specific thermal-sensitive regions, *Journal of Biotechnology* 164, 354-362.
- [187] Xie, Y., An, J., Yang, G., Wu, G., Zhang, Y., Cui, L., and Feng, Y. (2014) Enhanced enzyme kinetic stability by increasing rigidity within the active site, *Journal of Biological Chemistry*.
- [188] Borgo, B., and Havranek, J. J. (2012) Automated selection of stabilizing mutations in designed and natural proteins, *Proceedings of the National Academy of Sciences of the United States of America* 109, 1494-1499.
- [189] Elcock, A. H. (1998) The stability of salt bridges at high temperatures: implications for hyperthermophilic proteins, *Journal of molecular biology* 284, 489-502.
- [190] Yano, J. K., Blasco, F., Li, H., Schmid, R. D., Henne, A., and Poulos, T. L. (2003) Preliminary characterization and crystal structure of a thermostable cytochrome P450 from *Thermus thermophilus*, *Journal of Biological Chemistry* 278, 608-616.
- [191] Whitehouse, C. J. C., Bell, S. G., and Wong, L.-L. (2012) P450BM3 (CYP102A1): connecting the dots, *Chemical Society Reviews* 41, 1218-1260.
- [192] Bell, S. G., and Wong, L. L. (2007) P450 enzymes from the bacterium *Novosphingobium aromaticivorans*, *Biochem Biophys Res Commun* 360, 666-672.
- [193] Leys, D., Mowat, C. G., McLean, K. J., Richmond, A., Chapman, S. K., Walkinshaw, M. D., and Munro, A. W. (2003) Atomic structure of Mycobacterium tuberculosis CYP121 to 1.06 Å reveals novel features of cytochrome P450, *J Biol Chem* 278, 5141-5147.
- [194] Schroer, K., Kittelmann, M., and Lütz, S. (2010) Recombinant human cytochrome P450 monooxygenases for drug metabolite synthesis, *Biotechnol. Bioeng.* 106, 699-706.
- [195] Di Nardo, G., and Gilardi, G. (2012) Optimization of the bacterial cytochrome P450 BM3 system for the production of human drug metabolites, *Int. J. Mol. Sci.* 13, 15901-15924.
- [196] Sawayama, A. M., Chen, M. M., Kulanthaivel, P., Kuo, M. S., Hemmerle, H., and Arnold, F. H. (2009) A panel of cytochrome P450 BM3 variants to produce drug metabolites and diversify lead compounds, *Chem. Eur. J* 15, 11723-11729.
- [197] Di Nardo, G., Fantuzzi, A., Sideri, A., Panicco, P., Sassone, C., Giunta, C., and Gilardi, G. (2007) Wild-type CYP102A1 as a biocatalyst: Turnover of drugs usually metabolised by human liver enzymes, *J. Biol. Inorg. Chem.* 12, 313-323.
- [198] Damsten, M. C., van Vugt-Lussenburg, B. M. A., Zeldenthuis, T., de Vlioger, J. S. B., Commandeur, J. N. M., and Vermeulen, N. P. E. (2008) Application of drug metabolising mutants of cytochrome P450 BM3 (CYP102A1) as biocatalysts for the generation of reactive metabolites, *Chem.-Biol. Interact.* 171, 96-107.
- [199] Capoferri, L., Leth, R., ter Haar, E., Mohanty, A. K., Grootenhuys, P. D. J., Vottero, E., Commandeur, J. N. M., Vermeulen, N. P. E., Jørgensen, F. S., Olsen, L., and Geerke, D. P. (2016) Insights into regioselective metabolism of mefenamic acid by cytochrome P450 BM3 mutants through crystallography, docking, molecular dynamics, and free energy calculations, *Proteins: Struct., Funct., Bioinf.* 84, 383-396.
- [200] Sono, M., Roach, M. P., Coulter, E. D., and Dawson, J. H. (1996) Heme-containing oxygenases, *Chem. Rev.* 96, 2841-2888.

- [201] Di Nardo, G., Dell'Angelo, V., Catucci, G., Sadeghi, S. J., and Gilardi, G. (2016) Subtle structural changes in the Asp251Gly/Gln307His P450 BM3 mutant responsible for new activity toward diclofenac, tolbutamide and ibuprofen, *Arch. Biochem. Biophys.* 602, 106-115.
- [202] Whitehouse, C. J., Yang, W., Yorke, J. A., Tufton, H. G., Ogilvie, L. C., Bell, S. G., Zhou, W., Bartlam, M., Rao, Z., and Wong, L. L. (2011) Structure, electronic properties and catalytic behaviour of an activity-enhancing CYP102A1 (P450(BM3)) variant, *Dalton. Trans.* 40, 10383-10396.
- [203] Haines, D. C., Tomchick, D. R., Machius, M., and Peterson, J. A. (2001) Pivotal role of water in the mechanism of P450BM-3, *Biochemistry* 40, 13456-13465.
- [204] Gotoh, O. (1992) Substrate recognition sites in cytochrome P450 family 2 (CYP2) proteins inferred from comparative analyses of amino acid and coding nucleotide sequences, *J Biol Chem* 267, 83-90.
- [205] Cojocar, V., Winn, P. J., and Wade, R. C. (2007) The ins and outs of cytochrome P450s, *Biochim Biophys Acta* 1770, 390-401.
- [206] Wade, R. C., Winn, P. J., Schlichting, I., and Sudarko. (2004) A survey of active site access channels in cytochromes P450, *J Inorg Biochem* 98, 1175-1182.
- [207] Kitazume, T., Haines, D. C., Estabrook, R. W., Chen, B., and Peterson, J. A. (2007) Obligatory intermolecular electron-transfer from FAD to FMN in dimeric P450BM-3, *Biochemistry* 46, 11892-11901.
- [208] Whitehouse, C. J. C., Yang, W., Yorke, J. A., Rowlatt, B. C., Strong, A. J. F., Blanford, C. F., Bell, S. G., Bartlam, M., Wong, L.-L., and Rao, Z. (2010) Structural basis for the properties of two single-site proline mutants of CYP102A1 (P450BM3), *Chembiochem : a European journal of chemical biology* 11, 2549-2556.
- [209] Jeffreys, L. N., Poddar, H., Golovanova, M., Levy, C. W., Girvan, H. M., McLean, K. J., Voice, M. W., Leys, D., and Munro, A. W. (2019) Novel insights into P450 BM3 interactions with FDA-approved antifungal azole drugs, *Sci Rep* 9, 1577.
- [210] Matsumoto, S., and Yamazoe, Y. (2001) Involvement of multiple human cytochromes P450 in the liver microsomal metabolism of astemizole and a comparison with terfenadine, *Br J Clin Pharmacol* 51, 133-142.
- [211] Benowitz, N. L., Hukkanen, J., and Jacob, P., 3rd. (2009) Nicotine chemistry, metabolism, kinetics and biomarkers, *Handb Exp Pharmacol*, 29-60.
- [212] Barnhart, J. W. (1980) The urinary excretion of dextromethorphan and three metabolites in dogs and humans, *Toxicol Appl Pharmacol* 55, 43-48.
- [213] Bort, R., Mace, K., Boobis, A., Gomez-Lechon, M. J., Pfeifer, A., and Castell, J. (1999) Hepatic metabolism of diclofenac: role of human CYP in the minor oxidative pathways, *Biochem Pharmacol* 58, 787-796.
- [214] Wang, R. W., Kari, P. H., Lu, A. Y., Thomas, P. E., Guengerich, F. P., and Vyas, K. P. (1991) Biotransformation of lovastatin. IV. Identification of cytochrome P450 3A proteins as the major enzymes responsible for the oxidative metabolism of lovastatin in rat and human liver microsomes, *Arch Biochem Biophys* 290, 355-361.
- [215] de la Torre, R., Farre, M., Roset, P. N., Pizarro, N., Abanades, S., Segura, M., Segura, J., and Cami, J. (2004) Human pharmacology of MDMA: pharmacokinetics, metabolism, and disposition, *Ther Drug Monit* 26, 137-144.
- [216] Segre, E. J. (1975) Naproxen metabolism in man, *J Clin Pharmacol* 15, 316-323.

- [217] Kaminsky, L. S., and Zhang, Z.-Y. (1997) Human P450 metabolism of warfarin, *Pharmacol. Ther.* 73, 67-74.
- [218] Morris, G. M., Huey, R., Lindstrom, W., Sanner, M. F., Belew, R. K., Goodsell, D. S., and Olson, A. J. (2009) AutoDock4 and AutoDockTools4: Automated docking with selective receptor flexibility, *J. Comput. Chem.* 30, 2785-2791.
- [219] Bayly, C. I., Cieplak, P., Cornell, W., and Kollman, P. A. (1993) A well-behaved electrostatic potential based method using charge restraints for deriving atomic charges: The RESP model, *J. Phys. Chem.* 97, 10269-10280.
- [220] Case, D. A., Babin, V., Berryman, J. T., Betz, R. M., Cai, Q., Cerutti, D. S., Cheatham III, T. E., Darden, T. A., Duke, R. E., Gohlke, H., Goetz, A. W., Gusarov, S., Homeyer, N., Janowski, P., Kaus, J., Kolossváry, I., Kovalenko, A., Lee, T. S., LeGrand, S., Luchko, T., Luo, R., Madej, B., Merz, K. M., Paesani, F., Roe, D. R., Roitberg, A., Sagui, C., Salomon-Ferrer, R., Seabra, G., Simmerling, C. L., Smith, W., Swails, J., Walker, R. C., Wang, J., Wolf, R. M., Wu, X., and Kollman, P. A. AMBER 14, University of California, San Francisco.
- [221] Phillips, J. C., Braun, R., Wang, W., Gumbart, J., Tajkhorshid, E., Villa, E., Chipot, C., Skeel, R. D., Kalé, L., and Schulten, K. (2005) Scalable molecular dynamics with NAMD, *J. Comput. Chem.* 26, 1781-1802.
- [222] Case, D. A., Berryman, J. T., Betz, R. M., Cerutti, D. S., Cheatham III, T. E., Darden, T. A., Duke, R. E., Giese, T. J., Gohlke, H., Goetz, A. W., Homeyer, N., Izadi, S., Janowski, P., Kaus, J., Kovalenko, A., Lee, T. S., LeGrand, S., Li, P., Luchko, T., Luo, R., Madej, B., Merz, K. M., Monard, G., Needham, P., Nguyen, H., Nguyen, H. T., Omelyan, I., Onufriev, A., Roe, D. R., Roitberg, A., Salomon-Ferrer, R., Simmerling, C. L., Smith, W., Swails, J., Walker, R. C., Wang, J., Wolf, R. M., Wu, X., York, D. M., and Kollman, P. A. AMBER 2015, University of California, San Francisco.
- [223] Jiang, W., Hodoscek, M., and Roux, B. (2009) Computation of absolute hydration and binding free energy with Free Energy Perturbation Distributed Replica-Exchange Molecular Dynamics (FEP/REMD), *J. Chem. Theory Comput.* 5, 2583-2588.
- [224] Shirts, M. R., and Chodera, J. D. (2008) Statistically optimal analysis of samples from multiple equilibrium states, *J. Chem. Phys.* 129, 124105.
- [225] Isin, E. M., and Guengerich, F. P. (2008) Substrate binding to cytochromes P450, *Anal. Bioanal. Chem.* 392, 1019.
- [226] Kunze, K. L., Eddy, A. C., Gibaldi, M., and Trager, W. F. (1991) Metabolic enantiomeric interactions: The inhibition of human (S)-warfarin-7-hydroxylase by (R)-warfarin, *Chirality* 3, 24-29.
- [227] Poulos, T. L., and Raag, R. (1992) Cytochrome P450cam: Crystallography, oxygen activation, and electron transfer, *FASEB J.* 6, 674-679.
- [228] Sibbesen, O., Zhang, Z., and Ortiz de Montellano, P. R. (1998) Cytochrome P450cam substrate specificity: Relationship between structure and catalytic oxidation of alkylbenzenes, *Arch. Biochem. Biophys.* 353, 285-296.
- [229] Lin, Y.-L., and Roux, B. (2013) Computational analysis of the binding specificity of gleevec to Abl, c-Kit, Lck, and c-Src tyrosine kinases, *J. Am. Chem. Soc.* 135, 14741-14753.

- [230] Zhou, S.-F., Zhou, Z.-W., and Huang, M. (2010) Polymorphisms of human cytochrome P450 2C9 and the functional relevance, *Toxicology* 278, 165-188.
- [231] Tang, W., Stearns, R. A., Wang, R. W., Chiu, S.-H. L., and Baillie, T. A. (1999) Roles of human hepatic cytochrome P450s 2C9 and 3A4 in the metabolic activation of diclofenac, *Chem. Res. Toxicol.* 12, 192-199.
- [232] Miners, J. O., Coulter, S., Tukey, R. H., Veronese, M. E., and Birkett, D. J. (1996) Cytochromes P450, 1A2, and 2C9 are responsible for the human hepatic O-demethylation of R- and S-naproxen, *Biochem. Pharmacol.* 51, 1003-1008.
- [233] Williams, P. A., Cosme, J., Ward, A., Angove, H. C., Matak Vinkovic, D., and Jhoti, H. (2003) Crystal structure of human cytochrome P450 2C9 with bound warfarin, *Nature* 424, 464-468.
- [234] Transon, C., Leemann, T., and Dayer, P. (1996) In vitro comparative inhibition profiles of major human drug metabolising cytochrome P450 isozymes (CYP2C9, CYP2D6 and CYP3A4) by HMG-CoA reductase inhibitors, *European journal of clinical pharmacology* 50, 209-215.
- [235] Garcia, M. J., Reinoso, R. F., Sanchez Navarro, A., and Prous, J. R. (2003) Clinical pharmacokinetics of statins, *Methods and findings in experimental and clinical pharmacology* 25, 457-481.
- [236] Wester, M. R., Yano, J. K., Schoch, G. A., Yang, C., Griffin, K. J., Stout, C. D., and Johnson, E. F. (2004) The structure of human cytochrome P450 2C9 complexed with flurbiprofen at 2.0-Å resolution, *J. Biol. Chem.* 279, 35630-35637.
- [237] Wang, B., Yang, L.-P., Zhang, X.-Z., Huang, S.-Q., Bartlam, M., and Zhou, S.-F. (2009) New insights into the structural characteristics and functional relevance of the human cytochrome P450 2D6 enzyme, *Drug Metab. Rev.* 41, 573-643.
- [238] Rowland, P., Blaney, F. E., Smyth, M. G., Jones, J. J., Leydon, V. R., Oxbrow, A. K., Lewis, C. J., Tennant, M. G., Modi, S., Eggleston, D. S., Chenery, R. J., and Bridges, A. M. (2006) Crystal structure of human cytochrome P450 2D6, *J. Biol. Chem.* 281, 7614-7622.
- [239] Yu, A., Dong, H., Lang, D., and Haining, R. L. (2001) Characterization of dextromethorphan O- and N-demethylation catalyzed by highly purified recombinant human CYP2D6, *Drug metabolism and disposition: the biological fate of chemicals* 29, 1362-1365.
- [240] Meyer, M. R., Peters, F. T., and Maurer, H. H. (2009) The role of human hepatic cytochrome P450 isozymes in the metabolism of racemic 3,4-methylenedioxyethylamphetamine and its single enantiomers, *Drug metabolism and disposition: the biological fate of chemicals* 37, 1152-1156.
- [241] Matsumoto, S., and Yamazoe, Y. (2001) Involvement of multiple human cytochromes P450 in the liver microsomal metabolism of astemizole and a comparison with terfenadine, *Br. J. Clin. Pharmacol.* 51, 133-142.
- [242] Paine, M. J. I., McLaughlin, L. A., Flanagan, J. U., Kemp, C. A., Sutcliffe, M. J., Roberts, G. C. K., and Wolf, C. R. (2003) Residues glutamate 216 and aspartate 301 are key determinants of substrate specificity and product regioselectivity in cytochrome P450 2D6, *J. Biol. Chem.* 278, 4021-4027.
- [243] Wang, A., Stout, C. D., Zhang, Q., and Johnson, E. F. (2015) Contributions of ionic interactions and protein dynamics to cytochrome P450 2D6 (CYP2D6) substrate and inhibitor binding, *J. Biol. Chem.* 290, 5092-5104.

- [244] Coutts, R. T., Su, P., and Baker, G. B. (1994) Involvement of CYP2D6, CYP3A4, and other cytochrome P-450 isozymes in N-dealkylation reactions, *J. Pharmacol. Toxicol. Methods* 31, 177-186.
- [245] Sun, H., and Scott, D. O. (2011) Metabolism of 4-aminopiperidine drugs by cytochrome P450s: Molecular and quantum mechanical insights into drug design, *ACS Med. Chem. Lett.* 2, 638-643.
- [246] Xu, C., Goodz, S., Sellers, E. M., and Tyndale, R. F. (2002) CYP2A6 genetic variation and potential consequences, *Adv. Drug Delivery Rev.* 54, 1245-1256.
- [247] DeVore, N. M., and Scott, E. E. (2012) Nicotine and 4-(methylnitrosamino)-1-(3-pyridyl)-1-butanone binding and access channel in human cytochrome P450 2A6 and 2A13 enzymes, *J. Biol. Chem.* 287, 26576-26585.
- [248] Murphy, S. E., Johnson, L. M., and Pullo, D. A. (1999) Characterization of multiple products of cytochrome P450 2A6-catalyzed cotinine metabolism, *Chem. Res. Toxicol.* 12, 639-645.
- [249] Bao, Z., He, X.-Y., Ding, X., Prabhu, S., and Hong, J.-Y. (2005) Metabolism of nicotine and cotinine by human cytochrome P450 2A13, *Drug metabolism and disposition: the biological fate of chemicals* 33, 258.
- [250] Liddle, G. W., Island, D., Lance, E. M., and Harris, A. P. (1958) Alterations of adrenal steroid patterns in man resulting from treatment with a chemical inhibitor of 11 beta-hydroxylation, *J Clin Endocrinol Metab* 18, 906-912.
- [251] Leibman, K. C. (1969) Effects of metyrapone on liver microsomal drug oxidations, *Mol Pharmacol* 5, 1-9.
- [252] Williams, P. A., Cosme, J., Vinkovic, D. M., Ward, A., Angove, H. C., Day, P. J., Vonrhein, C., Tickle, I. J., and Jhoti, H. (2004) Crystal structures of human cytochrome P450 3A4 bound to metyrapone and progesterone, *Science* 305, 683-686.
- [253] Murata, H., Higuchi, T., and Otagiri, M. (2016) Oral pharmacokinetics and in-vitro metabolism of metyrapone in male rats, *J. Pharm. Pharmacol.* 68, 970-979.
- [254] Loida, P. J., and Sligar, S. G. (1993) Molecular recognition in cytochrome P-450: Mechanism for the control of uncoupling reactions, *Biochemistry* 32, 11530-11538.
- [255] Guallar, V., and Olsen, B. (2006) The role of the heme propionates in heme biochemistry, *J. Inorg. Biochem.* 100, 755-760.
- [256] Poulos, T. L. (2007) The Janus nature of heme, *Nat. Prod. Rep.* 24, 504-510.
- [257] Guallar, V., Baik, M.-H., Lippard, S. J., and Friesner, R. A. (2003) Peripheral heme substituents control the hydrogen-atom abstraction chemistry in cytochromes P450, *Proc. Natl. Acad. Sci. U. S. A.* 100, 6998-7002.
- [258] Danielson, P. B. (2002) The cytochrome P450 superfamily: biochemistry, evolution and drug metabolism in humans, *Curr Drug Metab* 3, 561-597.
- [259] Ghosh, D., Griswold, J., Erman, M., and Pangborn, W. (2009) Structural basis for androgen specificity and oestrogen synthesis in human aromatase, *Nature* 457, 219-223.
- [260] Geronimo, I., Denning, C. A., Rogers, W. E., Othman, T., Huxford, T., Heidary, D. K., Glazer, E. C., and Payne, C. M. (2016) Effect of Mutation and Substrate Binding on the Stability of Cytochrome P450BM3 Variants, *Biochemistry* 55, 3594-3606.
- [261] Fedurco, M., Augustynski, J., Indiani, C., Smulevich, G., Antalík, M., Bano, M., Sedlak, E., Glascock, M. C., and Dawson, J. H. (2004) The heme iron coordination

- of unfolded ferric and ferrous cytochrome c in neutral and acidic urea solutions. Spectroscopic and electrochemical studies, *Biochim Biophys Acta* 1703, 31-41.
- [262] Jones, C. M., Henry, E. R., Hu, Y., Chan, C. K., Luck, S. D., Bhuyan, A., Roder, H., Hofrichter, J., and Eaton, W. A. (1993) Fast events in protein folding initiated by nanosecond laser photolysis, *Proc Natl Acad Sci U S A* 90, 11860-11864.
- [263] Lee, J. C., Gray, H. B., and Winkler, J. R. (2001) Cytochrome c' folding triggered by electron transfer: fast and slow formation of four-helix bundles, *Proc Natl Acad Sci U S A* 98, 7760-7764.
- [264] Pascher, T., Chesick, J. P., Winkler, J. R., and Gray, H. B. (1996) Protein folding triggered by electron transfer, *Science* 271, 1558-1560.
- [265] Schejter, A., Ryan, M. D., Blizzard, E. R., Zhang, C., Margoliash, E., and Feinberg, B. A. (2006) The redox couple of the cytochrome c cyanide complex: the contribution of heme iron ligation to the structural stability, chemical reactivity, and physiological behavior of horse cytochrome c, *Protein Sci* 15, 234-241.
- [266] Zhong, F., Lisi, G. P., Collins, D. P., Dawson, J. H., and Pletneva, E. V. (2014) Redox-dependent stability, protonation, and reactivity of cysteine-bound heme proteins, *Proc Natl Acad Sci U S A* 111, E306-315.
- [267] Omura, T., and Sato, R. (1964) The Carbon Monoxide-Binding Pigment of Liver Microsomes. Ii. Solubilization, Purification, and Properties, *J Biol Chem* 239, 2379-2385.
- [268] Ost, T. W., Clark, J. P., Anderson, J. L., Yellowlees, L. J., Daff, S., and Chapman, S. K. (2004) 4-cyanopyridine, a versatile spectroscopic probe for cytochrome P450 BM3, *J Biol Chem* 279, 48876-48882.
- [269] van Vugt-Lussenburg, B. M., Stjernschantz, E., Lastdrager, J., Oostenbrink, C., Vermeulen, N. P., and Commandeur, J. N. (2007) Identification of critical residues in novel drug metabolizing mutants of cytochrome P450 BM3 using random mutagenesis, *J Med Chem* 50, 455-461.
- [270] Whitehouse, C. J., Bell, S. G., Yang, W., Yorke, J. A., Blanford, C. F., Strong, A. J., Morse, E. J., Bartlam, M., Rao, Z., and Wong, L. L. (2009) A highly active single-mutation variant of P450BM3 (CYP102A1), *Chembiochem : a European journal of chemical biology* 10, 1654-1656.
- [271] Whitehouse, C. J., Yang, W., Yorke, J. A., Rowlatt, B. C., Strong, A. J., Blanford, C. F., Bell, S. G., Bartlam, M., Wong, L. L., and Rao, Z. (2010) Structural basis for the properties of two single-site proline mutants of CYP102A1 (P450BM3), *Chembiochem : a European journal of chemical biology* 11, 2549-2556.
- [272] Reinen, J., Postma, G., Tump, C., Bloemberg, T., Engel, J., Vermeulen, N. P., Commandeur, J. N., and Honing, M. (2016) Application of a cocktail approach to screen cytochrome P450 BM3 libraries for metabolic activity and diversity, *Anal Bioanal Chem* 408, 1425-1443.
- [273] Reinen, J., van Leeuwen, J. S., Li, Y., Sun, L., Grootenhuis, P. D., Decker, C. J., Saunders, J., Vermeulen, N. P., and Commandeur, J. N. (2011) Efficient screening of cytochrome P450 BM3 mutants for their metabolic activity and diversity toward a wide set of drug-like molecules in chemical space, *Drug Metab Dispos* 39, 1568-1576.
- [274] Vallee, B. L., and Williams, R. J. (1968) Metalloenzymes: the entatic nature of their active sites, *Proc Natl Acad Sci U S A* 59, 498-505.

- [275] Conner, K. P., Woods, C. M., and Atkins, W. M. (2011) Interactions of cytochrome P450s with their ligands, *Arch Biochem Biophys* 507, 56-65.
- [276] Sligar, S. G., Cinti, D. L., Gibson, G. G., and Schenkman, J. B. (1979) Spin state control of the hepatic cytochrome P450 redox potential, *Biochem Biophys Res Commun* 90, 925-932.
- [277] Wells, A. V., Li, P., Champion, P. M., Martinis, S. A., and Sligar, S. G. (1992) Resonance Raman investigations of Escherichia coli-expressed Pseudomonas putida cytochrome P450 and P420, *Biochemistry* 31, 4384-4393.
- [278] Bennion, B. J., and Daggett, V. (2003) The molecular basis for the chemical denaturation of proteins by urea, *Proc Natl Acad Sci U S A* 100, 5142-5147.
- [279] Hua, L., Zhou, R., Thirumalai, D., and Berne, B. J. (2008) Urea denaturation by stronger dispersion interactions with proteins than water implies a 2-stage unfolding, *Proc Natl Acad Sci U S A* 105, 16928-16933.
- [280] Jha, S. K., and Marqusee, S. (2014) Kinetic evidence for a two-stage mechanism of protein denaturation by guanidinium chloride, *Proc Natl Acad Sci U S A* 111, 4856-4861.
- [281] Clark, J. P., Miles, C. S., Mowat, C. G., Walkinshaw, M. D., Reid, G. A., Daff, S. N., and Chapman, S. K. (2006) The role of Thr268 and Phe393 in cytochrome P450 BM3, *J Inorg Biochem* 100, 1075-1090.
- [282] Daff, S. N., Chapman, S. K., Turner, K. L., Holt, R. A., Govindaraj, S., Poulos, T. L., and Munro, A. W. (1997) Redox control of the catalytic cycle of flavocytochrome P-450 BM3, *Biochemistry* 36, 13816-13823.
- [283] Girvan, H. M., Levy, C. W., Williams, P., Fisher, K., Cheesman, M. R., Rigby, S. E., Leys, D., and Munro, A. W. (2010) Glutamate-haem ester bond formation is disfavoured in flavocytochrome P450 BM3: characterization of glutamate substitution mutants at the haem site of P450 BM3, *The Biochemical journal* 427, 455-466.
- [284] Whitehouse, C. J., Yang, W., Yorke, J. A., Tufton, H. G., Ogilvie, L. C., Bell, S. G., Zhou, W., Bartlam, M., Rao, Z., and Wong, L. L. (2011) Structure, electronic properties and catalytic behaviour of an activity-enhancing CYP102A1 (P450(BM3)) variant, *Dalton Trans* 40, 10383-10396.
- [285] Ost, T. W., Miles, C. S., Munro, A. W., Murdoch, J., Reid, G. A., and Chapman, S. K. (2001) Phenylalanine 393 exerts thermodynamic control over the heme of flavocytochrome P450 BM3, *Biochemistry* 40, 13421-13429.
- [286] Laroche-Clary, A., Morvan, V. L., Yamori, T., and Robert, J. (2010) Cytochrome P450 1B1 Gene Polymorphisms as Predictors of Anticancer Drug Activity: Studies with In vitro Models, *Mol. Cancer Ther.* 9, 3315-3321.
- [287] Rochat, B., Morsman, J. M., Murray, G. I., Figg, W. D., and McLeod, H. L. (2001) Human CYP1B1 and Anticancer Agent Metabolism: Mechanism for Tumor-Specific Drug Inactivation?, *J. Pharmacol. Exp. Ther.* 296, 537-541.
- [288] Guengerich, F. P. (2006) Cytochrome P450s and other enzymes in drug metabolism and toxicity, *AAPS J* 8, E101-E111.
- [289] Brueggemeier, R. W., Hackett, J. C., and Diaz-Cruz, E. S. (2005) Aromatase Inhibitors in the Treatment of Breast Cancer, *Endocr. Rev.* 26, 331-345.

- [290] Conte, P., and Frassoldati, A. (2007) Aromatase Inhibitors in the Adjuvant Treatment of Postmenopausal Women with Early Breast Cancer: Putting Safety Issues into Perspective, *Breast J.* 13, 28-35.
- [291] Haque, R., Ahmed, S. A., Fisher, A., Avila, C. C., Shi, J., Guo, A., Craig Cheetham, T., and Schottinger, J. E. (2012) Effectiveness of aromatase inhibitors and tamoxifen in reducing subsequent breast cancer, *Cancer Med.* 1, 318-327.
- [292] Van Poznak, C. H., and Hayes, D. F. (2006) Aromatase Inhibitors for the Treatment of Breast Cancer: Is Tamoxifen of Historical Interest Only?, *J. Natl. Cancer Inst.* 98, 1261-1263.
- [293] Ayres, L. R., Baldoni, d. A. O., Borges, A. d. P. S., and Pereira, L. R. L. (2014) Adherence and discontinuation of oral hormonal therapy in patients with hormone receptor positive breast cancer, *Int. J. Clin. Pharm.* 36, 45-54.
- [294] Attard, G., Belldgrun, A. S., and De Bono, J. S. (2005) Selective blockade of androgenic steroid synthesis by novel lyase inhibitors as a therapeutic strategy for treating metastatic prostate cancer, *BJU Int.* 96, 1241-1246.
- [295] de Bono, J. S., Logothetis, C. J., Molina, A., Fizazi, K., North, S., Chu, L., Chi, K. N., Jones, R. J., Goodman, O. B. J., Saad, F., Staffurth, J. N., Mainwaring, P., Harland, S., Flaig, T. W., Hutson, T. E., Cheng, T., Patterson, H., Hainsworth, J. D., Ryan, C. J., Sternberg, C. N., Ellard, S. L., Fléchon, A., Saleh, M., Scholz, M., Efstathiou, E., Zivi, A., Bianchini, D., Loriot, Y., Chieffo, N., Kheoh, T., Haqq, C. M., and Scher, H. I. (2011) Abiraterone and Increased Survival in Metastatic Prostate Cancer, *N. Engl. J. Med.* 364, 1995-2005.
- [296] DeVore, N. M., and Scott, E. E. (2012) Structures of cytochrome P450 17A1 with prostate cancer drugs abiraterone and TOK-001, *Nature* 482, 116-119.
- [297] Stein, M. N., Goodin, S., and DiPaola, R. S. (2012) Abiraterone in Prostate Cancer: A New Angle to an Old Problem, *Clin. Cancer Res.* 18, 1848-1854.
- [298] McFadyen, M. C. E., Melvin, W. T., and Murray, G. I. (2004) Cytochrome P450 enzymes: Novel options for cancer therapeutics, *Mol. Cancer Ther.* 3, 363-371.
- [299] Bruno, R. D., and Njar, V. C. O. (2007) Targeting cytochrome P450 enzymes: A new approach in anti-cancer drug development, *Bioorg. Med. Chem.* 15, 5047-5060.
- [300] Nieman, L. K. (2002) Medical Therapy of Cushing's Disease, *Pituitary* 5, 77-82.
- [301] Lynch, T., and Price, A. (2007) The effect of cytochrome P450 metabolism on drug response, interactions, and adverse effects, *American family physician* 76, 391-396.
- [302] Bibi, Z. (2008) Role of cytochrome P450 in drug interactions, *Nutr. Metab.* 5, 1-10.
- [303] Young, D. D., and Deiters, A. (2007) Photochemical control of biological processes, *Org. Biomol. Chem.* 5, 999-1005.
- [304] Zayat, L., Calero, C., Albores, P., Baraldo, L., and Etchenique, R. (2003) A new strategy for neurochemical photodelivery: metal-ligand heterolytic cleavage, *J. Am. Chem. Soc.* 125, 882-883.
- [305] Nikolenko, V., Yuste, R., Zayat, L., Baraldo, L. M., and Etchenique, R. (2005) Two-photon uncaging of neurochemicals using inorganic metal complexes, *Chem. Commun.* 13, 1752-1754.
- [306] Zayat, L., Salierno, M., and Etchenique, R. (2006) Ruthenium(II) bipyridyl complexes as photolabile caging groups for amines, *Inorg. Chem.* 45, 1728-1731.

- [307] Ciesiński, K. L., Haas, K. L., Dickens, M. G., Tesema, Y. T., and Franz, K. J. (2008) A photolabile ligand for light-activated release of caged copper, *J. Am. Chem. Soc.* *130*, 12246-12247.
- [308] Ciesiński, K. L., Hyman, L. M., Yang, D. T., Haas, K. L., Dickens, M. G., Holbrook, R. J., and Franz, K. J. (2010) A Photo-Caged Platinum(II) Complex That Increases Cytotoxicity upon Light Activation, *Eur. J. Inorg. Chem.* *2010*, 2224-2228.
- [309] Ciesiński, K. L., and Franz, K. J. (2011) Keys for unlocking photolabile metal-containing cages, *Angew. Chem. Int. Ed.* *50*, 814-824.
- [310] Respondek, T., Garner, R. N., Herroon, M. K., Podgorski, I., Turro, C., and Kodanko, J. J. (2011) Light activation of a cysteine protease inhibitor: caging of a peptidomimetic nitrile with Ru(II)(bpy)₂, *J. Am. Chem. Soc.* *133*, 17164-17167.
- [311] Prakash, J., and Kodanko, J. J. (2013) Metal-based methods for protein inactivation, *Curr. Opin. Chem. Biol.* *17*, 197-203.
- [312] Respondek, T., Sharma, R., Herroon, M. K., Garner, R. N., Knoll, J. D., Cueny, E., Turro, C., Podgorski, I., and Kodanko, J. J. (2014) Inhibition of cathepsin activity in a cell-based assay by a light-activated ruthenium compound, *ChemMedChem* *9*, 1306-1315.
- [313] Omura, T. (2006) Mitochondrial P450s, *Chem. Biol. Interact.* *163*, 86-93.
- [314] Berger, M. L., Hammerschmidt, F., Qian, R., Hahner, S., Schirbel, A., Stichelberger, M., Schibli, R., Yu, J., Arion, V. B., Woschek, A., Öhler, E., and Zolle, I. M. (2013) [3H]Metyrapol and 4-[131I]Iodometomidate Label Overlapping, but Not Identical, Binding Sites on Rat Adrenal Membranes, *Mol. Pharm.* *10*, 1119-1130.
- [315] Díaz-Valenzuela, M. B., Phillips, S. D., France, M. B., Gunn, M. E., and Clarke, M. L. (2009) Enantioselective Hydrogenation and Transfer Hydrogenation of Bulky Ketones Catalysed by a Ruthenium Complex of a Chiral Tridentate Ligand, *Eur. J. Chem.* *15*, 1227-1232.
- [316] Wachter, E., Howerton, B. S., Hall, E. C., Parkin, S., and Glazer, E. C. (2014) A new type of DNA "light-switch": a dual photochemical sensor and metalating agent for duplex and G-quadruplex DNA, *Chemical Communications* *50*, 311-313.
- [317] Heidary, D. K., and Glazer, E. C. (2014) A light-activated metal complex targets both DNA and RNA in a fluorescent in vitro transcription and translation assay, *Chembiochem : a European journal of chemical biology* *15*, 507-511.
- [318] Howerton, B. S., Heidary, D. K., and Glazer, E. C. (2012) Strained Ruthenium Complexes Are Potent Light-Activated Anticancer Agents, *J. Am. Chem. Soc.* *134*, 8324-8327.
- [319] Griepenburg, J. C., Rapp, T. L., Carroll, P. J., Eberwine, J., and Dmochowski, I. J. (2015) Ruthenium-caged antisense morpholinos for regulating gene expression in zebrafish embryos, *Chem. Sci.* *6*, 2342-2346.
- [320] Mosquera, J., Sanchez, M. I., Vazquez, M. E., and Mascarenas, J. L. (2014) Ruthenium bipyridyl complexes as photocleavable dimerizers: deactivation of DNA-binding peptides using visible light, *Chem. Commun.* *50*, 10975-10978.
- [321] Karaoun, N., and Renfrew, A. K. (2015) A luminescent ruthenium(II) complex for light-triggered drug release and live cell imaging, *Chem. Commun.* *51*, 14038-14041.

- [322] Albani, B. A., Durr, C. B., and Turro, C. (2013) Selective Photoinduced Ligand Exchange in a New Tris-Heteroleptic Ru(II) Complex, *J. Phys. Chem. A* 117, 13885-13892.
- [323] van Vugt-Lussenburg, B. M. A., Stjernschantz, E., Lastdrager, J., Oostenbrink, C., Vermeulen, P. E., and Commandeur, J. N. M. (2007) Identification of Critical Residues in Novel Drug Metabolizing Mutants of Cytochrome P450 BM3 Using Random Mutagenesis, *J. Med. Chem.* 50, 455-461.
- [324] Munro, A. W., Leys, D. G., McLean, K. J., Marshall, K. R., Ost, T. W., Daff, S., Miles, C. S., Chapman, S. K., Lysek, D. A., Moser, C. C., Page, C. C., and Dutton, P. L. (2002) P450 BM3: the very model of a modern flavocytochrome, *Trends Biochem. Sci.* 27, 250-257.
- [325] Locuson, C. W., Hutzler, J. M., and Tracy, T. S. (2007) Visible Spectra of Type II Cytochrome P450-Drug Complexes: Evidence that "Incomplete" Heme Coordination Is Common, *Drug metabolism and disposition: the biological fate of chemicals* 35, 614-622.
- [326] Hosea, N. A., Miller, G. P., and Guengerich, F. P. (2000) Elucidation of Distinct Ligand Binding Sites for Cytochrome P450 3A4†, *Biochem.* 39, 5929-5939.
- [327] Jefcoate, C. R. (1978) Measurement of substrate and inhibitor binding to microsomal cytochrome P-450 by optical-difference spectroscopy, *Methods Enzymol* 52, 258-279.
- [328] Lee, Y.-T., Glazer, E. C., Wilson, R. F., Stout, C. D., and Goodin, D. B. (2011) Three Clusters of Conformational States in P450cam Reveal a Multistep Pathway for Closing of the Substrate Access Channel, *Biochem.* 50, 693-703.
- [329] Hays, A.-M. A., Dunn, A. R., Chiu, R., Gray, H. B., Stout, C. D., and Goodin, D. B. (2004) Conformational States of Cytochrome P450cam Revealed by Trapping of Synthetic Molecular Wires, *J. Mol. Biol.* 344, 455-469.
- [330] Dunn, A. R., Hays, A.-M. A., Goodin, D. B., Stout, C. D., Chiu, R., Winkler, J. R., and Gray, H. B. (2002) Fluorescent Probes for Cytochrome P450 Structural Characterization and Inhibitor Screening, *J. Am. Chem. Soc.* 124, 10254-10255.
- [331] Dunn, A. R., Dmochowski, I. J., Bilwes, A. M., Gray, H. B., and Crane, B. R. (2001) Probing the open state of cytochrome P450cam with ruthenium-linker substrates, *Proc. Natl. Acad. Sci. U.S.A.* 98, 12420-12425.
- [332] Contakes, S. M., Juda, G. A., Langley, D. B., Halpern-Manners, N. W., Duff, A. P., Dunn, A. R., Gray, H. B., Dooley, D. M., Guss, J. M., and Freeman, H. C. (2005) Reversible inhibition of copper amine oxidase activity by channel-blocking ruthenium(II) and rhenium(I) molecular wires, *Proc. Natl. Acad. Sci. U.S.A.* 102, 13451-13456.
- [333] Durham, B., and Millett, F. (2012) Design of photoactive ruthenium complexes to study electron transfer and proton pumping in cytochrome oxidase, *BBA-Bioenergetics* 1817, 567-574.
- [334] Yang, X.-J., Drepper, F., Wu, B., Sun, W.-H., Haehnel, W., and Janiak, C. (2005) From model compounds to protein binding: syntheses, characterizations and fluorescence studies of [RuII(bipy)(terpy)L]2+ complexes (bipy = 2,2[prime or minute]-bipyridine; terpy = 2,2[prime or minute]:6[prime or minute],2[double prime]-terpyridine; L = imidazole, pyrazole and derivatives, cytochrome c), *Dalton Trans.* 2, 256-267.

- [335] Szaciłowski, K., Macyk, W., Drzewiecka-Matuszek, A., Brindell, M., and Stochel, G. (2005) Bioinorganic Photochemistry: Frontiers and Mechanisms, *Chem. Rev.* 105, 2647-2694.
- [336] Burke, M. D., Thompson, S., Weaver, R. J., Wolf, C. R., and Mayer, R. T. (1994) Cytochrome P450 specificities of alkoxyresorufin O-dealkylation in human and rat liver, *Biochem Pharmacol* 48, 923-936.
- [337] Goyal, N., Liu, J., Lovings, L., Dupart, P., Taylor, S., Bellow, S., Mensah, L., McClain, E., Dotson, B., Sridhar, J., Zhang, X., Zhao, M., and Foroozesh, M. (2014) Ethynylflavones, highly potent, and selective inhibitors of cytochrome P450 1A1, *Chem Res Toxicol* 27, 1431-1439.
- [338] Jia, L., and Liu, X. (2007) The conduct of drug metabolism studies considered good practice (II): in vitro experiments, *Curr. Drug Metab.* 8, 822-829.
- [339] Ortiz de Montellano, P. R. (2005) *Cytochrome P450 : structure, mechanism, and biochemistry*, 3rd ed., Kluwer Academic/Plenum Publishers, New York.
- [340] Bellon, S. F., Coleman, J. H., and Lippard, S. J. (1991) DNA Unwinding Produced by Site-Specific Intrastrand Cross-Links of the Antitumor Drug Cis-Diamminedichloroplatinum(II), *Biochemistry* 30, 8026-8035.
- [341] Keck, M. V. (2000) DNA topology analysis in the undergraduate biochemistry laboratory., *J. Chem. Educ.* 77, 1471-1473.
- [342] Keck, M. V., and Lippard, S. J. (1992) Unwinding of supercoiled DNA by platinum-ethidium and related complexes, *J. Am. Chem. Soc.* 114, 3386-3390.
- [343] Wachter, E., Heidary, D. K., Howerton, B. S., Parkin, S., and Glazer, E. C. (2012) Light-activated ruthenium complexes photobind DNA and are cytotoxic in the photodynamic therapy window, *Chem. Commun.* 48, 9649-9651.
- [344] Hidayatullah, A. N., Wachter, E., Heidary, D. K., Parkin, S., and Glazer, E. C. (2014) Photoactive Ru(II) complexes with dioxinophenanthroline ligands are potent cytotoxic agents, *Inorg Chem* 53, 10030-10032.
- [345] Knoll, J. D., Albani, B. A., and Turro, C. (2015) New Ru(II) complexes for dual photoreactivity: ligand exchange and (1)O₂ generation, *Acc Chem Res* 48, 2280-2287.
- [346] Seliskar, M., and Rozman, D. (2007) Mammalian cytochromes P450--importance of tissue specificity, *Biochim Biophys Acta* 1770, 458-466.
- [347] Poulos, T. L. (2003) Cytochrome P450 flexibility, *Proc Natl Acad Sci U S A* 100, 13121-13122.
- [348] Bolwell, G. P., Bozak, K., and Zimmerlin, A. (1994) Plant cytochrome P450, *Phytochemistry* 37, 1491-1506.
- [349] Morant, M., Bak, S., Moller, B. L., and Werck-Reichhart, D. (2003) Plant cytochromes P450: tools for pharmacology, plant protection and phytoremediation, *Curr Opin Biotechnol* 14, 151-162.
- [350] Vanden Bossche, H., Marichal, P., and Odds, F. C. (1994) Molecular mechanisms of drug resistance in fungi, *Trends Microbiol* 2, 393-400.
- [351] Lupetti, A., Danesi, R., Campa, M., Del Tacca, M., and Kelly, S. (2002) Molecular basis of resistance to azole antifungals, *Trends Mol Med* 8, 76-81.
- [352] Marichal, P., Koymans, L., Willemsens, S., Bellens, D., Verhasselt, P., Luyten, W., Borgers, M., Ramaekers, F. C. S., Odds, F. C., and Vanden Bossche, H. (1999) Contribution of mutations in the cytochrome P450 14alpha-demethylase (Erg11p,

Cyp51p) to azole resistance in *Candida albicans*, *Microbiology* 145 (Pt 10), 2701-2713.

[353] Box, G. E. P. (2013) *An accidental statistician : the life and memories of George E.P. Box*, p 1 online resource, John Wiley and Sons, Inc., Hoboken, New Jersey.

VITA

Catherine Alexandria Denning- Jannace

Personal Information

Place of Birth: Raleigh, NC U.S.A.

Education

Western Carolina University

Cullowhee, NC U.S.A.

Bachelors of Science in Chemistry (2013)

University of Kentucky

Lexington, KY U.S.A.

Doctoral Studies (2013-2020)

Advisor: Dr. Edith C. Glazer

Awards and Scholarships

UK Department of Chemistry Dissertation Year Award – 2018

Research Challenge Trust Fund Fellowship – 2016 – 2018

Naff Symposium Poster Competition – Honorable Mention – Spring 2015

UK Department of Chemistry “100% Plus” Award – Spring 2015

UK College of A&S Outstanding Teaching Award – Spring 2015

NIDA T32 Fellowship – 2014 – 2016

Max Steckler Fellowship – 2014

Department of Chemistry Fellowship – 2013 – 2018

ACS Scholar – 2011-2013

GlaxoSmithKline Women in Science Scholar – 2011 – 2013

North Carolina Biotechnology Center Undergraduate Fellow – 2011 – 2013

Undergraduate Academic Project Grant Recipient – 2011 – 2013

Publications

In preparation

C. A. Denning-Jannace, D. K. Heidary, E. C. Glazer. Correlations Between the Promiscuity of Cytochrome P450_{BM3} Variants and Oxidation State Dependent Stability.

Manuscript in preparation.

Published

I. Geronimo, **C. A. Denning**, D. K. Heidary, E. C. Glazer, C. M. Payne. Molecular Determinants of Small Molecule Affinity and Enzyme Activity of a Cytochrome P450_{BM3} Variant. *Biophysical Journal*, **2018**, 115, 1251 – 1263.

C.A. Denning*, A. Zamora*, E. Wachter, L. A. Nease, D. K. Heidary, J. Ruiz, E. C. Glazer. Ruthenium-containing P450 inhibitors for dual antitumor activity. *Dalton Transactions*, **2017**, 46, 2165 - 2173. * *Co-first authors*

I. Geronimo, **C. A. Denning**, W. E. Rogers, T. Othman, T. Huxford, D. K. Heidary, E. C. Glazer, C. M. Payne. Effect of Mutation and Substrate Binding on the Stability of Cytochrome P450_{BM3} Variants. *Biochemistry*, **2016**, 3594 - 3606.

Presentations

C. A. Denning-Jannace, E. C. Glazer. Impact of Fe oxidation state on the stability of P450_{BM3}. Invited talk at the American Chemical Society's National Meeting and Exposition. Pittsburgh, PA. March 2020. Conference cancelled due to Covid 19.

C. A. Denning, E. C. Glazer. P450_{BM3}: A Model Heme Protein. Oral presentation at: Appalachian State University's Department of Chemistry; March 2017; Boone, NC. Invited Talk.

C. A. Denning, E. C. Glazer. Nicotine and its Metabolites: Effects on a Model Cytochrome P450's Structure and Function. Oral presentation at: 2016 National Institute of Drug Abuse (NIDA) T32 Symposium; April 2016; Lexington, KY.

C. A. Denning, D. K. Heidary, E. C. Glazer. Effect of Iron Charge State on P450_{BM3} Stability. Poster presented at: 2016 Naff Symposium; April 2016, Lexington, KY.

C. A. Denning, D. K. Heidary, E. C. Glazer. Effect of Iron Charge State on P450_{BM3} Stability. Poster presented at: 250th American Chemical Society National Meeting; March 2016, San Diego, CA.

C. A. Denning, I. Geronimo, W. E. Rogers, T. Othman, T. Huxford, D. K. Heidary, E. C. Glazer, C. M. Payne. Effect of Mutations and Substrates on the Stability of a P450. Oral Presentation at: 2015 Pharmaceuticals Graduate Student Research Meeting (PGSRM); June 2015, Lexington, KY.

C. A. Denning, E. C. Glazer. Effect of Non-Native Substrates on the Stability of a Promiscuous P450. Talk presented at: 2015 NIDA T32 Symposium; April 2015, April 2015, Lexington, KY.

C.A. Denning, D. K. Heidary, E. C. Glazer. Effect of Mutations on the Stability of P450_{BM3} as determined by Chemical and Thermal Denaturation. Poster presented at: 249th American Chemical Society National Meeting; March 2015, Denver, CO.

C.A. Denning, D. K. Heidary, E. C. Glazer. Effect of Mutations on the Stability of P450_{BM3} as determined by Chemical and Thermal Denaturation. Poster Presented at: 2015 Naff Symposium; March 2015, Lexington, KY.

C. A. Denning, M. Van Dyke. Determining a Structure/Activity Relationship for the Triplex and Quadruplex Binding Protein: Stm1p. Poster presented at: National Conference of Undergraduate Research (NCUR); March 2012, Ogden, UT.

C. A. Denning, D. Livingston. Third Party Candidates and Political Debates. Oral presentation at: NCUR; March 2012, Ogden, UT.

C. A. Denning, C. Cooper. Happiness and Type of Government. Oral presentation at: NCUR; March 2011, Ithaca, NY.